CHC CANADIAN HYDRAULICS CENTRE
CENTRE D'HYDRAULIQUE CANADIEN

# INVENTORY OF CANADA'S MARINE RENEWABLE ENERGY RESOURCES

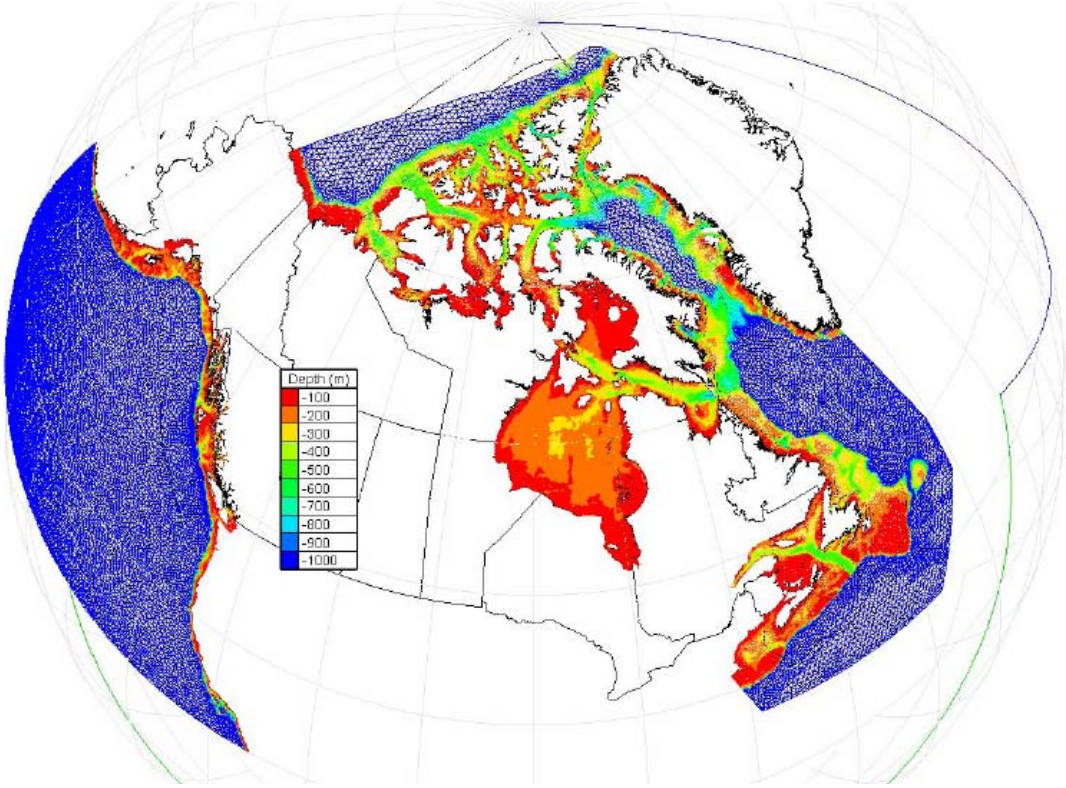


**A. Cornett**

**CHC-TR-041**

**April 2006**

National Research Council Canada
Conseil national de recherches Canada

CANADIAN HYDRAULICS CENTRE
CENTRE D'HYDRAULIQUE CANADIEN

# INVENTORY OF CANADA'S MARINE RENEWABLE ENERGY RESOURCES

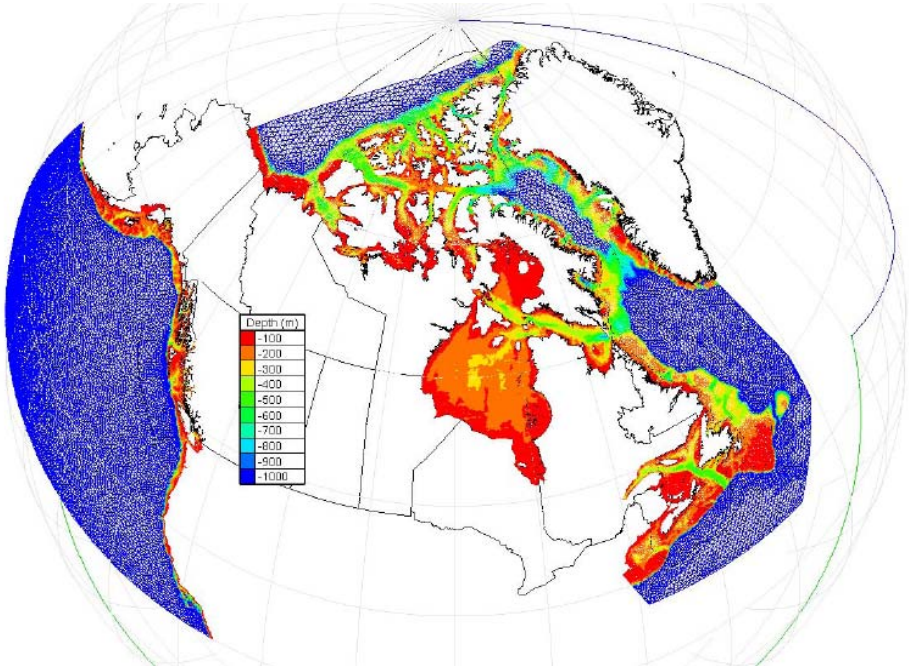


**Technical Report**

**CHC-TR-041**

**April 2006**

A. Cornett, Ph.D., P.Eng.
Canadian Hydraulics Centre
National Research Council Canada
Ottawa, K1A 0R6, Canada

# Abstract

This report presents results of studies conducted to quantify and map Canada's renewable marine energy resources due to waves and tidal currents. These studies constitute the initial phase of a multi-year project that aims to create a digital atlas of Canadian renewable marine energy resources.

The waters off Canada's Pacific and Atlantic coasts are endowed with rich wave energy resources. The results presented herein define the scale of these resources, as well as their significant spatial and seasonal variations. The annual mean wave power along the 1,000 m isobath off Canada's Pacific coast totals roughly 37,000 MW, equivalent to over 55% of Canadian electricity consumption, while the annual mean wave power along the 1,000 m isobath off Canada's Atlantic coast sums to roughly 146,500 MW or more than double current electricity demand. The wave energy available in winter is generally four to seven times greater than in summer. It is important to recognize that due to various factors including environmental considerations, losses associated with power conversion, and socio-economic factors, only a fraction of the available wave energy resource can be extracted and converted into useful power. Even so, the Canadian resources are considered sufficient to justify further research into their development as an important source of renewable green energy for the future.

Canada is also endowed with sizeable tidal current energy resources. Compared to other renewable energy sources such as solar, winds and waves, tidal currents have the distinct advantage of being reliable and highly predictable. A total of 190 sites with potential mean power greater than 1 MW have been identified. The total mean potential power at these 190 sites exceeds 42,000 MW, equivalent to roughly 63% of current electricity demand. Classified by Province and Territory, Nunavut has by far the largest potential resource, while British Columbia has the most sites with mean power greater than 1 MW. It is important to note that, as in the case of wave energy, only a fraction of the available tidal current resource can be converted into useable energy without noticeable impact on tides and tidal flows. The effects of extracting energy from tidal currents and from ocean waves should be assessed carefully on a case-by-case basis.

This report includes several recommendations for further work, including new modelling studies of nearshore wave conditions and tidal flows in selected regions, and the creation of a web-enabled digital atlas of Canadian marine renewable energy resources.

# Table of Contents

# List of Tables

Page

# List of Figures

# 1. Introduction

Global warming, the Kyoto protocol, the depletion of conventional reserves and the rising cost of electricity generation have sparked renewed interest in renewable ocean energy within Canada and internationally. Significant advances in ocean energy converters have been made in recent years, and there is a growing realization in many countries, particularly those in Europe, that these technologies will be ready for large scale deployments within the next five to ten years. One notable Canadian example of these advances is the tidal current energy demonstration project being conducted at Race Rocks, near Victoria, B.C. by Clean Current, in collaboration with EnCana and Pearson College.[1] In spite of these recent developments, the scale and distribution of the Canadian resource was poorly defined and uncertain.

The Ocean Energy (OE) Atlas project was conceived at an industry-government roundtable on ocean renewable energy held at Vancouver during March, 2005. At this meeting, the development of a comprehensive assessment of the pan-Canadian resource was recognized as a fundamental and important step towards the development of ocean energy in Canada. Several speakers noted that the Canadian Wind Energy Atlas[2], launched in 2004, played a pivotal role in boosting support for Canadian wind farms. A parallel Ocean Energy Atlas would provide a similar, much needed boost to Canada's emerging ocean energy industry.

A proposal to create a Digital Atlas of Canadian Marine Renewable Energy Resources was prepared during April and May 2005 and circulated to various Federal Government Departments and Agencies for funding. A three-year project was proposed, with a heavy emphasis in the first year on resource assessment based on existing data. The study was launched in August 2005, with funding for the first year (to March 31, 2006) provided by the Technology and Innovation Research and Development Program, administered by Natural Resources Canada.

The principal aims of the Ocean Energy Atlas project are as follows.

- To quantify and map, at a regional scale, Canada's renewable ocean energy resources due to tidal currents, waves and winds.
- To make the results available to all Canadians through an interactive digital atlas internet website.

The project is being conducted by a government-industry team led by the Canadian Hydraulics Centre of the National Research Council (NRC-CHC) in collaboration with Triton Consultants the federal department of Fisheries and Oceans (DFO), the Meteorological Service of Environment Canada (MSC), Powertech Labs and the Ocean Renewable Energy Group (OREG).

The purpose of this report is to provide a synopsis of the progress to date, including the results of preliminary assessments of Canada's wave and tidal current energy resources. The study team looks forward to securing funding for the second and third years of the project, so that these assessments can be refined and the goal of creating a digital atlas of marine renewable energy resources can be fulfilled.

[1] http://www.racerocks.com/racerock/energy/tidalenergy/tidalenergy.htm

[2] http://www.windatlas.ca/en/index.php

Further information on the proposed resource atlas is presented in Chapter 2. Chapter  provides a description and initial inventory of Canada's wave energy resources. Canada's tidal current energy resources are described, mapped and tallied in Chapter 4. Recommendations for further studies are presented in Chapter 5.

## *1.1. Targeted Renewable Energy Technologies*

Tidal barrage style energy projects have been built and successfully demonstrated at several sites around the world, including Annapolis Royal, NS[3]. However, tidal barrages tend to alter water levels, modify tidal currents, and impact eco-systems over a wide area. These side-effects suggest that traditional tidal barrages will remain unattractive for the foreseeable future in Canada. For these reasons, the Ocean Energy Atlas project will not be considering tidal barrage style developments. Instead, the project will quantify and map the resources that may one day be exploited using three different classes of energy converters:

- devices that extract energy from tidal currents (kinetic hydropower technologies);
- devices that extract energy from surface waves (wave energy converters); and
- devices that extract energy from winds (wind turbines).

Several different classes of kinetic hydropower devices have been developed and tested in recent years including: horizontal axis turbines; vertical axis turbines; water wheels; and oscillating hydroplanes. EPRI (2005) provide a recent review of the latest technologies. In addition to extracting energy from tidal currents, some of these devices can be adapted to harvest energy from the flows in rivers and open channels. The horizontal and vertical axis turbines are similar to wind turbines, but are optimized for working in water rather than air. Five examples of kinetic hydraulic turbines are shown in Figure 1. The Stingray tidal stream generator, a leading example of an oscillating hydroplane, is shown in Figure 2. One of the main advantages of marine kinetic hydropower compared with other forms of renewable energy is that unlike wind, wave and solar resources, tidal flows are entirely predictable and reliable. This predictability and reliability makes it much easier for utilities to incorporate the energy into their supply mix.

Many different types of wave energy converters have been proposed and developed in recent years. WaveNet (2003) and EPRI (2004) provide reviews of the latest technologies. These devices generally fall into two classes: *nearshore* devices that are rigidly mounted to the sea bottom or a rocky shore, and *offshore* devices which incorporate one or more semi-buoyant or floating oscillating bodies. One class of fixed device is the oscillating water column (OWC). Several full size oscillating water column prototypes have been built around the world in recent years, including Norway (1985), Japan (1990), India (1990), Portugal (1999), UK (1997, 2000), Australia (2005). Two of these devices are shown in Figure 3. Leading examples of floating devices include the Pelamis developed in the UK, the Archimedes Wave Swing developed in the Netherlands, the Wave Dragon developed in Denmark, and the OPT PowerBuoy developed in the USA. Figure 4 shows six examples of offshore wave energy converters that have all been ocean tested.

[3] Operating since 1984 with a peak output of 20 MW.

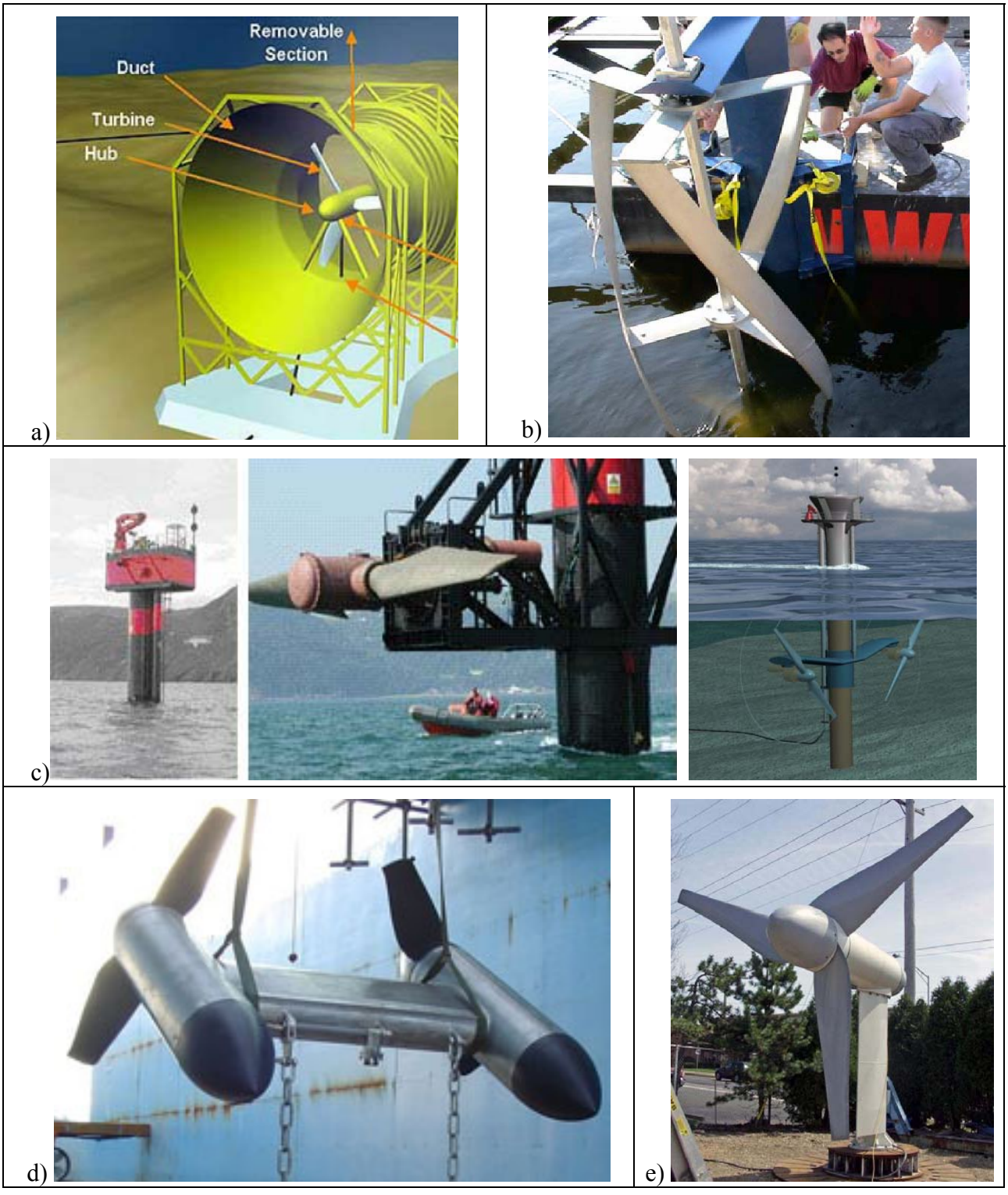


Figure 1. Five examples of kinetic hydraulic turbines: a) Lunar Energy; b) GCK Technology; c) MCT SeaGen; d) SMD Hydrovision TidEL; e) Verdant Power.

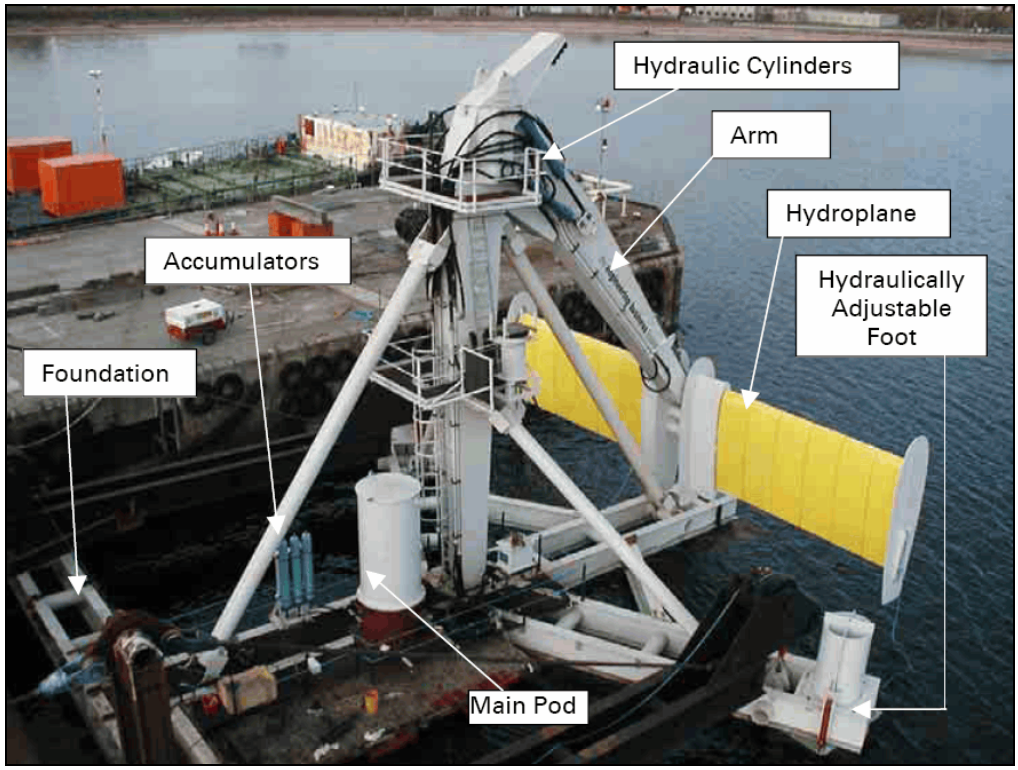


Figure 2. Stingray tidal stream generator prior to deployment.

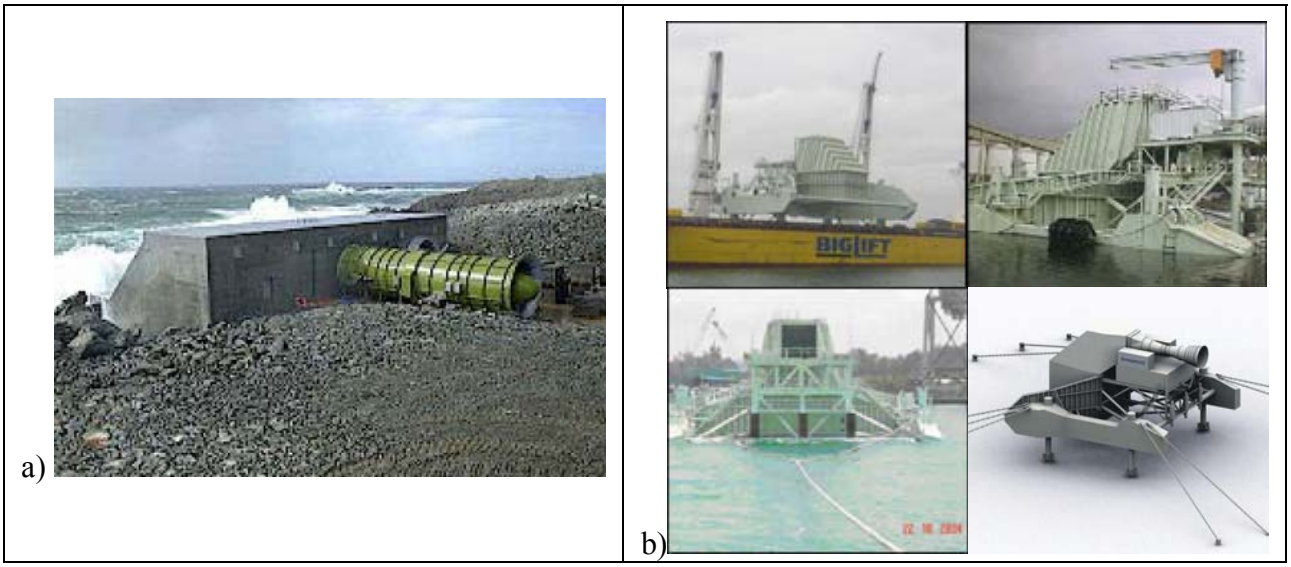


Figure 3. Two examples of nearshore wave energy converters: a) Limpet OWC; b) Energetech OWC.


Figure 4. Six examples of offshore wave energy converters: a) Pelamis; b) Archimedes Wave Swing; c) IPS Buoy; d) Technocean Hose-Pump; e) Wave Dragon; f) OPT PowerBuoy.

Winds tend to be steadier and stronger over open water than over land. Coastal and offshore winds represent a sizeable energy resource that is already being harnessed in several European countries, including Denmark, Sweden, the Netherlands, Ireland and the UK. Renewable energy project developers are also considering ocean energy farms designed to extract energy from more than one source at a single site. For example, an offshore wind farm could be equipped with wave energy converters to extract energy from waves and winds at the same site. Extracting energy from two sources would make the energy supply steadier and less intermittent. There would also be significant reductions in development costs, as much of the infrastructure could be shared between the two technologies. To support these initiatives, the Canadian Ocean Energy Atlas will include regional information on offshore winds for Canadian waters, borrowed from the existing database of the Wind Energy Atlas.

# 2. Vision for a Renewable Marine Energy Resource Atlas

## *2.1. General Description of the Atlas*

The proposed Ocean Energy Resource Atlas will feature a geo-referenced database containing tidal current, wave climate and wind data and meta-data for all Canadian waters, integrated with an interactive viewer/mapper and wrapped in a user-friendly interface. Additional layers featuring relevant climatic, environmental and socio-economic variables such as ice regime, marine parks, communities, ports and harbours, shipping lanes, and more will be included to enhance the value and utility of the Atlas to a broad and diverse community. The digital atlas will be equipped with a toolbox of statistical, temporal and spatial analysis tools for analysing and interpreting the data. The atlas will be web-enabled, like the Canadian Wind Energy Atlas, so that it can be accessed by all. The Atlas is not intended to replace the need for project developers to conduct detailed investigations of particular sites. However, the Atlas will help identify promising sites and will make it easier for others to conduct more detailed site-specific investigations.

The Atlas will help address the needs of a diverse community of users, including:

- developers of renewable ocean energy projects and technologies (for site identification);
- governments and non-governmental organizations (to help shape renewable energy policy);
- scientists and engineers (for environmental assessment and technical analysis);
- energy companies, power utilities and regulators;
- communities and municipalities;
- coastal resource managers;
- students and teachers; and
- media.

A sketch of the conceptual design for the Ocean Energy Atlas architecture is shown in Figure 5. The core of the atlas will be a geo-referenced database containing pan-Canadian information on bathymetry, wave climate, tidal flows, winds, ice regimes and more. The public will access the contents of the database through a public web interface with functionality for interactive mapping

and analysis. Users will be able to interrogate the database, perform analysis operations and create customized maps, charts and graphics. Technical users will be able to access the database contents and add new data using GIS software or through GIS-type applications such as EnSim[4]

### 2.1.1. Ancillary Benefits and Applications

The OE Atlas, with its geo-referenced database of met-ocean parameters, will provide ancillary benefits to several different communities of users. For the ocean energy sector, the atlas database will make it easier to apply computer models to conduct detailed site selection studies and perform detailed resource assessments for complex coastal areas. The Atlas database will also facilitate the use of computer models to study the potential environmental impacts of proposed installations. For example, a tidal model linked to the database could be used to investigate the impact of a proposed tidal current energy farm on the local and far-field tidal currents and water levels. Similarly, wave models and coastal process models linked to the database could be used to study the potential impact of a wave energy farm on neighbouring shores and coastal processes. By providing much of the required background data, the database will facilitate these kinds of studies.

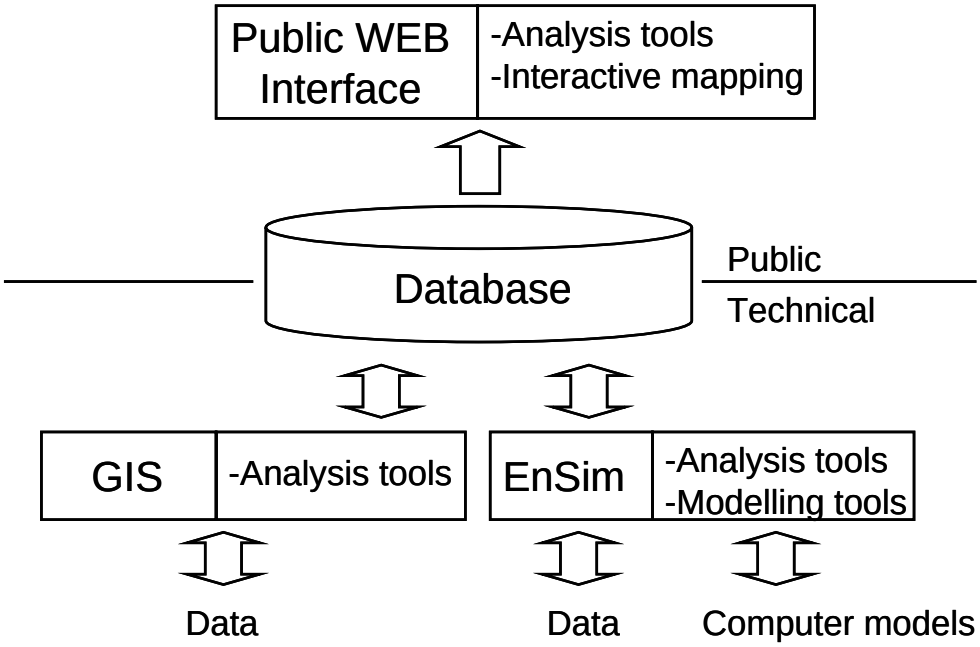


Figure 5. Preliminary system architecture for the Ocean Energy Atlas.

[4] EnSim software was developed at NRC-CHC as an environmental simulation toolkit for working with computer simulations of free surface flows in rivers, lakes, estuaries and oceans. EnSim creates a virtual environment where simulation results from different tide and wave models can be viewed, animated and analysed in two and three dimensions. A version of EnSim tailored specifically to the needs of the wind energy community was developed earlier this year.

### 2.1.2. Proposed Work Plans

As initially proposed, the OE Atlas project would have a three year duration. The main tasks for year one were:

- Review international resource assessment studies and methodologies;
- Assemble and analyse existing relevant data on tidal currents and wave conditions;
- Develop first-order estimates of provincial and national tidal stream resources;
- Develop first-order estimates of provincial and national wave energy resources;
- Develop a conceptual design of the digital OE atlas; and
- Communicate with stakeholders, disseminate interim results.

The main tasks for year two (2006/07) are as follows:

- Perform modelling studies to fill gaps and improve resource definition for nearshore waves
- Perform modelling studies to fill gaps and improve resource definition for high-velocity tidal currents
- Identify promising high-energy sites
- Complete final design of the Canadian Atlas of Renewable Ocean Energy
- Develop beta-version of the Atlas
- Communicate with stakeholders and disseminate results through technical workshops, conference presentations and papers.

The main tasks for year three (2007/08) are:

- Perform additional modelling studies to fill gaps and improve resource definition for nearshore waves.
- Perform modelling studies to fill gaps and improve resource definition for high-velocity tidal currents.
- Test and de-bug the beta-version of the Atlas
- Develop and launch the Atlas website.
- Estimate the scale of the recoverable resource and what impact its recovery might have on oceanographic processes (tides, waves, ocean circulation).
- Incorporate new data into the Atlas as it becomes available.
- Incorporate new tools for spatial and temporal analysis into the Atlas as much as possible.
- Incorporate new layers into the Atlas containing information on factors such as ice cover, surficial geology, parks and protected areas, aquaculture sites, navigation channels and routes, communities, road networks, political boundaries and the electricity grid).
- Communicate with stakeholders and disseminate results through technical workshops, conference presentations and papers.

# 3. Inventory of Wave Energy Resources

## *3.1. General Introduction*

Ocean surface waves can be considered as a concentrated form of solar energy, since these waves are generated by winds produced by weather systems that form in response to the differential solar heating of the earth's surface and atmosphere. Surface waves have long been recognized as an attractive source of renewable energy.

The power or energy flux in a wave is proportional to the square of the wave height (or amplitude) and to the wave period (or wave length). Large-amplitude, long-period waves contain more power than do smaller waves with shorter periods. The wave conditions at any site are highly variable over several different time scales. Each seastate contains many individual waves featuring a wide range of wave heights, periods and directions. The resulting surface elevation and energy flux are continuous stochastic processes. The prevailing seastate can also vary on an hourly or daily basis in response to changes in local winds, the passage of storms, and the arrival of swell from distant storms. Seasonal variations in wave climate are also common, and these tend to mirror the seasonal variations in global weather patterns. For example, wave climates at higher latitudes in the northern hemisphere tend to be considerably more energetic in winter than in summer. Wave energy is unevenly distributed around the globe. Increased wave energy can be found between the latitudes of ~40° to ~60° in both hemispheres, and on the western margin of the major continents.

Global warming, the depletion of conventional energy reserves and the rising cost of electricity generation have sparked renewed interest in renewable wave energy within Canada and internationally. Significant advances in wave energy converters have been made in recent years, and there is a growing realization in many countries, particularly those in Europe, that these technologies will be ready for large scale deployments within the next five to ten years (ABP, 2004). Despite these recent developments, very little effort has been directed to quantifying and mapping wave energy resources in Canada in the past. Due to this inattention, Canada's wave energy resources remain poorly defined and uncertain.

In the late 1970's the National Research Council Canada (NRC) investigated methods to determine wave energy flux from buoy measurements (Mansard, 1978), and quantified the wave energy resource at sites near Tofino B.C. and Logy Bay Nfld. (Baird and Mogridge, 1976). During 1991-1993, Transport Canada funded the development and published a Wind and Wave Climate Atlas of Canada in four volumes, each focusing on a different geographic region. These reports presented detailed information on wind speeds, wave heights and wave periods, but no information was given on wave energy flux or power. Allievi and Bhuyan (1994) analysed data from eleven buoys for a single year (1991) to estimate wave power in deep water off the coast of British Columbia; however, their results are inconsistent with other studies. Very recently, Cornett (2005) presented results from a preliminary analysis of wave buoy measurements from over 60 sites in the NE Pacific and the NW Atlantic near Canada.

This report extends the contribution of Cornett (2005) by presenting results from a recent study in which the wave energy resource in Canada's Pacific and Atlantic waters is defined by analysing a large quantity of data obtained from three main sources:

- direct wave measurements obtained at over sixty stations;

- a wind-wave hindcast of the North Atlantic, known as the AES40 hindcast, generated using the OWI-3G model (Swail et al, 2000); and
- wind-wave hindcasts of the Northeast Pacific and Northwest Atlantic generated by the WAVEWATCH-III model (Tolman, 2002).

The main purpose of the present work is to improve the definition of wave energy resources in the NE Pacific and the NW Atlantic near Canada. Wave energy resources in the Arctic Ocean are relatively small and difficult to exploit, due in large part to the fact that these waters remain ice-covered for much of the year. Hence, this survey has focused on the wave energy resources in the Atlantic and Pacific Oceans near Canada, where the resource is both larger and can be harvested more easily. The author is not aware of any previous studies that have attempted a comprehensive assessment of wave energy resources in the NE Pacific and the NW Atlantic near Canada.

## *3.2. Theoretical Basis for Resource Assessment*

Various methods have been proposed to estimate the wave power (P) or energy flux from field measurements of wave properties. Six methods for calculating wave power from measured data were compared by Mansard (1978), who found that some approximate methods yielded erroneous and misleading estimates. This study highlights the importance of employing a methodology that is accurate and reliable.

The energy flux or power (P) transmitted by a regular wave per unit crest width can be written as

$$P = \frac{1}{8}\rho g H^{2} C_{g} \quad , \tag{1}$$

where ρ is the fluid density (~1,030 kg/m$^3$), H is the wave height, and $C_g$ is the group velocity, defined as

$$C_{g} = \frac{1}{2}\left(1 + \frac{2kh}{\sinh(2kh)}\right)\frac{L}{T} \quad , \tag{2}$$

in which h is the local water depth, L is the wave length, T is the wave period, $k = 2\pi/L$ is the wave number and $C = L/T$ is the wave celerity. The wave length, depth and period are related through the dispersion equation:

$$L = T\sqrt{\frac{g}{k}\tanh(kh)} \quad . \tag{3}$$

In shallow water ($h < L/2$), the following explicit equation for L can be used without noticeable error:

$$L = \frac{gT^{2}}{2\pi}\left\{\tanh\left[\left(\frac{\omega^{2}h}{g}\right)^{3/4}\right]\right\}^{2/3} \quad . \tag{4}$$

In deep water ($h > L/2$), $C = L/T = 2C_g$ and $L = L_o = gT^2/2\pi$, therefore

$$P_{o} = \frac{1}{32\pi}\rho g^{2} H^{2} T \quad \text{(regular wave in deep water)} \tag{5}$$

Real seastates are often described as a summation of a large number of regular waves having different frequencies, amplitudes and directions. The mix of amplitudes, frequencies and directions is often described by a variance spectral density function or 3D wave spectrum S(f,θ). In this case, the power transmitted per unit width can be written as

$$P = \rho g \int_0^{2\pi} \int_0^{\infty} C_g(f) S(f,\theta) df\, d\theta \quad , \tag{6}$$

with

$$C_g(f) = \frac{1}{2}\left[1 + \frac{2kh}{\sinh(2kh)}\right]\sqrt{\frac{g}{k}\tanh(kh)} \quad , \tag{7}$$

where k(f) is the frequency dependent wave number and h is the local water depth.

Figure 6 shows the significant dependence of energy flux on water depth for seastates with identical $H_s$ and $T_p$. This figure illustrates the importance of taking the local water depth into account when computing wave energy at sites with water depths less than 200m. This figure does not illustrate the variation in energy flux as waves propagate from deep to shallow water, or vice-versa.

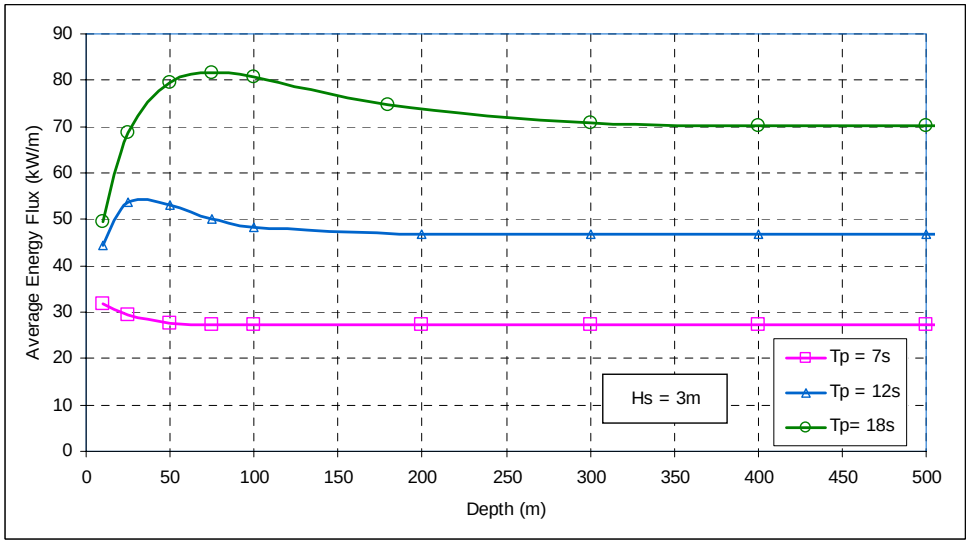


Figure 6. Influence of water depth on energy flux for selected seastates.

The wave power per unit width transmitted by irregular waves can be approximated as

$$P \approx \frac{\rho g}{16} H_s^2 C_g(T_e) \quad , \tag{8}$$

where $T_e$ is known as the energy period and $C_g(T_e)$ is the group velocity of a wave with period $T_e$. The energy period can be defined in terms of spectral moments as

$$T_e = \frac{m_{-1}}{m_0} = \frac{\int_0^\infty f^{-1} S(f)df}{\int_0^\infty S(f)df} \quad . \tag{9}$$

In deep water, the approximate expression for wave power transmitted per unit width simplifies further to

$$P_o \approx \frac{\rho g^2}{64\pi} T_e H_s^2 \quad \text{(deep water)} \, . \tag{10}$$

Measured seastates are often defined in terms of significant wave height $H_s$ and either peak period $T_p$ or mean period $T_z$. The energy period $T_e$ is rarely specified and must be estimated from other variables when the spectral shape is unknown. For example, in preparing the Atlas of UK Marine Renewable Energy Resources, it was assumed that $T_e=1.14T_z$ (ABP, 2004). Another approach when $T_p$ is known is to assume

$$T_e = \alpha T_p \quad . \tag{11}$$

The coefficient α depends on the shape of the wave spectrum: α=0.86 for a Pierson-Moskowitz spectrum, and α increases towards unity with decreasing spectral width. In assessing the wave energy resource in southern New England, Hagerman (2001) assumed that $T_e=T_p$. In this study, we have taken the more conservative assumption that $T_e=0.9T_p$, which is equivalent to assuming a standard JONSWAP spectrum with a peak enhancement factor of γ=3.3. It is readily acknowledged that this necessary assumption introduces some uncertainty into the resulting wave power estimates, particularly when the real seastate is comprised of multiple wave systems (sea plus one or more swells approaching from different directions).

## *3.3. Direct Measurements*

The Marine Environmental Data Services (MEDS) of the Department of Fisheries and Oceans Canada maintains an on-line archive of wave data measured in Canadian waters dating back to the early 1970's. MEDS currently acquires wave data from several sources, including:

- buoys operated by the Meteorological Service of Canada (MSC);
- selected buoys operated by the U.S. National Data Buoy Center (NDBC); and
- data submitted by researchers, universities, regional institutes and the oil and gas industry.

MEDS databases contain over 8 million observed wave spectra from roughly 500 locations in the Canadian area of interest. However, many of the stations are located in inland waters or contain data for relatively short periods. Wave measurements obtained mainly by wave buoys at 68 stations (38 stations in the Atlantic, 30 stations in the Pacific) have been analysed to determine the monthly, seasonal and annual wave energy regime at each site. All available sites with over 300 good days of record were selected for this analysis.

### 3.3.1. Analysis Methodology

The measured seastates are described in terms of a characteristic wave height $H_s$ (derived from the spectral moment) and a peak wave period $T_p$. Only observations classified by MEDS as "good" or "acceptable" were considered in the analysis. A program was written to determine the

frequency of occurrence for 110 different combinations of $H_s$ and $T_p$. The energy flux for each seastate bin was computed using the central values of $H_s$ and $T_p$ in equation (8) presented previously. In these calculations, the influence of water depth on group velocity and energy flux was taken into account, and the energy period for each seastate was computed as $T_e=0.9T_p$. The total energy flux at each site was obtained by summing the contributions from all 110 bins, weighted by the appropriate frequency of occurrence. Computations were performed to determine the mean wave power at each station for every month and for a typical year.

Data for Station C46147 (South Moresby) located in 2,000m water depth near South Moresby Island at longitude -131.20°, latitude 51.82°, will be used to illustrate this procedure. For this station, the MEDS archive contains 94,035 good or acceptable observations spread over 4,091 days (over 11 years). The good observations are also fairly evenly distributed by month, so that all seasons are well represented in the dataset. Table 1 shows the annual wave climate at station C46147, expressed in terms of the frequency of occurrence (in %) for 110 combinations of $H_s$ and $T_p$. The annual distributions of $H_s$ and $T_p$ are presented graphically in Figure 7. The wave power for each seastate bin, $P(H_s,T_p)$, computed using the central values of $H_s$ and $T_p$ in equation (10), are shown in Table 2, and plotted in Figure 8. This power surface applies to station C46147 and all other deep water sites. The power surface in shallow water is modified according to equation (8). The annual distribution of wave energy (kW-hr/m) with $H_s$ and $T_p$ for station C46147 is shown in Table 3, and presented graphically in Figure 9. The annual mean wave power for this site is obtained by dividing the total annual energy by the number of hours in a year (8,766), which in this case is 429,526/8,766 or 49.0 kW/m.

| $T_p$ (s) | 0 - 3 | 3 - 6 | 6 - 9 | 9 - 12 | 12 - 15 | 15 - 18 | 18 - 21 | 21 - 24 | 24 - 27 | 27 – 30 | >30 | All |
|---|---|---|---|---|---|---|---|---|---|---|---|---|
| $H_s$ (m) | | | | | | | | | | | | |
| >10 | 0.00 | 0.00 | 0.00 | 0.00 | 0.04 | 0.04 | 0.00 | 0.00 | 0.00 | 0.00 | 0.00 | 0.07 |
| 9 – 10 | 0.00 | 0.00 | 0.00 | 0.01 | 0.07 | 0.04 | 0.00 | 0.00 | 0.00 | 0.00 | 0.00 | 0.12 |
| 8 – 9 | 0.00 | 0.00 | 0.00 | 0.05 | 0.17 | 0.09 | 0.01 | 0.00 | 0.00 | 0.00 | 0.00 | 0.32 |
| 7 – 8 | 0.00 | 0.00 | 0.00 | 0.22 | 0.43 | 0.20 | 0.03 | 0.00 | 0.00 | 0.00 | 0.00 | 0.88 |
| 6 – 7 | 0.00 | 0.00 | 0.01 | 0.67 | 0.92 | 0.41 | 0.06 | 0.01 | 0.00 | 0.00 | 0.00 | 2.07 |
| 5 – 6 | 0.00 | 0.00 | 0.15 | 1.73 | 1.77 | 0.65 | 0.08 | 0.01 | 0.00 | 0.00 | 0.00 | 4.40 |
| 4 – 5 | 0.00 | 0.00 | 0.66 | 3.83 | 3.09 | 0.92 | 0.11 | 0.01 | 0.00 | 0.00 | 0.00 | 8.61 |
| 3 – 4 | 0.00 | 0.00 | 2.34 | 7.80 | 4.89 | 1.33 | 0.24 | 0.01 | 0.00 | 0.00 | 0.00 | 16.61 |
| 2 – 3 | 0.00 | 0.17 | 6.40 | 11.91 | 4.71 | 1.25 | 0.32 | 0.04 | 0.00 | 0.00 | 0.00 | 24.80 |
| 1 – 2 | 0.00 | 1.52 | 13.80 | 10.64 | 4.36 | 4.49 | 0.78 | 0.05 | 0.00 | 0.00 | 0.00 | 35.65 |
| 0 – 1 | 0.00 | 0.21 | 1.63 | 0.74 | 1.96 | 1.69 | 0.19 | 0.04 | 0.01 | 0.00 | 0.00 | 6.47 |
| All | 0.00 | 1.90 | 25.00 | 37.59 | 22.40 | 11.10 | 1.82 | 0.17 | 0.01 | 0.01 | 0.00 | |

Table 1. Annual distribution of $H_s$ and $T_p$ for station C46147 (frequency in %).

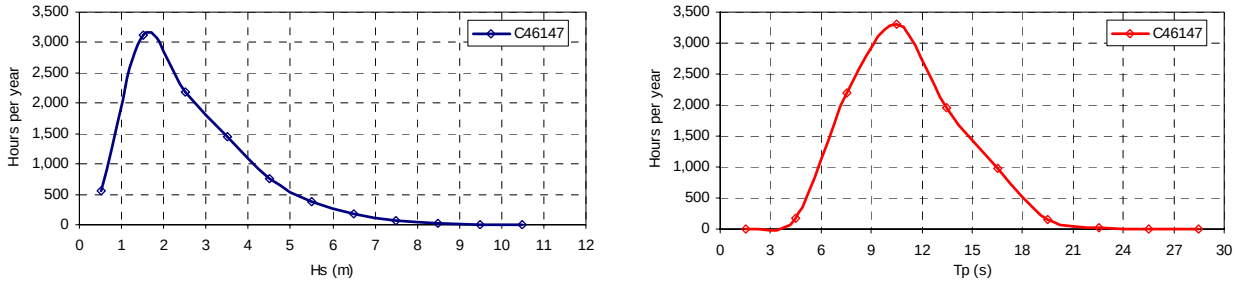


Figure 7. Annual distribution of $H_s$ and $T_p$ for station C46147.

| $T_p$ (s) | 0 - 3 | 3 - 6 | 6 - 9 | 9 - 12 | 12 - 15 | 15 - 18 | 18 - 21 | 21 - 24 | 24 - 27 | 27 – 30 | >30 | All |
|---|---|---|---|---|---|---|---|---|---|---|---|---|
| $H_s$ (m) | | | | | | | | | | | | |
| >10 | 73 | 219 | 365 | 511 | 657 | 803 | 948 | 1094 | 1240 | 1386 | | |
| 9 – 10 | 60 | 179 | 299 | 418 | 538 | 657 | 776 | 896 | 1015 | 1135 | | |
| 8 – 9 | 48 | 143 | 239 | 335 | 430 | 526 | 622 | 717 | 813 | 908 | | |
| 7 – 8 | 37 | 112 | 186 | 261 | 335 | 409 | 484 | 558 | 633 | 707 | | |
| 6 – 7 | 28 | 84 | 140 | 196 | 252 | 308 | 363 | 419 | 475 | 531 | | |
| 5 – 6 | 20 | 60 | 100 | 140 | 180 | 220 | 260 | 300 | 340 | 380 | | |
| 4 – 5 | 13 | 40 | 67 | 94 | 121 | 147 | 174 | 201 | 228 | 255 | | |
| 3 – 4 | 8 | 24 | 41 | 57 | 73 | 89 | 105 | 122 | 138 | 154 | | |
| 2 – 3 | 4 | 12 | 21 | 29 | 37 | 45 | 54 | 62 | 70 | 79 | | |
| 1 – 2 | 1 | 4 | 7 | 10 | 13 | 16 | 19 | 22 | 25 | 28 | | |
| 0 – 1 | 0 | 0 | 1 | 1 | 1 | 2 | 2 | 2 | 3 | 3 | | |
| All | | | | | | | | | | | | |

Table 2. Variation of wave power (kW/m) with $H_s$ and $T_p$ for station C46147.

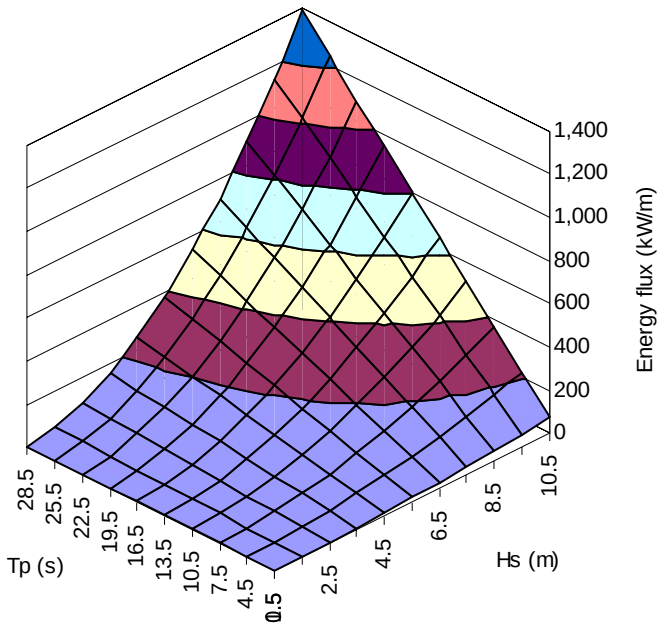


Figure 8. Variation in wave energy flux (wave power) with peak period and significant wave height (for all deep water sites including station C46147).

| $T_p$ (s) | 0 - 3 | 3 - 6 | 6 - 9 | 9 - 12 | 12 - 15 | 15 - 18 | 18 - 21 | 21 - 24 | 24 - 27 | 27 – 30 | >30 | All |
|---|---|---|---|---|---|---|---|---|---|---|---|---|
| $H_s$ (m) | | | | | | | | | | | | |
| >10 | 0 | 0 | 0 | 46 | 2030 | 2481 | 86 | 0 | 0 | 0 | 0 | 4,643 |
| 9 – 10 | 0 | 0 | 0 | 380 | 3176 | 2508 | 212 | 0 | 0 | 0 | 0 | 6,276 |
| 8 – 9 | 0 | 0 | 0 | 1582 | 6259 | 4112 | 339 | 0 | 0 | 0 | 0 | 12,292 |
| 7 – 8 | 0 | 0 | 0 | 4974 | 12745 | 7259 | 1144 | 102 | 0 | 0 | 0 | 26,223 |
| 6 – 7 | 0 | 0 | 165 | 11431 | 20245 | 10945 | 1817 | 267 | 0 | 0 | 0 | 44,871 |
| 5 – 6 | 0 | 0 | 1347 | 21279 | 28007 | 12521 | 1774 | 273 | 0 | 0 | 0 | 65,201 |
| 4 – 5 | 0 | 0 | 3898 | 31466 | 32650 | 11833 | 1631 | 201 | 0 | 0 | 0 | 81,679 |
| 3 – 4 | 0 | 4 | 8296 | 38775 | 31289 | 10388 | 2251 | 133 | 0 | 0 | 0 | 91,137 |
| 2 – 3 | 0 | 183 | 11600 | 30224 | 15380 | 4982 | 1525 | 214 | 0 | 0 | 0 | 64,107 |
| 1 – 2 | 0 | 596 | 9005 | 9725 | 5122 | 6452 | 1318 | 95 | 0 | 8 | 0 | 32,321 |
| 0 – 1 | 0 | 9 | 118 | 75 | 255 | 270 | 36 | 9 | 2 | 1 | 0 | 776 |
| All | 0 | 792 | 34430 | 149957 | 157157 | 73750 | 12135 | 1294 | 2 | 9 | 0 | 429,526 |

Table 3. Distribution of annual wave energy by seastate (kW-hr/m) for station C46147.

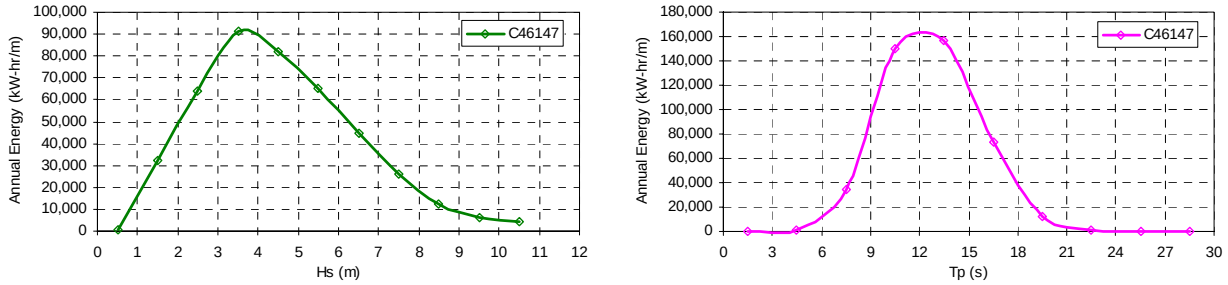


Figure 9. Distribution of annual wave energy with $H_s$ and $T_p$ for station C46147.

### 3.3.2. Results

Table 4 and Table 5 show the number of good and acceptable observations by month for all Atlantic and Pacific stations. The number of observations (related to the period of record) and their distribution throughout the year will have a direct impact on the accuracy and reliability of any wave power predictions. The most accurate and reliable predictions apply to stations with a large number of observations for every month of the year. It is important to note that the wave power predictions become less reliable as the number of monthly observations decreases.

The annual and monthly mean wave power for all east coast stations is presented in Table 6, while results for the west coast stations are shown in Table 7. The annual mean wave power results are also mapped in Figure 10 and Figure 11.

| | | | | Number of good and acceptable observations | | | | | | | | | | | |
|---|---|---|---|---|---|---|---|---|---|---|---|---|---|---|---|
| Station ID | Station Name | Long | Lat | Jan | Feb | Mar | Apr | May | Jun | Jul | Aug | Sep | Oct | Nov | Dec |
| WEL407 | HIBERNIA-MIROS | -48.78 | 46.75 | 3888 | 4022 | 2535 | 4121 | 4244 | 4229 | 4225 | 4281 | 3969 | 3560 | 4246 | 4364 |
| C44141 | Laurentian Fan | -56.13 | 42.12 | 6769 | 5798 | 6190 | 5262 | 5727 | 6303 | 6846 | 7194 | 6202 | 7173 | 7256 | 6671 |
| C44138 | SW Grand Banks | -53.62 | 44.25 | 4218 | 3079 | 3412 | 3862 | 5022 | 4744 | 4743 | 5644 | 3629 | 4693 | 5091 | 5639 |
| C44140 | Tail of the Bank | -50.61 | 42.73 | 5270 | 4739 | 5103 | 4560 | 4211 | 4675 | 5448 | 5385 | 5424 | 7171 | 6244 | 5386 |
| C44137 | East Scotian Slope | -61.35 | 41.32 | 6355 | 5654 | 5229 | 4928 | 5180 | 5272 | 5785 | 5768 | 5453 | 6471 | 6787 | 6795 |
| C44139 | Banquereau | -57.35 | 44.32 | 4055 | 2945 | 2946 | 2544 | 4136 | 4295 | 4375 | 4181 | 5120 | 6261 | 5829 | 5363 |
| meds189 | Glomar Labrador I | -58.35 | 44.44 | 1121 | 715 | 1123 | 1005 | 425 | 311 | 313 | 269 | 316 | 266 | 454 | 544 |
| meds016 | Torbay | -52.47 | 47.64 | 9652 | 2903 | 1554 | 205 | 223 | 2578 | 9180 | 12601 | 13377 | 15936 | 15658 | 14001 |
| C44142 | La Have Bank | -64.2 | 42.49 | 4861 | 4967 | 5386 | 4597 | 5503 | 5284 | 6465 | 6500 | 5494 | 5766 | 5528 | 5678 |
| WEL437 | Terra Nova L-98 | -48.43 | 46.48 | 1486 | 1239 | 1117 | 1920 | 1482 | 1438 | 1474 | 1065 | 1104 | 0 | 101 | 1484 |
| C44251 | Nickerson Bank | -53.39 | 46.44 | 3209 | 2516 | 2609 | 2631 | 2749 | 2291 | 2200 | 1999 | 1514 | 2007 | 2844 | 2818 |
| WEL416 | COPAN 1993 | -60.6 | 43.85 | 6491 | 4914 | 5265 | 4343 | 5150 | 5329 | 5168 | 4606 | 5301 | 5884 | 6647 | 6229 |
| WEL411 | Terra Nova G-90 | -48.47 | 46.49 | 1480 | 1403 | 2897 | 2850 | 2846 | 2556 | 3215 | 4748 | 1376 | 2291 | 1937 | 1442 |
| C44131 | Gannet Rock | -51 | 45.9 | 1127 | 858 | 0 | 0 | 0 | 0 | 175 | 682 | 606 | 503 | 508 | 938 |
| meds298 | Rowan Gorilla III | -60.73 | 43.81 | 1710 | 1373 | 1478 | 1395 | 1734 | 1886 | 1366 | 942 | 1174 | 1473 | 1773 | 1939 |
| meds142 | Rowan Juneau | -59.54 | 44.03 | 333 | 765 | 942 | 691 | 719 | 860 | 776 | 658 | 919 | 1025 | 800 | 839 |
| meds037 | Osborne Head | -63.46 | 44.54 | 19569 | 18143 | 18539 | 17088 | 19101 | 17580 | 16369 | 15529 | 14723 | 18742 | 19462 | 20565 |
| C44153 | Hibernia | -63.33 | 47.37 | 0 | 238 | 249 | 0 | 48 | 500 | 760 | 809 | 835 | 952 | 794 | 164 |
| meds031 | Western Head | -64.6 | 44.01 | 663 | 523 | 587 | 546 | 459 | 431 | 264 | 349 | 624 | 742 | 501 | 679 |
| C44258 | Halifax Harbour | -63.4 | 44.5 | 1690 | 1979 | 2653 | 3231 | 3577 | 3045 | 3317 | 3054 | 3006 | 3054 | 2634 | 2957 |
| meds032 | Cape Roseway | -65.2 | 43.52 | 395 | 279 | 300 | 390 | 465 | 386 | 480 | 485 | 447 | 463 | 237 | 365 |
| C44255 | NE Burgeo Bank | -57.35 | 47.28 | 2155 | 1662 | 1679 | 1508 | 1249 | 1699 | 1984 | 2120 | 2579 | 2877 | 2869 | 2204 |
| meds043 | Magdalen (Outer) | -61.3 | 47.6 | 0 | 0 | 0 | 0 | 64 | 258 | 859 | 858 | 826 | 665 | 600 | 243 |
| meds048 | Magdalen (Inner) | -61.52 | 47.63 | 0 | 0 | 0 | 0 | 0 | 18 | 509 | 634 | 607 | 597 | 533 | 41 |
| meds151 | Rolls Cove | -52.69 | 47.57 | 233 | 131 | 173 | 152 | 197 | 217 | 250 | 198 | 221 | 226 | 215 | 204 |
| meds028 | Gabarus Bay (Inner) | -60.07 | 45.82 | 236 | 79 | 0 | 17 | 232 | 292 | 430 | 448 | 262 | 401 | 465 | 436 |
| meds318 | Port-Aux-Basques Inn | -59.13 | 47.57 | 990 | 0 | 0 | 0 | 530 | 251 | 2113 | 2956 | 2763 | 2884 | 2848 | 2654 |
| meds143 | Saulnierville | -66.17 | 44.26 | 446 | 324 | 388 | 222 | 256 | 402 | 487 | 422 | 407 | 345 | 380 | 367 |
| meds040 | Tiner Point | -66.2 | 45.13 | 186 | 199 | 399 | 402 | 398 | 234 | 223 | 246 | 218 | 226 | 227 | 212 |
| C44150 | Point Sapin | -64.64 | 46.85 | 0 | 0 | 0 | 0 | 646 | 1272 | 1793 | 1764 | 1035 | 1367 | 1241 | 546 |
| meds260 | Ste Flavie Inner (K) | -68.17 | 48.64 | 0 | 0 | 0 | 0 | 114 | 286 | 482 | 480 | 476 | 472 | 187 | 0 |
| meds152 | Point Sapin | -64.68 | 46.99 | 0 | 0 | 0 | 0 | 396 | 514 | 547 | 542 | 559 | 549 | 315 | 22 |
| meds045 | Fox River A | -64.38 | 49.01 | 0 | 0 | 0 | 0 | 217 | 462 | 366 | 422 | 394 | 343 | 273 | 27 |
| meds042 | Cape Tormentine | -63.77 | 46.14 | 0 | 0 | 0 | 0 | 0 | 132 | 384 | 468 | 426 | 495 | 271 | 0 |
| meds149 | Lunenberg (WB) | -64.29 | 44.35 | 228 | 151 | 218 | 221 | 194 | 216 | 202 | 173 | 223 | 190 | 207 | 139 |
| meds027 | Minas Basin | -64.15 | 45.29 | 0 | 0 | 0 | 128 | 239 | 196 | 441 | 371 | 405 | 389 | 296 | 2 |
| meds310 | St-Bride's Outer | -54.18 | 46.92 | 393 | 477 | 235 | 10 | 339 | 439 | 533 | 484 | 580 | 645 | 496 | 444 |
| meds299 | Bay de Verde Inner | -52.9 | 48.08 | 584 | 198 | 85 | 0 | 246 | 377 | 343 | 516 | 294 | 303 | 591 | 890 |
| meds051 | Sept Iles | -66.38 | 50.2 | 0 | 0 | 0 | 12 | 207 | 327 | 332 | 197 | 208 | 391 | 388 | 197 |

Table 4. Number of good and acceptable observations by month for Atlantic stations.

| | | | | Number of good and acceptable observations | | | | | | | | | | | |
|---|---|---|---|---|---|---|---|---|---|---|---|---|---|---|---|
| Station ID | Station Name | Long | Lat | Jan | Feb | Mar | Apr | May | Jun | Jul | Aug | Sep | Oct | Nov | Dec |
| C46004 | Middle Nomad | -135.87 | 50.94 | 8155 | 7426 | 8375 | 7695 | 9147 | 9034 | 9598 | 9744 | 8583 | 9584 | 8283 | 8180 |
| C46036 | South Nomad | -133.86 | 48.3 | 9212 | 8469 | 9764 | 9428 | 10726 | 10886 | 11147 | 10521 | 10037 | 11677 | 11194 | 10464 |
| meds503w | Queen Charlotte | -129.97 | 51.3 | 741 | 545 | 322 | 211 | 345 | 450 | 585 | 551 | 642 | 812 | 788 | 774 |
| C46184 | North Nomad | -138.76 | 53.96 | 10255 | 9078 | 9932 | 9728 | 10317 | 10396 | 11182 | 10267 | 9289 | 11072 | 10521 | 10310 |
| C46207 | East Dellwood | -129.91 | 50.86 | 8895 | 8898 | 9847 | 9290 | 9132 | 8668 | 8438 | 8559 | 8188 | 9699 | 9585 | 9181 |
| C46147 | South Moresby | -131.2 | 51.82 | 7799 | 7073 | 7664 | 7100 | 7880 | 8475 | 9209 | 9100 | 7504 | 7587 | 7283 | 7361 |
| meds211 | Langara West | -133.32 | 54.45 | 2529 | 2235 | 1958 | 1513 | 622 | 254 | 1030 | 1227 | 1063 | 1177 | 792 | 2084 |
| C46208 | West Moresby | -132.7 | 52.5 | 8610 | 8191 | 8875 | 8489 | 8769 | 9889 | 10198 | 10051 | 8322 | 9513 | 9082 | 8779 |
| C46205 | West Dixon Entrance | -133.4 | 54.3 | 7923 | 7485 | 9405 | 9355 | 9623 | 9537 | 9975 | 9866 | 7975 | 9111 | 8139 | 8720 |
| meds226 | Cape Scott | -128.91 | 50.77 | 900 | 344 | 273 | 330 | 120 | 114 | 88 | 248 | 239 | 313 | 289 | 316 |
| C46132 | South Brooks | -127.92 | 49.73 | 6323 | 6628 | 7583 | 7437 | 7436 | 6890 | 6295 | 7084 | 6516 | 7503 | 7077 | 6077 |
| meds103 | Tofino | -125.74 | 48.99 | 4395 | 5212 | 5911 | 5764 | 6210 | 6417 | 5287 | 4924 | 4678 | 4833 | 4589 | 5425 |
| C46204 | West Sea Otter | -128.74 | 51.38 | 8357 | 7675 | 9139 | 9196 | 8264 | 7303 | 7321 | 7557 | 7961 | 9346 | 7888 | 8314 |
| C46185 | South Hecate Strait | -129.8 | 52.42 | 8476 | 7909 | 8987 | 7694 | 7670 | 7767 | 8010 | 7587 | 7536 | 8525 | 7721 | 7903 |
| meds502w | Hecate Strait | -130.33 | 52.2 | 374 | 454 | 733 | 548 | 460 | 445 | 596 | 494 | 573 | 712 | 562 | 293 |
| C46145 | Central Dixon Entran | -132.43 | 54.38 | 9238 | 8371 | 9636 | 8580 | 8797 | 9655 | 10297 | 10395 | 8897 | 8974 | 9125 | 9299 |
| meds213 | Bonilla Island | -130.72 | 53.32 | 3471 | 3272 | 3741 | 2313 | 2256 | 1819 | 2775 | 3296 | 3117 | 2269 | 2900 | 3659 |
| C46183 | North Hecate Strait | -131.14 | 53.57 | 8177 | 7976 | 8561 | 7770 | 8216 | 8151 | 8238 | 8230 | 6977 | 7940 | 8388 | 7750 |
| C46131 | Sentry Shoal | -124.99 | 49.91 | 6131 | 6114 | 6825 | 6855 | 6294 | 6203 | 6791 | 6714 | 6439 | 6356 | 6549 | 6403 |
| meds108 | Roberts Bank | -123.27 | 49.02 | 241 | 348 | 427 | 121 | 251 | 399 | 438 | 342 | 397 | 472 | 237 | 240 |
| meds102 | Sturgeon Bank | -123.31 | 49.17 | 428 | 557 | 688 | 413 | 416 | 307 | 458 | 333 | 177 | 172 | 302 | 338 |
| C46146 | Halibut Bank | -123.73 | 49.34 | 5987 | 5911 | 6972 | 6863 | 6996 | 6316 | 6904 | 6978 | 6404 | 6720 | 6539 | 6865 |
| meds122 | Point Grey | -123.27 | 49.28 | 182 | 149 | 206 | 203 | 85 | 170 | 367 | 142 | 205 | 212 | 171 | 157 |
| meds106 | West Vancouver | -123.23 | 49.35 | 838 | 805 | 553 | 387 | 373 | 212 | 245 | 244 | 236 | 244 | 233 | 514 |
| meds123 | Fishermans Cove (WB) | -123.7 | 49.35 | 246 | 213 | 209 | 171 | 244 | 228 | 221 | 237 | 211 | 240 | 206 | 234 |
| C46181 | Nanakwa Shoal | -128.84 | 53.82 | 4902 | 4060 | 4752 | 4689 | 5179 | 4544 | 4176 | 4447 | 5068 | 5438 | 5554 | 5169 |
| meds317 | Esquimalt Harbour | -123.45 | 48.43 | 1509 | 874 | 975 | 1440 | 1430 | 1252 | 1478 | 1488 | 1329 | 1259 | 2640 | 2687 |
| meds124 | Fishermans Cove (K) | -123.27 | 49.35 | 200 | 204 | 225 | 138 | 200 | 238 | 248 | 248 | 165 | 67 | 201 | 201 |
| C46134 | Pat Bay Test Buoy | -123.45 | 48.66 | 1482 | 1348 | 1961 | 1888 | 1949 | 2291 | 1536 | 1364 | 1057 | 1137 | 1425 | 1311 |
| meds121 | Gibsons Landing | -123.5 | 49.4 | 188 | 214 | 240 | 257 | 247 | 207 | 247 | 231 | 230 | 238 | 236 | 245 |

Table 5. Number of good and acceptable observations by month for Pacific stations.

| | | | | Mean Wave Power (kW/m) | | | | | | | | | | | | |
|---|---|---|---|---|---|---|---|---|---|---|---|---|---|---|---|---|
| Station ID | Station Name | Long | Lat | Annual | Jan | Feb | Mar | Apr | May | Jun | Jul | Aug | Sep | Oct | Nov | Dec |
| WEL407 | HIBERNIA-MIROS | -48.78 | 46.75 | 45.1 | 98.8 | 47.1 | 34.2 | 47.3 | 22.4 | 14.8 | 10.9 | 11.7 | 45.9 | 74.0 | 52.2 | 83.4 |
| C44141 | Laurentian Fan | -56.13 | 42.12 | 44.2 | 79.6 | 72.6 | 66.3 | 45.3 | 24.4 | 14.6 | 12.3 | 12.7 | 25.9 | 41.0 | 54.6 | 83.4 |
| C44138 | SW Grand Banks | -53.62 | 44.25 | 43.4 | 79.8 | 62.3 | 64.4 | 38.8 | 18.6 | 12.2 | 9.8 | 12.6 | 20.0 | 42.8 | 64.7 | 85.4 |
| C44140 | Tail of the Bank | -50.61 | 42.73 | 42.2 | 84.8 | 68.1 | 59.4 | 32.6 | 18.5 | 15.1 | 11.4 | 10.2 | 23.9 | 39.7 | 60.5 | 72.4 |
| C44137 | East Scotian Slope | -61.35 | 41.32 | 36.7 | 60.7 | 57.6 | 57.6 | 26.4 | 21.0 | 10.9 | 9.8 | 12.1 | 20.5 | 35.8 | 47.4 | 65.2 |
| C44139 | Banquereau | -57.35 | 44.32 | 34.1 | 61.8 | 55.7 | 56.0 | 28.5 | 16.0 | 10.3 | 8.2 | 12.1 | 19.1 | 35.8 | 44.0 | 60.0 |
| meds189 | Glomar Labrador I | -58.35 | 44.44 | 30.5 | 46.5 | 37.4 | 43.2 | 32.6 | 15.4 | 13.8 | 8.4 | 6.1 | 13.0 | 38.8 | 39.5 | 55.4 |
| meds016 | Torbay | -52.47 | 47.64 | 28.9 | 48.4 | 33.5 | 51.2 | 33.7 | 16.0 | 9.3 | 7.4 | 9.5 | 20.6 | 32.2 | 37.9 | 54.8 |
| C44142 | La Have Bank | -64.2 | 42.49 | 25.8 | 45.0 | 42.0 | 40.5 | 22.7 | 13.8 | 8.3 | 6.8 | 8.8 | 16.1 | 23.9 | 38.6 | 50.6 |
| WEL437 | Terra Nova L-98 | -48.43 | 46.48 | 24.3 | 40.8 | 37.6 | 30.5 | 25.7 | 18.4 | 13.5 | 8.9 | 8.5 | 16.9 | NA | 37.3 | 37.5 |
| C44251 | Nickerson Bank | -53.39 | 46.44 | 24.0 | 38.5 | 39.0 | 34.9 | 17.0 | 11.6 | 5.8 | 7.4 | 6.7 | 13.1 | 24.8 | 27.5 | 43.8 |
| WEL416 | COPAN 1993 | -60.6 | 43.85 | 22.4 | 50.2 | 33.8 | 34.0 | 19.7 | 12.2 | 6.2 | 6.1 | 9.3 | 14.6 | 20.6 | 27.5 | 43.9 |
| WEL411 | Terra Nova G-90 | -48.47 | 46.49 | 22.0 | 35.0 | 35.4 | 31.0 | 25.6 | 17.1 | 10.6 | 9.2 | 11.9 | 16.1 | 25.8 | 30.4 | 42.2 |
| C44131 | Gannet Rock | -51 | 45.9 | 21.9 | 36.8 | 37.4 | NA | NA | NA | NA | 1.6 | 1.5 | 12.2 | 8.7 | 5.6 | 28.1 |
| meds298 | Rowan Gorilla III | -60.73 | 43.81 | 20.3 | 48.1 | 30.0 | 32.5 | 19.3 | 11.9 | 7.0 | 5.8 | 6.1 | 7.3 | 20.0 | 24.6 | 40.2 |
| meds142 | Rowan Juneau | -59.54 | 44.03 | 20.2 | 37.5 | 31.4 | 30.6 | 24.8 | 9.1 | 9.0 | 7.1 | 5.2 | 12.6 | 17.1 | 35.9 | 34.5 |
| meds037 | Osborne Head | -63.46 | 44.54 | 11.6 | 20.2 | 18.8 | 17.8 | 12.6 | 7.0 | 5.9 | 4.3 | 4.4 | 7.0 | 10.0 | 13.3 | 18.0 |
| C44153 | Hibernia | -63.33 | 47.37 | 11.1 | NA | 66.9 | 58.0 | NA | 1.3 | 1.4 | 1.4 | 5.7 | 5.0 | 8.1 | 11.7 | 23.5 |
| meds031 | Western Head | -64.6 | 44.01 | 10.4 | 10.3 | 22.6 | 16.4 | 12.1 | 6.5 | 3.2 | 3.1 | 4.7 | 4.0 | 8.5 | 14.3 | 13.0 |
| C44258 | Halifax Harbour | -63.4 | 44.5 | 9.0 | 12.7 | 12.4 | 14.1 | 10.4 | 7.1 | 4.4 | 4.0 | 3.3 | 5.7 | 11.0 | 10.3 | 16.7 |
| meds032 | Cape Roseway | -65.2 | 43.52 | 8.5 | 10.9 | 16.9 | 19.0 | 9.3 | 8.0 | 3.8 | 3.9 | 5.6 | 4.4 | 7.0 | 10.8 | 10.9 |
| C44255 | NE Burgeo Bank | -57.35 | 47.28 | 8.3 | 6.6 | 12.7 | 18.1 | 13.5 | 7.8 | 5.0 | 5.3 | 3.4 | 4.1 | 8.7 | 9.3 | 8.3 |
| meds043 | Magdalen (Outer) | -61.3 | 47.6 | 6.2 | NA | NA | NA | NA | 10.1 | 1.4 | 2.8 | 3.2 | 4.6 | 9.3 | 10.3 | 19.9 |
| meds048 | Magdalen (Inner) | -61.52 | 47.63 | 4.8 | NA | NA | NA | NA | NA | 0.5 | 1.3 | 2.0 | 5.0 | 6.7 | 8.7 | 9.4 |
| meds151 | Rolls Cove | -52.69 | 47.57 | 3.6 | 4.3 | 1.8 | 7.2 | 2.4 | 0.9 | 1.0 | 1.1 | 0.6 | 2.9 | 2.8 | 13.9 | 2.9 |
| meds028 | Gabarus Bay (Inner) | -60.07 | 45.82 | 3.4 | 5.4 | 6.0 | NA | 0.8 | 1.7 | 1.1 | 1.3 | 1.6 | 2.6 | 2.1 | 4.4 | 9.3 |
| meds318 | Port-Aux-Basques Inn | -59.13 | 47.57 | 3.4 | 4.8 | NA | NA | NA | 9.0 | 2.4 | 1.3 | 1.0 | 2.7 | 3.4 | 3.9 | 6.6 |
| meds143 | Saulnierville | -66.17 | 44.26 | 2.6 | 6.6 | 2.1 | 4.4 | 1.9 | 1.5 | 0.6 | 0.6 | 0.4 | 0.9 | 2.5 | 3.2 | 5.7 |
| meds040 | Tiner Point | -66.2 | 45.13 | 2.5 | 7.0 | 1.3 | 2.9 | 2.1 | 1.2 | 0.8 | 1.1 | 0.6 | 0.8 | 3.6 | 3.9 | 6.2 |
| C44150 | Point Sapin | -64.64 | 46.85 | 2.4 | NA | NA | NA | NA | 11.0 | 0.6 | 0.4 | 0.5 | 2.0 | 3.2 | 3.7 | 4.6 |
| meds260 | Ste Flavie Inner (K) | -68.17 | 48.64 | 1.4 | NA | NA | NA | NA | 0.6 | 0.6 | 0.4 | 0.8 | 1.4 | 1.8 | 6.1 | NA |
| meds152 | Point Sapin | -64.68 | 46.99 | 1.4 | NA | NA | NA | NA | 1.4 | 0.7 | 1.2 | 0.7 | 1.0 | 2.7 | 2.5 | 0.6 |
| meds045 | Fox River A | -64.38 | 49.01 | 1.0 | NA | NA | NA | NA | 1.0 | 1.0 | 0.5 | 0.6 | 0.6 | 1.5 | 1.5 | 3.8 |
| meds042 | Cape Tormentine | -63.77 | 46.14 | 0.4 | NA | NA | NA | NA | NA | 0.3 | 0.2 | 0.2 | 0.3 | 0.7 | 0.7 | NA |
| meds149 | Lunenberg (WB) | -64.29 | 44.35 | 0.3 | 0.8 | 0.2 | 0.5 | 0.3 | 0.2 | 0.1 | 0.1 | 0.1 | 0.1 | 0.2 | 0.2 | 0.4 |
| meds027 | Minas Basin | -64.15 | 45.29 | 0.3 | NA | NA | NA | 0.1 | 0.3 | 0.2 | 0.1 | 0.1 | 0.2 | 0.4 | 0.8 | 0.5 |
| meds310 | St-Bride's Outer | -54.18 | 46.92 | 0.2 | 0.8 | 0.2 | 0.2 | 0.1 | 0.0 | 0.1 | 0.1 | 0.1 | 0.0 | 0.2 | 0.3 | 0.6 |
| meds299 | Bay de Verde Inner | -52.9 | 48.08 | 0.2 | 0.2 | 1.4 | 0.1 | NA | 0.1 | 0.1 | 0.1 | 0.0 | 0.0 | 0.2 | 0.1 | 0.2 |
| meds051 | Sept Iles | -66.38 | 50.2 | 0.1 | NA | NA | NA | 0.0 | 0.0 | 0.0 | 0.0 | 0.1 | 0.1 | 0.1 | 0.1 | 0.2 |

Table 6. Annual and monthly mean wave power for Atlantic stations (NA = not available).

| | | | | Mean Wave Power (kW/m) | | | | | | | | | | | | |
|---|---|---|---|---|---|---|---|---|---|---|---|---|---|---|---|---|
| Station ID | Station Name | Long | Lat | Annual | Jan | Feb | Mar | Apr | May | Jun | Jul | Aug | Sep | Oct | Nov | Dec |
| C46004 | Middle Nomad | -135.87 | 50.94 | 53.8 | 89.4 | 80.4 | 64.8 | 51.0 | 27.0 | 17.9 | 11.1 | 14.8 | 33.3 | 64.9 | 96.8 | 113.8 |
| C46036 | South Nomad | -133.86 | 48.3 | 53.3 | 90.8 | 79.2 | 73.8 | 50.7 | 26.6 | 19.6 | 11.3 | 15.0 | 27.2 | 59.2 | 86.8 | 107.1 |
| meds503w | Queen Charlotte | -129.97 | 51.3 | 52.9 | 103.4 | 73.8 | 57.6 | 72.9 | 25.3 | 22.7 | 10.5 | 10.5 | 22.3 | 35.9 | 83.9 | 85.8 |
| C46184 | North Nomad | -138.76 | 53.96 | 50.9 | 79.6 | 73.0 | 62.5 | 44.6 | 22.7 | 16.8 | 10.3 | 14.7 | 35.3 | 62.6 | 84.9 | 103.3 |
| C46207 | East Dellwood | -129.91 | 50.86 | 49.0 | 82.4 | 75.3 | 59.9 | 39.3 | 22.1 | 16.1 | 9.9 | 11.4 | 23.9 | 56.7 | 77.4 | 100.5 |
| C46147 | South Moresby | -131.2 | 51.82 | 49.0 | 79.4 | 82.3 | 64.9 | 42.1 | 21.8 | 16.9 | 10.1 | 11.8 | 26.3 | 63.1 | 79.1 | 101.0 |
| meds211 | Langara West | -133.32 | 54.45 | 45.7 | 106.2 | 101.3 | 55.9 | 48.7 | 20.7 | 12.3 | 7.8 | 9.6 | 21.0 | 37.7 | 63.3 | 72.3 |
| C46208 | West Moresby | -132.7 | 52.5 | 44.7 | 72.8 | 69.7 | 56.6 | 39.1 | 22.8 | 16.2 | 9.7 | 12.8 | 25.8 | 56.0 | 73.0 | 95.8 |
| C46205 | West Dixon Entrance | -133.4 | 54.3 | 43.6 | 73.0 | 57.6 | 53.1 | 40.0 | 23.3 | 15.3 | 9.5 | 13.3 | 28.2 | 53.5 | 81.2 | 91.0 |
| meds226 | Cape Scott | -128.91 | 50.77 | 43.3 | 101.1 | 53.9 | 49.9 | 54.4 | 22.4 | 11.7 | 7.2 | 13.5 | 15.4 | 55.7 | 29.3 | 53.0 |
| C46132 | South Brooks | -127.92 | 49.73 | 43.3 | 71.7 | 71.8 | 60.0 | 35.8 | 19.4 | 15.1 | 9.0 | 9.8 | 21.4 | 51.2 | 67.0 | 87.1 |
| meds103 | Tofino | -125.74 | 48.99 | 31.9 | 58.2 | 53.5 | 45.6 | 32.5 | 18.6 | 12.4 | 7.8 | 8.3 | 13.7 | 34.2 | 52.2 | 55.7 |
| C46204 | West Sea Otter | -128.74 | 51.38 | 30.7 | 51.8 | 41.6 | 39.7 | 25.5 | 14.7 | 10.6 | 6.7 | 7.7 | 15.4 | 35.9 | 48.8 | 61.2 |
| C46185 | South Hecate Strait | -129.8 | 52.42 | 23.0 | 42.8 | 34.1 | 27.3 | 20.6 | 11.8 | 7.9 | 5.4 | 5.9 | 10.5 | 23.0 | 36.4 | 47.0 |
| meds502w | Hecate Strait | -130.33 | 52.2 | 18.2 | 31.7 | 20.4 | 32.3 | 21.8 | 10.3 | 10.6 | 4.9 | 4.1 | 7.9 | 18.3 | 33.0 | 21.2 |
| C46145 | Central Dixon Entranc | -132.43 | 54.38 | 17.7 | 22.2 | 26.0 | 24.0 | 14.5 | 8.2 | 5.0 | 3.4 | 4.8 | 12.7 | 22.0 | 30.7 | 41.7 |
| meds213 | Bonilla Island | -130.72 | 53.32 | 12.1 | 23.2 | 13.9 | 16.4 | 14.4 | 7.7 | 4.8 | 3.2 | 2.6 | 4.9 | 10.1 | 24.4 | 17.6 |
| C46183 | North Hecate Strait | -131.14 | 53.57 | 11.2 | 21.3 | 16.9 | 13.0 | 10.4 | 5.0 | 3.0 | 2.3 | 3.5 | 5.3 | 11.5 | 17.9 | 24.0 |
| C46131 | Sentry Shoal | -124.99 | 49.91 | 0.6 | 0.8 | 0.5 | 0.8 | 0.6 | 0.2 | 0.2 | 0.1 | 0.1 | 0.2 | 0.7 | 1.1 | 1.2 |
| meds108 | Roberts Bank | -123.27 | 49.02 | 0.4 | 0.2 | 0.5 | 0.6 | 0.4 | 0.4 | 0.6 | 0.2 | 0.2 | 0.2 | 0.4 | 0.5 | 0.5 |
| meds102 | Sturgeon Bank | -123.31 | 49.17 | 0.4 | 0.3 | 0.4 | 0.5 | 0.5 | 0.3 | 0.4 | 0.2 | 0.2 | 0.2 | 0.3 | 0.4 | 0.4 |
| C46146 | Halibut Bank | -123.73 | 49.34 | 0.3 | 0.3 | 0.2 | 0.3 | 0.2 | 0.2 | 0.2 | 0.2 | 0.2 | 0.2 | 0.3 | 0.4 | 0.6 |
| meds122 | Point Grey | -123.27 | 49.28 | 0.2 | 0.1 | 0.1 | 0.2 | 0.1 | 0.1 | 0.2 | 0.1 | 0.1 | 0.1 | 0.2 | 0.2 | 0.3 |
| meds106 | West Vancouver | -123.23 | 49.35 | 0.1 | 0.1 | 0.1 | 0.1 | 0.1 | 0.1 | 0.1 | 0.2 | 0.1 | 0.1 | 0.1 | 0.1 | 0.1 |
| meds123 | Fishermans Cove (WB) | -123.7 | 49.35 | 0.1 | 0.1 | 0.0 | 0.1 | 0.1 | 0.0 | 0.1 | 0.0 | 0.0 | 0.0 | 0.1 | 0.0 | 0.1 |
| C46181 | Nanakwa Shoal | -128.84 | 53.82 | 0.0 | 0.2 | 0.1 | 0.0 | 0.0 | 0.0 | 0.0 | 0.0 | 0.0 | 0.0 | 0.0 | 0.1 | 0.1 |
| meds317 | Esquimalt Harbour | -123.45 | 48.43 | 0.0 | 0.0 | 0.0 | 0.0 | 0.0 | 0.0 | 0.0 | 0.0 | 0.0 | 0.0 | 0.0 | 0.0 | 0.1 |
| meds124 | Fishermans Cove (K) | -123.27 | 49.35 | 0.0 | 0.0 | 0.0 | 0.0 | 0.0 | 0.0 | 0.0 | 0.0 | 0.0 | 0.0 | 0.0 | 0.0 | 0.0 |
| C46134 | Pat Bay Test Buoy | -123.45 | 48.66 | 0.0 | 0.0 | 0.0 | 0.0 | 0.0 | 0.0 | 0.0 | 0.0 | 0.0 | 0.0 | 0.0 | 0.0 | 0.0 |
| meds121 | Gibsons Landing | -123.5 | 49.4 | 0.0 | 0.0 | 0.0 | 0.0 | 0.0 | 0.0 | 0.0 | 0.0 | 0.0 | 0.0 | 0.0 | 0.0 | 0.0 |

Table 7. Annual and monthly mean wave power for Pacific stations.

Many stations on both coasts are located in sheltered inshore locations with relatively mild wave climates. However, there are also a good number of stations in exposed sites featuring energetic wave climates. These results indicate that the mean annual wave energy flux at exposed sites in deep water off the B.C. coast is typically in the range of 45 to 55 kW/m, while the mean wave power available near the western shores of the Queen Charlotte Islands and Vancouver Island is on the order of 30 to 45 kW/m. On the Grand Banks east of Newfoundland, the mean annual wave energy flux is in the range of 42 to 45 kW/m, while the mean wave power available near the SE coast of Newfoundland is on the order of 25 to 30 kW/m. Annual mean wave power values around 20 to 25 kW/m seem representative for the waters near Sable Island, while values near 10 kW/m are representative of conditions along the southern shore of Nova Scotia.

As noted previously, the wave power along a coast can vary considerably due to sheltering and bathymetric effects such as wave diffraction and refraction. Hence, there likely will be pronounced local variations in wave conditions and energy potential close to shore. Clearly, these local variations cannot be identified and are beyond the scope of the present analysis.

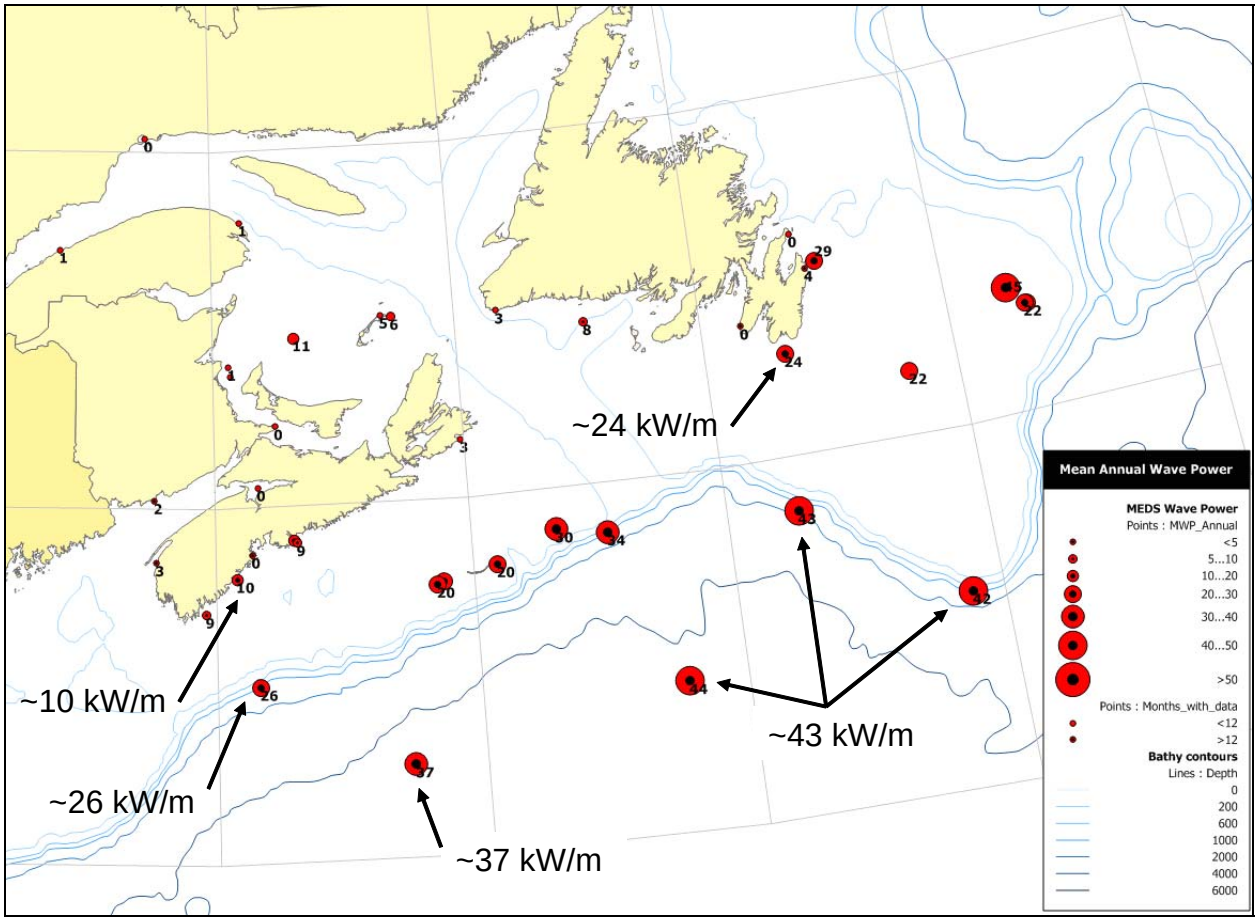


Figure 10. Annual mean wave power for sites in the NW Atlantic.

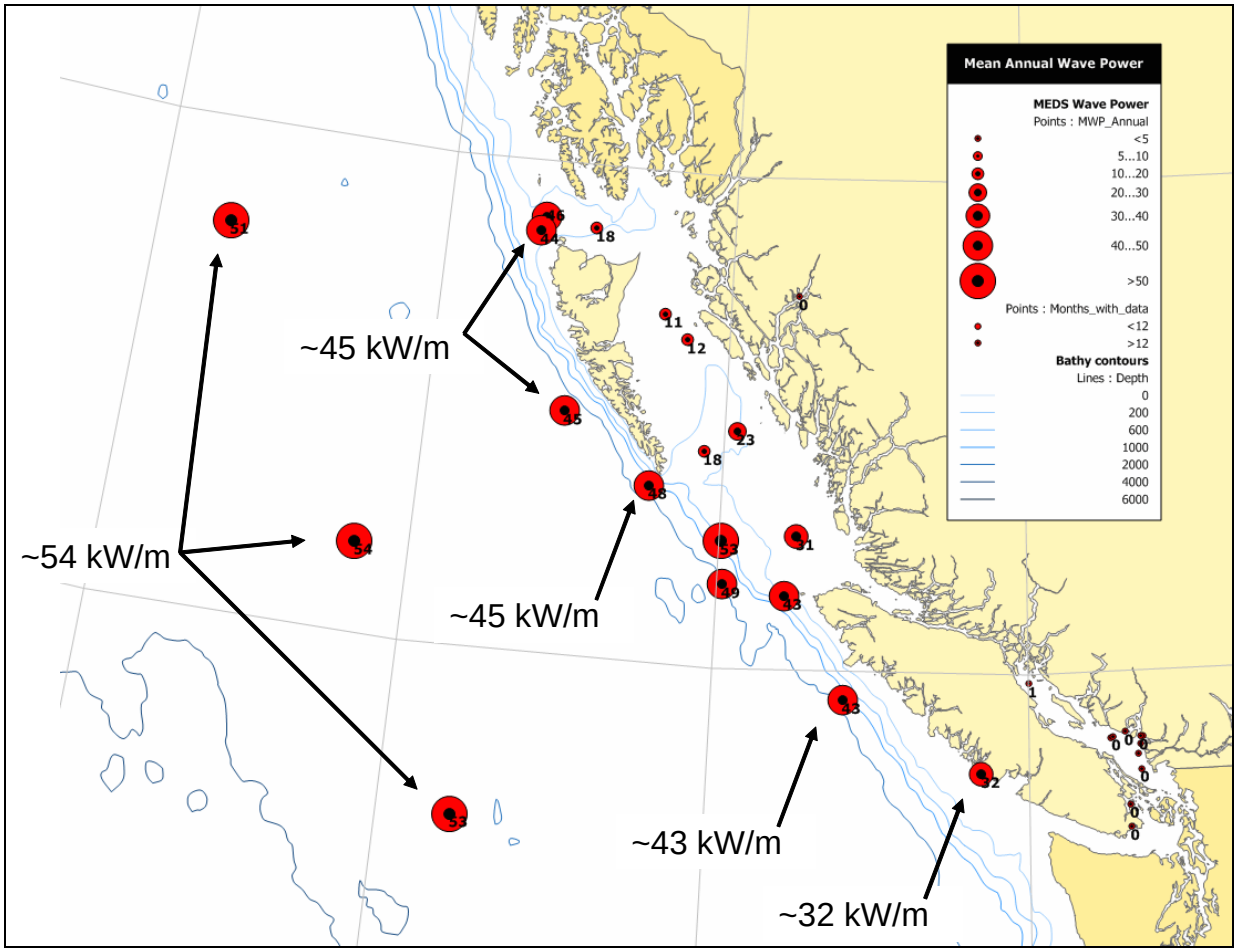


Figure 11. Annual mean wave power for sites in the NE Pacific.

These results indicate a strong seasonal variation in the wave energy available along both coasts. The monthly variation in mean wave power for nineteen stations in the Atlantic and eighteen stations in the Pacific are plotted in Figure 12 and Figure 13. In these figures, the monthly mean power for each station has been normalized by the annual mean power for that station, so that a value of 2 indicates a monthly mean power that is double the annual mean value. In the NW Atlantic (see Figure 12), the mean wave power in winter (December - February) is roughly four or five times larger than in summer (June - August). On the B.C coast (see Figure 13), the mean wave power in winter is approximately six or seven times greater than in summer.

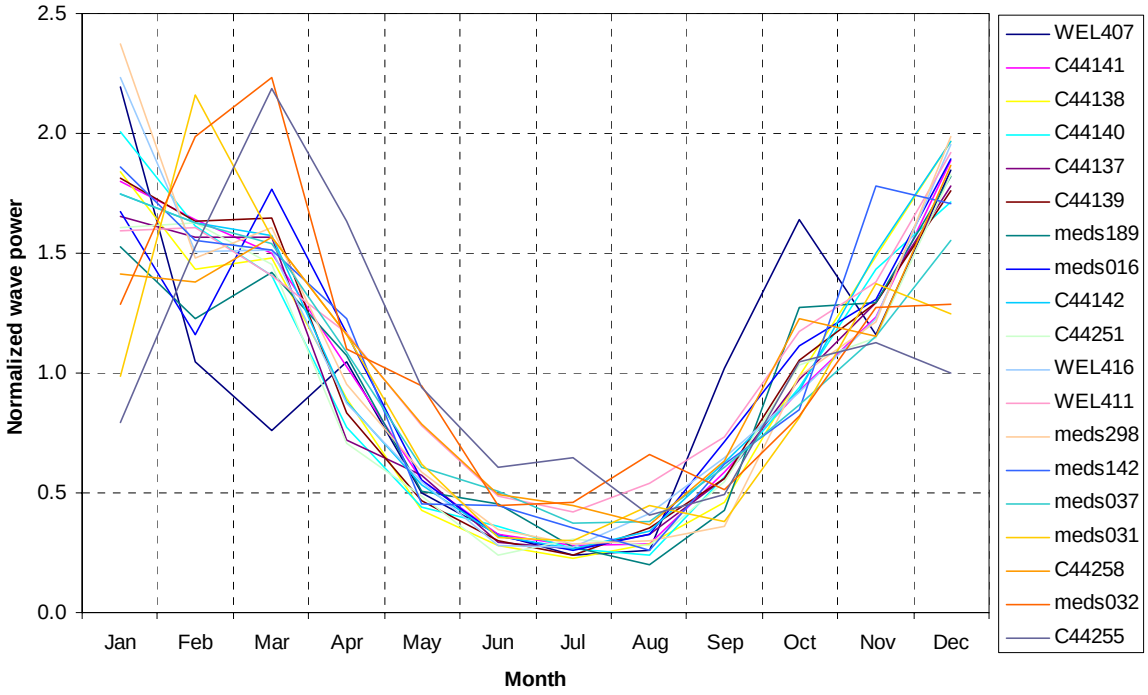


Figure 12. Seasonal variation in mean wave power for Atlantic stations.

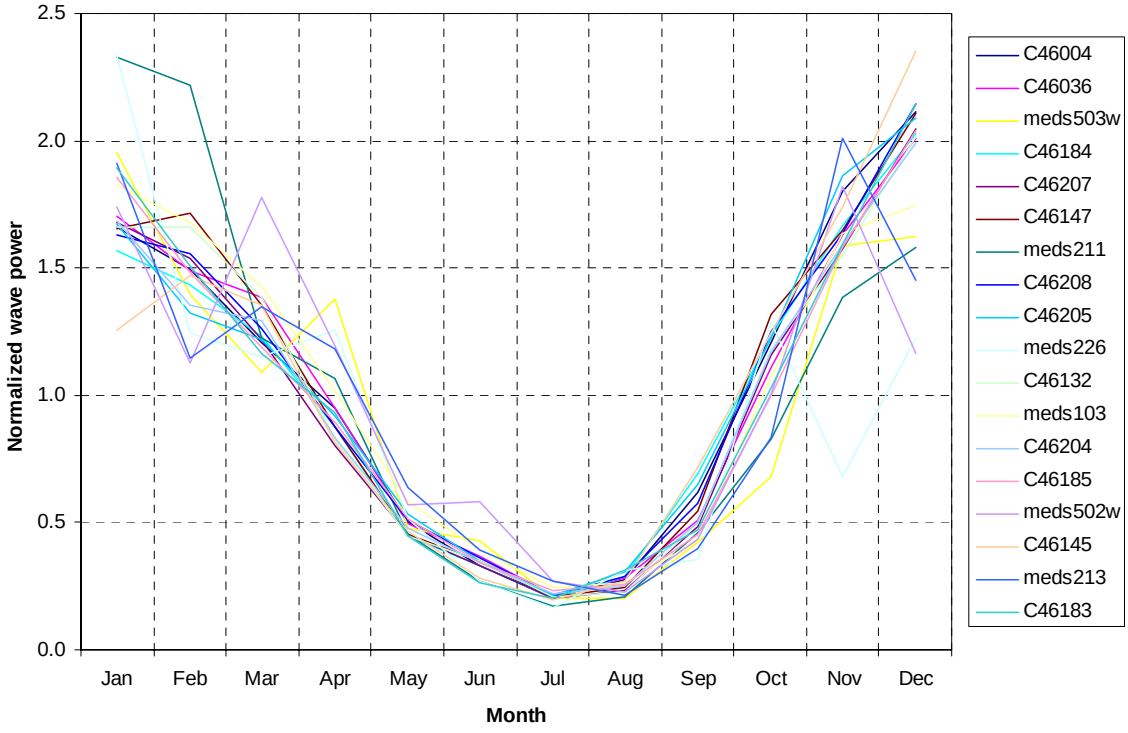


Figure 13. Seasonal variation in mean wave power for Pacific stations.

## *3.4. AES40 Wave Climatology*

The AES40 wind and wave climatology was developed by the firm Oceanweather Inc. for the Climate Research Branch of Environment Canada (Swail et al., 1998). The climatology was developed by applying the 3rd generation wave model OWI-3G to predict the wave fields in the North Atlantic over a continuous 40 year period, going back to 1958. (The hindcast period has since been extended to 50 years.) The historical wind fields used to drive the model were derived by synthesizing data from a number of sources, including wind fields developed by the NCEP-NCAR Reanalysis Project and a kinematic reanalysis of all major storms.

The AES40 wave hindcast was performed on a 0.625° by 0.833° grid containing 9,023 nodes spanning the North Atlantic between latitudes 0° and 75°N and longitudes 82°W to 20°E. This domain extends northwards past the northern tip of Baffin Island and includes all Canadian waters in the North Atlantic. The influence of ice cover was included using ice cover charts updated monthly. The 5/10 ice concentration contour was used to define the ice edge – points with ice concentrations greater than 5/10 were considered as land by the model.

The resulting wave climatology has been well validated and has been widely used in wave climate and engineering studies for the North Atlantic, particularly in the region offshore the east coast of Canada (Swail et al., 2000). The AES40 hindcast appears to provide a good description of the wave climate at exposed deep water sites. However, because the grid is relatively coarse and the wave model did not include shallow water effects, the model is not well suited to predicting wave climatology close to land or in smaller partially enclosed water bodies such as the Bay of Fundy, Northumberland Strait, the Strait of Belle Isle or the Gulf of St. Lawrence. Predictions for these areas should be approached with caution.

### 3.4.1. Analysis Methodology

AES40 hindcast results for all 9,032 grid points were obtained from MSC for a five year period between January 1997 and December 2001. Seventeen variables were available at each node, including:

- mean 10m wind speed and direction
- peak period, variance and vector mean direction of the total spectrum (including sea and swell)
- peak period, variance and vector mean direction of the primary part of the spectrum (the sea)
- peak period, variance and vector mean direction of the secondary part of the spectrum (the swell)

The first three years of data were computed at a 6-hour interval, while a 3-hour interval was used in the final two years. A 1,415-point subset of the original grid containing all nodes north of 38°N and west of -42°W was retained for analysis. The following derived variables were computed for all time steps at each node of the sub-grid.

- significant wave height for the sea, swell and total seastate,
- wave energy flux for the sea, swell and total seastate (equation (8) with $T_e=0.9T_p$),
- the mean wave period, and
- the wind power density.

Next, the five years of data were grouped to form datasets describing conditions annually and during each month (January to December) and season (winter, spring, summer and autumn). winter was defined from December to February, spring from March to May, summer from June to August, and autumn from September to November. Finally, for every combination of variable, month and season, a set of simple statistics was computed to describe conditions at every node in the sub-grid. These statistics included the minimum, maximum, mean, standard deviation and root-mean-square values, plus the values corresponding to cumulative probabilities of 10%, 25%, 50%, 75% and 90%.

### 3.4.2. Results

Figure 14 shows the mean annual wave power derived from the AES40 data. The contributions to annual mean wave power due to sea and swell are compared in Figure 15. It is interesting to note that roughly half of the annual wave energy along the exposed coasts or Newfoundland and Nova Scotia is due to swells arriving from distant storms. The mean wave power in winter (December - February), spring (March – May), summer (June – August) and autumn (September – November) are compared in Figure 16.

The probability distribution of energy flux (wave power) at the node nearest to MEDS station C44140 for the months of January, April, July, and October are compared in Figure 17. In January the energy flux varies between 10 and 500 kW/m, while the energy flux during July varies between 2 and 60 kW/m. The median energy fluxes (the value exceeded 50% of the time) in January and July are 55 and 9 kW/m, respectively

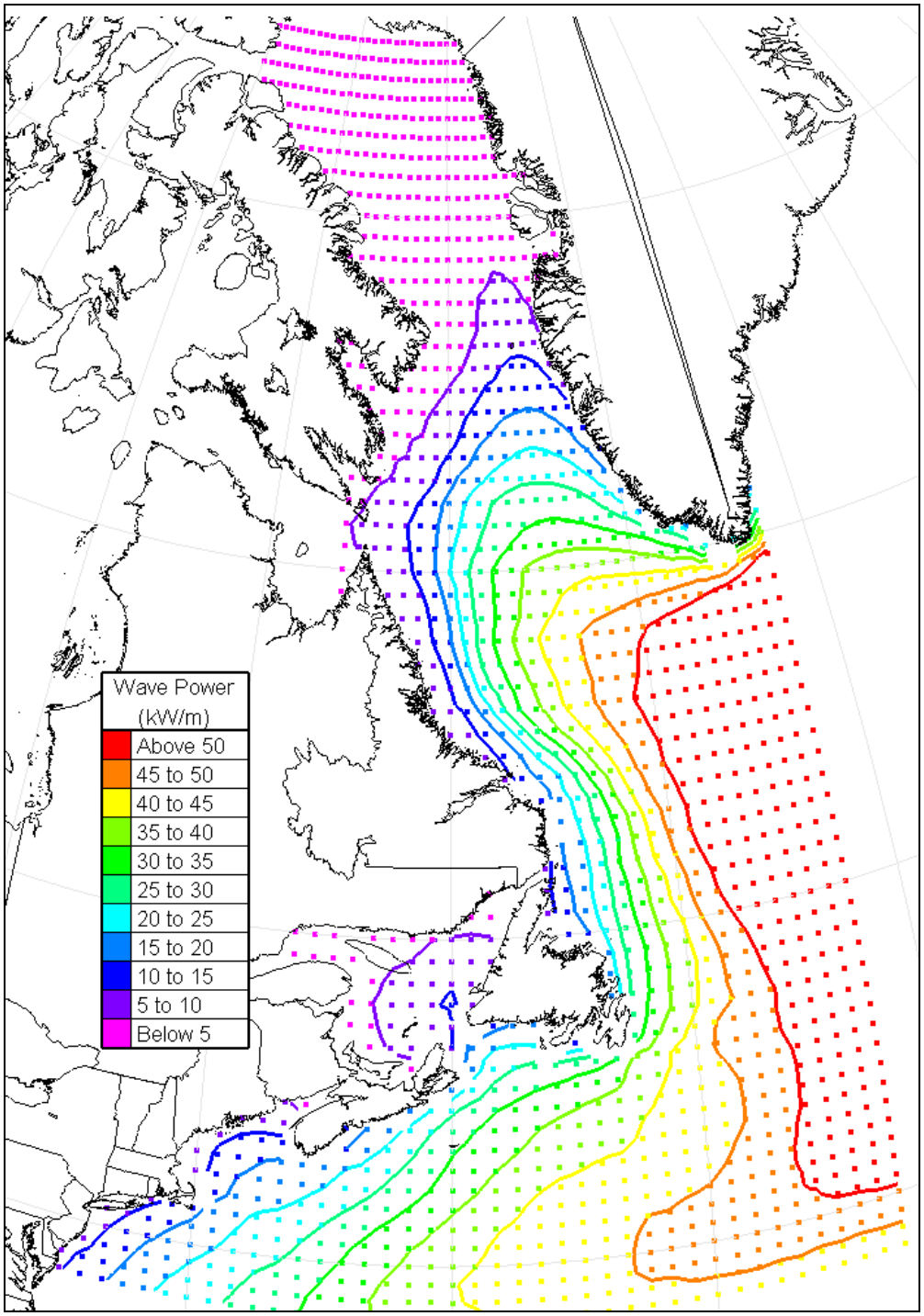


Figure 14. Mean annual wave power derived from AES40 hindcast data. (Points denote AES40 nodes.)

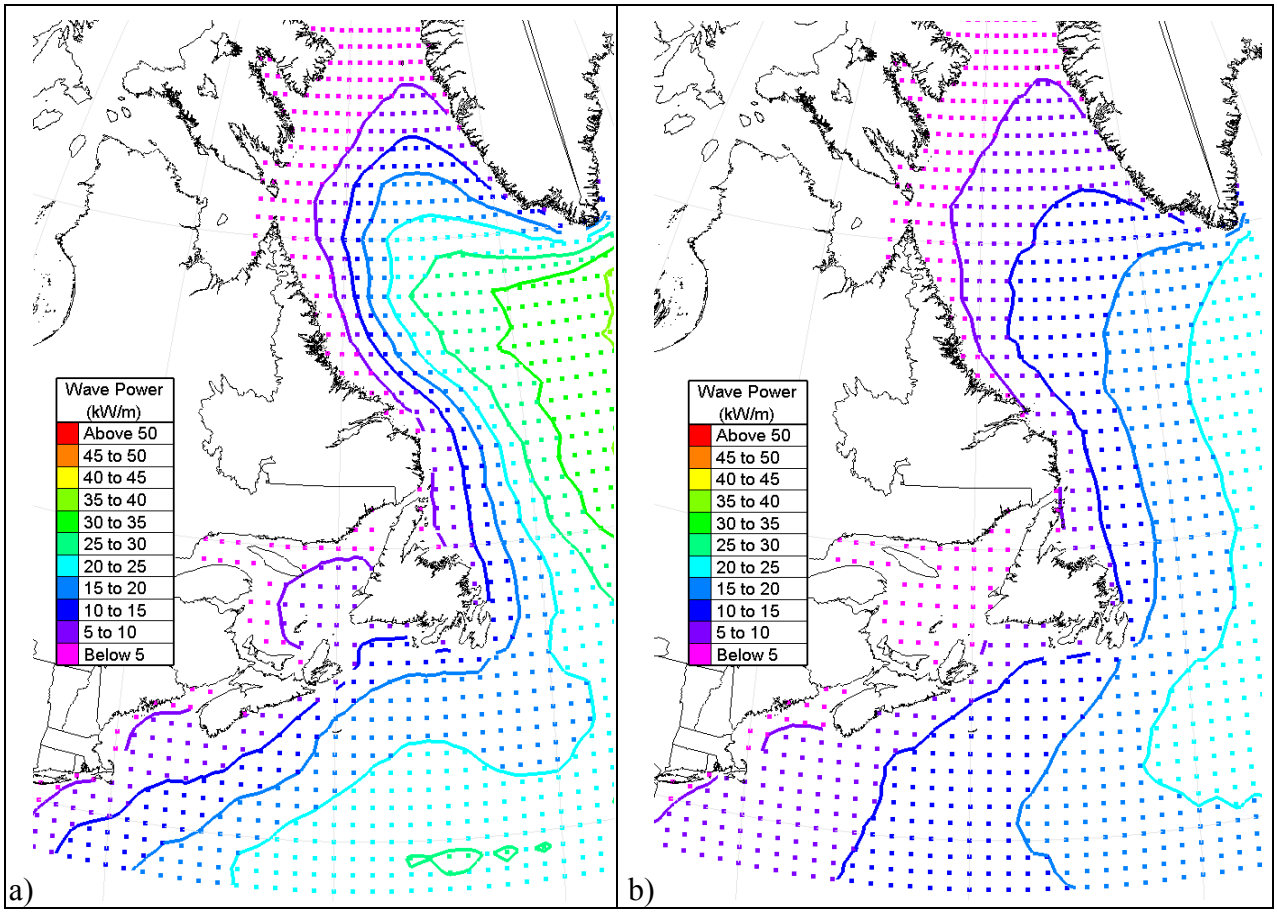


Figure 15. Contribution to mean annual wave power in the NW Atlantic due to a) sea and b) swell. (Points denote AES40 nodes.)

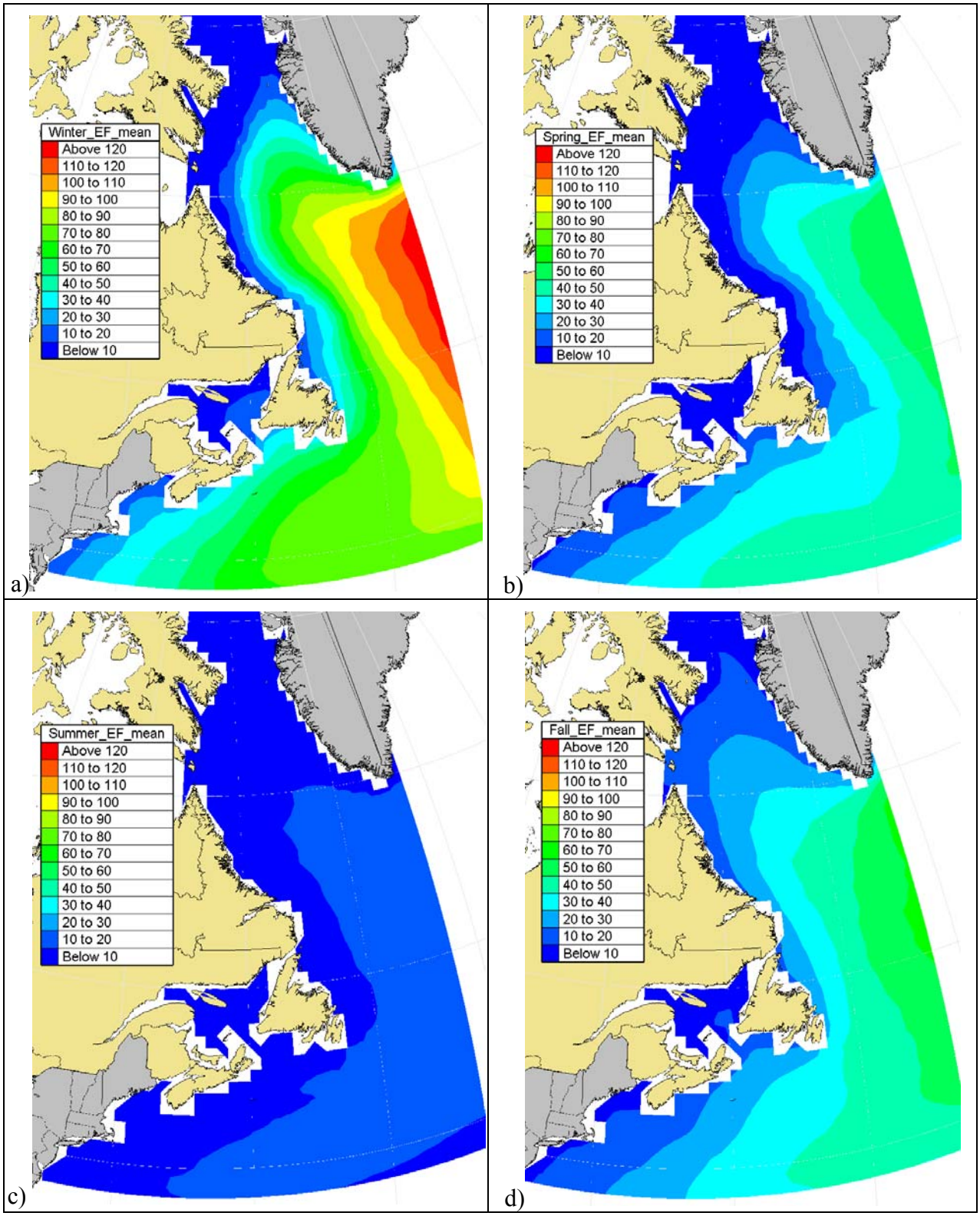


Figure 16. Mean wave power in the NW Atlantic during a) winter; b) spring; c) summer; and d) autumn; from AES40 data.

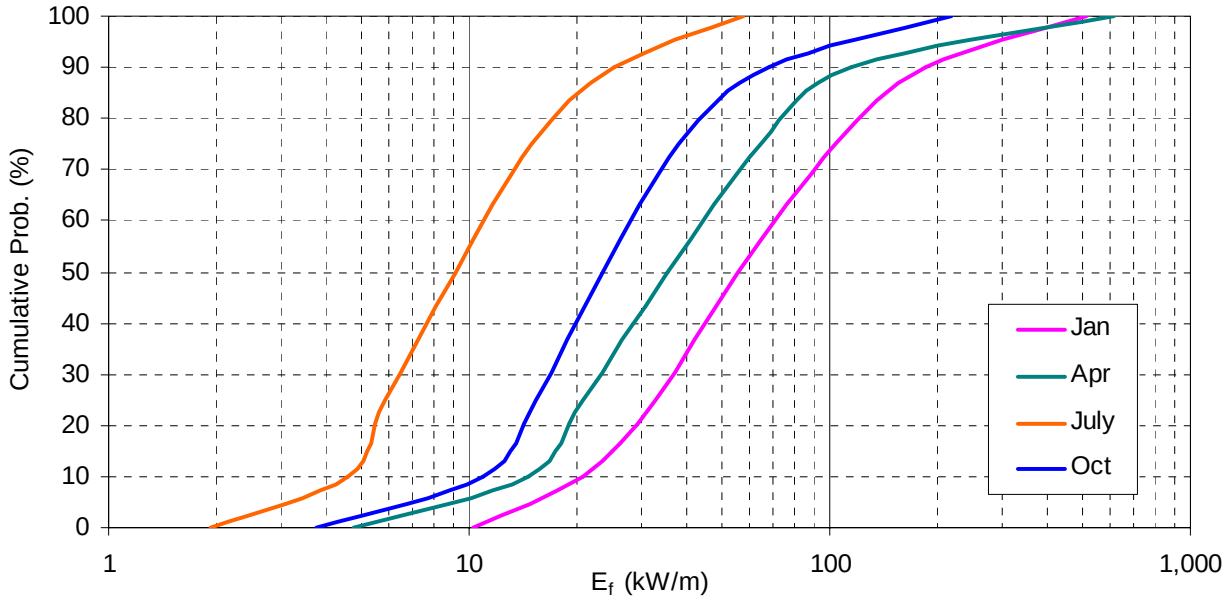


Figure 17. Monthly cumulative probability of wave energy flux near MEDS station C44140, from AES40 data.

## *3.5. WAVEWATCH III Hindcasts*

The Marine Modeling and Analysis Branch (MMAB) of the U.S. National Oceanic and Atmospheric Administration (NOAA) performs continuous operational forecasts of the ocean wave climate around the globe. The wave predictions are performed using a sophisticated third generation spectral wind-wave model known as WAVEWATCH III or WW3 (Tolman, 2002). The wind fields used to drive the model are obtained from operational products prepared by the U.S. National Centers for Environmental Prediction (NCEP).

WW3 solves the spectral action density balance equation for wave number-direction spectra. The implicit assumption of this equation is that properties of the medium (water depth and current) as well as the wave field itself vary on time and space scales that are much larger than the variation scales of a single wave. A further constraint is that the parameterizations of physical processes included in the model do not address conditions where the waves are strongly depth-limited. These two basic assumptions imply that the model can generally be applied on spatial scales (grid increments) larger than 1 to 10 km, and outside the surf zone.

The WW3 model has been validated by comparison with data from buoys and satellites. Results of this validation can be viewed at http://polar.ncep.noaa.gov/waves/validation.

The MMAB has implemented the WW3 model on several different regular grids, spanning various ocean basins. Results from two of these grids, namely the Eastern North Pacific (ENP) and the Western North Atlantic (WNA), can be used to describe the wave climate and the wave energy resource along Canada's Pacific and Atlantic coasts. The ENP grid features a 0.25° by 0.25° resolution and contains over 81,000 nodes spanning the region between latitudes 5°N to 60.25°N and longitudes 170°W to 77.5°W. The WNA grid has a 0.25° by 0.25° resolution and

contains over 54,000 nodes spanning the region between latitudes 0°N to 50°N and longitudes 98°W to 30°W. The ENP grid covers all Canadian waters in the Pacific Ocean, but the WNA grid covers only the southern portion of Canadian waters in the Atlantic. Due to their finer resolution, these grids provide a more realistic representation of land boundaries and smaller water bodies. For this reason, and because shallow water effects are included in the WW3 model, the WW3-ENP and WW3-WNA models may be better suited to predicting wave climate close to shore and in smaller partially enclosed water bodies such as the Bay of Fundy. However, as discussed by Pontes (2003), shallow-water wave transformation models and high resolution grids must be used to provide reliable estimates of wave power in coastal waters. Such models are routinely used to provide detailed estimates of nearshore wave climates for coastal engineering studies.

In addition to operational forecasting, the suite of WW3 models have been applied, using archived wind fields and ice cover charts, to hindcast historical wave fields at 3-hour intervals over several years. The model results (hindcasts and forecasts) are freely available via the internet as binary files in GRIB format. The hindcast WW3 model results are being used for engineering studies of wave climate around the globe.

### 3.5.1. Analysis Methodology

Data files in binary GRIB format containing results from the WW3-ENP hindcast for a three year period between October 2002 and September 2005 were obtained from the MMAB ftp server. These files contained results for the following variables computed at 3 hour intervals for all nodes:

- significant wave height of combined wind waves and swell, $H_s$
- peak wave period, $T_p$
- primary wave direction, and
- u and v components of the mean 10m wind.

A sub-grid containing 676 nodes focused on Canada's Pacific coast was defined to reduce the computational effort. The sub-grid extended from latitude 42°N to 59°N and from longitude -145°W to -124°W, and featured a 0.25° resolution close to the coast and a 1° resolution in the open ocean.

The following derived variables were computed for all times at each node of the sub-grid:

- the wave energy flux (equation (8) with $T_e=0.9T_p$),
- the wind speed; and
- the wind power density.

The post-processing of these given and derived variables was similar to the methods applied to analyse the AES40 data, described earlier. The results were grouped into datasets describing annual, seasonal and monthly conditions, and simple statistical quantities were computed to characterize the temporal variations at each node during these periods.

The processing and analysis of data from the WW3-WNA hindcast was very similar to the methodology described above; however, in this case, data files were obtained containing results at 3-hour intervals for a five year period, beginning in October 2000. Another sub-grid with variable resolution – 0.25° close to the coast and 1° in the open ocean – was defined between latitude 38°N and 50°N and longitude -75°W to -43°W. As before, the results were grouped into datasets describing annual, seasonal and monthly conditions, and simple statistical quantities were computed to characterize the temporal variations at each node.

### 3.5.2. Results

The mean annual wave power computed from the WW3-ENP data is plotted in Figure 18. The mean wave power in winter and summer are compared in Figure 19.

Figure 20 shows the mean annual wave power computed from the WW3-WNA data. The mean wave power in summer and winter are compared in Figure 21.

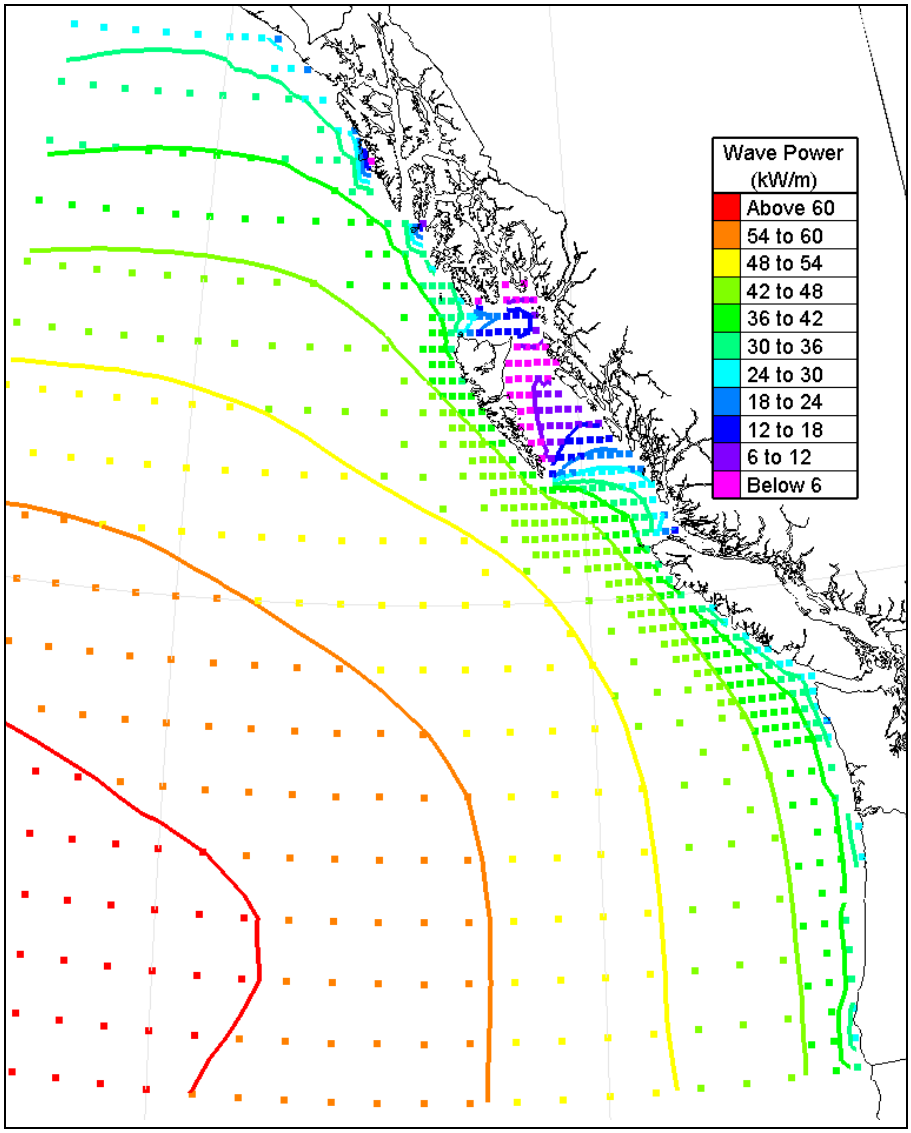


Figure 18. Mean annual wave power in the NE Pacific derived from WW3-ENP hindcast data. (points denote sub-grid nodes.)

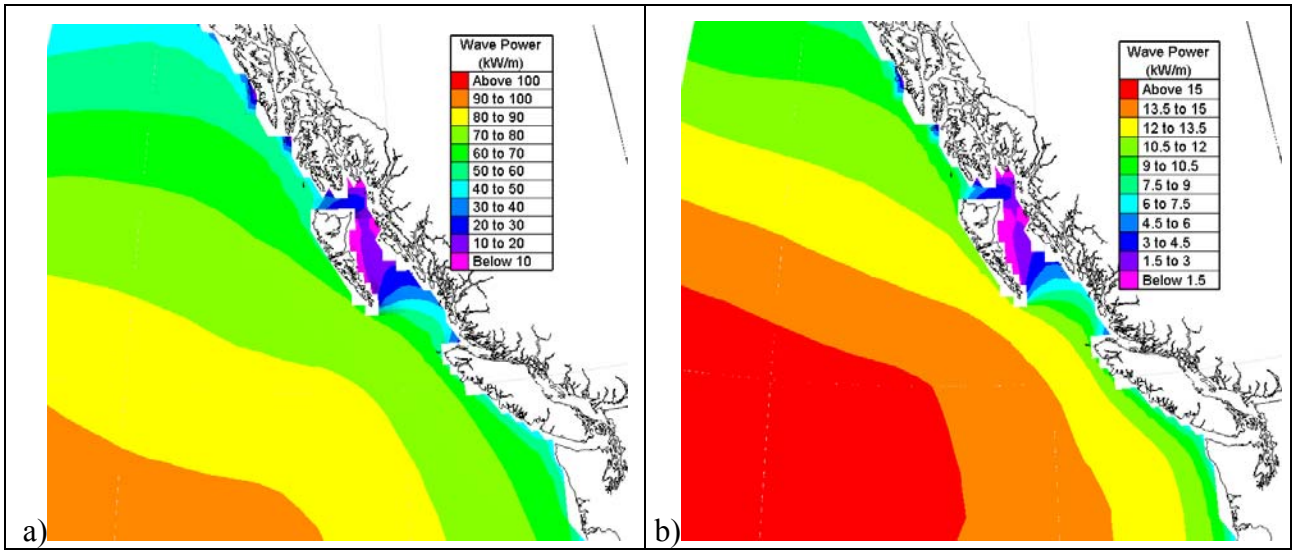


Figure 19. Mean wave power in the NE Pacific during a) winter and b) summer, from WW3-ENP data. (Note that different colour scales are used.)

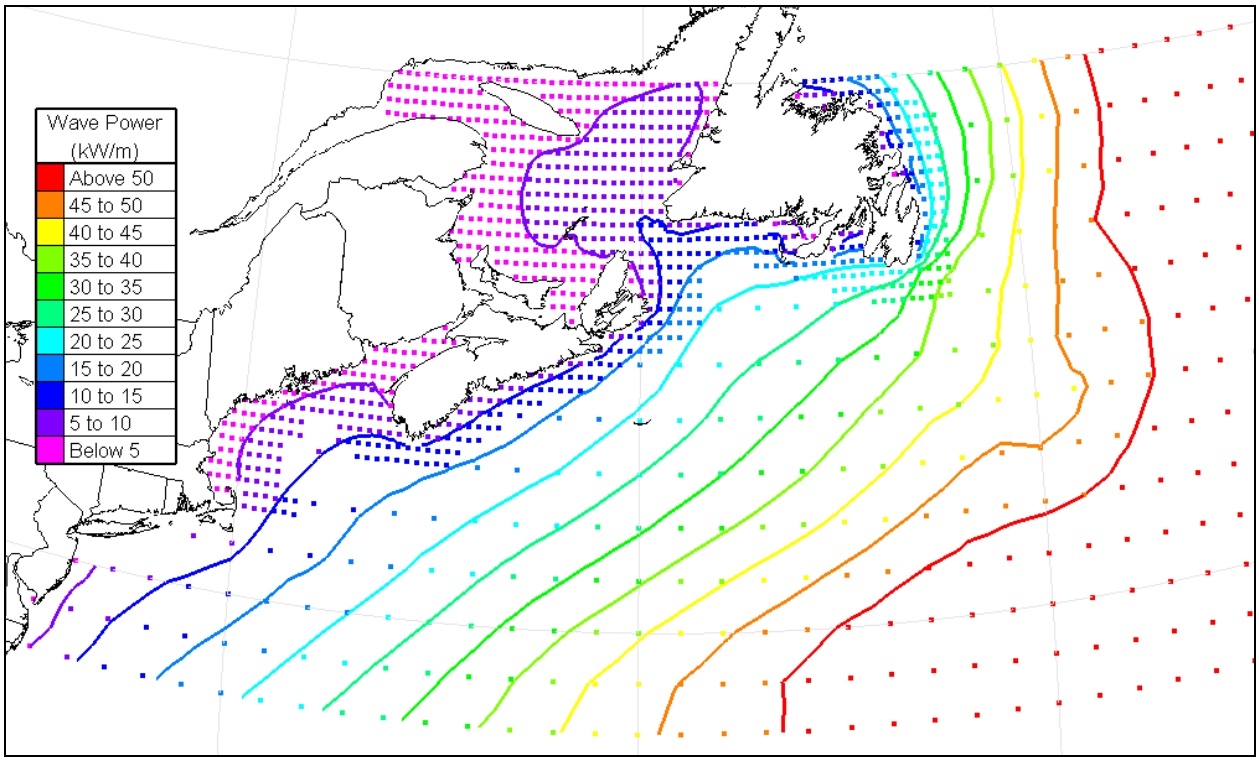


Figure 20. Mean annual wave power in the NW Atlantic derived from WW3-WNA hindcast data. (Points denote sub-grid nodes.)

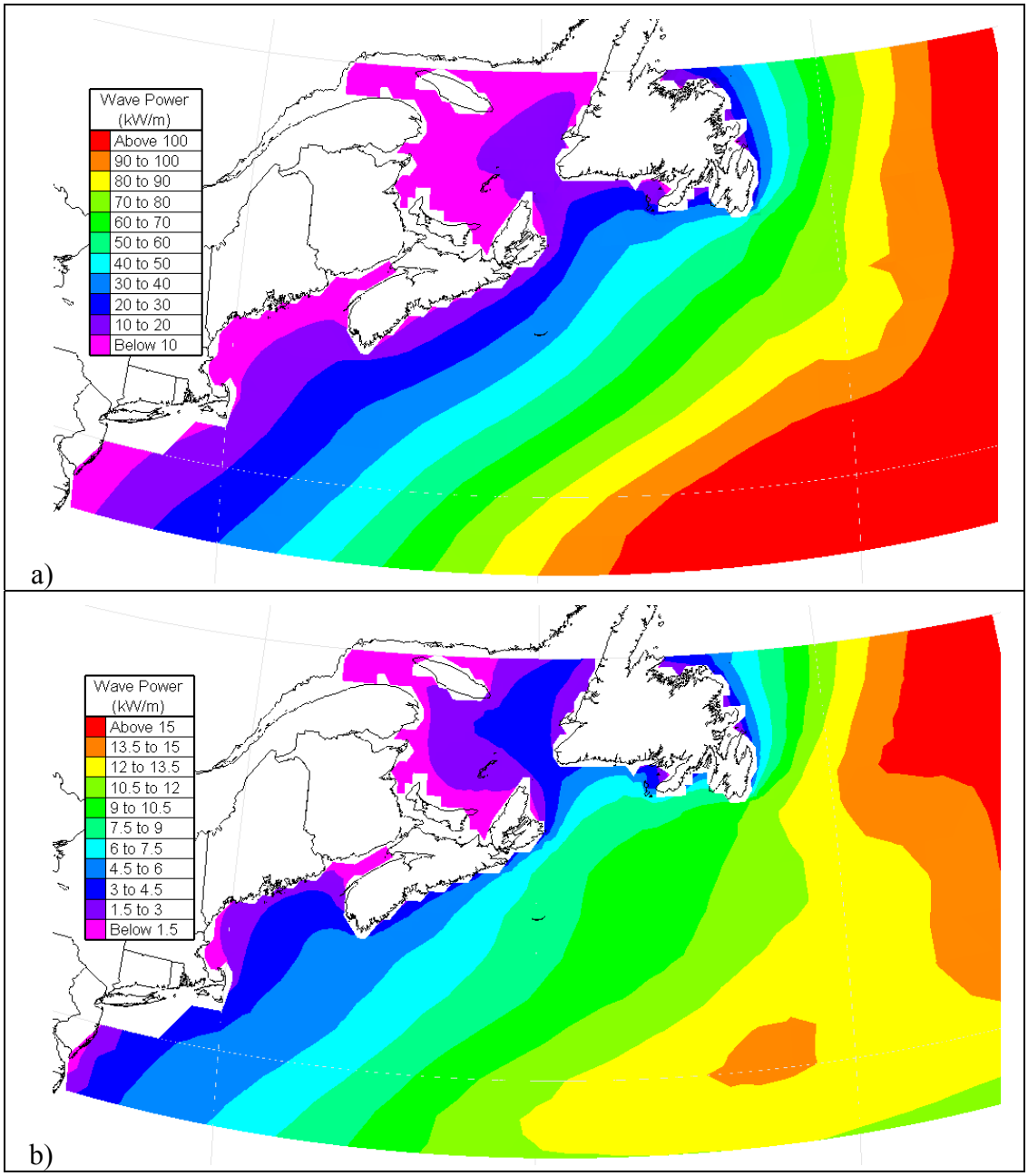


Figure 21. Mean wave power in the NW Atlantic during a) winter and b) summer, from WW3-NWA data. (Note that different colour scales are used.)

## *3.6. Inter-Comparison of Results*

Some confidence in the derived wave power predictions can be gained by comparing results obtained from different data sets. The estimates of mean annual wave power obtained from analysis of the AES40 and WW3-WNA hindcasts are compared graphically in Figure 22. Interestingly, the most noticeable difference is in the southeast part of the overlapping domain, far from land and beyond the continental shelf, where the mean annual wave power estimate

derived from the WW3-WNA data exceeds the estimate derived from the AES40 data by as much as 10 kW/m. However, over most of the continental shelf, including the Scotian Shelf and the Grand Banks, the two estimates agree within a tolerance of 5 kW/m or better. Some of this discrepancy may relate to differences in the methodologies applied in generating the wave hindcasts, while some of it may be due to the fact that two different five year periods were considered in the analysis.

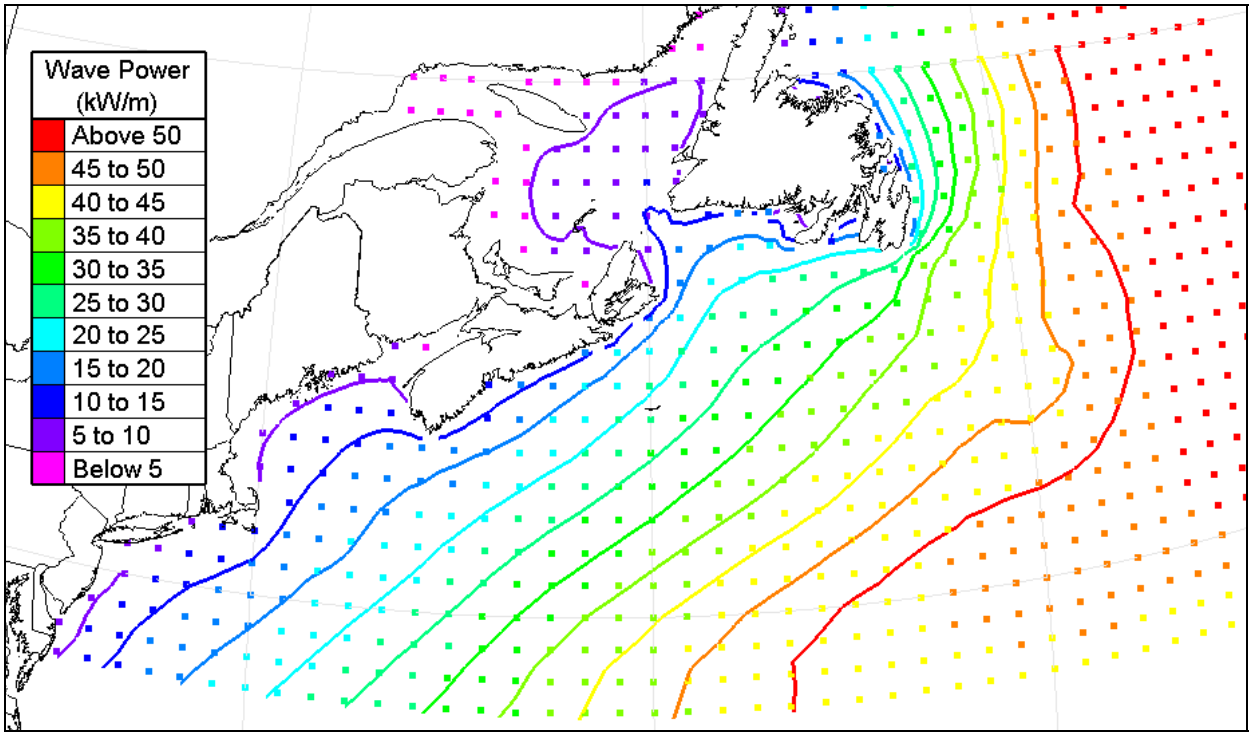


Figure 22. Mean annual wave power derived from AES40 data (points) and WW3-WNA data (isolines).

Figure 23 shows a comparison between the mean monthly wave power estimates derived from analysis of buoy measurements and from the AES40 and WW3-WNA wave hindcasts for MEDS station C44140, located on the southern edge of the Grand Banks at latitude 42.7°N, longitude -50.6°W. Figure 23 also provides a typical illustration of the strong seasonal variation of the wave energy resource in the northwest Atlantic, where the wave energy in summer (June to August) is typically only one-third of the annual resource. In this case, the seasonal trends in wave energy derived from the measured and hindcast wave data show overall good agreement. Some of the small divergence could be due to the fact that the measured and hindcast wave data were not exactly co-located and did not span the same period.

Similar comparisons for some other Atlantic stations are presented in Figure 24 - Figure 30. In general, the agreement is good at offshore stations with lengthy records, but the agreement at nearshore stations is sometimes less satisfactory. This suggests that the AES40 and WW3-WNA hindcasts are reasonably accurate offshore, but less reliable in nearshore regions. It is noted that

the gradient in wave energy can be very large close to shore, so that small differences in location can lead to sizeable differences in energy.

Figure 31 shows a similar comparison of mean monthly wave power estimates derived from measured wave data and the WW3-ENP hindcast for MEDS station C46208, located off the western shore of the Queen Charlotte Islands at latitude 52.5°N, longitude -132.7°W. Again, the energy levels and the seasonal trends in wave energy derived from the measured and hindcast wave data show good agreement.

Similar comparisons for some other Pacific stations are presented in Figure 32 - Figure 40.

In general, the agreement is satisfactory for offshore stations with lengthy records. This suggests that the WW3-ENP hindcast is reasonably accurate offshore and suggests that a three-year simulation is sufficient to capture the main features of the wave climate in this region. As in the Atlantic, the agreement is less satisfactory at nearshore stations where the spatial gradient in wave climate is large, and the WWW-ENP hindcast is less precise.

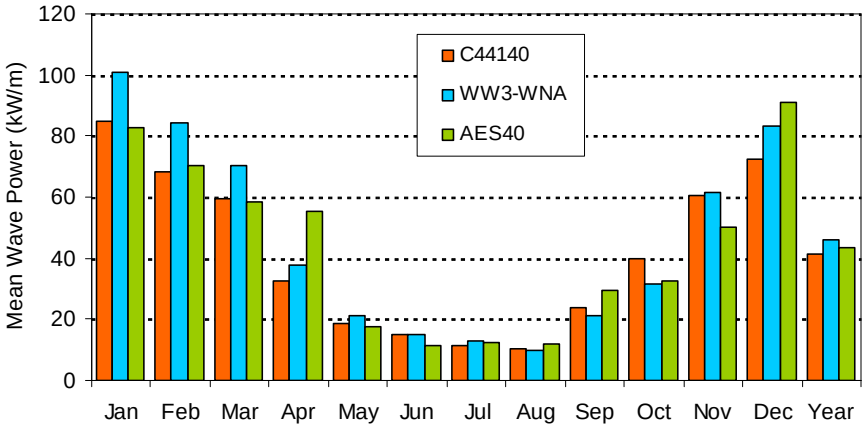


Figure 23. Comparison of mean monthly wave power from buoy measurements and wave hindcasts, station C44140.

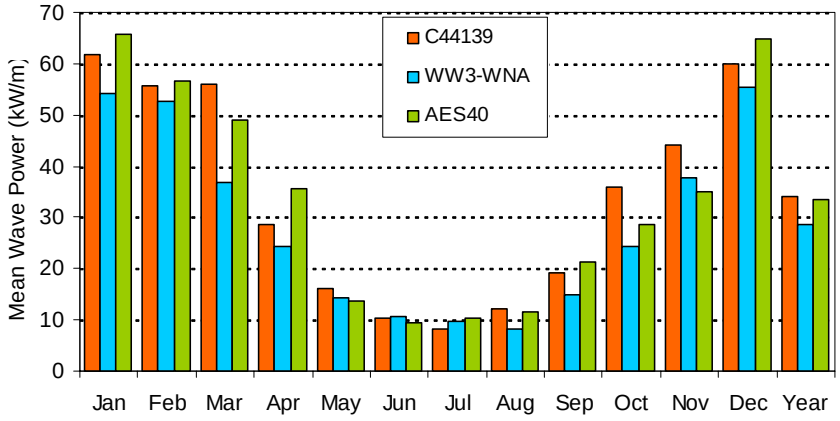


Figure 24. Comparison of mean monthly wave power from buoy measurements and wave hindcasts, station C44139.

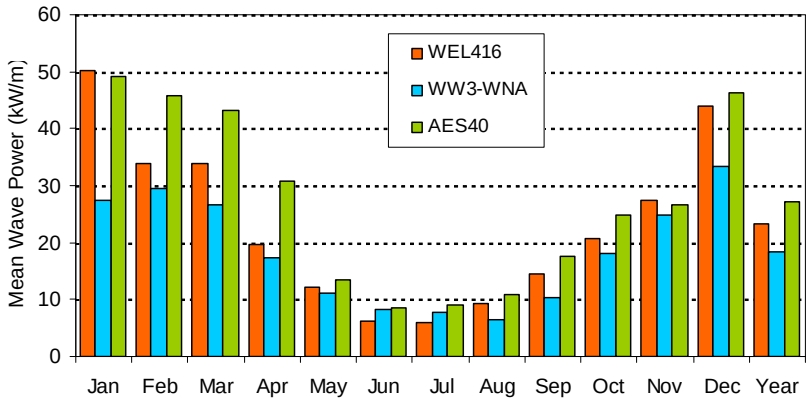


Figure 25. Comparison of mean monthly wave power from buoy measurements and wave hindcasts, station wel416.

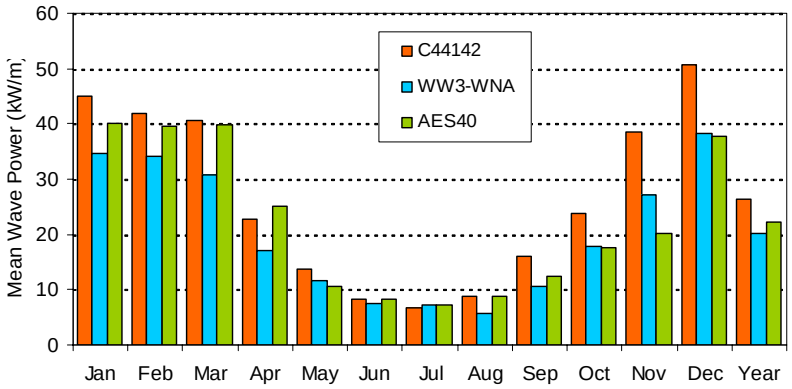


Figure 26. Comparison of mean monthly wave power from buoy measurements and wave hindcasts, station C44142.

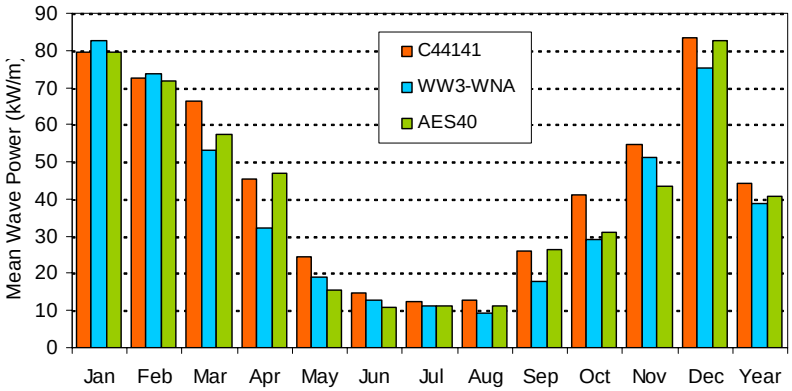


Figure 27. Comparison of mean monthly wave power from buoy measurements and wave hindcasts, station C44141.

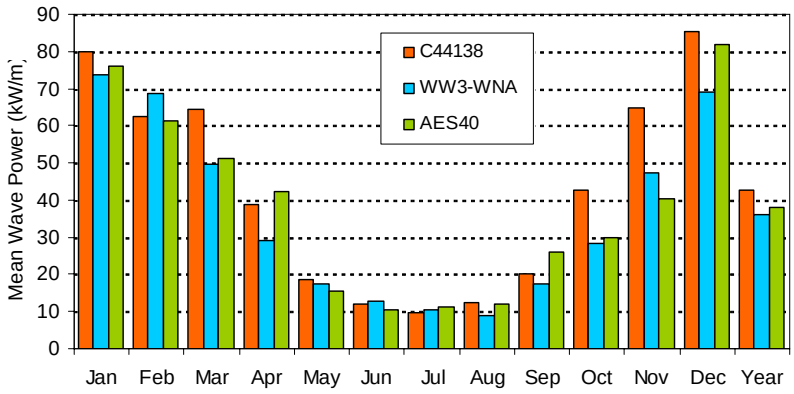


Figure 28. Comparison of mean monthly wave power from buoy measurements and wave hindcasts, station C44138.

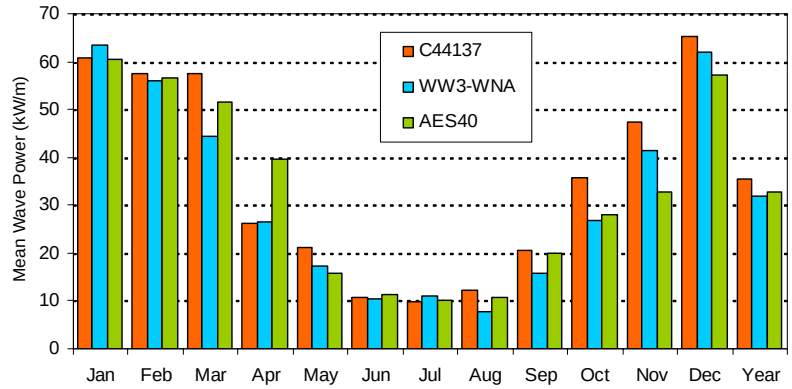


Figure 29. Comparison of mean monthly wave power from buoy measurements and wave hindcasts, station C44137.

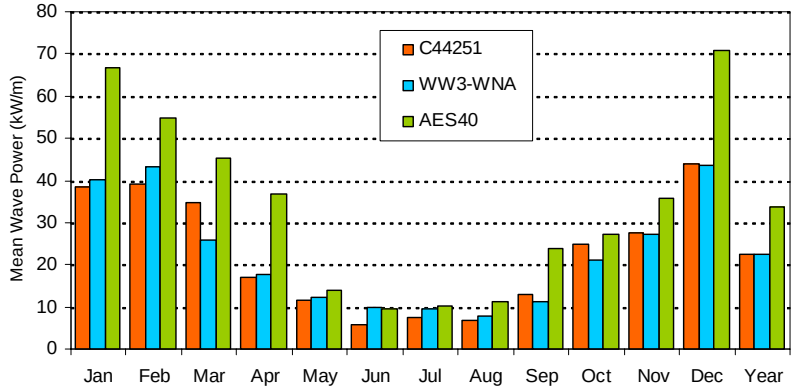


Figure 30. Comparison of mean monthly wave power from buoy measurements and wave hindcasts, station C44251.

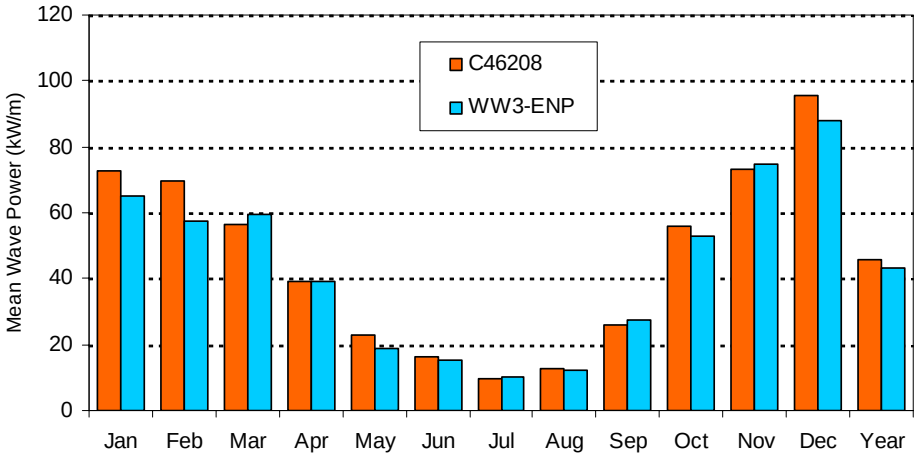


Figure 31. Comparison of mean monthly wave power from buoy measurements and WW3-ENP hindcast, station C46208.

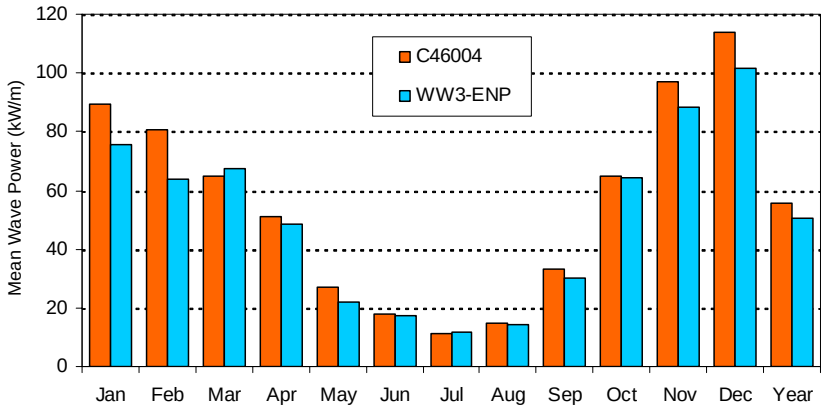


Figure 32. Comparison of mean monthly wave power from buoy measurements and WW3-ENP hindcast, station C46004.

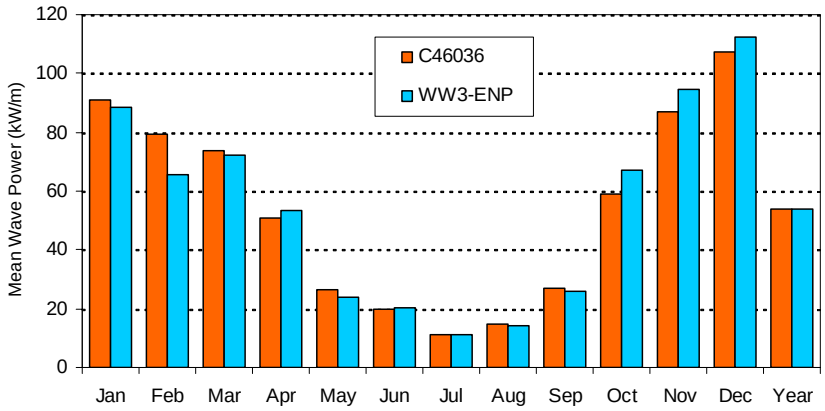


Figure 33. Comparison of mean monthly wave power from buoy measurements and WW3-ENP hindcast, station C46036.

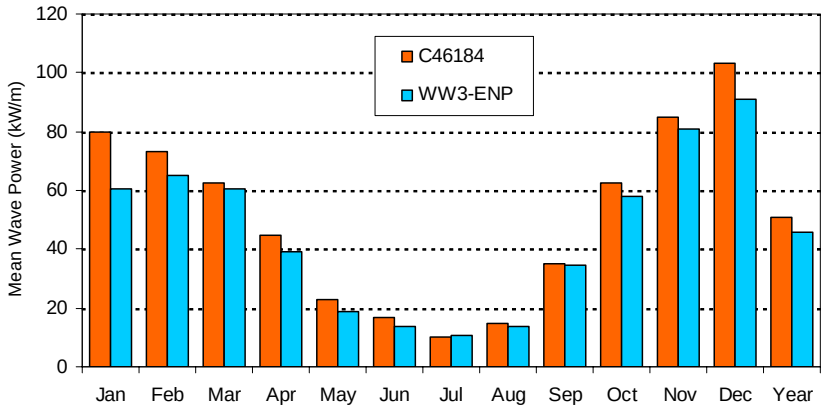


Figure 34. Comparison of mean monthly wave power from buoy measurements and WW3-ENP hindcast, station C46184.

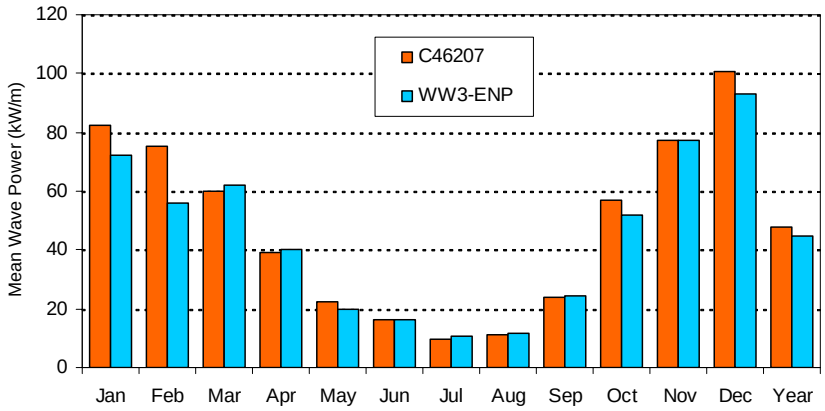


Figure 35. Comparison of mean monthly wave power from buoy measurements and WW3-ENP hindcast, station C46207.

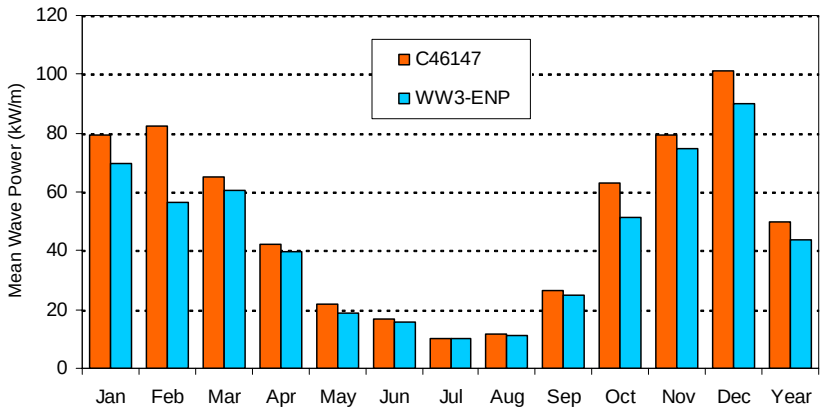


Figure 36. Comparison of mean monthly wave power from buoy measurements and WW3-ENP hindcast, station C46147.

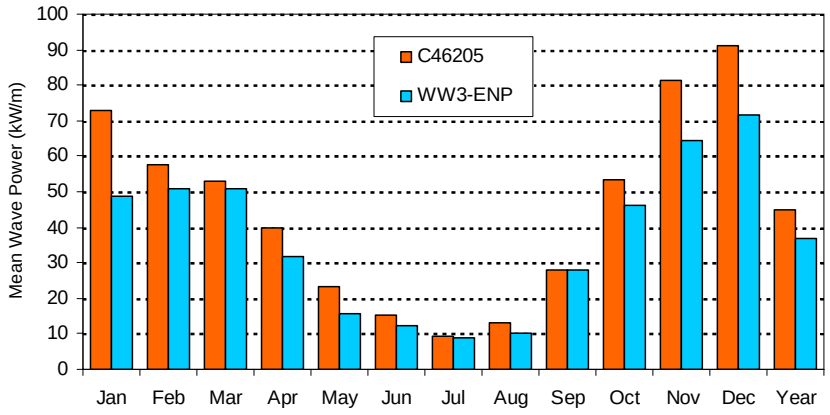


Figure 37. Comparison of mean monthly wave power from buoy measurements and WW3-ENP hindcast, station C46205.

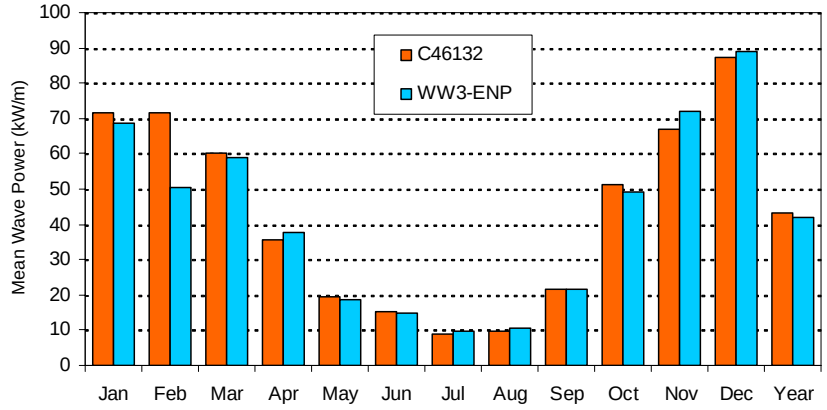


Figure 38. Comparison of mean monthly wave power from buoy measurements and WW3-ENP hindcast, station C46132.

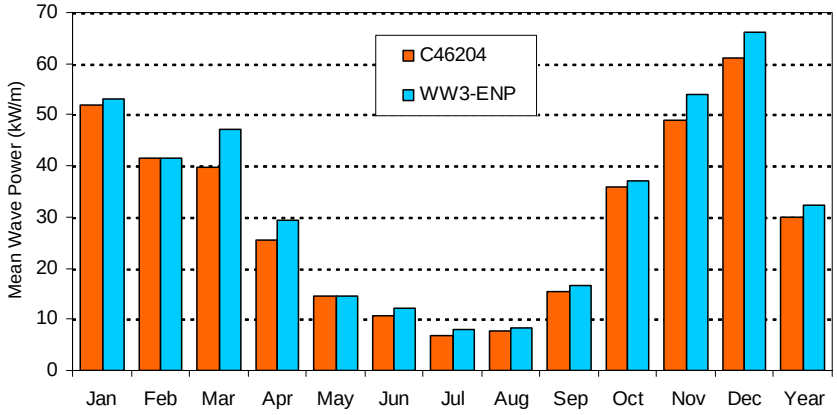


Figure 39. Comparison of mean monthly wave power from buoy measurements and WW3-ENP hindcast, station C46204.

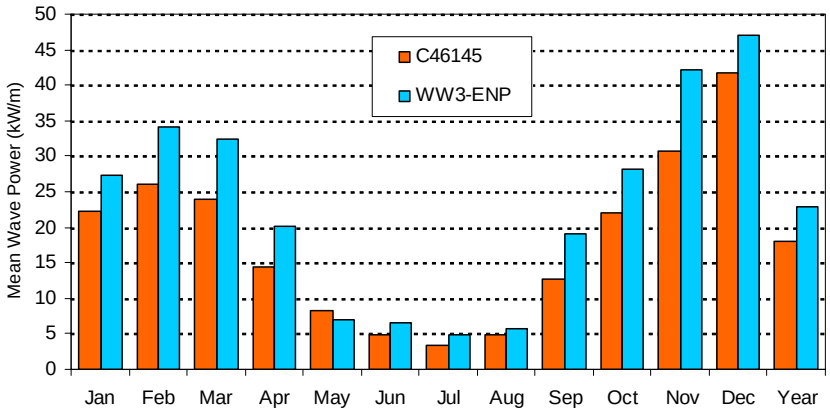


Figure 40. Comparison of mean monthly wave power from buoy measurements and WW3-ENP hindcast, station C46145.

## *3.7. Discussion of Results*

Canadian electricity demand now totals roughly 580 TWh per year, or roughly 18 MWh annually per person. This is equivalent to a mean power of 66,165 MW or roughly 2 kW/person. The three leading electricity demand sectors are manufacturing (38%) residential (28%) and commercial and institutional (22%). Assuming that only 10% of the available wave power is converted into electrical energy, a 1 km wide site with a mean annual power of 25 kW per meter of wave crest could potentially generate 21.9 GWh per year, enough to supply the residential electrical needs of over 4,300 typical Canadians.

Wave energy resources in the NE Pacific are largest in the open ocean far from shore, and decrease as you cross the continental shelf and approach land. The annual mean wave energy flux for exposed deep-water sites located 100 km off Canada's Pacific coast is on the order of 40 to 45 kW/m. Approaching Vancouver Island from the west along the 49°N parallel, the mean annual wave power decreases from ~43 kW/m 150 km offshore, to ~39 kW/m 75 km offshore, to ~25 kW/m at the coast. Moving east along the 53°N parallel, the mean annual wave power decreases from ~44 kW/m 100 km offshore to ~36 kW/m at the western shore of the Queen Charlotte Islands. Wave energy resources in the northeast Pacific also feature a strong seasonal variability – the mean wave energy flux in winter (December to Februrary) is typically around six to eight times larger than in summer (June to August).

Meanwhile, the annual mean wave power at exposed deep-water sites near the edge of the continental shelf in the northwest Atlantic varies from around 21 kW/m off southern Nova Scotia to around 50 kW/m on the edge of the Grand Banks east of Newfoundland. The continental shelf in the northwest Atlantic is much wider than in the northeast Pacific, and there is generally more attenuation of wave energy across the shelf, so that the wave energy resources close to shore are often significantly smaller than at the shelf edge. For example, on a line projected across the Scotian Shelf southeast from Halifax, the mean annual wave energy increases from ~9 kW/m at the coast, to ~20 kW/m roughly 200 km offshore, and to ~30 kW/m roughly 400 km offshore. Wave energy resources in the northwest Atlantic also feature a strong seasonal variability – the mean wave energy flux in summer is typically around one-third of the annual value. In eastern

Canada, the richest wave energy resources close to land lie near the southeastern tip of Newfoundland and around Sable Island. The mean annual wave power in these nearshore regions is on the order of 25 kW/m.

By comparison, the mean annual wave energy at exposed deep-water locations off the western coast of Europe varies between ~25 kW/m near the Canary Islands, up to ~75 kW/m off Ireland and Scotland (Pontes, 1998). The European resource is also seasonally variable: the mean wave power in summer is typically between 25% to 50% of the annual value. The European resource also decreases as you approach shore. For example, Pontes et al. (2003) reports that the nearshore wave energy resource along the coast of Portugal varies between ~8 kW/m and ~25 kW/m, while the offshore resource is on the order of 39 kW/m.

The new results presented here are generally consistent with recent analyses of wave energy resources along the Atlantic and Pacific coasts of the U.S. performed by the Electrical Power Research Institute (EPRI, 2005). The EPRI studies indicate that the mean annual wave power at exposed deep-water sites off the coasts of Washington State and Maine are about 40 kW/m, and 25 kW/m, respectively.

The total mean annual wave power off Canada's Atlantic and Pacific coasts has been estimated by integrating the power density along the 1,000m isobath and along the outer edge of the 200-mile fishing zone. The results, summarized in Table 8, show that the mean wave power along the 1,000 m isobath off Canada's Pacific coast totals roughly 37,000 MW or over 55% of Canadian electricity consumption, while the mean waver power along the 1,000 m isobath off Canada's Atlantic coast sums to 146,500 MW, or more than double current electricity demand.

The waters off Canada's Pacific and Atlantic coasts are endowed with rich wave energy resources. The results presented here define the scale of these resources, as well as their significant spatial and seasonal variations. It is important to recognize that due to various factors including environmental considerations and losses associated with power conversion, only a fraction of the available wave energy resource can be extracted and converted into useful power. Even so, the Canadian resources are considered sufficient to justify further research into their development as an important source of renewable energy for the future.

This work has aimed to quantify and map Canadian offshore wave energy resources. As noted previously, the wave power along a coast (above the ~150 m depth contour) can vary considerably due to sheltering and bathymetric effects such as wave shoaling, refraction and diffraction. These processes will create pronounced local variations in wave conditions and energy potential close to shore, particularly in regions with complex bathymetry. Clearly, these important local variations are beyond the scope of the present analysis.

Further work is clearly required to improve the definition of Canada's nearshore wave energy resources. Shallow water wave transformation models can be applied to study and quantify nearshore wave conditions provided that the necessary high-resolution bathymetry data is available. A logical next step is to apply such models to extend the present results into selected nearshore regions. Further work is also planned to consider the directionality of the Canadian wave energy resources described herein, and to assess the implications of directionality on resource assessment and energy extraction.

| Line of integration | from latitude deg | to Latitude deg | Length km | Mean annual wave power MW | Mean annual power density kW/m |
|---|---|---|---|---|---|
| Pacific Ocean | | | | | |
| 200 mile limit | 46.54 | 53.49 | 1,070 | 54,300 | 50.7 |
| 1,000m isobath | 48.13 | 54.31 | 915 | 37,000 | 40.4 |
| Atlantic Ocean | | | | | |
| 200 mile limit | 40.0 | 45.0 | 1,660 | 62,667 | 37.8 |
| 200 mile limit | 45.0 | 50.0 | 590 | 27,616 | 46.8 |
| 200 mile limit | 50.0 | 55.0 | 600 | 29,079 | 48.5 |
| 200 mile limit | 55.0 | 60.0 | 680 | 29,196 | 42.9 |
| 200 mile limit | 60.0 | 65.0 | 570 | 12,062 | 21.2 |
| 200 mile limit | 65.0 | 70.0 | 590 | 1,334 | 2.3 |
| 200 mile limit | 40.0 | 70.0 | 4,690 | 161,955 | 34.5 |
| Atlantic Ocean | | | | | |
| 1,000m isobath | 41.1 | 45.0 | 1,840 | 61,897 | 33.6 |
| 1,000m isobath | 45.0 | 50.0 | 800 | 36,603 | 45.8 |
| 1,000m isobath | 50.0 | 55.0 | 660 | 24,955 | 37.8 |
| 1,000m isobath | 55.0 | 60.0 | 760 | 16,024 | 21.1 |
| 1,000m isobath | 60.0 | 64.1 | 540 | 7,047 | 13.0 |
| 1,000m isobath | 41.1 | 64.1 | 4,600 | 146,525 | 31.9 |

Table 8. Summary of offshore wave energy resources near Canadian waters.

# 4. Inventory of Tidal Current Energy Resources

## *4.1. General Description of Tides*

Tides are a regular and predictable phenomenon caused by the gravitational attraction of the moon and sun acting on the oceans of the rotating earth. Because of its relative proximity to the earth, the moon exerts roughly twice the tidal forcing as does the sun. The main lunar forcing oscillates with a period of 24 hours and 50 minutes, which is equal to the time required for a point on the earth to rotate back to the same position relative to the moon during each daily revolution.

The solar and lunar gravitational forces create two bulges in the earth's ocean waters: one directly under or closest to the moon, and the other on the opposite side of the earth (see Figure 41) These bulges are the twice-daily fluctuations in water levels observed in many places around the globe. In reality, this model is complicated by the fact that the earth's axis of rotation is tilted by 23.5° relative to the moon's orbit. The two bulges in the ocean are unequal unless the moon is over the equator. This daily difference in tide amplitude is called the diurnal inequality and repeats over a 14 day cycle as the moon rotates around the earth.

The largest tides are known as Spring tides: these occur at the time of new or full moon when the gravitational pull of the sun and moon are aligned. Neap tides are smaller and occur when the moon is waxing or waning, and the gravitational pull of the moon and sun are not aligned. The spring-neap cycle has a period of 15 days. The 15-day spring-neap cycle, combined with the 14 day diurnal inequality cycle, are responsible for much of the variability of the tides throughout the months of the year.

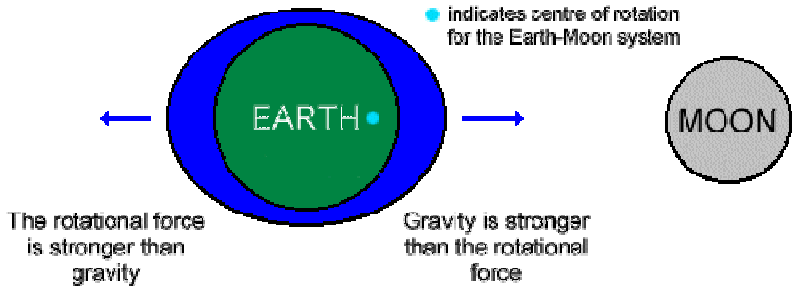


Figure 41. Tides are generated by the gravitational forcing of the moon and sun.

The tidal fluctuations at any point on earth are the cumulative effect of over a hundred harmonic constituents or cyclic components working together, each with their own amplitude, phase and period or frequency. These constituents combine so that tides completely repeat themselves every 18.6 years. The tide at any location can be completely described by summing the contributions from all constituent. In practice, reasonably accurate estimates can be obtained by considering the 5 to 8 leading constituents while disregarding the others. The principal semi-diurnal (twice daily) constituents are known as M2 (moon, twice daily) and S2 (sun, twice daily), while the principal diurnal (once daily) constituents are known as K1 and O1. Other important constituents include N2, K2 and M4.

Tides move as shallow water waves in the open ocean and in coastal waters. Tsunamis are shallow water waves generated by earthquakes or sub-marine landslides, rather than gravitational effects of the sun and moon. Despite their name, shallow water waves can exist in any water depth. One important characteristic of these waves is that the entire water column below the free surface moves in unison as the wave passes. Shallow water waves, tides included, propagate with a celerity proportional to the square root of the water depth, which can be several hundred kilometres per hour in the open ocean beyond the continental shelves. In the open ocean, tides are small, rarely exceeding 0.5 m in height. However, as a tide wave enters shallower coastal waters, it decelerates, shoals (increases in height) and eventually bumps into land. These coastal effects can be very important, as evidenced by the fact that a small amplitude deep ocean tide can generate 15 m tides in the upper Bay of Fundy. The reader is directed to the Canadian Tidal Manual (Forrester, 1983) for additional information concerning the nature and behaviour of tides.

Tidal currents result from the passage of tide waves. As the water level rises, tidal currents tend to flow in the direction of propagation of the tide wave. These flows are often referred to as the flood tide. During the ebb tide, when water levels recede, the tidal currents tend to reverse themselves and flow opposite to the propagation direction of the tide wave.

As noted above, the tidal current at any location varies over a wide range of time scales. The flow direction typically reverses between two and four times daily, depending on whether the tides are diurnal or semi-diurnal. In addition, the peak velocity during each ebb and flood varies over weeks, months and years. The entire pattern of temporal fluctuation repeats over an 18.6 year cycle. It is worth noting that semi-diurnal tides produce roughly twice the peak current of a diurnal tide of the same height. This is because the semi-diurnal tide rises and falls in half the time of the equivalent diurnal tide.

Coastal tidal flow patterns often feature strong shears and steep gradients, which is another way of stating that the velocities vary strongly with location. At many locations, high-velocity high-energy flows are confined to quite small areas. This characteristic can make it particularly difficult to quantify and assess tidal current energy resources. The spatial variation depends on how the tide waves interact with the local bathymetry of the area. One important factor is the presence of narrow passages or channels which can act to concentrate and accelerate the flows. However, the flow through a passage is also constrained by the loss of energy due to friction. The discharges and flow velocities in a passage result from a fine balance between the energy forcing the flow into the passage and the dissipation due to friction within the passage. Clearly, if the energy extracted from the flow within a passage increases, either by natural causes or the installation of an hydraulic turbine, then the discharge and velocity through the passage will be lowered. There is clearly an upper limit to the energy that can be extracted from such tidal flows. Another important factor is the phasing of the tidal flows. Very large currents can arise when the tide is high on one side of a passage at the same time that the tide is low on the other side. Such phase differences can also generate significant tidal flows near large Islands and major headlands.

Tidal currents in the open ocean are too weak for economically viable energy extraction using existing or anticipated technologies. For the foreseeable future, development will likely be restricted to sites with peak flow velocities on the order of 2 m/s or more, and mean flow velocities above 1 m/s. Such high-energy flows are typically confined to local areas, such as:

- entrances to estuaries and coastal embayments;
- narrow channels or passages between islands; and

- some major headlands.

## *4.2. Theoretical Basis for Resource Assessment*

The power (P) in a tidal flow is proportional to the cube of the flow velocity. Hence, the power increases rapidly with increasing flow velocity.

The power density (p) of a tidal flow can be written as

$$p = \frac{P}{A} = 0.5\rho U^3 \quad , \tag{12}$$

where P is the power [Watts], A is the cross-sectional area (normal to flow) under consideration [$m^2$], $\rho \approx 1{,}027$ kg/$m^3$ is the density of seawater, and U is the flow speed [m/s]. The annual mean power density for the site is equal to the average value of p over the year.

If we assume that the temporal variation in current speed at a site can be written as

$$u(t) = U_{\max} \sin(\frac{2\pi}{T} t) \quad , \tag{13}$$

where $U_{max}$ is the maximum speed and T is the period of oscillation, then the average speed over a half cycle is

$$\overline{u} = \frac{\int_0^{T/2} u(t)dt}{\int_0^{T/2} dt} = \frac{2}{\pi} U_{\max} \tag{14}$$

or 64% of $U_{max}$. The average power density over a half cycle is

$$\overline{p} = \frac{0.5\rho \int_0^{T/2} u^3(t)dt}{\int_0^{T/2} dt} = \frac{2\rho}{3\pi} U_{\max}^3 \approx 0.21\rho U_{\max}^3 \tag{15}$$

or 42% of the maximum power density. Expressed in terms of mean velocity, the average power density over a half cycle is

$$\overline{p} = \frac{\pi^2 \rho}{12} \overline{u}^3 \approx 0.82\rho \overline{u}^3 \tag{16}$$

One important result from this simple sinusoidal model is that the average power density over a half cycle is 1.64 times greater than the power density of the average speed over the same half cycle.

Many potential high-energy sites are located at narrow passages between islands or headlands. At any instant in time, the flow velocity within the passage will vary with depth, and with position across the channel. For typical sites, the strongest flows tend to occur within the upper half of the water column, and near the centre of the passage. It is important to account for these horizontal and vertical spatial variations when assessing energy resources due to tidal currents.

According to the well known Betz law, which applies to both wind turbines and hydraulic turbines, a theoretical maximum of 59% of the kinetic energy in a flow can be converted to mechanical energy using a turbine. Forty-one percent of the incident energy is required to ensure

that the fluid has enough kinetic energy to depart from the turbine. Once ecological considerations, power conversion efficiencies and other factors are taken into consideration, only a fraction of the available tidal stream energy resource can be extracted at any site. In other words, the recoverable resource will be a small fraction of the available resource.

## *4.3. Tide Modelling*

Numerous numerical simulations of tides (computer tide models) have been developed by many agencies, firms and individuals to describe and predict water levels and flows in the Oceans near Canada. In a nutshell, these models attempt to simulate the propagation of tides into coastal waters by solving a set of governing equations over a discretized model domain. By necessity, each model simulates the tide within a region, and results from multiple models must be combined to describe the flows in all of Canada's coastal waters.

In many models, the non-linear shallow water equations for sea level and depth averaged velocity are solved using a finite-element discretization in space and harmonic expansion in time. The domain is represented by a mesh of triangles, where the water depth and bottom roughness are specified at each node (the corners of the triangles). The node density (triangle size) is normally varied over the domain to suit the local water depth, the bathymetric variation, and the desired resolution. In general, densely packed nodes and very small triangles are required to obtain accurate and detailed flow predictions at sites where the bathymetry and/or the flow field feature strong gradients.

It is generally much easier to simulate water levels than to model tidal currents. This is because the spatial gradients in water level are much weaker than the gradients in velocity. Finer resolution models made up of a greater number of smaller and more densely packed triangles are required to provide accurate simulations of flow velocities in complex coastal regions. Such models require detailed information on bathymetry and bottom roughness. To yield accurate predictions, tide models generally need to be calibrated by comparison to measured water level and velocity data. A well-constructed and well-calibrated tide model can yield excellent predictions of water levels, and good predictions of depth averaged tidal currents. However, many existing models were developed to predict water levels and not flow velocities. Hence, their grids are not sufficiently refined to yield accurate velocity predictions in complex coastal regions.

### 4.3.1. Data Sources

Results from fourteen different tide models were obtained and analysed for this study. Some of the model characteristics are summarized in Table 9.

Six datasets with model results were obtained from the program WebTide, disseminated without charge over the internet by Fisheries and Oceans Canada (DFO). WebTide is a graphical user interface to a tidal prediction program. WebTide predictions are based on analysis of outputs from numerical models of tides implemented on seven different domains. The WebTide datasets provide a good description of the tides and tidal currents on a regional scale for almost all of Canada. (Unfortunately, the available data for Hudson Bay includes information on tidal elevations, but not tidal currents.) However, the WebTide grids are often too coarse to provide reliable tidal current predictions at narrow passages.

Four model result datasets were supplied by Triton Consultants Inc. The Triton model grid for the waters around Vancouver Island was developed by the Institute of Ocean Sciences with the assistance of Triton Consultants. The grid is considered to be one of the best available discretizations of B.C.'s coastal waters. In general, the Triton model grids feature a higher density of nodes in shallow water and thus have the potential to provide more accurate predictions of tidal currents in coastal waters than do the WebTide models. The Triton models have been calibrated by comparison with measured data and used to predict tides and tidal currents for engineering studies across Canada.

Results from high-resolution models of the upper Bay of Fundy and the Bras d'Or Lakes were contributed by Dr. John Loder of DFO's Bedford Institute of Oceanography (BIO). The upper Bay of Fundy model is described in Dupont et al. (2005), while the Bras d'Or Lakes model is described in Dupont et al. (2003). Both of these models have been validated by comparison with measured data and feature detailed high resolution grids. The intermittent wetting and drying of the extensive mud-flats within the upper Bay of Fundy is an important feature of the tidal flows within the Bay – and this process was included in the Fundy model.

Dr. Guoqi Han of DFO's Northwest Atlantic Fisheries Centre in St. John's contributed results from two medium-resolution regional models covering the Newfoundland Shelf (including the Grand Banks) and the Gulf of St. Lawrence. Both of these models were validated by comparison with measured current data.

In every case, the model results were expressed in terms of the amplitude and phase of the leading tidal constituents for every node in the model domain. In most cases, amplitude and phase values were supplied to describe the water surface elevation and the u and v components of depth averaged velocity at each node. The exceptions were the HB2 model, where only elevation constituents were available, and the NS and GSL2 models, were only velocity constituents were provided. In most cases, the location and water depth of each node was also supplied, along with the finite element mesh used in the modelling. The number of nodes and the number of constituents varied from model to model, as indicated in Table 9. The domain, bathymetry and finite element mesh for some of these models are shown in Figure 42 – Figure 49.

| No. | Name | Abbrev. | Source | No. of nodes | Constituents |
|---|---|---|---|---|---|
| | | | | | |
| 1 | Vancouver Island | VI | Triton | 132,022 | K1, O1, P1, Q1, K2, M2, N2, S2 |
| 2 | Queen Charlotte Isl. | QC | Triton | 7,575 | K1, O1, P1, Q1, M2, K2, N2 |
| 3 | Hudson Bay | HB1 | Triton | 45,230 | K1, S2, N2, M2, K2, M4, MS4 |
| 4 | Gulf of St. Lawrence | GSL1 | Triton | 7,763 | K1, O1, M2, S2, M2 |
| 5 | Bay of Fundy | Fundy | DFO - BIO | 74,934 | K1, O1, N2, S2, M2, M4 |
| 6 | Bras d'Or Lakes | BdO | DFO - BIO | 8,614 | K1, O1, N2, S2, M2, M4, Mf |
| 7 | Newfoundland Shelf | NS | DFO - NAFC | 10,927 | K1, O1, S2, M2, N2 |
| 8 | Gulf of St. Lawrence | GSL2 | DFO - NAFC | 7,734 | K1, O1, S2, M2, N2 |
| 9 | Scotian Shelf | SS | DFO - WebTide | 5,261 | K1, O1, M2, K2, N2, S2, L2, M4, NU2, 2N |
| 10 | NW Atlantic | NWA | DFO - WebTide | 17,055 | K1, O1, M2, N2, S2 |
| 11 | Arctic | Arctic | DFO - WebTide | 17,356 | K1, O1, M2, N2, S2 |
| 12 | Hudson Bay | HB2 | DFO - WebTide | 13,429 | K1, O1, M2, N2, S2, M4, MS4 |
| 13 | Quatsino Sound | QS | DFO - WebTide | 43,118 | K1, O1, P1, M2, N2, S2, Z0 |
| 14 | NE Pacific | NEP | DFO - WebTide | 51,330 | K1, O1, P1, Q1, M2, K2, N2, S2 |

Table 9. Summary of tide models considered in this study.

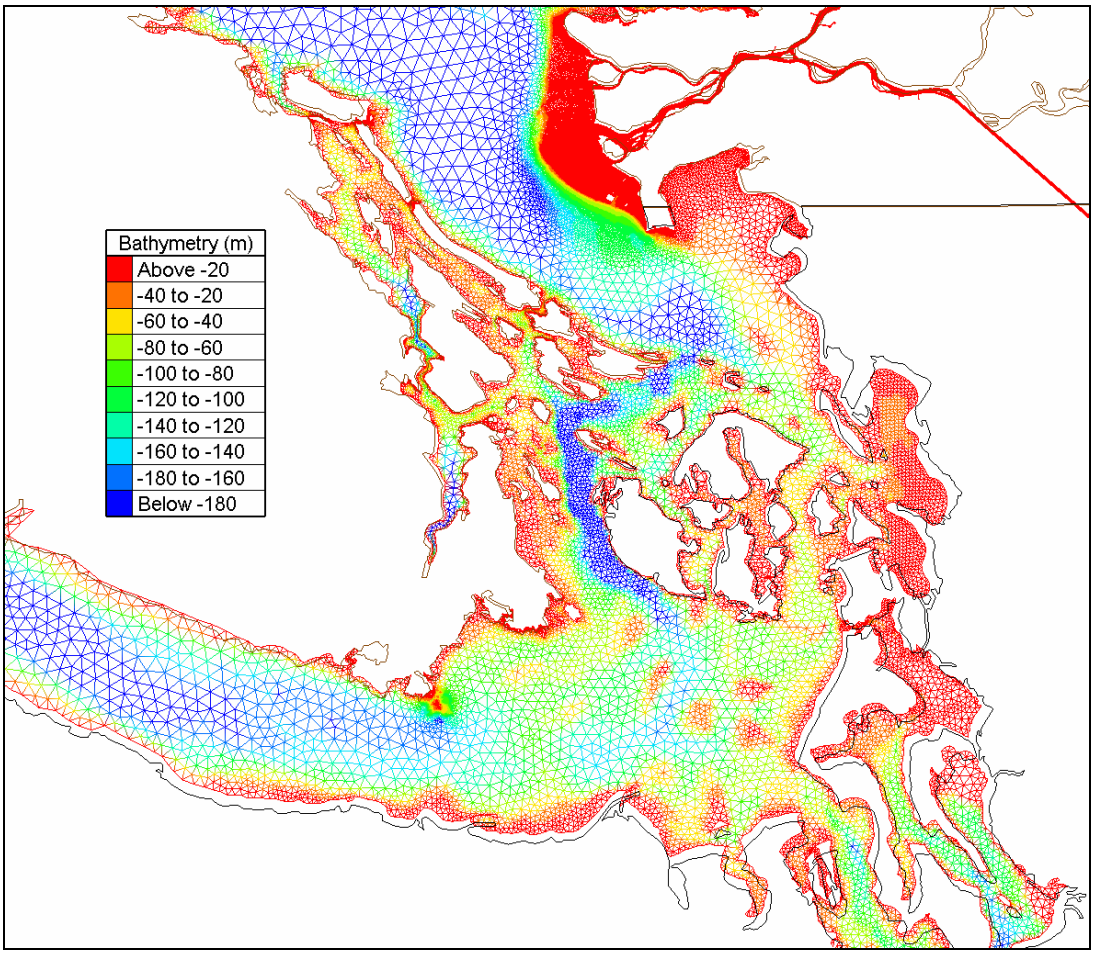


Figure 42. Bathymetry and mesh for the part of the Vancouver Island model (132,022 nodes, partial domain shown).

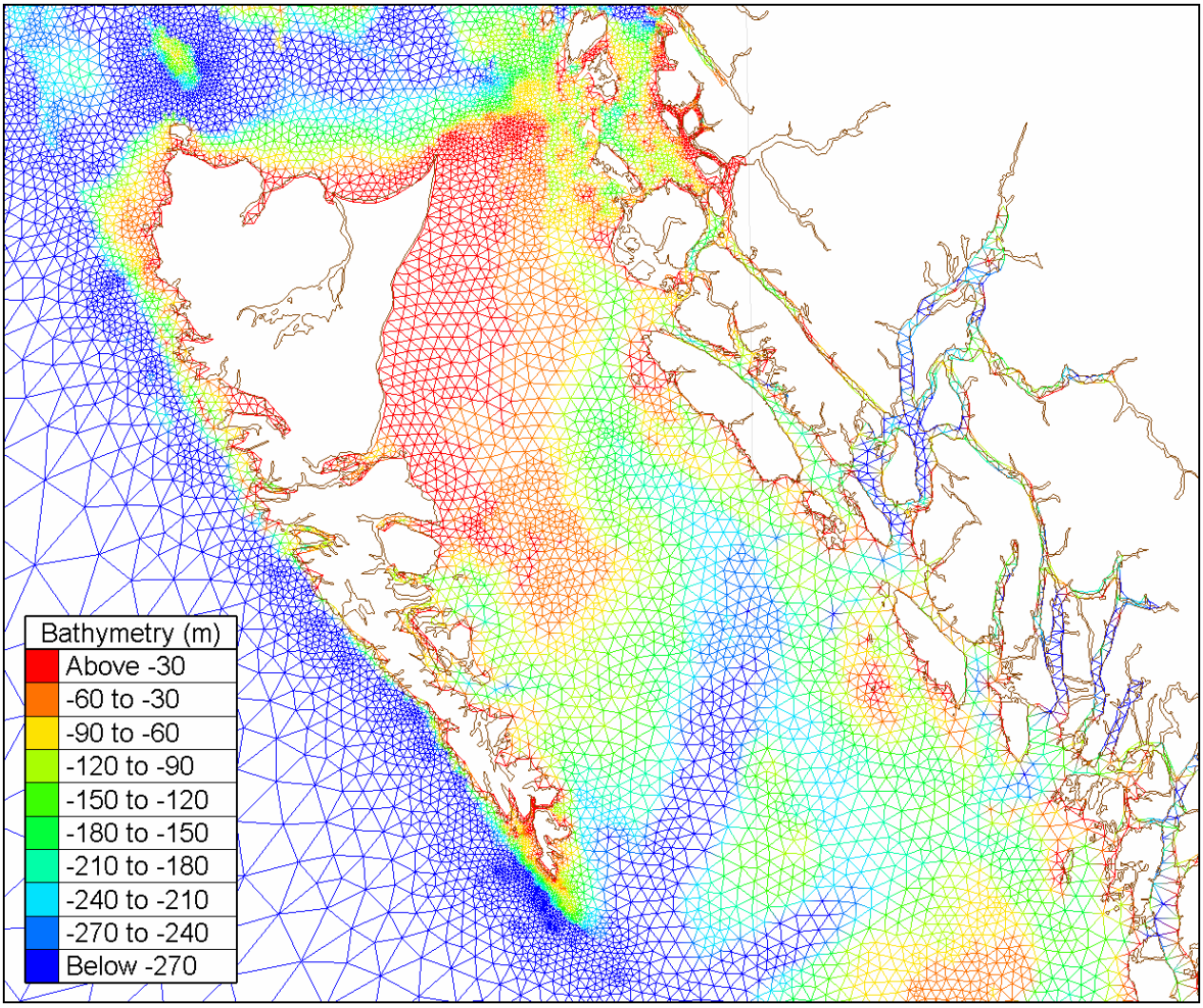


Figure 43. Bathymetry and mesh for part of the NE Pacific model (51,330 nodes, partial domain shown).

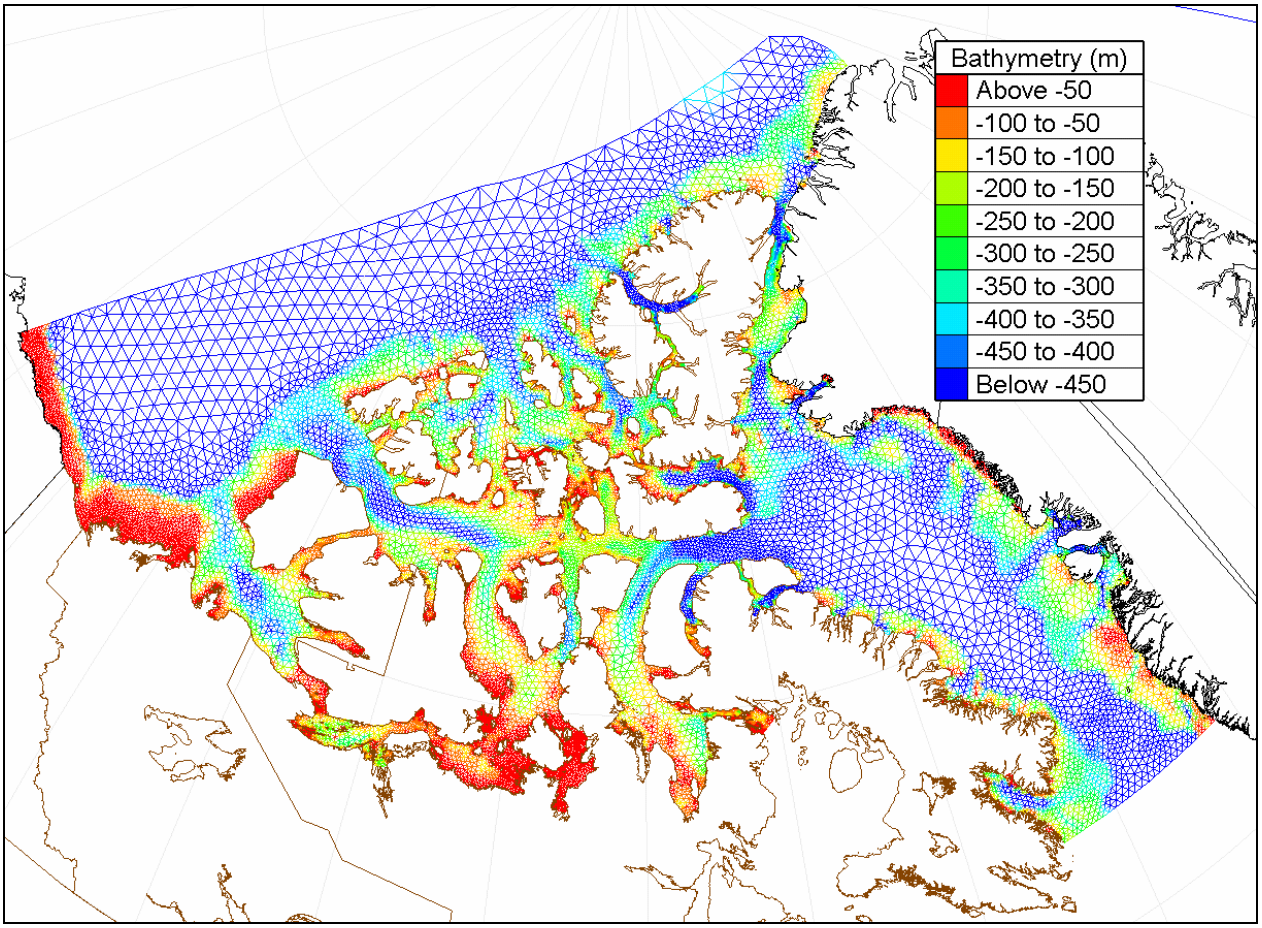


Figure 44. Bathymetry and mesh for the Arctic model (17,356 nodes).

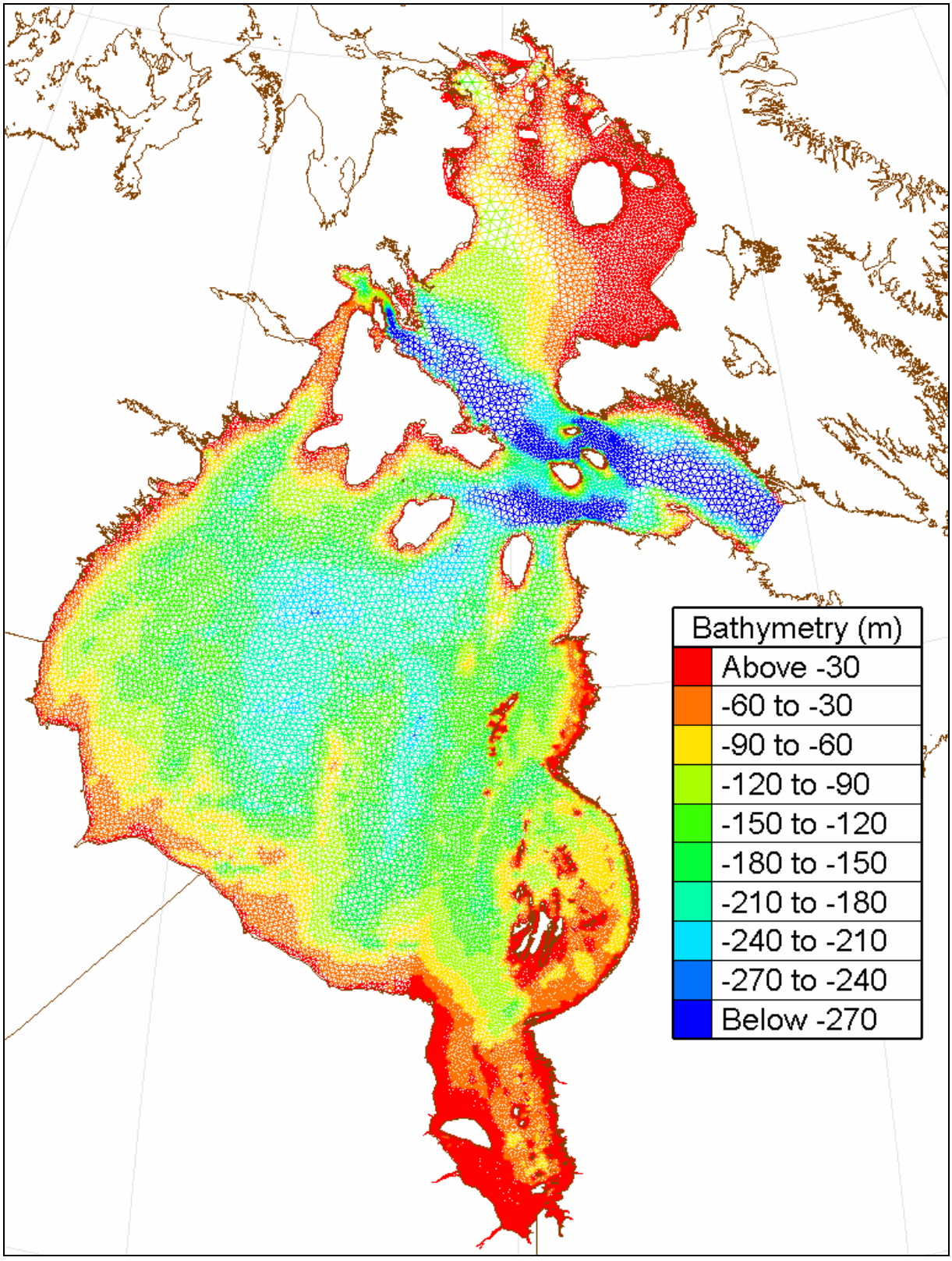


Figure 45. Bathymetry and mesh for the Hudson Bay (HB1) model (45,230 nodes).

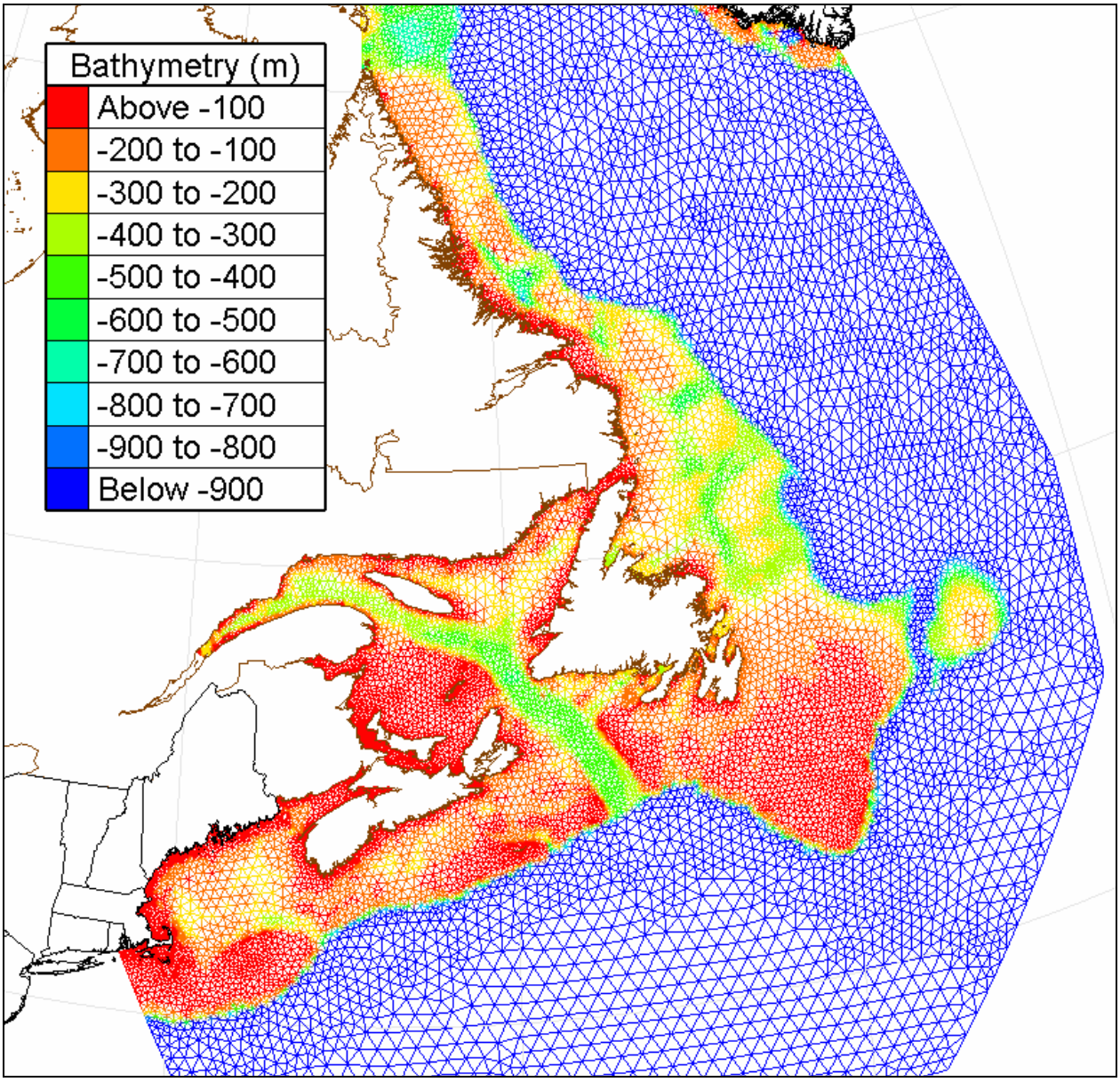


Figure 46. Bathymetry and mesh for the NW Atlantic model (17,055 nodes, partial domain shown).

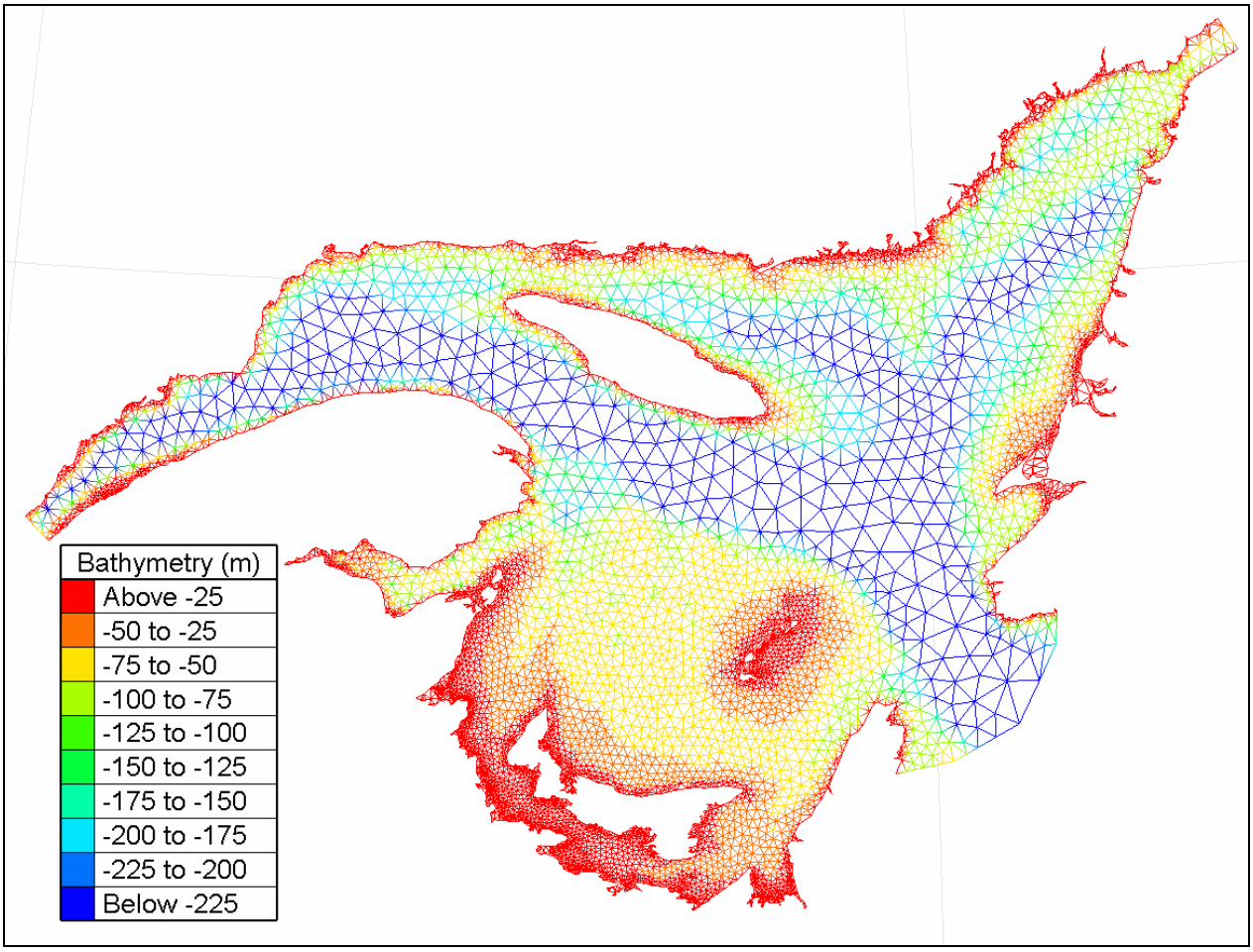


Figure 47. Bathymetry and mesh for the Gulf of St. Lawrence (GSL1) model (7,575 nodes).

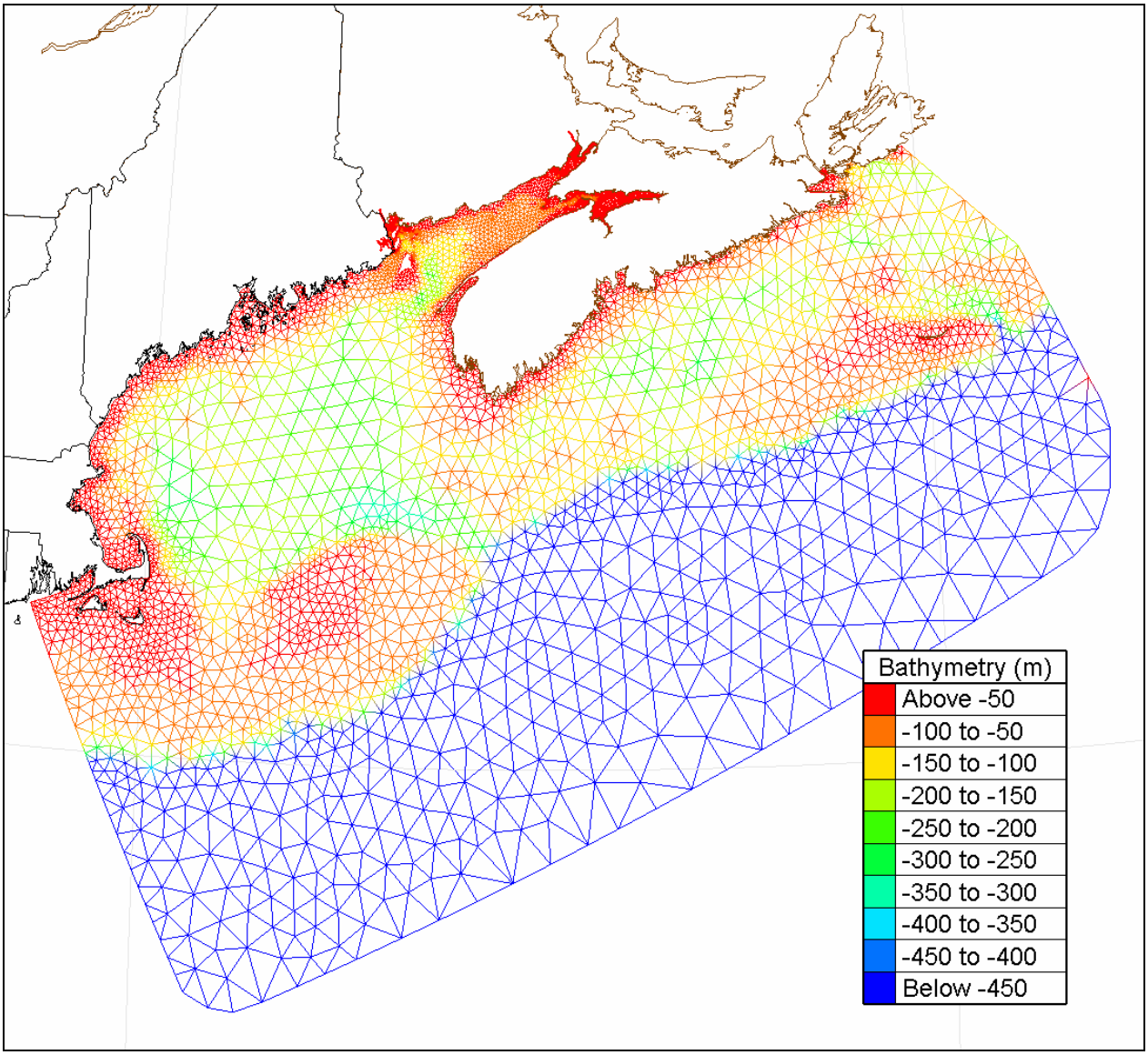


Figure 48. Bathymetry and mesh for the Scotain Shelf model (5,261 nodes).

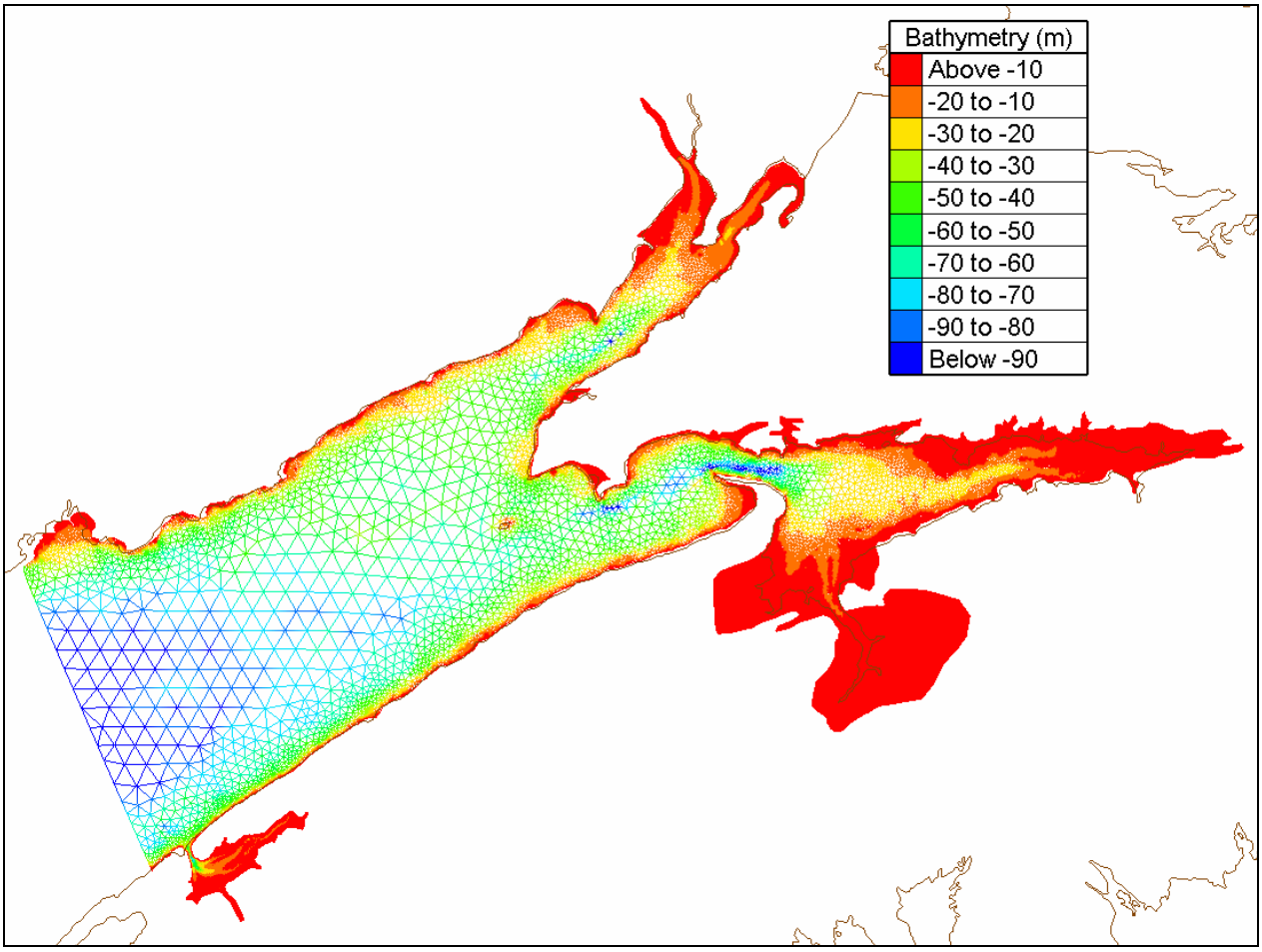


Figure 49. Bathymetry and mesh for the Fundy model (74,934 nodes).

### 4.3.2. Analysis Methodology

For each set of model results described in the previous section, an extensive set of marine resource parameters have been derived to describe the spatial and temporal variations of the tides, the tidal flows, and the power associated with those flows. The methodology used to compute these parameters is described in what follows.

Parameters were derived to describe:

- the tidal range;
- the depth averaged tidal flow;
- the power density of the depth averaged flow; and
- properties of the tidal ellipse for each constituent.

The time series of water surface elevation η(t) was computed according to

$$\eta(t) = \sum_{i=1}^{M} \eta_i \cos(\omega_i t - a_i) \quad , \tag{17}$$

where $\eta_i$, $a_i$ and $\omega_i$ are the amplitude, phase and frequency of the $i^{th}$ constituent, and M is the total number of constituents. Similarly, the time series of the E-W and N-S depth averaged velocity components u(t) and v(t) were computed according to

$$u(t) = \sum_{i=1}^{M} u_i \cos(\omega_i t - b_i) \quad , \tag{18}$$

$$v(t) = \sum_{i=1}^{M} v_i \cos(\omega_i t - c_i) \quad , \tag{19}$$

Where $u_i$ and $b_i$ are the amplitude and phase of the $i^{th}$ constituent for u(t), and $v_i$ and $c_i$ are the amplitude and phase of the $i^{th}$ constituent for v(t). The time series of depth averaged flow speed was defined as

$$s(t) = \left[u^2(t) + v^2(t)\right]^{1/2} \quad , \tag{20}$$

The time series of depth averaged power density was calculated as

$$p(t) = \frac{1}{2}\rho s^3(t) \quad , \tag{21}$$

All time series were computed at a one-hour time step for a one year (N=8766 hour) duration, with $\rho$=1027 kg/m$^3$.

A zero-crossing analysis was applied to determine the range (H) of each tidal cycle from $\eta(t)$.

The annual time series of elevation, speed and power density and the set of consecutive ranges were analysed to determine the following statistical parameters:

- minimum and maximum values;
- mean value: $\overline{\eta} = \frac{\sum \eta}{N}$ ;
- standard deviation ($\sigma$): $\eta_\sigma = \sqrt{\frac{\sum (\eta - \overline{\eta})^2}{N}}$ ;
- root-mean-squared (rms) value: $\eta_{rms} = \sqrt{\frac{\sum \eta^2}{N}}$ ; and
- the values corresponding to cumulative probabilities of 10%, 25%, 50%, 75%, and 90%.

For example, the parameter $s_{25\%}$ denotes the speed that is exceeded 75% of the time (not exceeded 25% of the time), while the parameter $p_{90\%}$ denotes the power density that is exceeded only 10% of the time (not exceeded 90% of the time).

In computing the annual time series it was assumed for simplicity that the amplitude and phase of each constituent remained constant throughout the year, whereas in reality these coefficients vary over an 18.6 year cycle. Thus, the annual time series that were synthesized can be considered representative of conditions during a "typical" year, rather than a specific calendar year. The effect of this simplification on the resulting speed and power density statistics was investigated for a number of sites and found to be small in all cases. (The main difference is that the extremes

(maximums) are slightly under-predicted by the approximate method. The non-extreme statistics are predicted with good accuracy using this method. Thus, the approximation is considered to be reasonable and sufficiently accurate for the purposes of this study. The sensitivity of these results to the time-step was also investigated to confirm that the one-hour time step was sufficient.

The methodology will be illustrated using data for two of Canada's largest tidal power sites: Minas Passage in the upper Bay of Fundy, and the channel between Mill Island and Salisbury Island in western Hudson Strait. Figure 50 shows time series of the tide level, depth averaged velocity, depth averaged speed and depth averaged power density near the centre of Minas Passage over a typical 14 day spring-neap cycle. The tides are strongly semi-diurnal and feature two similar ebbs and two similar floods each day. The cumulative distributions of speed and power density for this site (based on a one year simulation) are shown in Figure 51. This site features an average flow speed of 2.11 m/s and an average power density of 9.06 kW/m$^2$. The median speed (the speed exceeded 50% of the time) is 2.17 m/s and the median power density is 5.24 kW/m$^2$. Since the depth is 72 m, the average power of the tidal flows at this site per metre width across the passage is roughly 652 kW/m.

Figure 52 and Figure 53 show the corresponding time series and probability distributions for the channel between Mill Island and Salisbury Island, where the tide is also semi-diurnal. It is interesting to note that the flow speed remains above 0.4 m/s at all times, never becoming slack. The flows in this channel are less intense than at Minas Passage, but since the channel is roughly three times deeper and seven times wider than Minas Passage, they represent a significant tidal energy resource.

To illustrate conditions typical of a site where the tide is mixed (a mixture of diurnal and semi-diurnal oscillations), corresponding results for Cape St. James, located at the southern tip of the Queen Charlotte Islands, are presented in Figure 55 to Figure 56. Here, the tide features 2 ebbs and 2 floods on most days, but their intensity is often quite dissimilar.

The preceding analysis was applied at every node of the fourteen model domains discussed in Section 4.3.1 – a total of 442,348 locations in the oceans and coastal waters around Canada. These results may be used to help create a digital atlas of tidal energy resources.

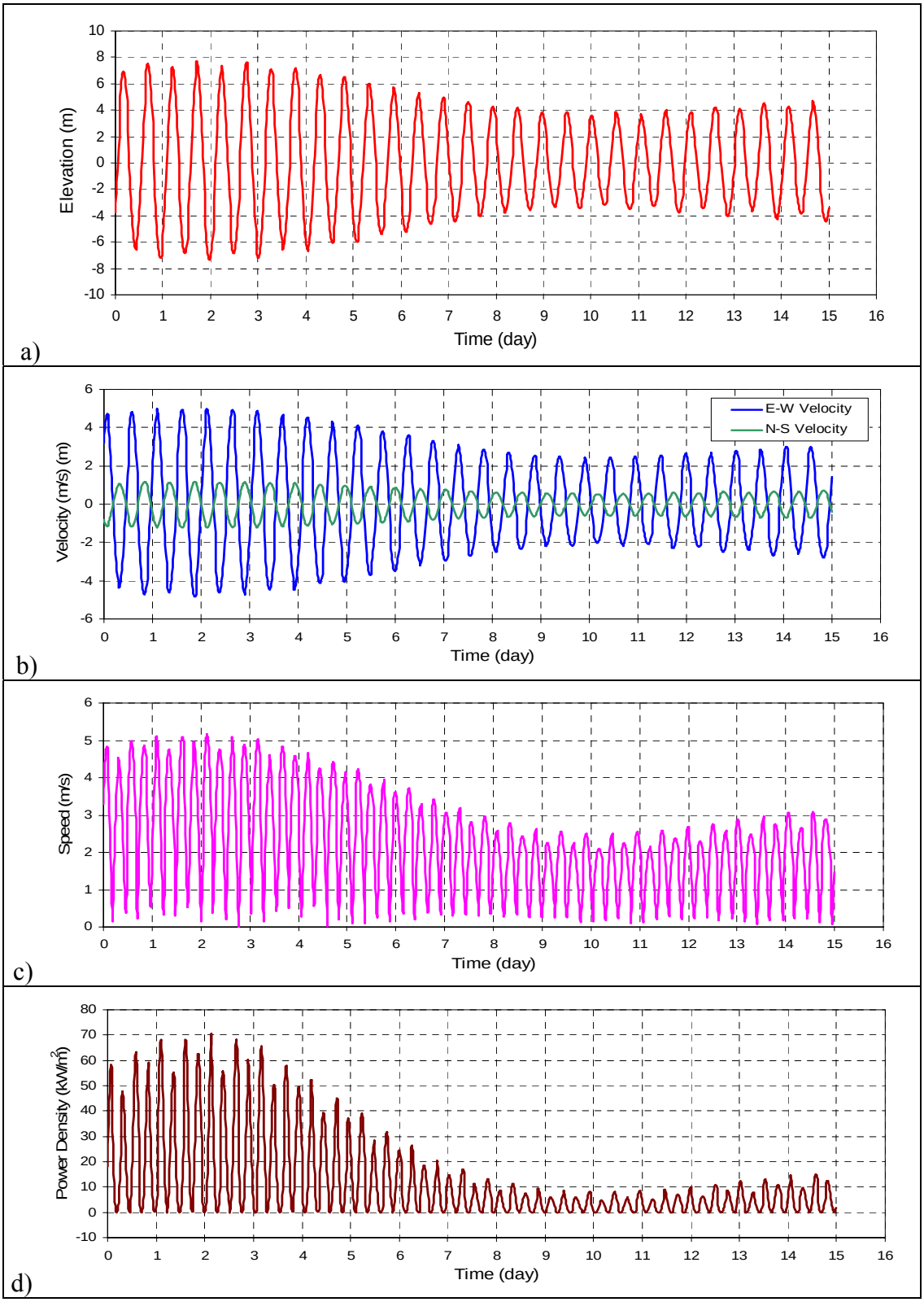


Figure 50. a) Tide level, b) depth averaged velocity; c) depth averaged speed; and d) depth averaged power density near the centre Minas Passage over a typical 15 day cycle.

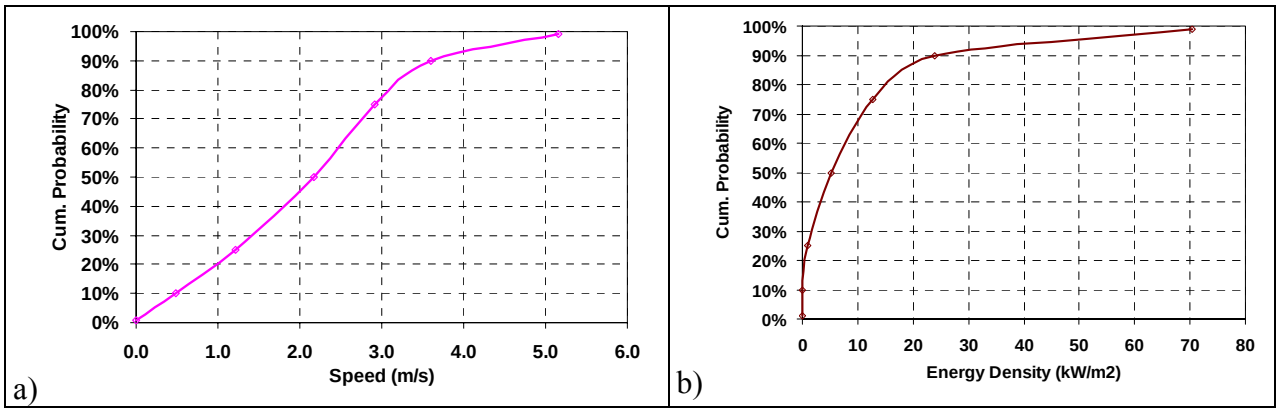


Figure 51. Cumulative distribution of a) depth averaged speed; and b) depth averaged power density near the centre of Minas Passage.

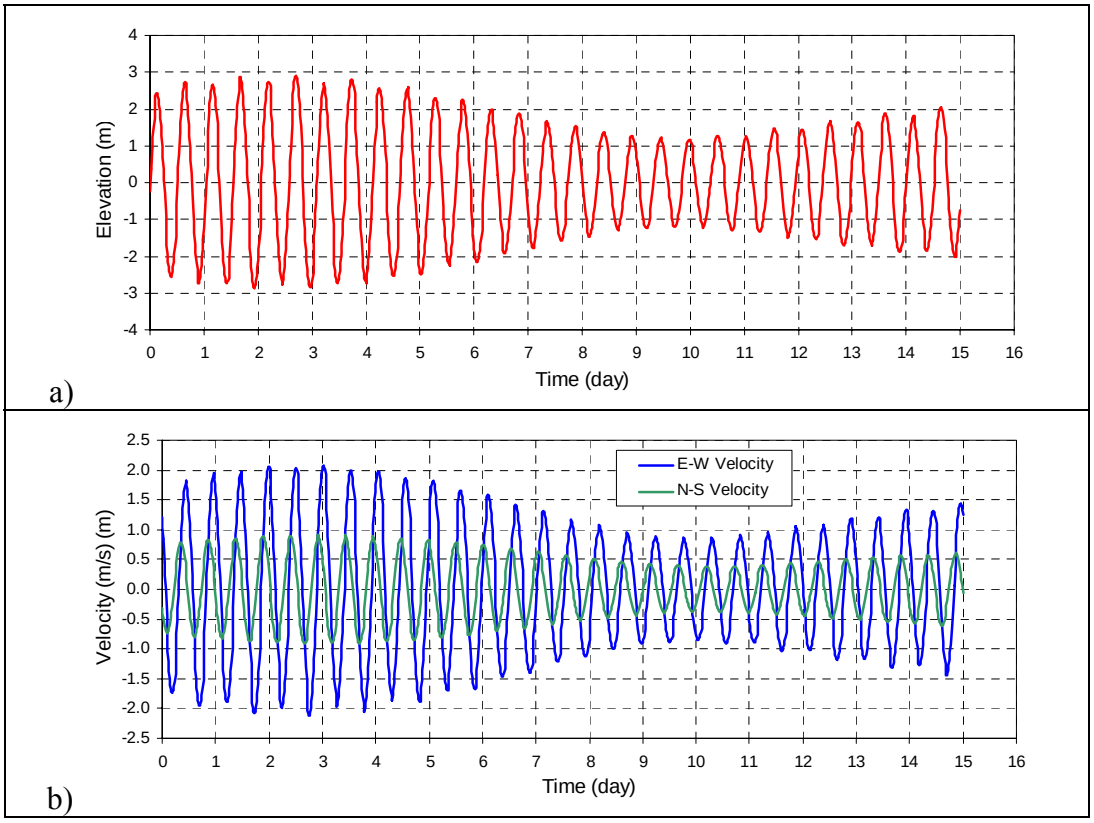

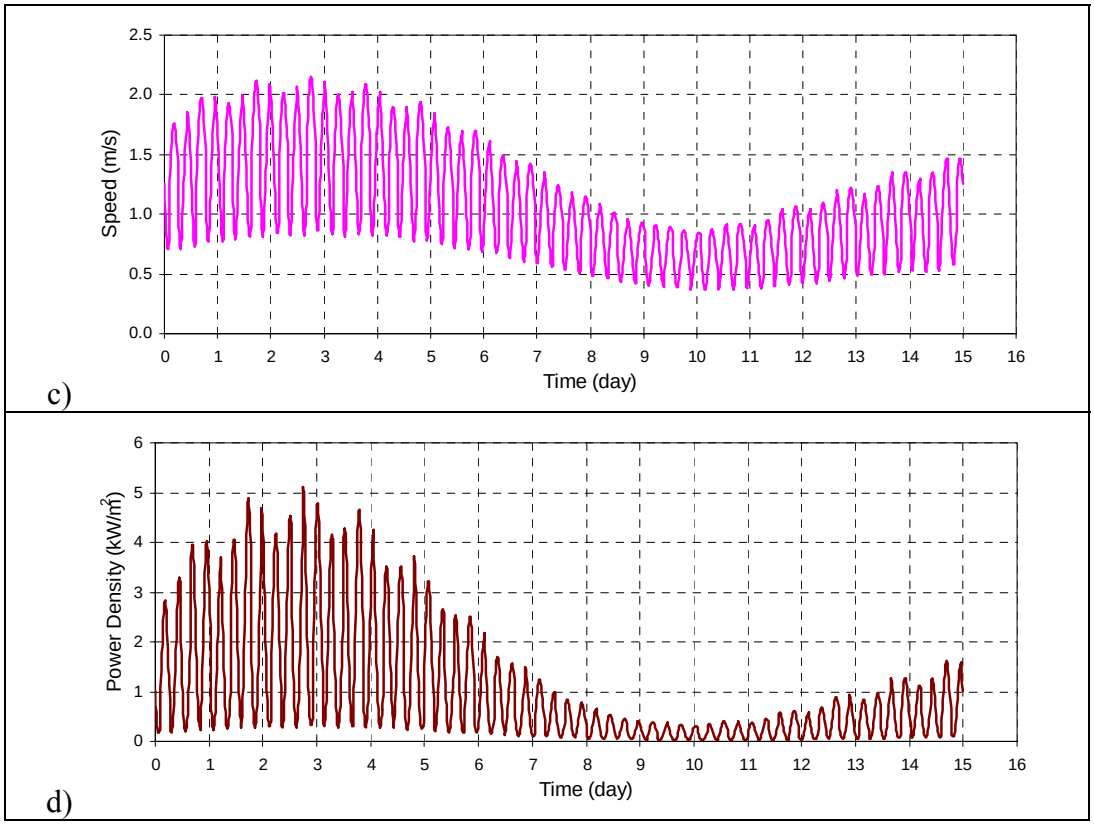


Figure 52. a) Tide level; b) depth averaged velocity; c) depth averaged speed; d) depth averaged power density between Mill Island and Salisbury Island over a typical 15 day cycle.

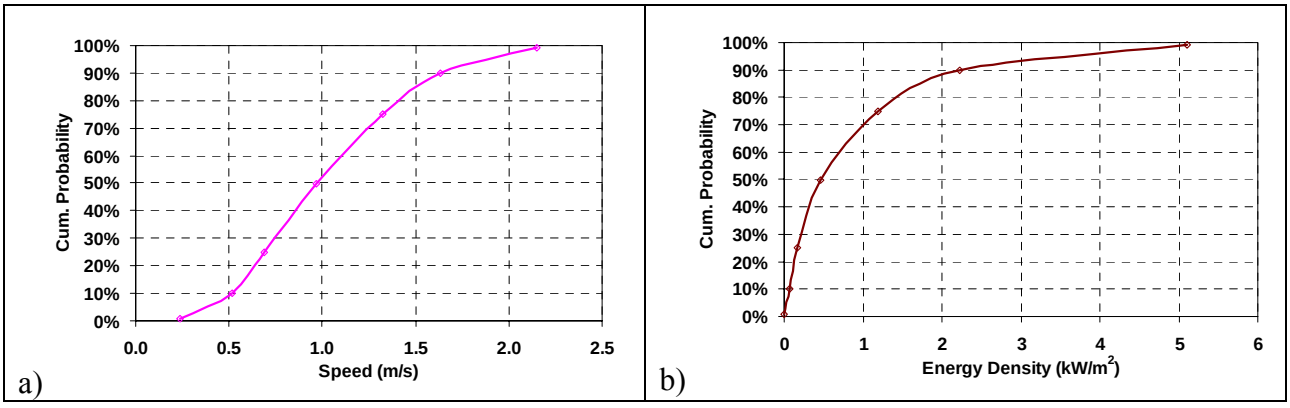


Figure 53. Cumulative distribution of a) depth averaged speed and b) depth averaged power density between Mill Island and Salisbury Island.

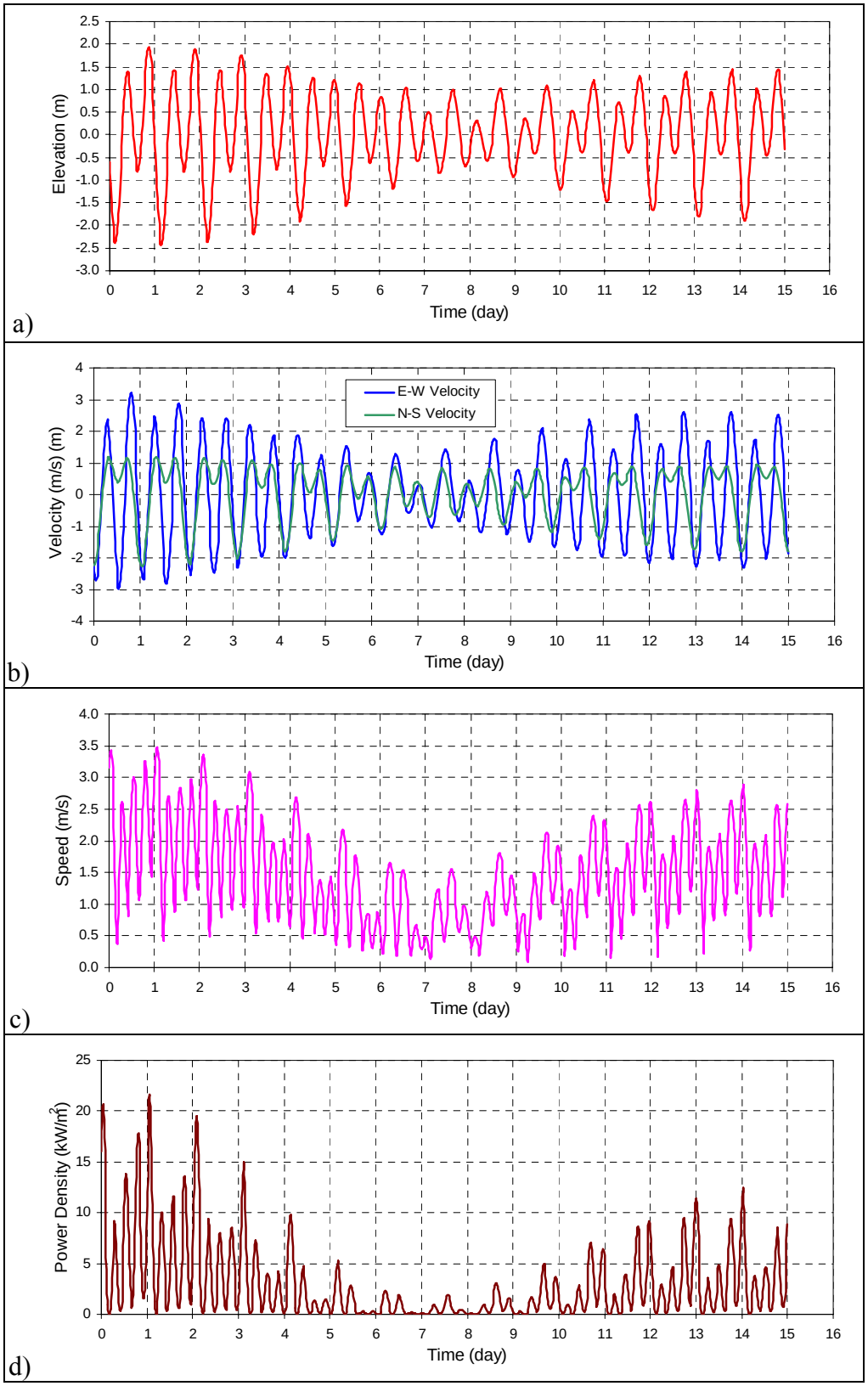


Figure 54. a) Tide level; b) depth averaged velocity; c) depth averaged speed; and d) depth averaged power density near Cape St. James over a typical 15 day cycle.

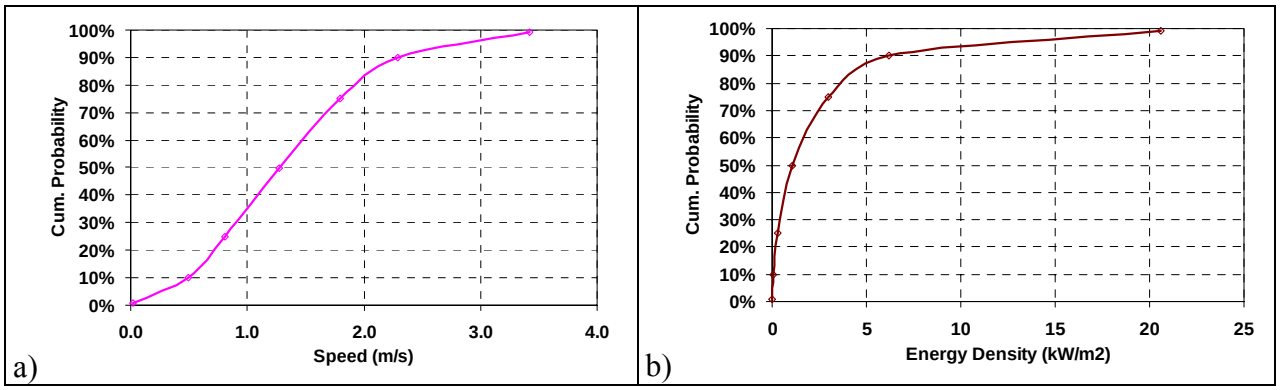


Figure 55. Cumulative distribution of a) depth averaged speed and b) depth averaged power density near Cape St. James.

### 4.3.3. Results

Selected results from the preceding analysis will be presented in what follows, arranged by ocean, starting with the Pacific.

***Pacific Ocean***

Figure 56 shows the mean tide range along the BC coast. The rms velocity of the tidal flows throughout the region, as predicted by the tidal models discussed above, is presented in Figure 57 to Figure 59. The mean power density of the tidal flows is plotted in Figure 60 to Figure 62.

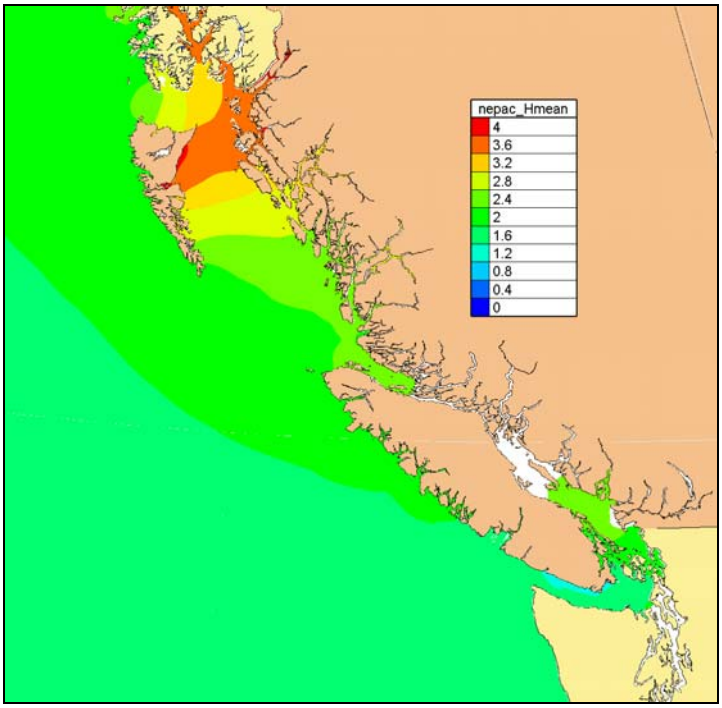


Figure 56. Mean tide range along the BC coast (m).

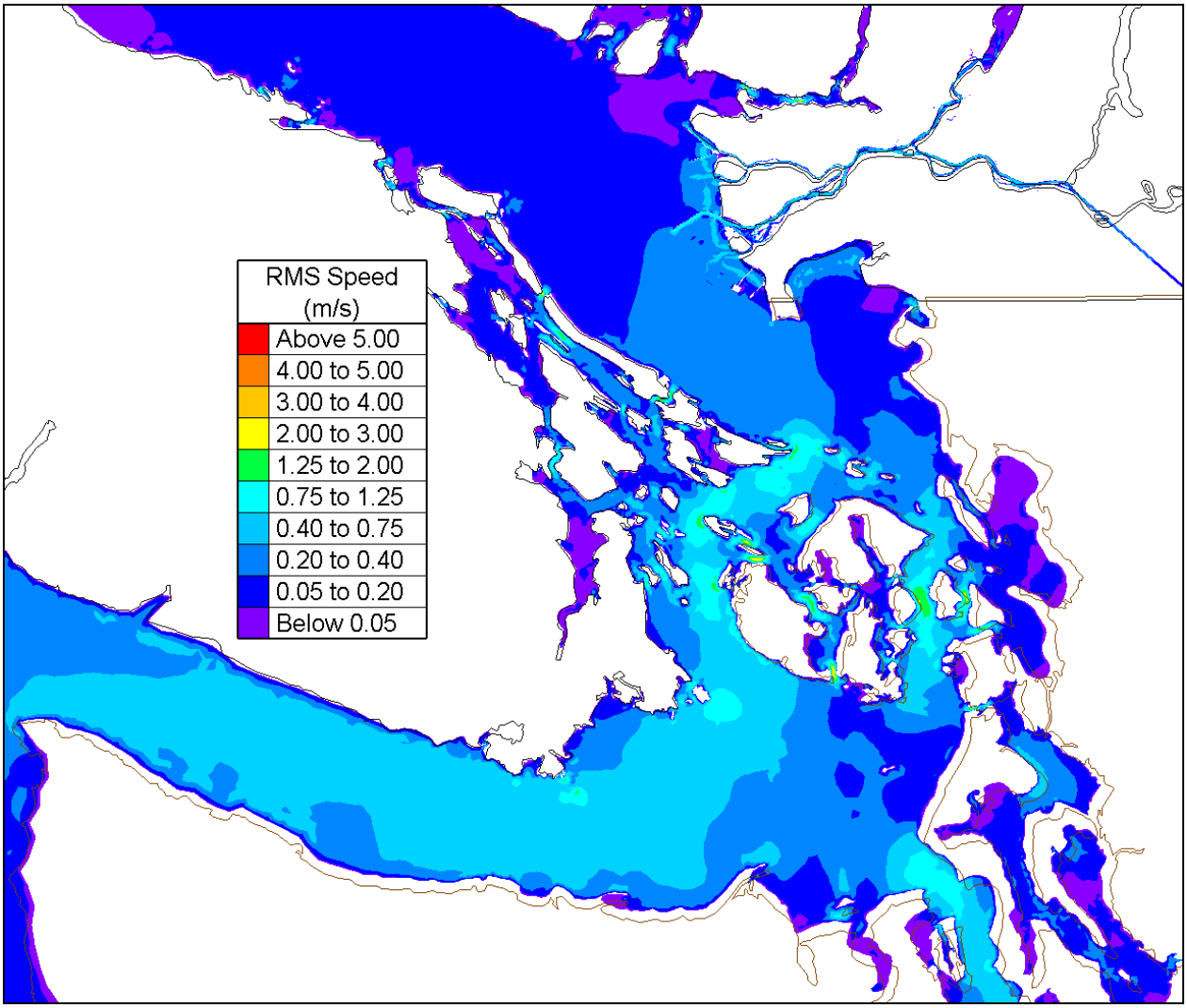


Figure 57. Root-mean-square tidal current speed, southern Vancouver Island.

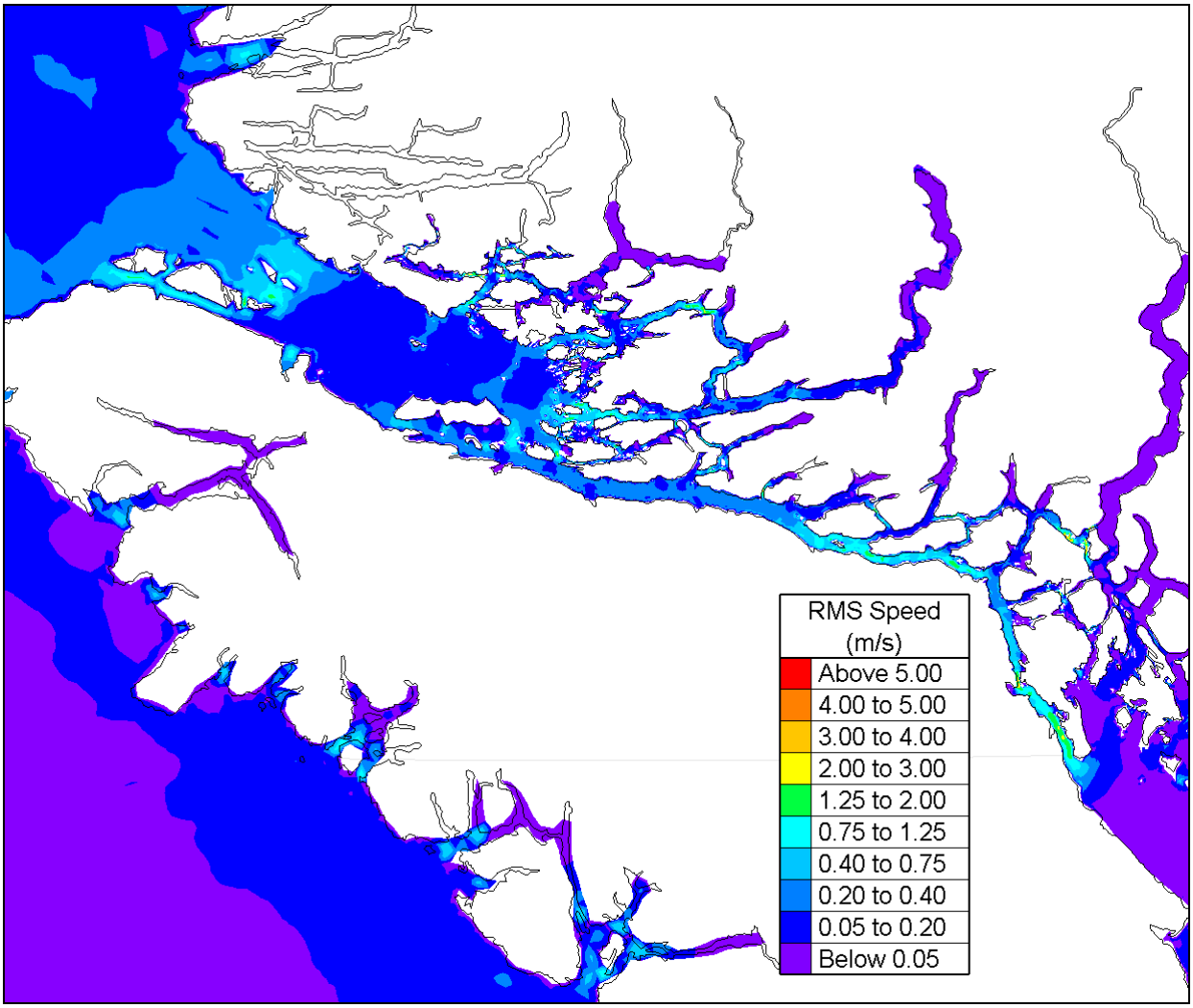


Figure 58. Root-mean-square tidal current speed, northern Vancouver Island.

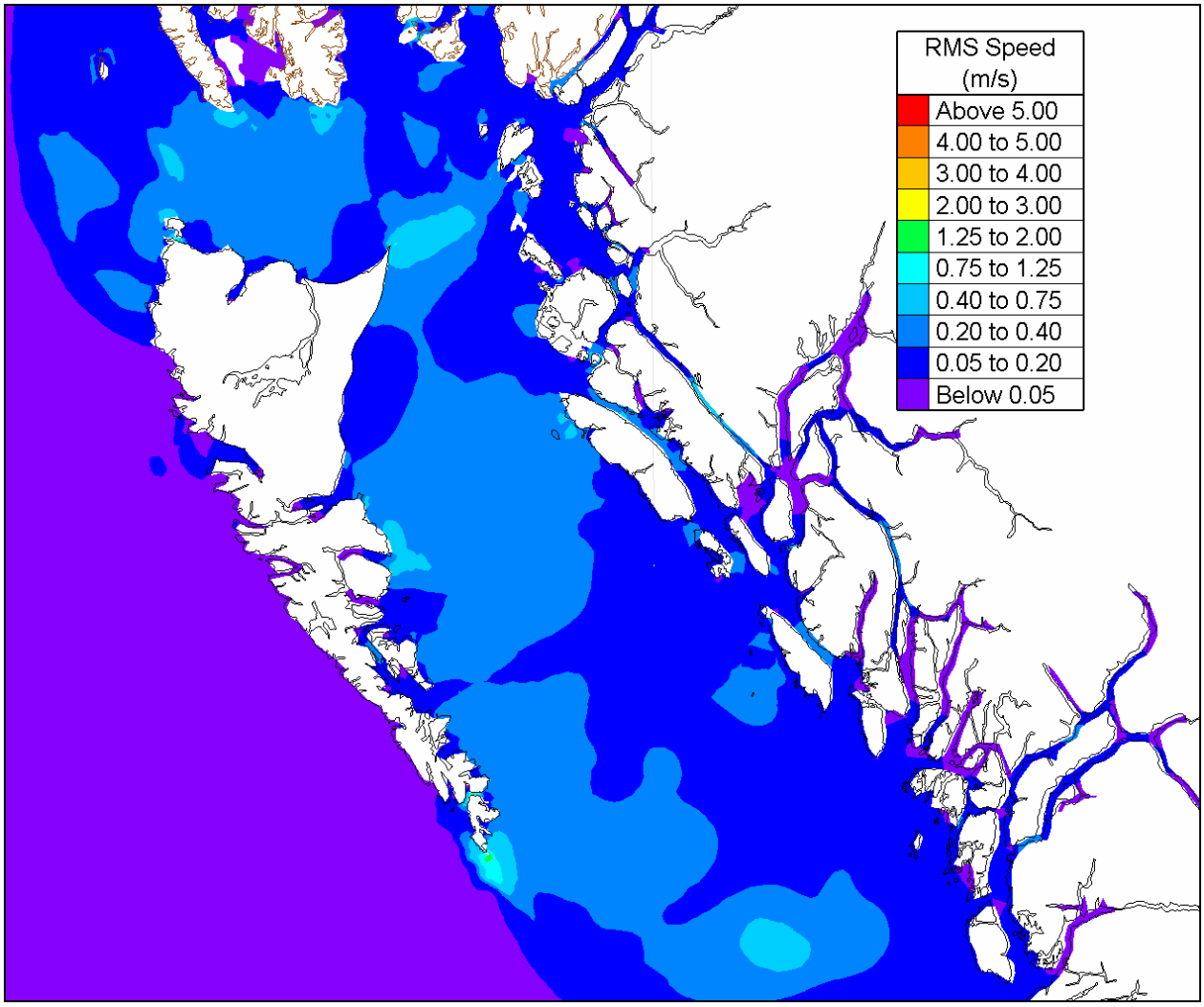


Figure 59. Root-mean-square tidal current speed, Queen Charlotte Islands.

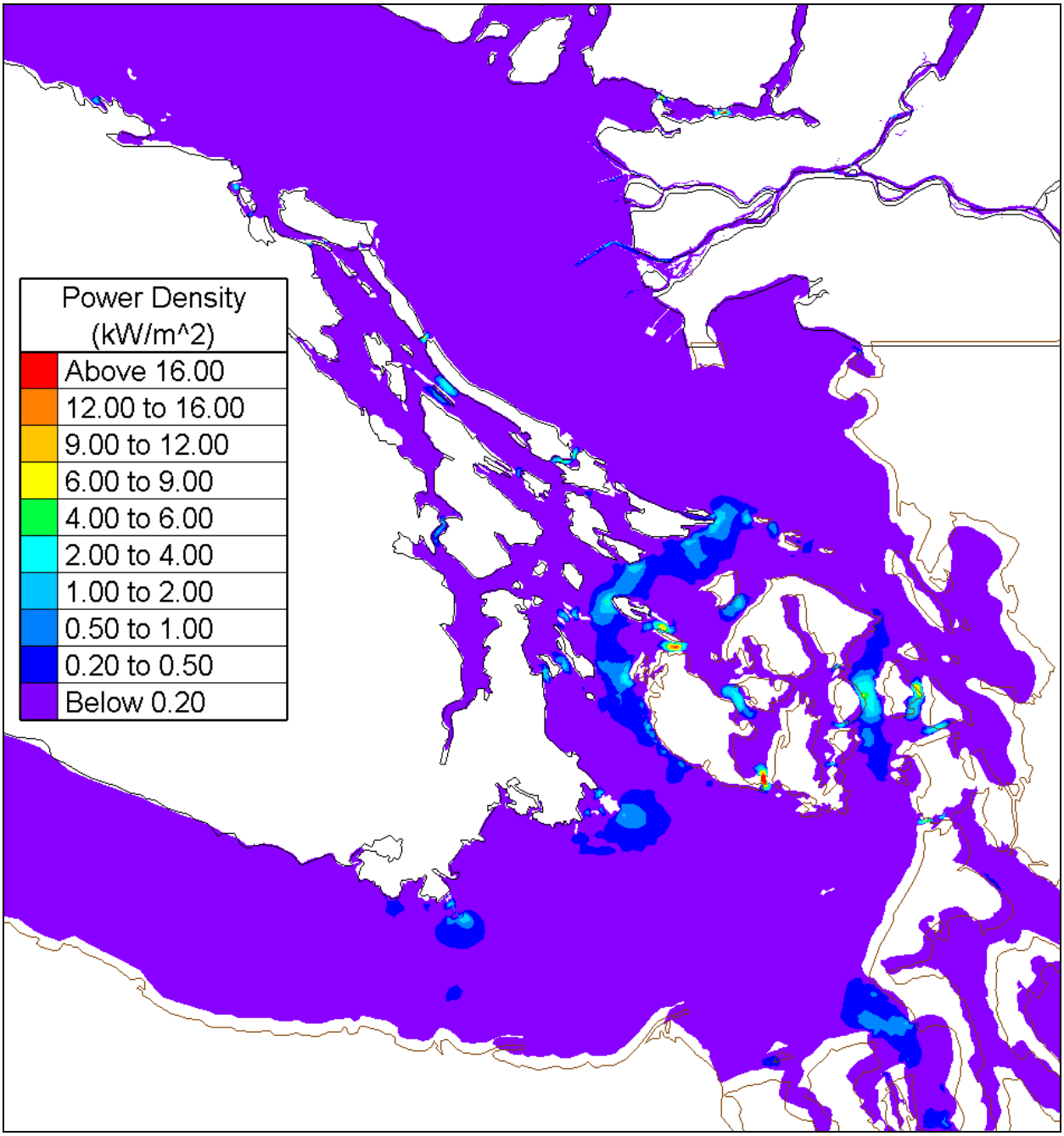


Figure 60. Mean power density, southern Vancouver Island.

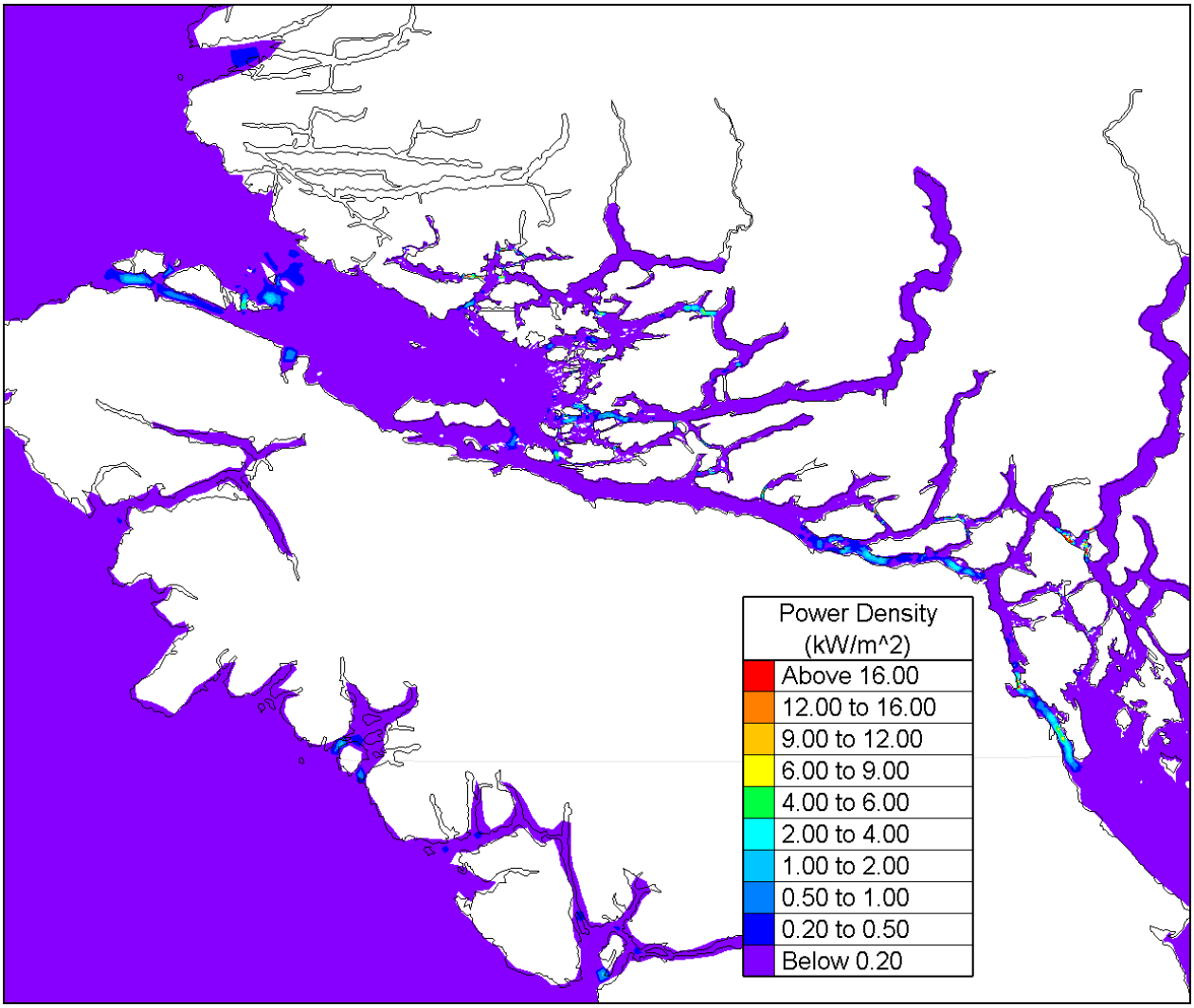


Figure 61. Mean power density, northern Vancouver Island.

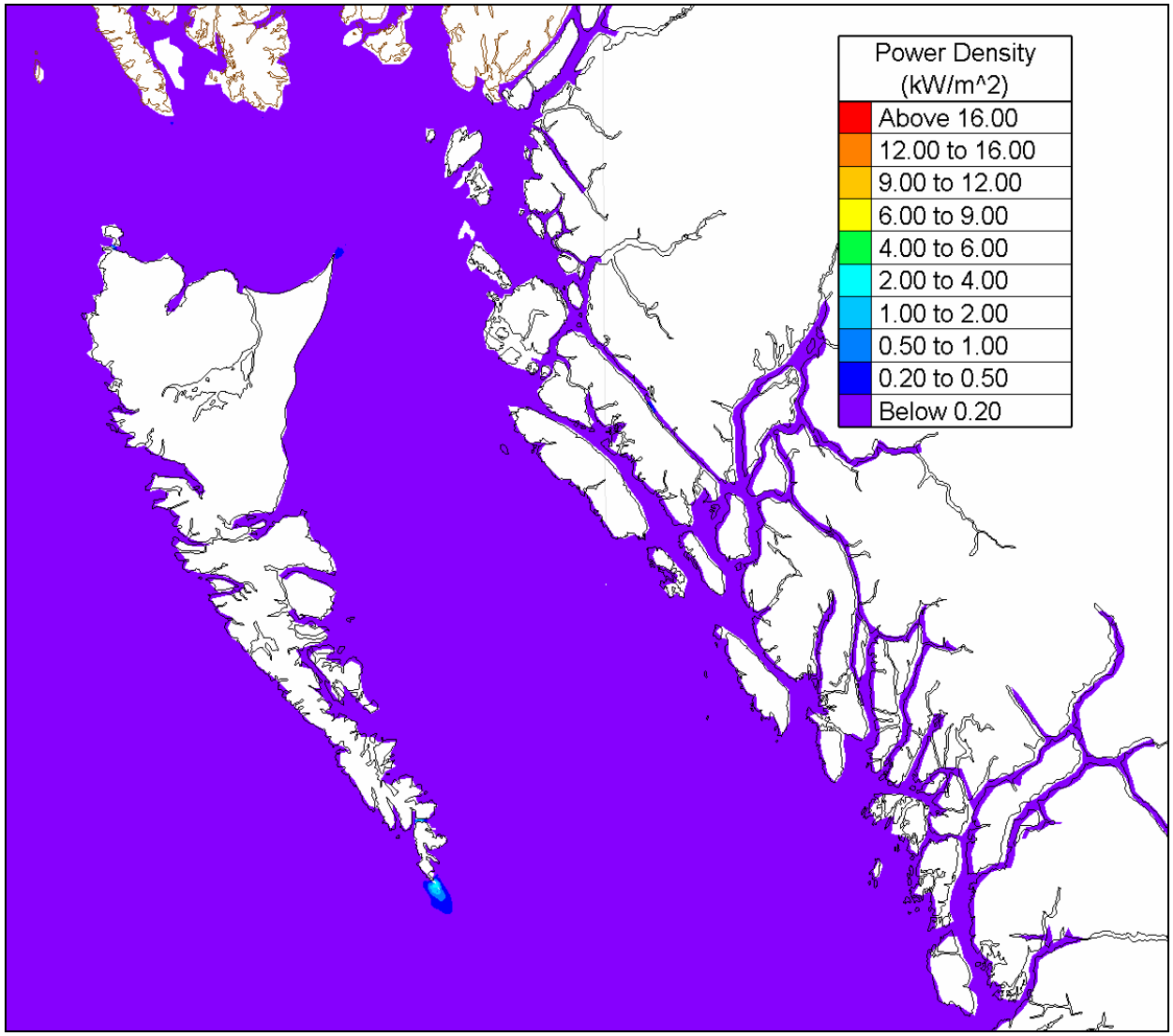


Figure 62. Mean power density, Queen Charlotte Islands.

### *Atlantic Ocean*

Figure 63 shows the mean tide range in eastern Canada. The rms velocity of the tidal flows throughout the region, as predicted by the tidal models discussed above, is presented in Figure 64. The mean power density of the tidal flows is Eastern Canada is plotted in Figure 65. Figure 66 to Figure 68 show the mean tide range, the rms velocity and the mean power density of the tidal flows in the Bay of Fundy.

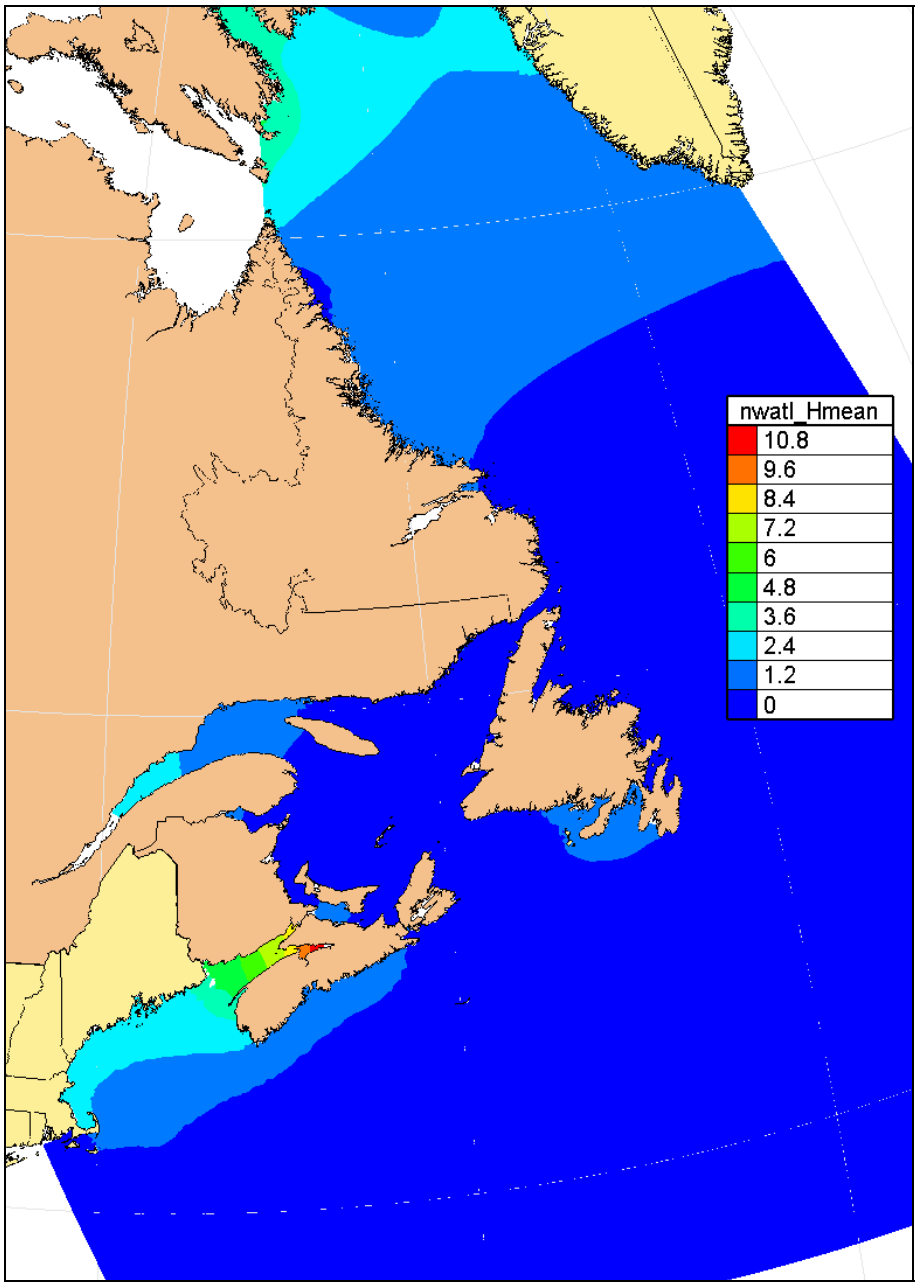


Figure 63. Mean tide range in eastern Canada.

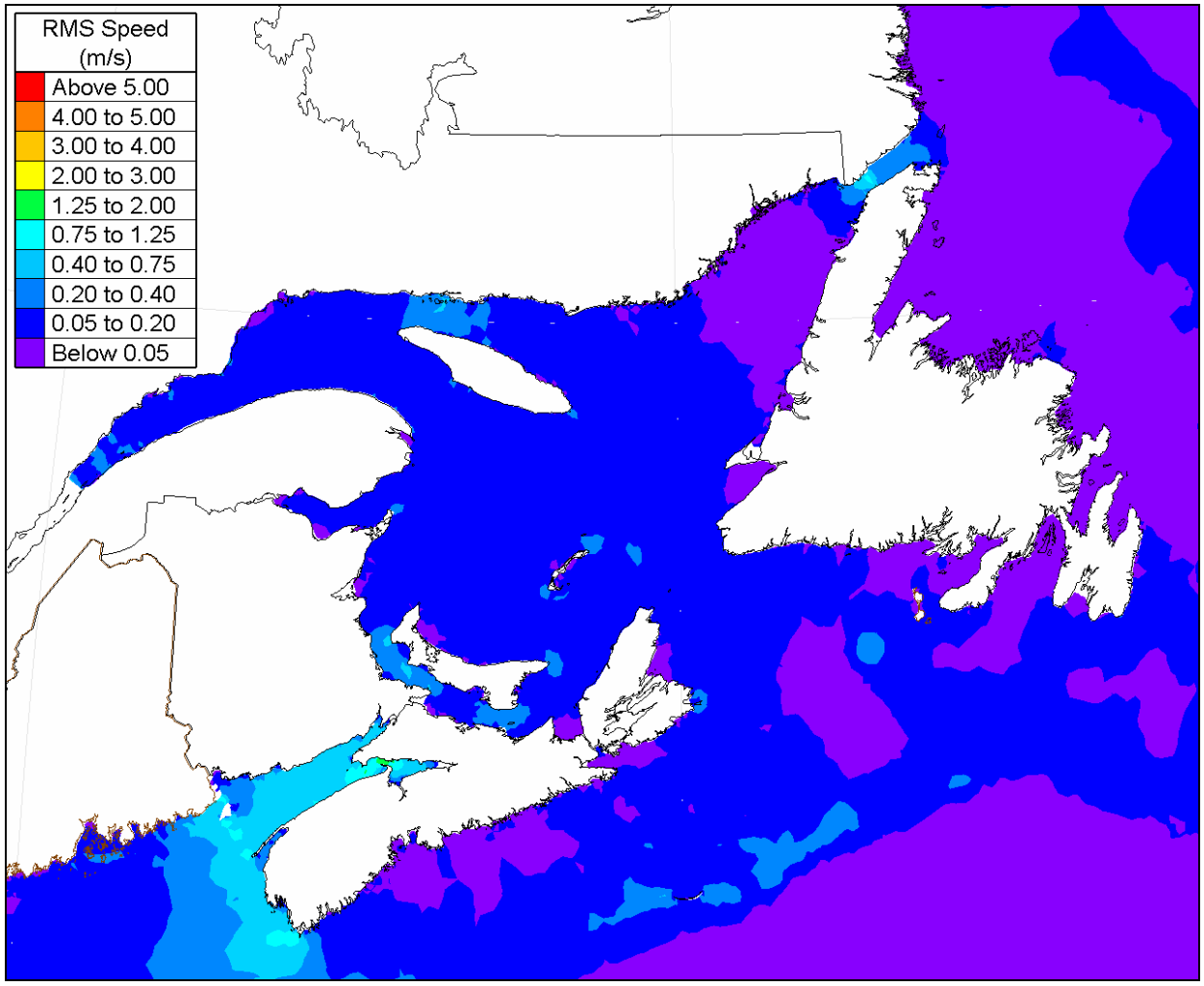


Figure 64. Root-mean-square tidal current speed, eastern Canada.

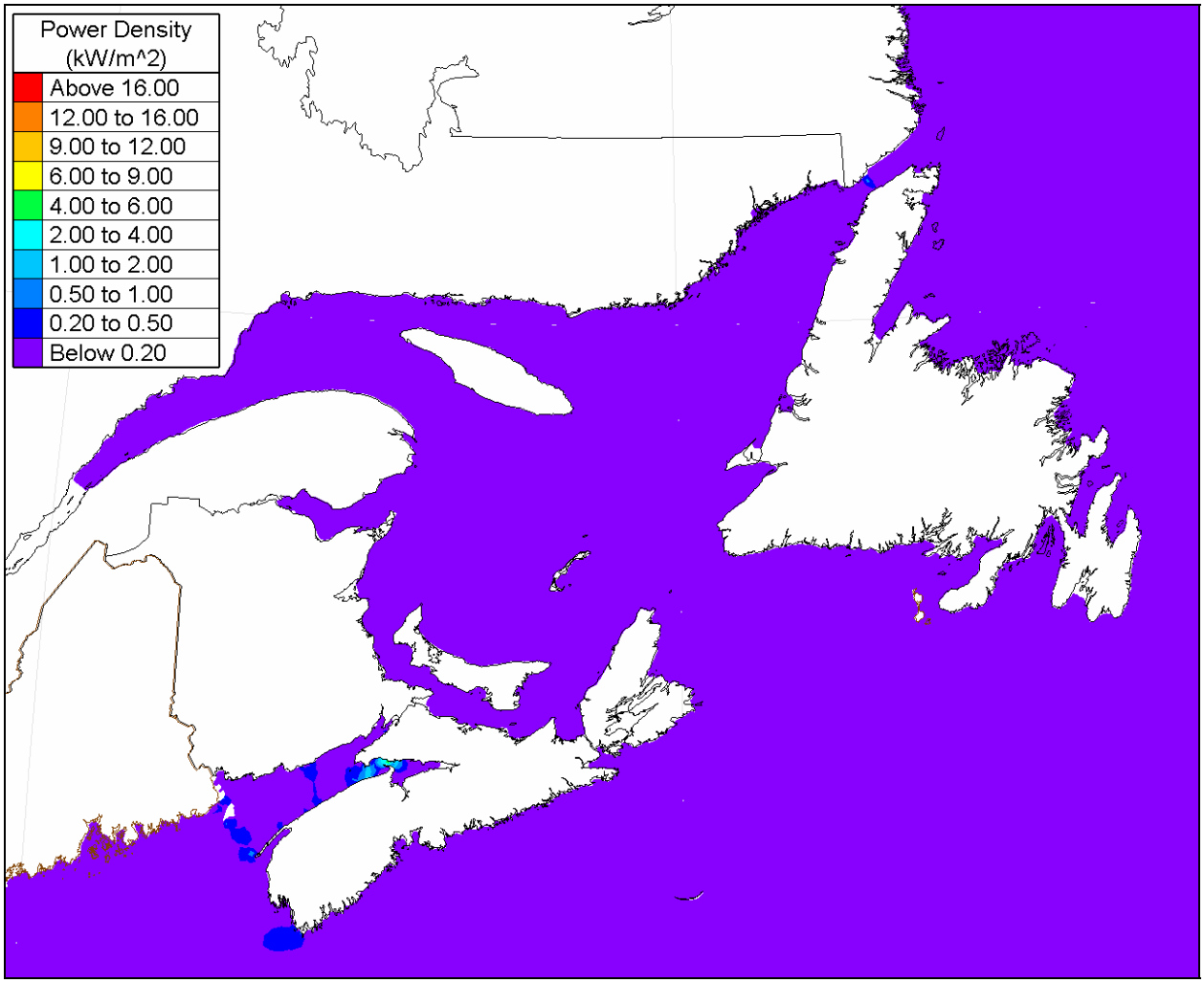


Figure 65. Mean power density, eastern Canada.

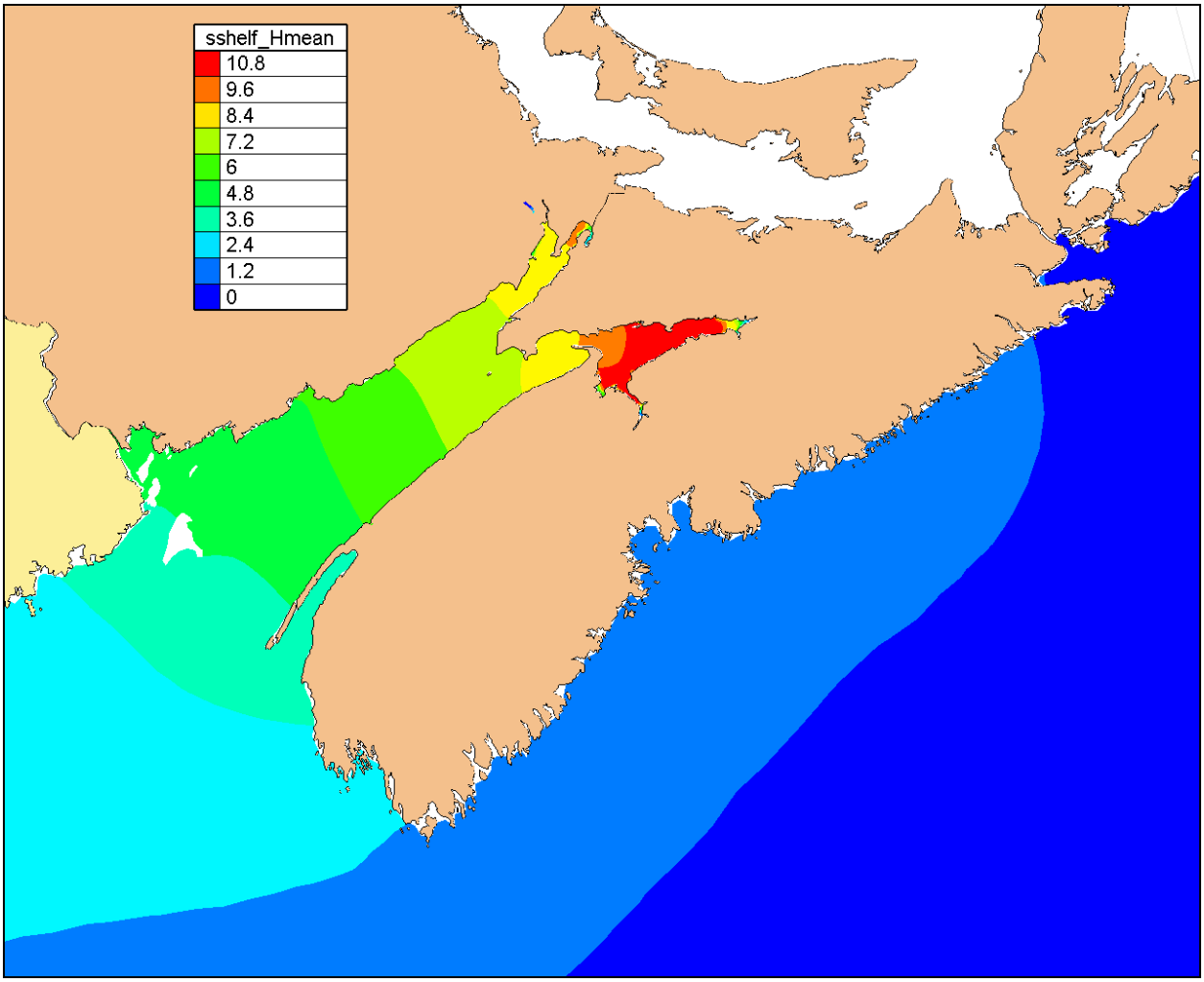


Figure 66. Mean tide range, Bay of Fundy and Scotian Shelf (m).

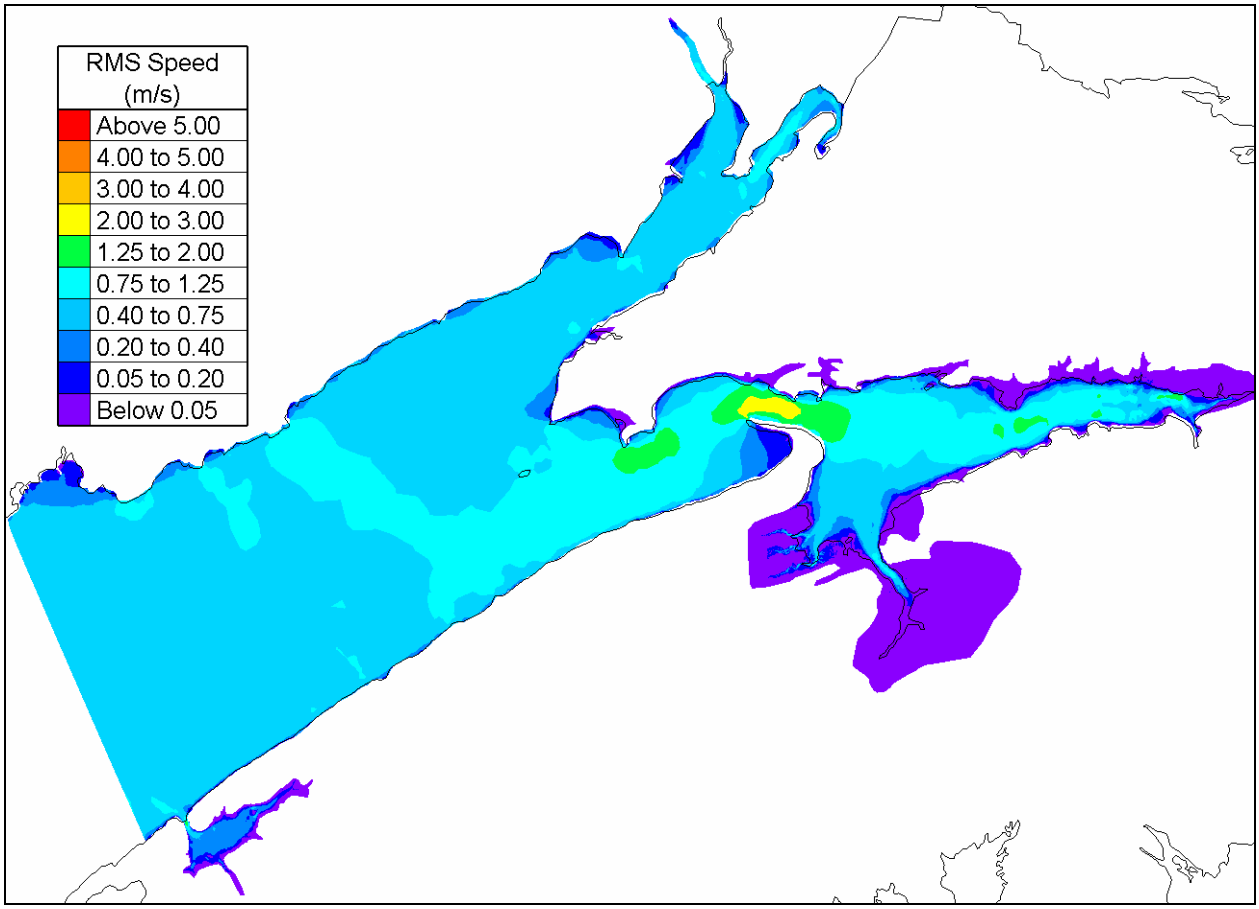


Figure 67. Root-mean-square tidal current speed, Bay of Fundy.

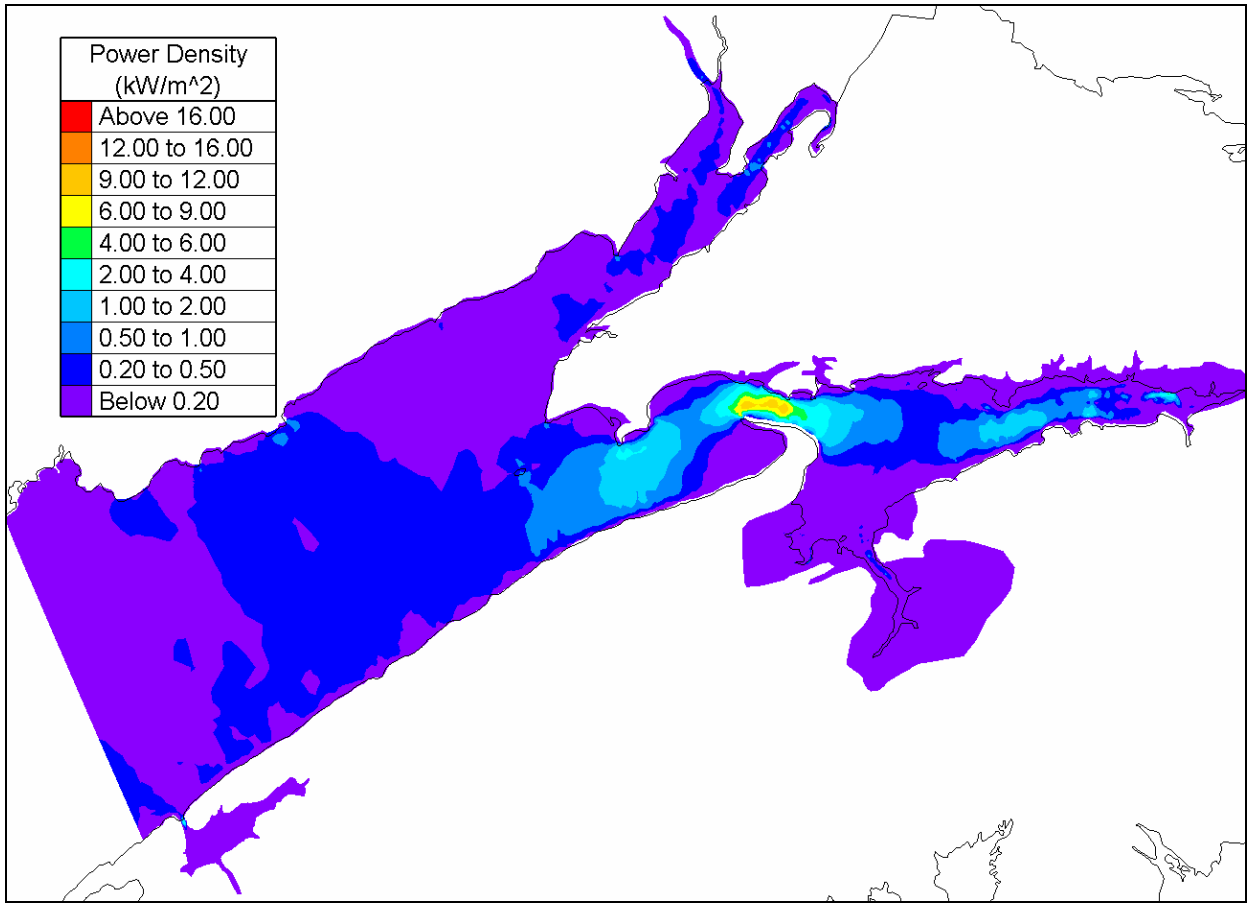


Figure 68. Mean power density, Bay of Fundy.

### *Arctic Ocean*

The mean tide range throughout Hudson Bay and the Arctic Archipelago is plotted in Figure 69 and Figure 70. RMS flow velocities throughout the region are plotted in Figure 71 to Figure 73. Finally, Figure 74 to Figure 75 show the mean power density of the flows in Hudson Bay and the Arctic Archipelago, as predicted by the tidal models discussed previously.

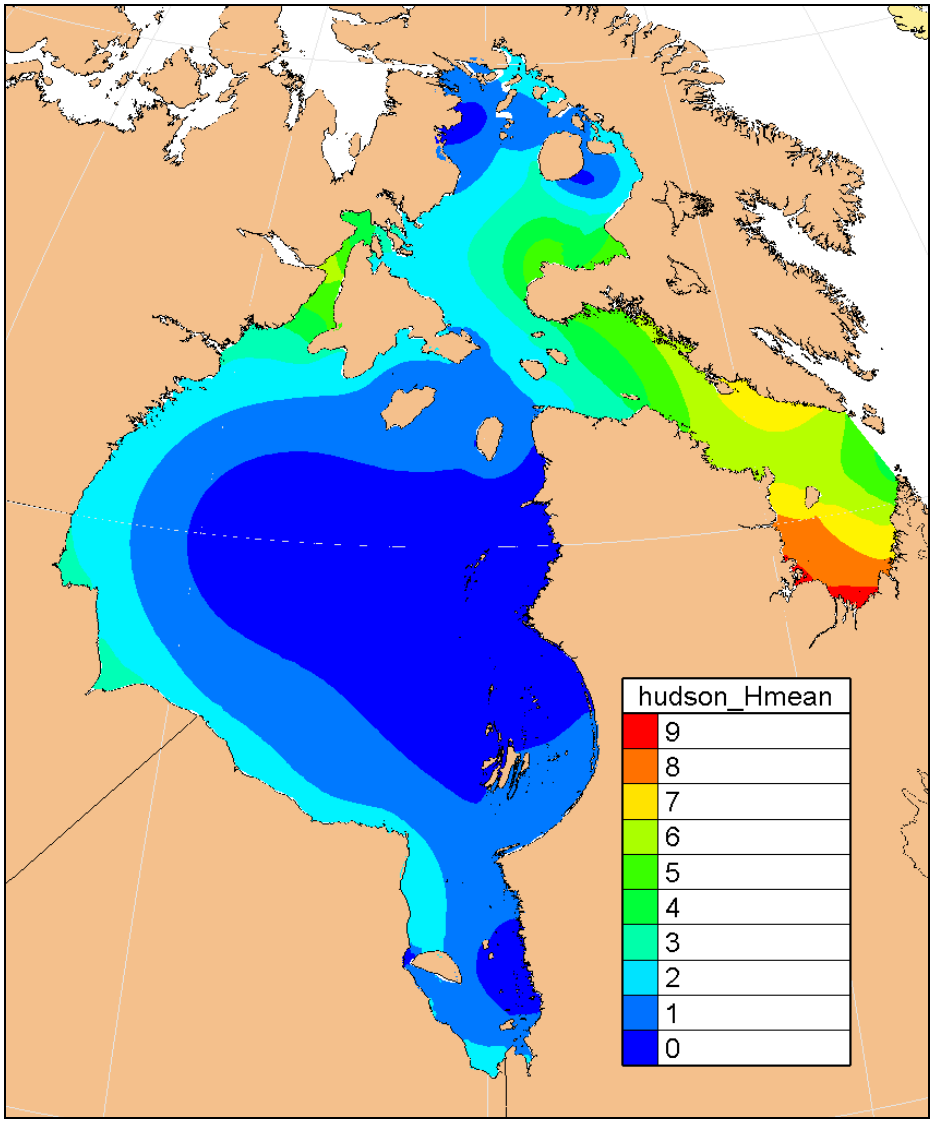


Figure 69. Mean tide range in Hudson Bay (m).

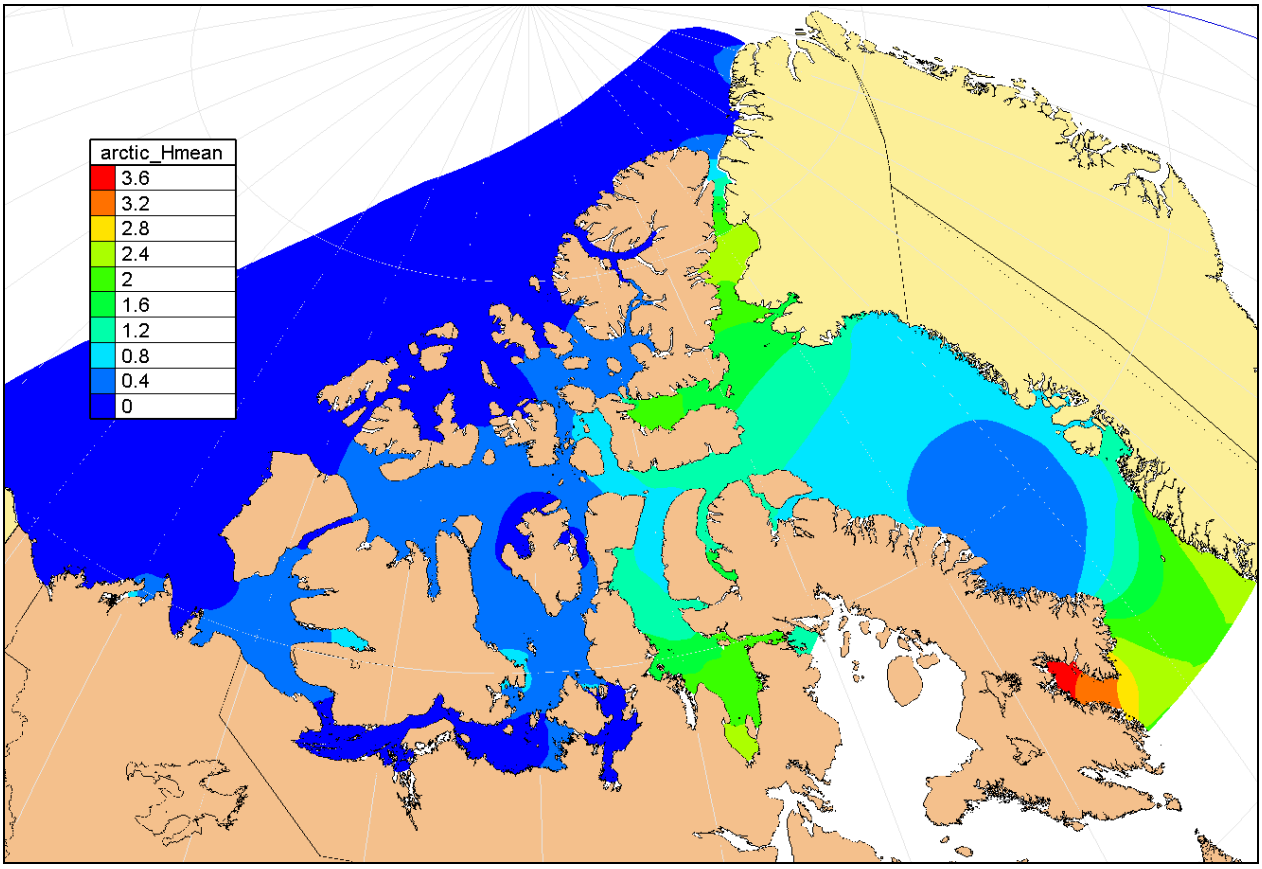


Figure 70. Mean tide range in the Arctic Archipelago (m).

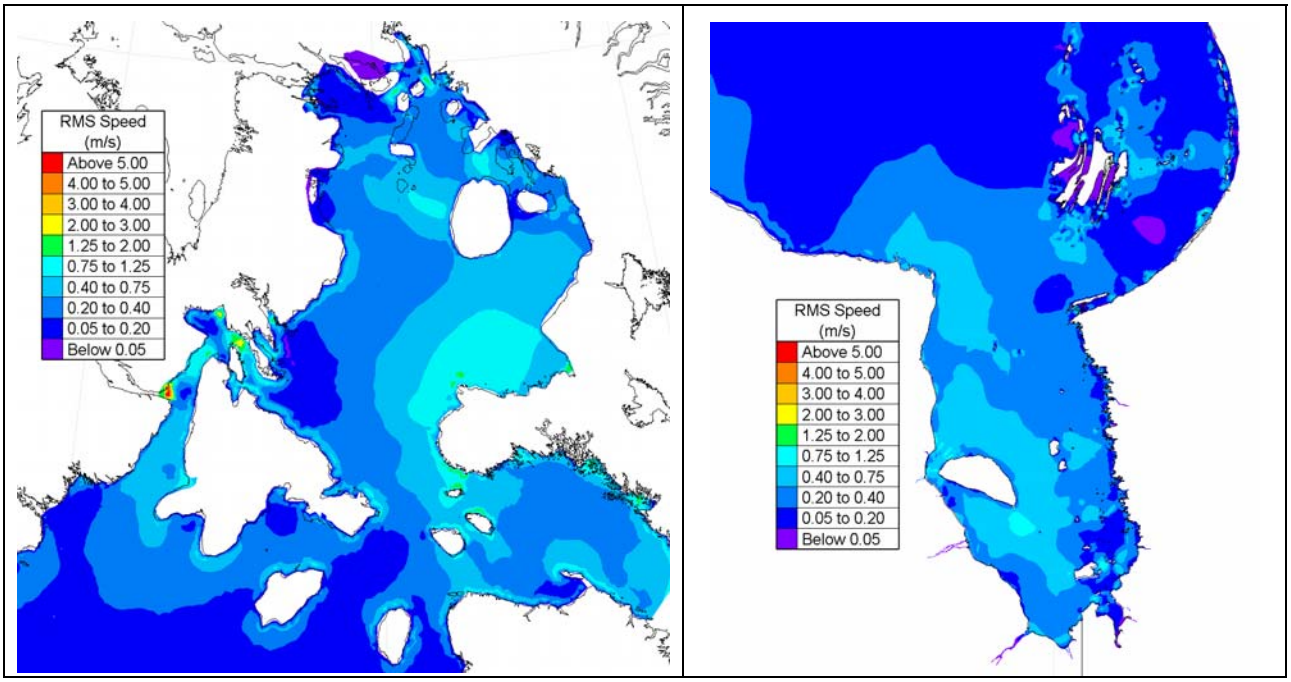


Figure 71. Root-mean-square tidal current speed, Hudson Bay.

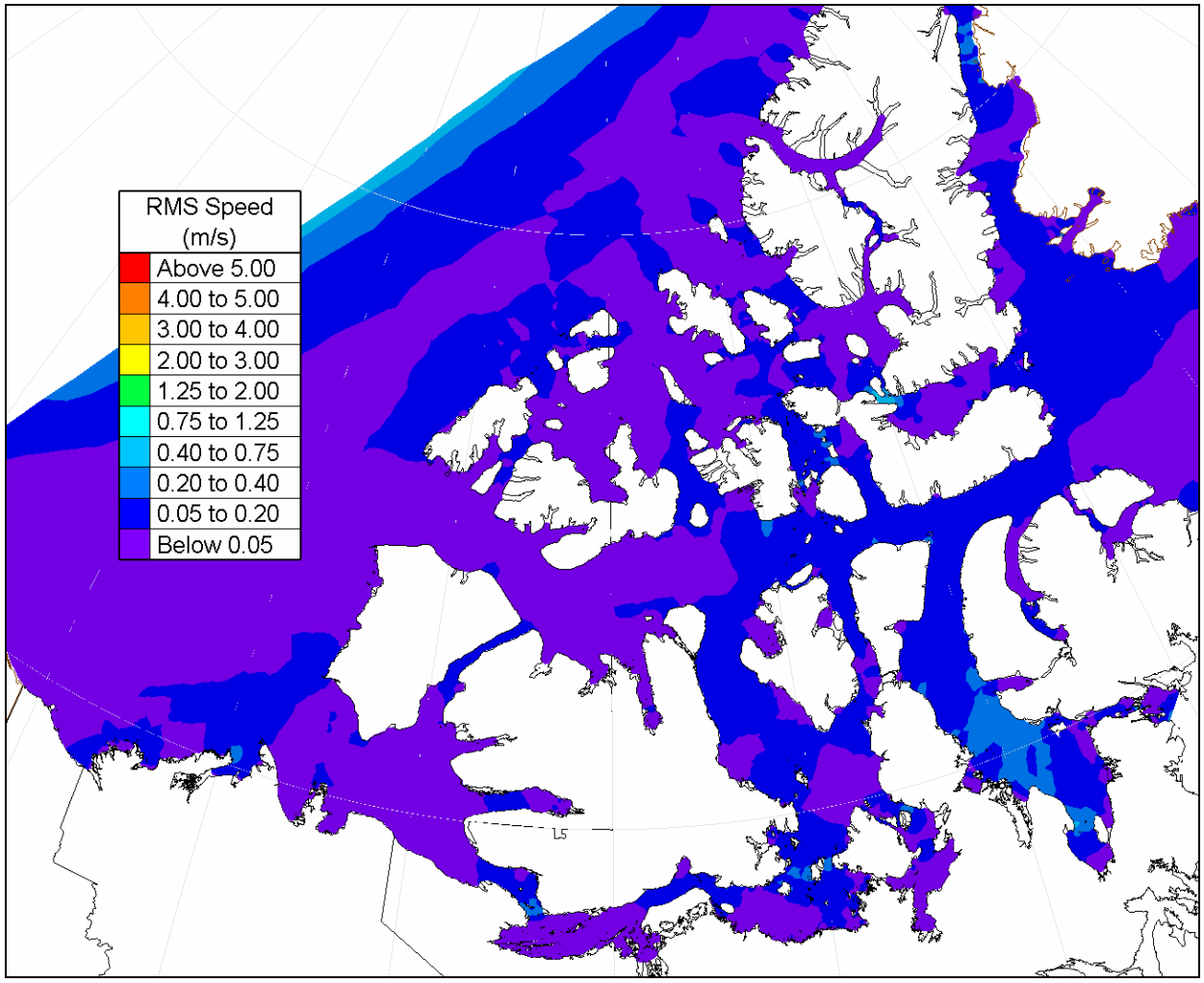


Figure 72. Root-mean-square tidal current speed, western Arctic.

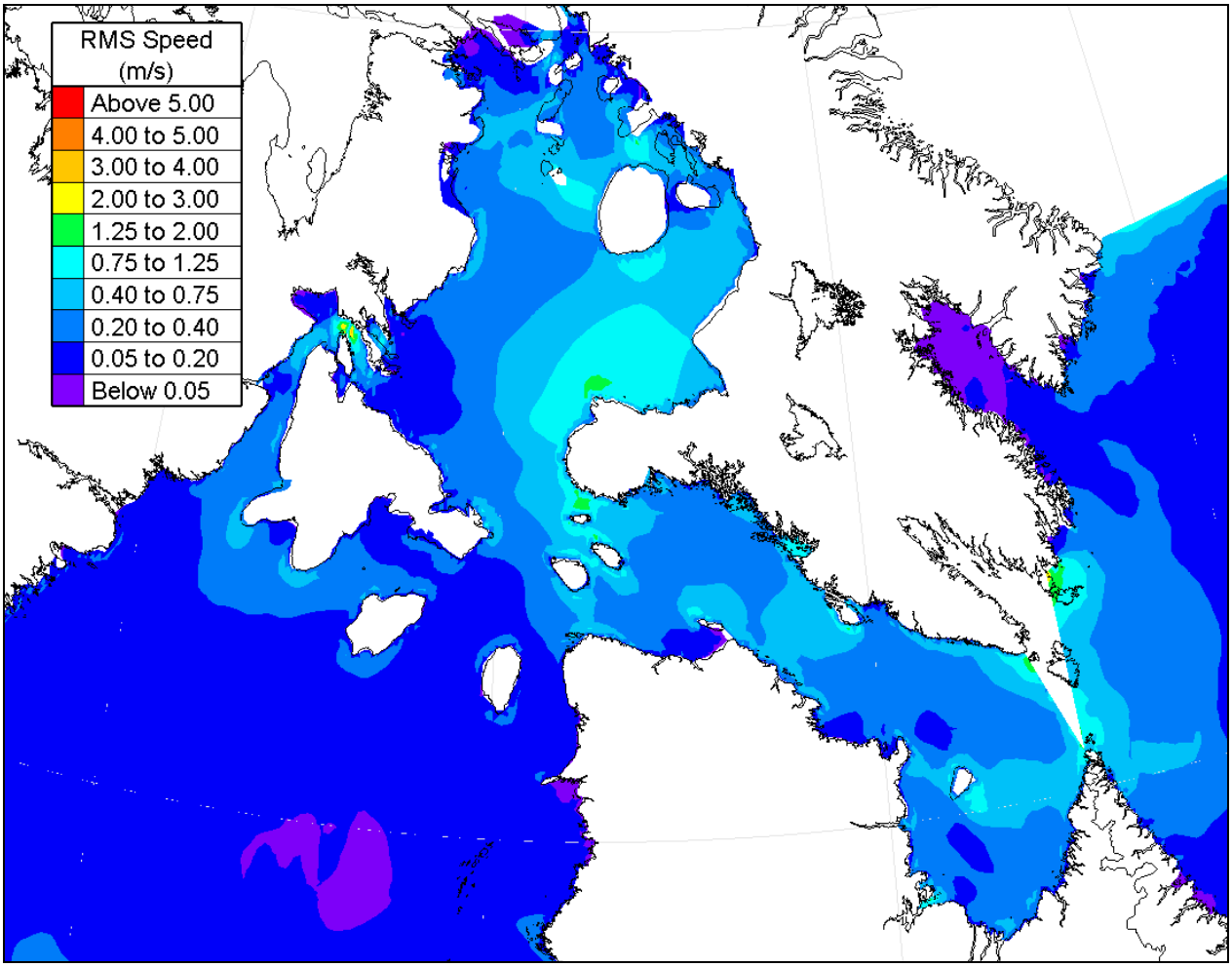


Figure 73. Root-mean-square tidal current speed, Hudson Bay and Hudson Strait.

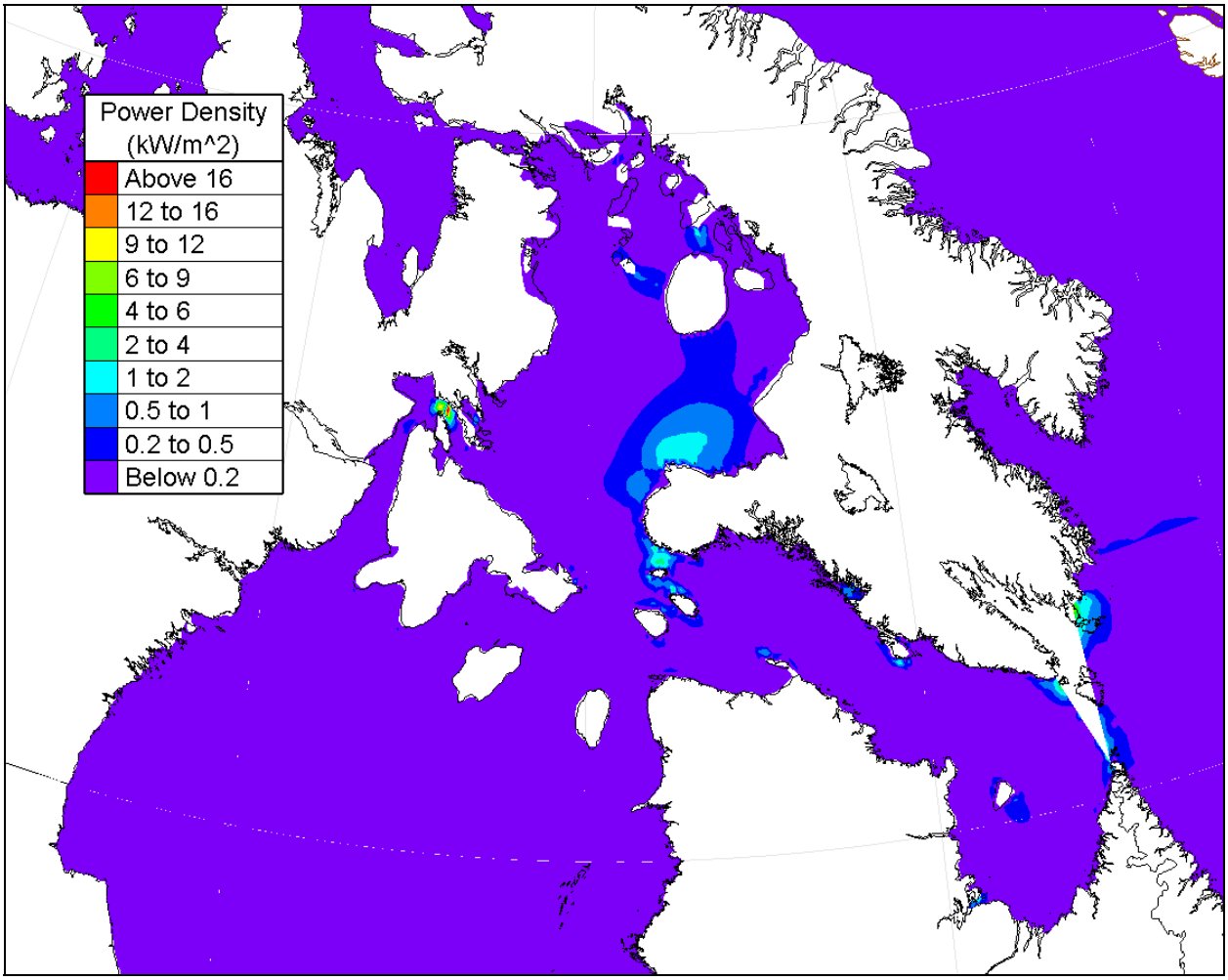


Figure 74. Mean power density, Hudson Bay and Hudson Strait.

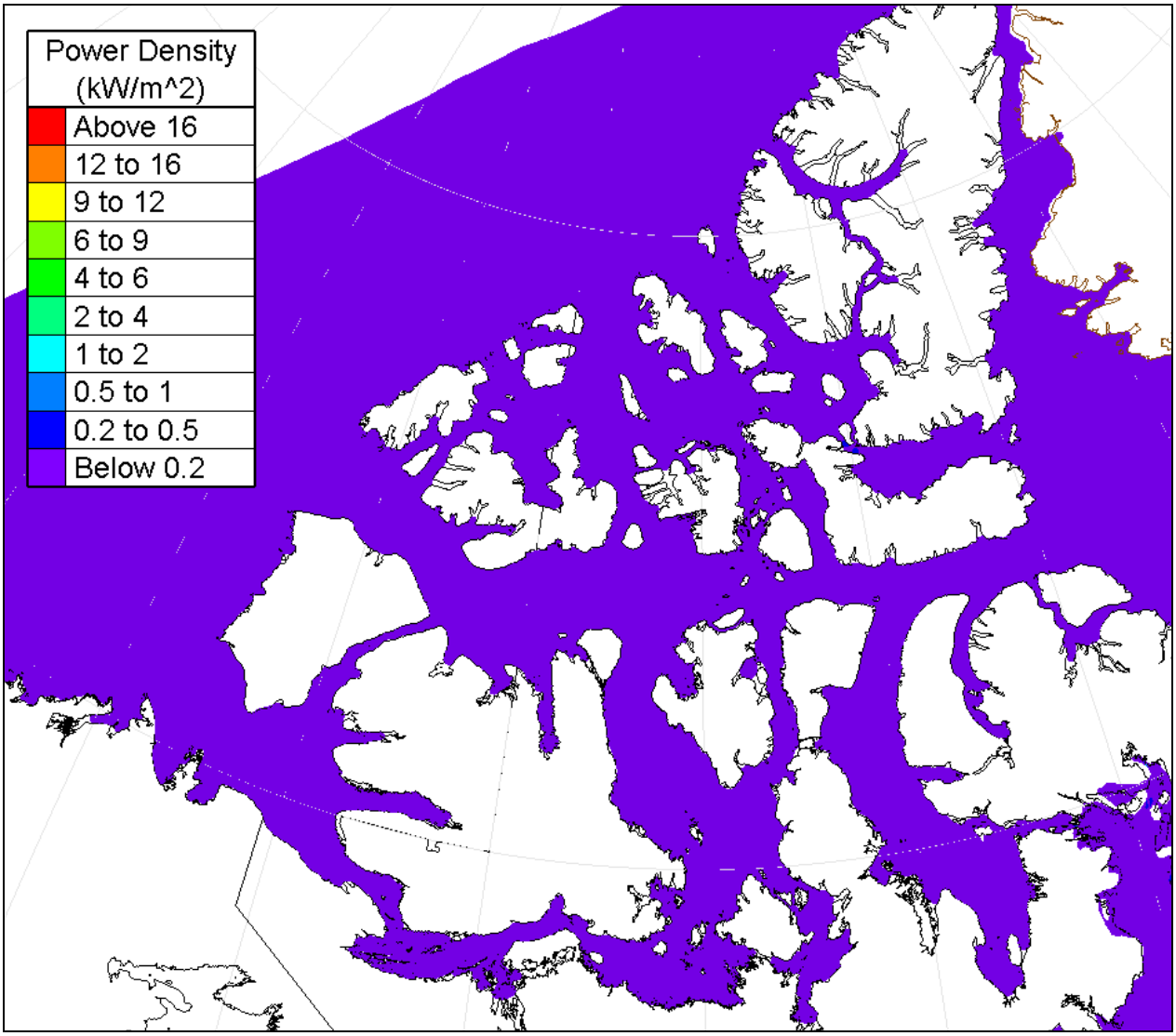


Figure 75. Mean power density, Arctic.

## *4.4. Site Identification and Resource Inventory*

Triton Consultants were commissioned to undertake an inventory of tidal current resources across Canada, using the methodology developed for their 2002 assessment of tidal current resources in British Columbia (Triton, 2002). A summary of their work is presented here for easy reference. Triton's complete report is presented as Annex A.

Before considering this study and its results, it is worth recalling that tidal currents vary rapidly with space and time. At most sites, the flow velocity goes to zero from two to four times per day, and reaches its peak annual value for only a few hours per year. The velocity fluctuation during each half cycle is roughly sinusoidal, but the peak speed varies from cycle to cycle as a consequence of the lunar and solar gravitational forcing. At most sites, the direction of flow also reverses between two and four times per day.

Tidal current resources are best characterized by the mean power, which represents an integration or averaging of these temporal fluctuations over time. The annual mean power is the average value of the instantaneous power throughout the year. Similarly, the mean power density is the average value of the instantaneous power density over time. The mean power density characterizes the average intensity of the flow at the site, while the mean power indicates the scale of the energy resource. Energy extraction will not be feasible if the power density is either too small (the flows are too weak for efficient operation of an energy conversion device) or too large (the flows are too strong for safe and efficient operation and maintenance).

It is important to note that the power values quoted in this report represent the energy resources available in tidal flows, and do not represent the economically realisable resources. For various reasons, only a small fraction of the available energy at any site can be extracted and converted into a more useful form. The recoverable resource will be limited by the following factors, among others:

- environmental and ecological considerations;
- adverse effects on tides and tidal currents;
- conflicting uses;
- the efficiency of the energy conversion device(s);
- economic factors;
- climate related factors (ice, climate change)

### 4.4.1. Methodology

Triton's method involves three steps:

- identifying passages and reaches with strong tidal currents;
- determining basic parameters for each site, including the passage width, average depth, and the maximum ebb and flood velocities during large tides; and
- estimating the annual mean power density and annual mean power from these basic parameters.

The inventory is based on a variety of data sources, including:

- Canadian *Sailing Directions* published by the Canadian Hydrographic Service (CHS);
- *Nautical Charts* and *Tide Books* issued by the CHS;
- Database of tide level and tidal current constituents developed by CHS; and
- Results from some of the numerical tidal models discussed in Section 4.3.1.

Triton examined a large number of publications, including roughly 700 nautical charts, 22 Sailing Directions, and 7 Tide and Current Tables.

At each potential site, the mean maximum depth averaged current speed ($U_{max}$) is estimated as

$$U_{\max} = 0.85\frac{V_f + V_e}{2} \tag{22}$$

where $V_f$ is the maximum speed at the surface in the passage during a large flood, $V_e$ is the maximum surface speed during a large ebb, and the factor 0.85 accounts for the lateral and vertical velocity variations across the channel. The annual mean power density is computed as

$$\overline{p} = \frac{2\rho}{3\pi} \frac{\left(a_f U_{\max}\right)^3 + \left(a_e U_{\max}\right)^3}{2} \tag{23}$$

Where $a_f U_{max}$ denotes the annual mean peak flood current velocity, and $a_e U_{max}$ denotes the annual mean of the current velocity at peak ebb. Triton assumed $a_f = 0.9$ and $a_e = 0.7$ at all locations except in British Columbia, where diurnal tidal currents are particularly strong. It was assumed that $a_e = 0.5$ for sites in southern B.C., and $a_e = 0.6$ for sites in northern B.C.. The annual mean power at the site was calculated according to

$$\overline{P} = w h_{ave} \overline{p} \tag{24}$$

where $w$ denotes the width of the passage and $h_{ave}$ is the average depth.

### 4.4.2. Results

A total of 260 potential sites were identified. Of these, 190 sites had potential mean power estimated to be greater that 1 MW. Table 10 shows the cumulative mean potential tidal current energy by Province and Territory. Nunavut has by far the greatest potential resource (30,567 MW), while British Columbia has the most sites greater than 1 MW (89 sites). Table 11 shows the distribution of mean potential power by region. Over 70% of the Canada's tidal current energy resources lie within Hudson Strait, which connects Hudson Bay with Baffin Bay and the Northwest Atlantic.

| Province | Potential Tidal Current Energy MW | Number of Sites | Average Size MW |
|---|---|---|---|
| Northwest Territories | 35 | 4 | 9 |
| British Columbia | 4,015 | 89 | 45 |
| Québec | 4,288 | 16 | 268 |
| Nunavut | 30,567 | 34 | 899 |
| New Brunswick | 636 | 14 | 45 |
| PEI | 33 | 4 | 8 |
| Nova Scotia | 2,122 | 15 | 141 |
| Newfoundland | 544 | 15 | 36 |
| TOTAL | 42,240 | 191 | 221 |

Table 10. Mean potential tidal current energy by Province and Territory.

| Region | Potential Tidal Current Energy MW | Number of Sites | Average Size MW |
|---|---|---|---|
| Vancouver Island Mainland | 3,580 | 62 | 58 |
| Pacific Mainland North | 353 | 18 | 20 |
| Queen Charlotte Islands | 81 | 9 | 9 |
| Arctic | 1,008 | 30 | 34 |
| Hudson Strait | 29,595 | 8 | 3,699 |
| Ungava | 4,112 | 10 | 411 |
| St. Lawrence River | 153 | 4 | 38 |
| Gulf of St Lawrence | 537 | 15 | 36 |
| Atlantic North | 65 | 6 | 11 |
| Atlantic South | 30 | 8 | 4 |
| Bay of Fundy | 2,725 | 21 | 130 |
| TOTAL | 42,240 | 191 | 221 |

Table 11. Mean potential tidal current energy by region.

All sites in southern and northern British Columbia with mean power greater than 1 MW are summarized in Table 12 and Table 13 respectively. Table 14 lists the sites in the Northwest Territories; Table 15 shows the sites in Nunavut; Table 16 shows the sites in Québec; Table 17 shows the sites in Newfoundland and Labrador; while Table 18, Table 19, and Table 20 list the sites in Nova Scotia, Prince Edward Island and in New Brunswick.

The leading tidal current energy sites across Canada are also mapped in Figure 76. Figure 77 , Figure 78 and Figure 79 show detailed views of this map, centred on the Pacific coast, the Arctic Archipelago, and the Atlantic coast, respectively. In these maps, the size and colour of the circles are scaled and shaded in proportion to the mean potential power of each site.

This inventory, while likely not fully comprehensive, represents the best possible pan-Canadian assessment that could be made considering the level of funding, the available information, and the vast extent of Canada's coastal waters. Despite best efforts, it is entirely possible that some good potential sites have been missed. Hence, this inventory should be considered as a lower bound estimate to both the number of sites and the total tidal stream energy resource.

| Site Name | Latitude | Longitude | Maximum Current Speed Flood | Maximum Current Speed Ebb | Mean Maximum Depth Average Current Speed | Mean Power Density | Width of Passage | Average Depth of Passage | Flow Cross-sectional Area | Mean Potential Power |
|---|---|---|---|---|---|---|---|---|---|---|
| | deg | deg | knot | m/s | m/s | kW/m$^2$ | m | m | m$^2$ | MW |
| Seymour Narrows | 50.13 | -125.35 | 16 | 14 | 6.56 | 18.16 | 769 | 41 | 33,331 | 786 |
| N. Boundary Passage | 48.79 | -123.01 | 4 | 4 | 1.75 | 0.50 | 5,158 | 140 | 734,949 | 366 |
| Discovery Pass. S. | 50.00 | -125.21 | 7 | 7 | 3.06 | 3.68 | 1,459 | 42 | 65,626 | 327 |
| Boundary passage | 48.69 | -123.27 | 3.5 | 3.5 | 1.53 | 0.33 | 4,472 | 175 | 793,760 | 265 |
| Current Passage 2 | 50.39 | -125.86 | 6 | 6 | 2.63 | 1.68 | 1,502 | 80 | 123,931 | 208 |
| Weyton Passage | 50.59 | -126.82 | 6 | 6 | 2.63 | 1.68 | 1,535 | 75 | 118,985 | 200 |
| Current Passage 1 | 50.41 | -125.87 | 5 | 5 | 2.19 | 0.97 | 1,398 | 100 | 143,331 | 139 |
| Dent Rapids | 50.41 | -125.21 | 11 | 8 | 4.16 | 6.67 | 420 | 45 | 19,955 | 133 |
| South Pender Is | 48.72 | -123.19 | 4 | 4 | 1.75 | 0.50 | 1,985 | 100 | 203,416 | 101 |
| Yaculta Rapids | 50.38 | -125.15 | 10 | 10 | 4.38 | 7.78 | 539 | 20 | 12,135 | 94 |
| Arran Rapids | 50.42 | -125.14 | 14 | 10 | 5.25 | 13.45 | 271 | 22 | 6,629 | 89 |
| Secheldt Rapids 2 | 49.74 | -123.90 | 14.5 | 16 | 6.67 | 27.60 | 261 | 8 | 2,739 | 76 |
| Gillard Passage 1 | 50.39 | -125.16 | 13 | 10 | 5.03 | 11.84 | 237 | 16 | 4,393 | 52 |
| Scott Channel | 50.79 | -128.50 | 3 | 3 | 1.31 | 0.21 | 9,970 | 22 | 244,256 | 51 |
| Active Pass | 48.86 | -123.33 | 8 | 8 | 3.50 | 3.98 | 561 | 20 | 12,628 | 50 |
| Nahwitti Bar 1 | 50.89 | -127.99 | 5.5 | 5.5 | 2.41 | 1.29 | 2,993 | 9 | 34,417 | 45 |
| Race Passage | 48.31 | -123.54 | 6 | 7 | 2.84 | 2.14 | 884 | 20 | 19,885 | 42 |
| Green Pt 2 | 50.45 | -125.52 | 6 | 6 | 2.63 | 1.68 | 538 | 35 | 20,157 | 34 |
| Blackney Passage | 50.57 | -126.69 | 5 | 5 | 2.19 | 0.97 | 814 | 40 | 34,598 | 34 |
| GreenPt Rap. 1 | 50.44 | -125.51 | 7 | 7 | 3.06 | 2.67 | 440 | 25 | 12,093 | 32 |
| Porlier Pass | 49.01 | -123.59 | 9 | 8 | 3.72 | 4.78 | 339 | 15 | 5,926 | 28 |
| Becher Bay | 48.32 | -123.62 | 3 | 3 | 1.31 | 0.21 | 2,148 | 60 | 134,263 | 28 |
| Upper rapids 2 | 50.31 | -125.23 | 9 | 9 | 3.94 | 5.67 | 242 | 18 | 4,955 | 28 |
| Gillard Passage 2 | 50.40 | -125.15 | 10 | 8 | 3.94 | 5.67 | 393 | 10 | 4,916 | 28 |
| Whirlpool Rapids | 50.46 | -125.76 | 7 | 7 | 3.06 | 2.67 | 321 | 28 | 9,804 | 26 |
| Surge Narrows | 50.23 | -125.16 | 6 | 6 | 2.63 | 1.68 | 413 | 30 | 13,432 | 23 |
| Chatham Islands | 48.45 | -123.26 | 6 | 6 | 2.63 | 1.68 | 903 | 12 | 13,099 | 22 |
| Quatsino Narrows | 50.55 | -127.56 | 9 | 8 | 3.72 | 4.78 | 207 | 18 | 4,240 | 20 |
| Hole-in-the-Wall 1 | 50.30 | -125.21 | 12 | 9.5 | 4.70 | 9.67 | 189 | 8 | 1,985 | 19 |
| Village Island | 50.64 | -126.51 | 3 | 3 | 1.31 | 0.21 | 1,234 | 70 | 89,461 | 19 |
| Green Pt 3 | 50.44 | -125.57 | 5 | 5 | 2.19 | 0.97 | 673 | 25 | 18,498 | 18 |
| Nahwitti Bar 2 | 50.87 | -127.99 | 5.5 | 5.5 | 2.41 | 1.29 | 2,012 | 4 | 13,078 | 17 |
| First Narrows | 49.32 | -123.14 | 6 | 6 | 2.63 | 1.68 | 418 | 16 | 7,734 | 13 |
| Buckholtz Ch 2 | 50.49 | -127.60 | 3 | 3 | 1.31 | 0.21 | 1,073 | 50 | 56,329 | 12 |
| Buckholtz Ch 1 | 50.49 | -127.67 | 3 | 3 | 1.31 | 0.21 | 997 | 50 | 52,357 | 11 |
| Tallac - Erasmus Is | 50.44 | -125.47 | 3 | 3 | 1.31 | 0.21 | 665 | 75 | 51,522 | 11 |
| Lower Rapids 1 | 50.31 | -125.26 | 7 | 7 | 3.06 | 2.67 | 371 | 8 | 3,891 | 10 |
| Picton Point | 50.46 | -125.40 | 3 | 3 | 1.31 | 0.21 | 881 | 50 | 46,235 | 10 |
| Charles Bay Rapids | 50.42 | -125.49 | 5 | 5 | 2.19 | 0.97 | 664 | 12 | 9,631 | 9 |
| Pearse Passage | 50.58 | -126.90 | 4 | 4 | 1.75 | 0.50 | 1,168 | 13 | 18,104 | 9 |
| Welcome Passage | 49.51 | -123.97 | 3 | 3 | 1.31 | 0.21 | 746 | 50 | 39,189 | 8 |
| Alert Bay | 50.57 | -126.93 | 3 | 3 | 1.31 | 0.21 | 1,771 | 18 | 36,311 | 8 |
| Gabriola Pass. | 49.13 | -123.70 | 8.5 | 9 | 3.83 | 5.21 | 137 | 8 | 1,435 | 7 |

| Site Name | Latitude | Longitude | Maximum Current Speed Flood | Maximum Current Speed Ebb | Mean Maximum Depth Average Current Speed | Mean Power Density | Width of Passage | Average Depth of Passage | Flow Cross-sectional Area | Mean Potential Power |
|---|---|---|---|---|---|---|---|---|---|---|
| | deg | deg | knot | m/s | m/s | kW/m$^2$ | m | m | m$^2$ | MW |
| Second Narrows | 49.29 | -123.02 | 6 | 6 | 2.63 | 1.68 | 254 | 14 | 4,159 | 7 |
| Haddington Passage 2 | 50.59 | -127.02 | 3 | 3 | 1.31 | 0.21 | 1,311 | 20 | 29,492 | 6 |
| Moresby Passage | 48.73 | -123.34 | 3 | 3 | 1.31 | 0.21 | 1,191 | 20 | 26,793 | 6 |
| Nitinat Narrows | 48.67 | -124.85 | 8 | 8 | 3.50 | 3.98 | 61 | 20 | 1,376 | 5 |
| Stuart Narrows | 50.90 | -126.94 | 6 | 7 | 2.84 | 2.14 | 261 | 7 | 2,478 | 5 |
| Hamber Island | 49.32 | -122.94 | 4 | 4 | 1.75 | 0.50 | 414 | 23 | 10,362 | 5 |
| Dodds Narrows | 49.14 | -123.82 | 9 | 8 | 3.72 | 4.78 | 91 | 9 | 1,047 | 5 |
| Sansum Narrows | 48.78 | -123.56 | 3 | 3 | 1.31 | 0.21 | 553 | 40 | 23,509 | 5 |
| Gillard Passage 3 | 50.39 | -125.16 | 10 | 8 | 3.94 | 5.67 | 92 | 5 | 686 | 4 |
| Haddington Passage 1 | 50.61 | -127.02 | 3 | 3 | 1.31 | 0.21 | 570 | 25 | 15,684 | 3 |
| Matlset Narrowsq | 49.24 | -125.80 | 4 | 4 | 1.75 | 0.50 | 464 | 10 | 5,799 | 3 |
| Tsownin Narrows | 49.78 | -126.65 | 3 | 3 | 1.31 | 0.21 | 283 | 45 | 13,460 | 3 |
| Hayden Passage | 49.40 | -126.11 | 4 | 4 | 1.75 | 0.50 | 312 | 15 | 5,457 | 3 |
| N Sydney Is | 48.67 | -123.35 | 3 | 3 | 1.31 | 0.21 | 1,029 | 9 | 11,833 | 2 |
| Scouler Pass | 50.31 | -127.82 | 4 | 4 | 1.75 | 0.50 | 512 | 4 | 3,327 | 2 |
| Dawley Passage | 49.15 | -125.79 | 3 | 3 | 1.31 | 0.21 | 289 | 20 | 6,509 | 1 |
| Neilson Is - Morpheus | 49.16 | -125.88 | 5 | 5 | 2.19 | 0.97 | 202 | 4 | 1,311 | 1 |
| Tsapee Narrows | 49.12 | -125.82 | 4 | 4 | 1.75 | 0.50 | 280 | 7 | 2,517 | 1 |
| Felice Is - Grice Pt | 49.15 | -125.91 | 3 | 3 | 1.31 | 0.21 | 339 | 12 | 4,915 | 1 |
| | | | | | | | | | Total: | 3,580 |

Table 12. Tidal current power sites in southern British Columbia.

| Site Name | Latitude | Longitude | Maximum Current Speed Flood | Maximum Current Speed Ebb | Mean Maximum Depth Average Current Speed | Mean Power Density | Width of Passage | Average Depth of Passage | Flow Cross-sectional Area | Mean Potential Power |
|---|---|---|---|---|---|---|---|---|---|---|
| | deg | deg | knot | m/s | m/s | kW/m$^2$ | m | m | m$^2$ | MW |
| Nakwakto Rapids | 51.10 | -127.50 | 14 | 16 | 6.56 | 29.06 | 434 | 10 | 5,643 | 164 |
| Otter Passage | 53.00 | -129.73 | 6 | 6 | 2.63 | 1.86 | 620 | 50 | 32,860 | 61 |
| Beaver Passage | 53.73 | -130.37 | 4 | 4 | 1.75 | 0.55 | 810 | 100 | 83,430 | 46 |
| Outer Narrows | 51.09 | -127.63 | 7 | 10 | 3.72 | 5.29 | 210 | 17 | 4,206 | 22 |
| Perceval Narrows | 52.33 | -128.38 | 5 | 5 | 2.19 | 1.08 | 382 | 25 | 10,709 | 12 |
| Hiekish Narrows | 52.88 | -128.49 | 4 | 4.5 | 1.86 | 0.66 | 571 | 25 | 16,000 | 11 |
| Draney Narrows` | 51.47 | -127.56 | 9 | 9 | 3.94 | 6.28 | 139 | 8 | 1,463 | 9 |
| Kildidt Narrows | 51.89 | -128.11 | 12 | 12 | 5.25 | 14.88 | 75 | 2 | 375 | 6 |
| Hidden Inlet | 54.95 | -130.33 | 9 | 9 | 3.94 | 6.28 | 142 | 3 | 781 | 5 |
| Porcher Narrows | 53.90 | -130.47 | 7 | 7 | 3.06 | 2.95 | 120 | 10 | 1,560 | 5 |
| Freeman Passage | 53.85 | -130.58 | 4 | 4 | 1.75 | 0.55 | 150 | 32 | 5,250 | 3 |
| Tuck Narrows | 54.40 | -130.26 | 6 | 6 | 2.63 | 1.86 | 138 | 7 | 1,379 | 3 |
| Eclipse Narrows | 51.09 | -126.77 | 6 | 5 | 2.41 | 1.43 | 141 | 6 | 1,269 | 2 |
| Clement Rapids | 53.20 | -129.04 | 6 | 6 | 2.63 | 1.86 | 80 | 7 | 800 | 1 |
| Schooner Channel | 51.06 | -127.52 | 6 | 6.5 | 2.73 | 2.10 | 72 | 6 | 648 | 1 |
| Hawkins Narrows | 53.41 | -129.42 | 8 | 8 | 3.50 | 4.41 | 55 | 3 | 301 | 1 |
| Higgins Passage 2 | 52.48 | -128.71 | 5 | 5 | 2.19 | 1.08 | 173 | 3 | 1,039 | 1 |
| Nelson Narrows 1 | 51.77 | -127.43 | 3.5 | 3.5 | 1.53 | 0.37 | 313 | 6 | 2,817 | 1 |
| Masset Sound | 53.98 | -132.00 | 5 | 5.5 | 2.30 | 1.25 | 750 | 20 | 17,250 | 21 |
| Rose Spit | 54.25 | -131.52 | 2.5 | 2.5 | 1.09 | 0.13 | 11,000 | 8 | 121,000 | 16 |
| Houston Stewart Channe | 52.16 | -131.12 | 5 | 5 | 2.19 | 1.08 | 610 | 17 | 12,200 | 13 |
| Parry Passage | 54.18 | -133.00 | 5 | 3 | 1.75 | 0.55 | 594 | 28 | 18,414 | 10 |
| Skidigate Entrance | 53.36 | -131.90 | 3 | 3 | 1.31 | 0.23 | 1,322 | 30 | 43,626 | 10 |
| Fairbairn Channel | 53.04 | -131.68 | 3 | 3 | 1.31 | 0.23 | 710 | 25 | 19,880 | 5 |
| Skuttle Passage | 52.66 | -131.68 | 2 | 3 | 1.09 | 0.13 | 510 | 45 | 24,480 | 3 |
| Alexandra Narrows | 54.05 | -132.57 | 2 | 2.5 | 0.98 | 0.10 | 420 | 25 | 11,760 | 1 |
| Tasu Narrows | 52.74 | -132.11 | 1.5 | 1.5 | 0.66 | 0.03 | 425 | 82 | 36,125 | 1 |
| | | | | | | | | | Total: | 434 |

Table 13. Tidal current power sites in northern British Columbia.

| Site Name | Latitude | Longitude | Maximum Current Speed Flood | Maximum Current Speed Ebb | Mean Maximum Depth Average Current Speed | Mean Power Density | Width of Passage | Average Depth of Passage | Flow Cross-sectional Area | Mean Potential Power |
|---|---|---|---|---|---|---|---|---|---|---|
| | deg | deg | knot | m/s | m/s | $kW/m^2$ | m | m | $m^2$ | MW |
| Cape Parry | 70.27 | -124.78 | 4 | 4 | 1.75 | 0.63 | 2,000 | 10 | 20,800 | 13 |
| Pearce Point | 69.83 | -122.69 | 4 | 4 | 1.75 | 0.63 | 2,000 | 10 | 20,800 | 13 |
| Cape Kellet | 71.98 | -126.13 | 2.5 | 2.5 | 1.09 | 0.15 | 2,000 | 20 | 40,800 | 6 |
| Observation Point | 70.66 | -128.27 | 2.5 | 2.5 | 1.09 | 0.15 | 2,000 | 10 | 20,800 | 3 |
| Cape Parry | 70.27 | -124.78 | 4 | 4 | 1.75 | 0.63 | 2,000 | 10 | 20,800 | 13 |
| | | | | | | | | | Total: | 35 |

Table 14. Tidal current power sites in the Northwest Territories.

| Site Name | Latitude | Longitude | Maximum Current Speed Flood | Maximum Current Speed Ebb | Mean Maximum Depth Average Current Speed | Mean Power Density | Width of Passage | Average Depth of Passage | Flow Cross-sectional Area | Mean Potential Power |
|---|---|---|---|---|---|---|---|---|---|---|
| | deg | deg | knot | m/s | m/s | kW/m$^2$ | m | m | m$^2$ | MW |
| Gray Strait | 60.54 | -64.69 | 6 | 6 | 2.63 | 2.11 | 6,000 | 550 | 3,307,800 | 6,979 |
| Lacy/Lawson Islands | 60.60 | -64.62 | 7 | 7 | 3.06 | 3.35 | 2,750 | 80 | 223,575 | 749 |
| McLelan Strait | 60.35 | -64.63 | 7 | 7 | 3.06 | 3.35 | 200 | 8 | 1,880 | 6 |
| Mill Isl.-Salisbury Isl. | 63.81 | -77.50 | 8 | 8 | - | 0.89 | 32,054 | 204 | 6,571,070 | 10,426 |
| Mill Island-Baffin Island | 64.15 | -77.57 | 8 | 8 | - | 1.02 | 26,125 | 229 | 6,008,750 | 7,584 |
| Nottingham Isl.-Ungava | 62.83 | -77.93 | 8 | 8 | - | 0.14 | 64,098 | 228 | 14,678,442 | 1,972 |
| Salisbury Isl.-Nottingham Isl. | 63.45 | -77.41 | 8 | 8 | - | 0.36 | 22,146 | 147 | 3,277,608 | 1,704 |
| Cape Enouolik | 64.95 | -78.33 | 5 | 5 | 2.19 | 1.22 | 5,000 | 25 | 142,500 | 174 |
| Labrador Narrows | 69.71 | -82.59 | 6 | 6 | 2.63 | 2.11 | 1,500 | 100 | 151,950 | 321 |
| Bellot Strait | 72.00 | -94.48 | 8 | 8 | 3.50 | 5.00 | 1,000 | 16 | 16,400 | 82 |
| Cache Pt Channel | 68.62 | -113.55 | 5 | 5 | 2.19 | 1.22 | 6,000 | 10 | 62,400 | 76 |
| James Ross Strait | 66.69 | -95.87 | 5 | 5 | 2.19 | 1.22 | 5,900 | 10 | 61,360 | 75 |
| Egg Island | 68.55 | -97.40 | 7 | 7 | 3.06 | 3.35 | 750 | 25 | 19,050 | 64 |
| Seahorse Point | 63.83 | -80.13 | 5 | 5 | 2.19 | 1.22 | 2,000 | 20 | 40,800 | 50 |
| Nettliling Fiord | 66.72 | -72.83 | 8 | 8 | 3.50 | 5.00 | 1,700 | 5 | 9,180 | 46 |
| Cardigan Strait | 76.51 | -90.30 | 3.5 | 3.5 | 1.53 | 0.42 | 6,000 | 15 | 92,400 | 39 |
| Hells Gate | 76.54 | -89.66 | 3.5 | 3.5 | 1.53 | 0.42 | 5,500 | 15 | 84,700 | 35 |
| Hurd Channel | 66.15 | -84.42 | 6 | 6 | 2.63 | 2.11 | 2,000 | 8 | 16,800 | 35 |
| Barrow Strait | 74.44 | -92.87 | 2 | 2 | 0.88 | 0.08 | 20,000 | 20 | 408,000 | 32 |
| Bathhurst Inlet | 67.31 | -107.88 | 5 | 5 | 2.19 | 1.22 | 2,000 | 10 | 20,800 | 25 |
| Spence Bay | 69.42 | 93.83 | 4 | 5 | 1.97 | 0.89 | 2,300 | 10 | 23,920 | 21 |
| Clifton Point | 69.22 | -118.62 | 4 | 4 | 1.75 | 0.63 | 2,000 | 10 | 20,800 | 13 |
| Sherman Inlet | 68.12 | -98.55 | 5 | 5 | 2.19 | 1.22 | 1,850 | 5 | 9,990 | 12 |
| Flagler Bay | 79.10 | -75.96 | 4 | 4 | 1.75 | 0.63 | 1,500 | 8 | 12,600 | 8 |
| Edinburgh Channel | 68.47 | -111.09 | 3 | 3 | 1.31 | 0.26 | 2,000 | 10 | 20,800 | 5 |
| Franklin Lake | 66.94 | -95.34 | 5 | 5 | 2.19 | 1.22 | 800 | 5 | 4,320 | 5 |
| Gibson's Cove | 65.27 | -75.92 | 6 | 6 | 2.63 | 2.11 | 430 | 5 | 2,322 | 5 |
| Cape Dorchester | 65.50 | -77.37 | 6 | 6 | 2.63 | 2.11 | 400 | 5 | 2,160 | 5 |
| Wager Bay Narrows | 65.31 | -87.74 | 6 | 7 | 2.84 | 2.68 | 3,600 | | 1,440 | 4 |
| Resolute Bay | 74.54 | -94.91 | 3 | 3 | 1.31 | 0.26 | 1,500 | 8 | 12,600 | 3 |
| Stormness Bay | 68.86 | -102.61 | 5 | 5 | 2.19 | 1.22 | 250 | 10 | 2,600 | 3 |
| Durban Harbour | 67.06 | -62.17 | 4 | 4 | 1.75 | 0.63 | 900 | 5 | 4,860 | 3 |
| Cape Young | 68.98 | -116.98 | 3 | 3 | 1.31 | 0.26 | 2,000 | 5 | 10,800 | 3 |
| Princess Royal Islands | 73.37 | -115.28 | 2 | 2 | 0.88 | 0.08 | 2,000 | 10 | 20,800 | 2 |
| | | | | | | | | | Total: | 30,567 |

Table 15. Tidal current power sites in Nunavut.

| Site Name | Latitude | Longitude | Maximum Current Speed Flood | Maximum Current Speed Ebb | Mean Maximum Depth Average Current Speed | Mean Power Density | Width of Passage | Average Depth of Passage | Flow Cross-sectional Area | Mean Potential Power |
|---|---|---|---|---|---|---|---|---|---|---|
| | deg | deg | knot | m/s | m/s | $kW/m^2$ | m | m | $m^2$ | MW |
| Smoky Narrows | 58.92 | -69.27 | 12 | 12 | 5.25 | 16.88 | 1,500 | 55 | 92,400 | 1,560 |
| Algernine Narrows | 58.79 | -69.60 | 10 | 10 | 4.38 | 9.77 | 2,000 | 59 | 130,400 | 1,274 |
| Riviere George Entrance | 58.76 | -66.12 | 8 | 8 | 3.50 | 5.00 | 3,000 | 35 | 125,100 | 626 |
| Riviere Arnaud (Payne) Entrance | 59.98 | -69.84 | 9 | 9 | 3.94 | 7.12 | 2,300 | 9 | 32,200 | 229 |
| Koksoak Entrance | 58.52 | -68.17 | 6 | 6 | 2.63 | 2.11 | 2,000 | 40 | 92,400 | 195 |
| Nakertok Narrows | 60.00 | -70.27 | 9 | 9 | 3.94 | 7.12 | 1,100 | 6 | 12,100 | 86 |
| Mikitok Narrows | 60.00 | -70.27 | 9 | 9 | 3.94 | 7.12 | 700 | 8 | 9,590 | 68 |
| Koksoak Narrows | 58.18 | -68.32 | 5 | 8.5 | 2.95 | 3.00 | 400 | 30 | 14,400 | 43 |
| Riviere George Narrows | 58.68 | 66.00 | 6 | 6 | 2.63 | 2.11 | 600 | 12 | 11,220 | 24 |
| McLean Strait | 60.35 | -64.63 | 7 | 7 | 3.06 | 3.35 | 200 | 8 | 2,200 | 7 |
| Passage de Ile aux Coudre | 47.43 | -70.43 | 5 | 6 | 2.41 | 1.63 | 1,700 | 30 | 56,100 | 91 |
| Travers de Saint-Roch | 47.36 | -70.26 | 7.5 | 7.5 | 3.28 | 4.12 | 500 | 15 | 9,000 | 37 |
| Traverse du Millieu | 47.33 | -70.38 | 4 | 5 | 1.97 | 0.89 | 2,000 | 10 | 26,000 | 23 |
| Havre St Pierre | 50.23 | -63.60 | 3 | 3 | 1.31 | 0.26 | 270 | 20 | 5,670 | 1 |
| Cap Gaspe | 48.70 | -64.08 | 3 | 3 | 1.31 | 0.26 | 2,400 | 20 | 50,400 | 13 |
| Pointe Heath | 49.06 | -61.59 | 2 | 2 | 0.88 | 0.08 | 3,900 | 29 | 117,780 | 9 |
| | | | | | | | | | Total: | 4,288 |

Table 16. Tidal current power sites in Québec.

| Site Name | Latitude | Longitude | Maximum Current Speed Flood | Maximum Current Speed Ebb | Mean Maximum Depth Average Current Speed | Mean Power Density | Width of Passage | Average Depth of Passage | Flow Cross-sectional Area | Mean Potential Power |
|---|---|---|---|---|---|---|---|---|---|---|
| | deg | deg | knot | m/s | m/s | kW/m$^2$ | m | m | m$^2$ | MW |
| Strait of Belle Isle | 51.45 | -56.68 | | | - | 0.20 | 26,069 | 49 | 1,298,236 | 373 |
| Forteau | 51.41 | -56.95 | 4 | 5 | 1.97 | 0.89 | 1,500 | 35 | 53,700 | 48 |
| Pointe Armour | 51.45 | -56.86 | 4 | 5 | 1.97 | 0.89 | 1,500 | 35 | 53,700 | 48 |
| Cape Bauld | 51.64 | -55.43 | 2 | 2 | 0.88 | 0.08 | 2,000 | 15 | 31,600 | 2 |
| Cape Anguille | 47.90 | -59.41 | 3 | 3 | 1.31 | 0.26 | 700 | 10 | 7,700 | 2 |
| Stearing Island | 49.93 | -57.81 | 2 | 2 | 0.88 | 0.08 | 1,650 | 13 | 23,100 | 2 |
| Cape St George | 48.46 | -59.28 | 3 | 3 | 1.31 | 0.26 | 200 | 18 | 3,800 | 1 |
| Pass Island Tickle | 47.50 | -56.19 | 4 | 3 | 1.53 | 0.42 | 300 | 7 | 2,490 | 1 |
| Placentia Gut | 47.25 | -53.96 | 9 | 9 | 3.94 | 7.12 | 80 | 3 | 336 | 2 |
| Pike Run | 54.10 | -58.36 | 6 | 5 | 2.41 | 1.63 | 580 | 45 | 26,680 | 43 |
| Cul-de-Sac | 54.06 | -58.56 | 6 | 5 | 2.41 | 1.63 | 360 | 14 | 5,400 | 9 |
| Cap Islet | 56.55 | -61.45 | 4 | 5 | 1.97 | 0.89 | 610 | 9 | 6,100 | 5 |
| Goose Bay Narrows | 54.43 | -59.99 | 3 | 5 | 1.75 | 0.63 | 813 | 7 | 6,504 | 4 |
| The Narrows | 53.67 | -57.07 | 3.5 | 3.5 | 1.53 | 0.42 | 260 | 18 | 4,940 | 2 |
| Bridges Passage | 56.45 | -61.56 | 4 | 4 | 1.75 | 0.63 | 280 | 5 | 1,680 | 1 |
| | | | | | | | | | Total: | 544 |

Table 17. Tidal current power sites in Newfoundland and Labrador.

| Site Name | Latitude | Longitude | Maximum Current Speed Flood | Maximum Current Speed Ebb | Mean Maximum Depth Average Current Speed | Mean Power Density | Width of Passage | Average Depth of Passage | Flow Cross-sectional Area | Mean Potential Power |
|---|---|---|---|---|---|---|---|---|---|---|
| | deg | deg | knot | m/s | m/s | kW/m$^2$ | m | m | m$^2$ | MW |
| Savage Harbour/Dulse Rocks | 45.64 | -62.45 | 5 | 5 | 2.19 | 1.22 | 160 | 6 | 1,184 | 1 |
| Minas Basin | 45.35 | -64.40 | 7.5 | 7.5 | 3.28 | 6.04 | 4,376 | 56 | 274,113 | 1,903 |
| Northwest Ledge | 44.30 | -66.42 | 4 | 4 | 1.75 | 0.63 | 5,334 | 18 | 117,348 | 73 |
| The Hospital | 43.44 | -66.00 | 4 | 4 | 1.75 | 0.63 | 3,600 | 18 | 79,200 | 50 |
| Petit Passage | 44.39 | -66.21 | 7 | 7 | 3.06 | 3.35 | 335 | 18 | 7,035 | 24 |
| Digby Gut | 44.68 | -65.76 | 5 | 5 | 2.19 | 1.22 | 573 | 25 | 16,904 | 21 |
| Grand Passage | 44.28 | -66.34 | 6 | 6 | 2.63 | 2.11 | 380 | 16 | 7,220 | 15 |
| Trinity Ledge | 44.00 | -66.29 | 2.5 | 2.5 | 1.09 | 0.15 | 2,520 | 14 | 42,840 | 7 |
| Ellewoods Channel | 43.66 | -66.05 | 4 | 4 | 1.75 | 0.63 | 350 | 4 | 2,275 | 1 |
| Cape Sable | 43.35 | -65.66 | 4 | 4 | 1.75 | 0.63 | 2,070 | 10 | 23,805 | 15 |
| Baccaro Point | 43.44 | -65.47 | 3 | 3 | 1.31 | 0.26 | 670 | 10 | 7,504 | 2 |
| Great Bras d'Or (entrance) | 46.29 | -60.41 | 5 | 5 | 2.19 | 1.22 | 320 | 8 | 2,832 | 3 |
| Barra Strait | 45.96 | -60.80 | 3 | 3 | 1.31 | 0.26 | 455 | 20 | 9,487 | 3 |
| Flint Island | 46.17 | -59.79 | 2.5 | 3 | 1.20 | 0.20 | 500 | 20 | 10,425 | 2 |
| St Ann's Harbour | 46.29 | -60.41 | 5 | 5 | 2.19 | 1.22 | 155 | 10 | 1,682 | 2 |
| | | | | | | | | | Total: | 2,122 |

Table 18. Tidal current power sites in Nova Scotia.

| Site Name | Latitude | Longitude | Maximum Current Speed Flood | Maximum Current Speed Ebb | Mean Maximum Depth Average Current Speed | Mean Power Density | Width of Passage | Average Depth of Passage | Flow Cross-sectional Area | Mean Potential Power |
|---|---|---|---|---|---|---|---|---|---|---|
| | deg | deg | knot | m/s | m/s | kW/m$^2$ | m | m | m$^2$ | MW |
| East Point/Milne Bank | 46.41 | -61.94 | 2.5 | 2.5 | 1.09 | 0.15 | 7,100 | 13 | 102,240 | 16 |
| Indian Rocks | 45.93 | -62.80 | 3 | 3 | 1.31 | 0.26 | 2,500 | 15 | 40,000 | 11 |
| WestReef/West Spit | 46.67 | -64.48 | 2.5 | 2.5 | 1.09 | 0.15 | 3,790 | 8 | 35,626 | 5 |
| Charlottetown Harbour Entrance | 46.20 | -63.13 | 2.5 | 2.5 | 1.09 | 0.15 | 490 | 15 | 8,232 | 1 |
| | | | | | | | | | Total: | 33 |

Table 19. Tidal current power sites in Prince Edward Island.

| Site Name | Latitude | Longitude | Maximum Current Speed Flood | Maximum Current Speed Ebb | Mean Maximum Depth Average Current Speed | Mean Power Density | Width of Passage | Average Depth of Passage | Flow Cross-sectional Area | Mean Potential Power |
|---|---|---|---|---|---|---|---|---|---|---|
| | deg | deg | knot | m/s | m/s | $kW/m^2$ | m | m | $m^2$ | MW |
| Miramichi Bay Islands | 47.15 | -65.04 | 3.5 | 3.5 | 1.53 | 0.42 | 1,920 | 5 | 10,944 | 5 |
| Clarks Ground | 44.59 | -66.64 | 6 | 6 | 2.63 | 2.11 | 4,092 | 22 | 102,300 | 216 |
| Devils Half Acre | 44.54 | -66.69 | 6 | 6 | 2.63 | 2.11 | 2,133 | 18 | 44,793 | 95 |
| Old Sow | 44.92 | -66.99 | 6 | 6 | 2.63 | 2.11 | 625 | 60 | 39,375 | 83 |
| Head Harbour Passage 1 | 44.95 | -66.93 | 5 | 5 | 2.19 | 1.22 | 890 | 65 | 60,520 | 74 |
| Gran Manan Channel | 44.78 | -66.86 | 2.5 | 2 | 0.98 | 0.11 | 5,446 | 80 | 452,018 | 50 |
| Quoddy River | 44.96 | -66.95 | 4.5 | 4 | 1.86 | 0.75 | 1,350 | 28 | 41,850 | 31 |
| Reversing Falls | 45.26 | -66.09 | 12 | 12 | 5.25 | 16.88 | 90 | 15 | 1,746 | 29 |
| Cumberland Basin | 45.74 | -64.47 | 4 | 5 | 1.97 | 0.89 | 2,125 | 6 | 26,988 | 24 |
| Letete Passage | 45.05 | -66.92 | 5 | 5 | 2.19 | 1.22 | 508 | 25 | 14,224 | 17 |
| Shepody Bay | 45.87 | -64.57 | 3 | 4 | 1.53 | 0.42 | 1,400 | 3 | 12,740 | 5 |
| Lubec Narrows | 44.86 | -66.98 | 6 | 8 | 3.06 | 3.35 | 180 | 3 | 1,080 | 4 |
| Little Letete Passage | 45.03 | -66.93 | 5 | 5 | 2.19 | 1.22 | 150 | 6 | 1,350 | 2 |
| Devils Head/St Stephen | 45.16 | -67.18 | 3 | 4 | 1.53 | 0.42 | 440 | 3 | 2,640 | 1 |
| | | | | | | | | | Total: | 636 |

Table 20. Tidal current power sites in New Brunswick.

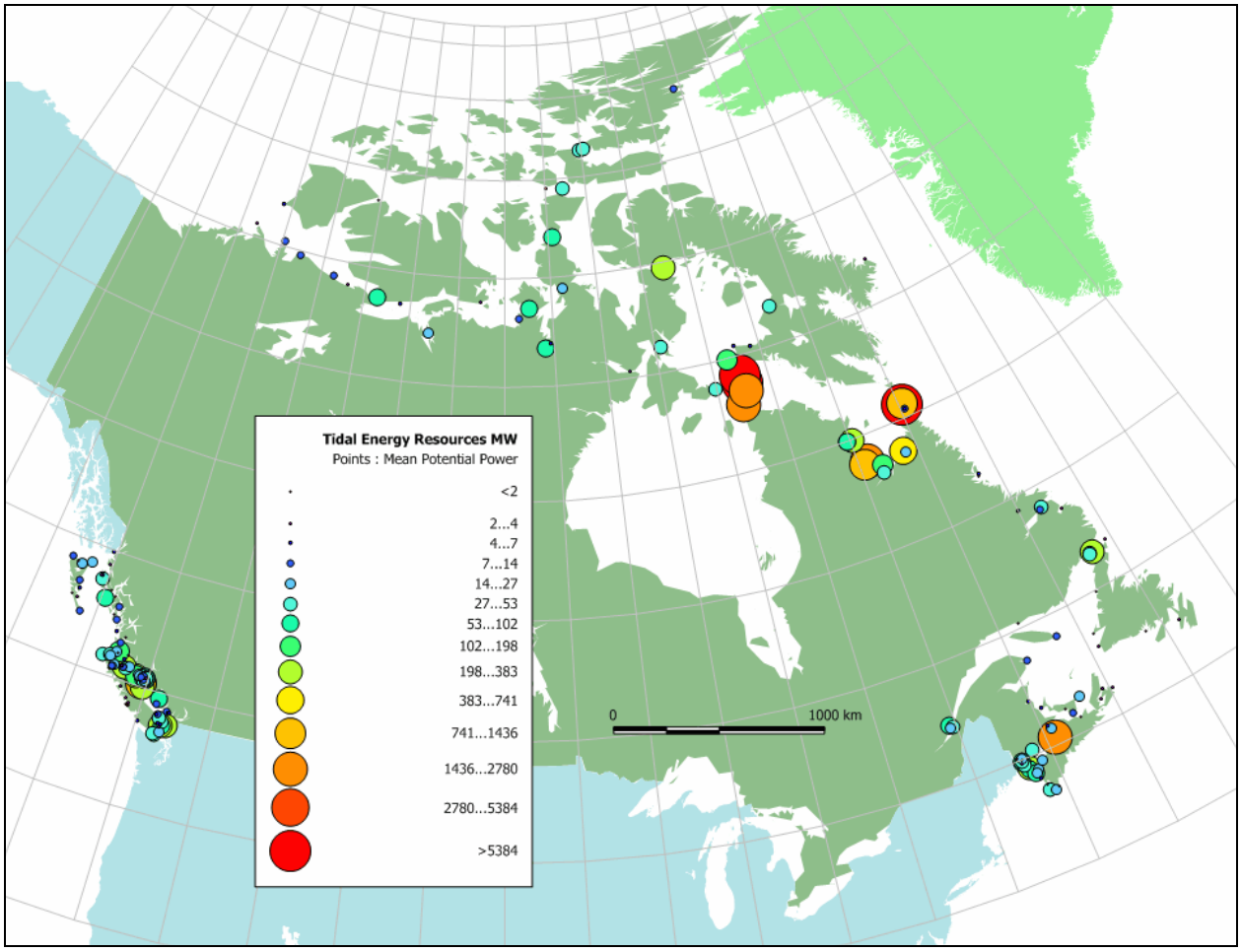


Figure 76. Leading tidal current power sites, Canada.

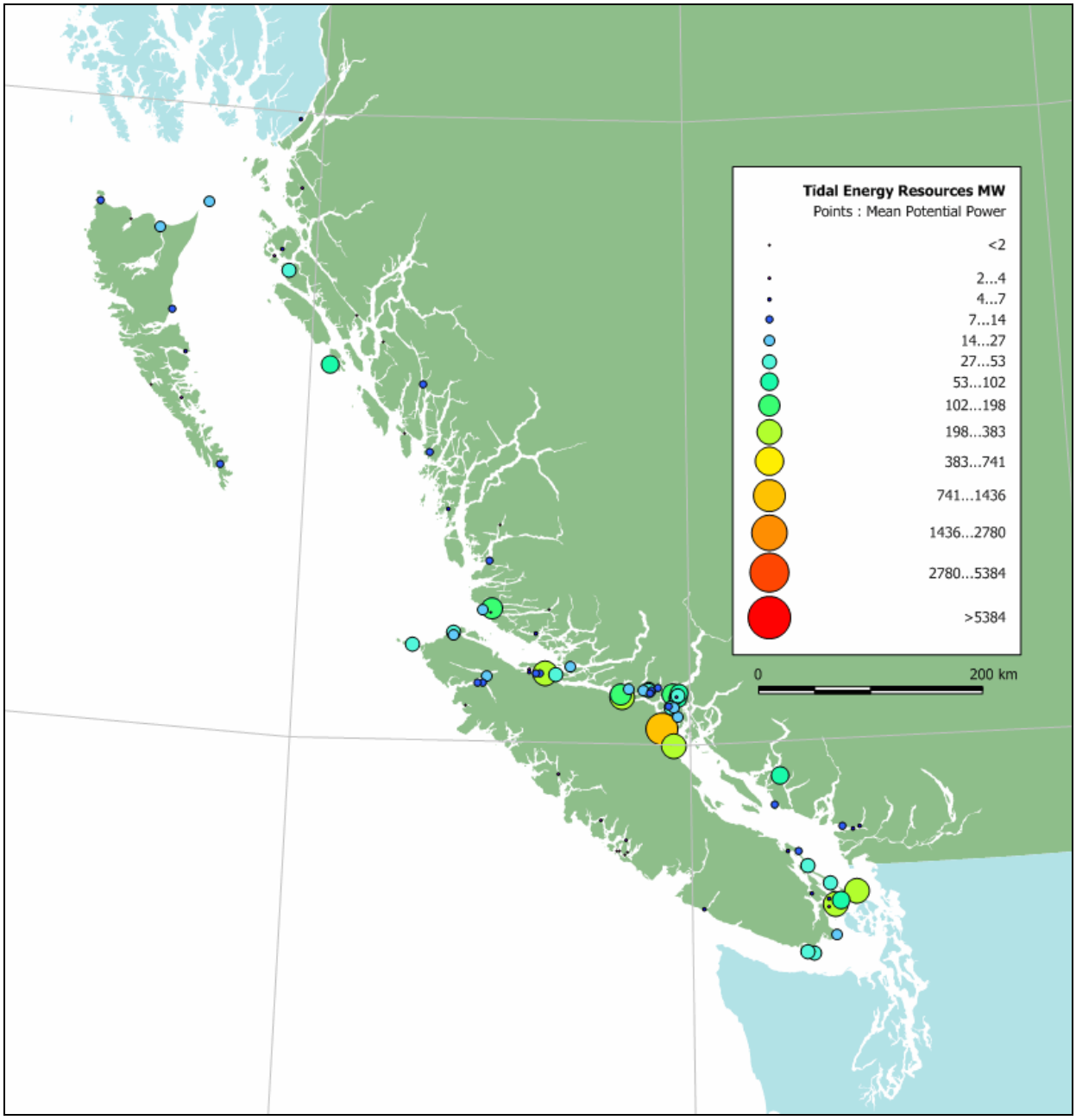


Figure 77. Leading tidal current power sites, Pacific coast.

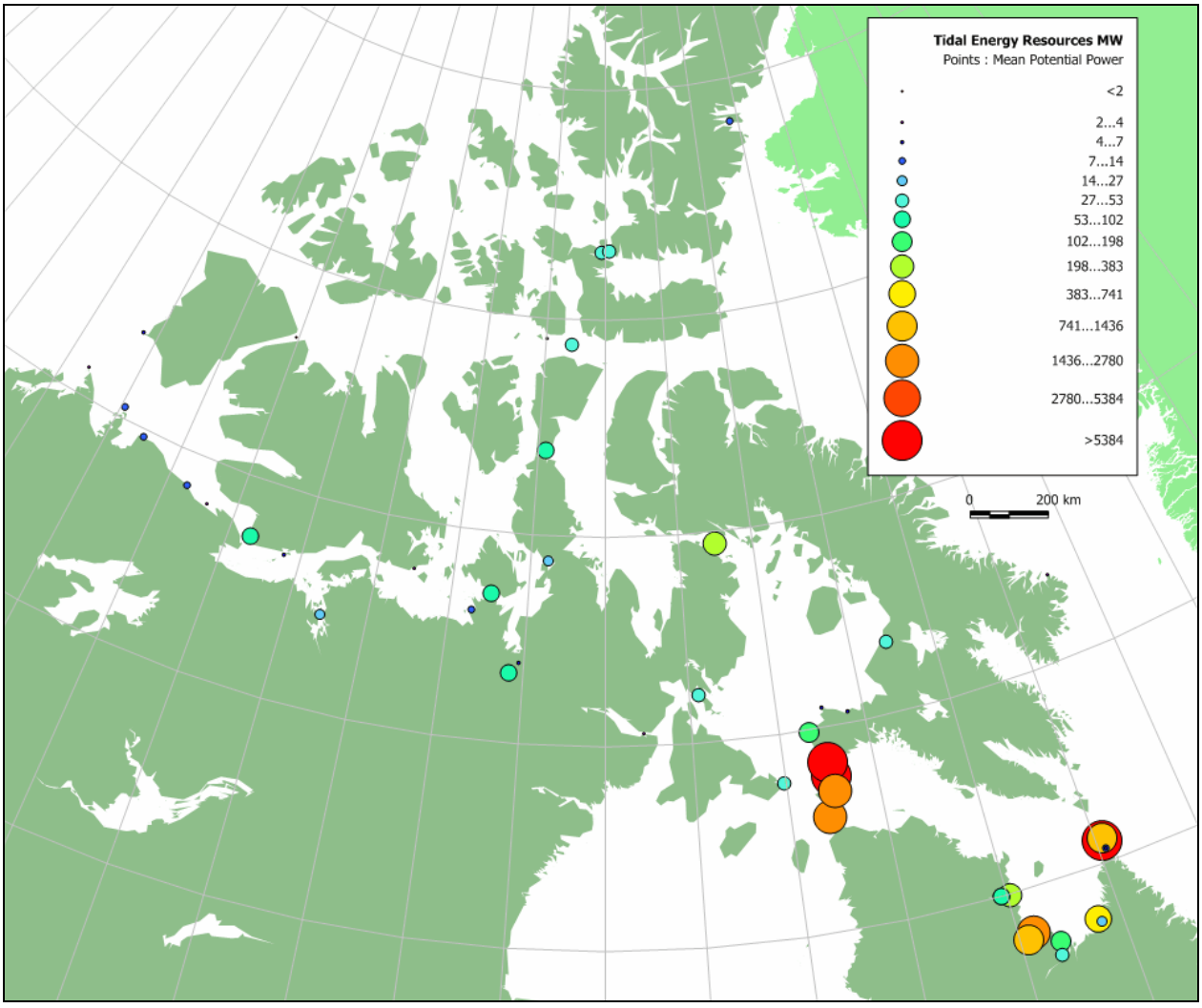


Figure 78. Leading tidal current power sites, Arctic Archipelago.

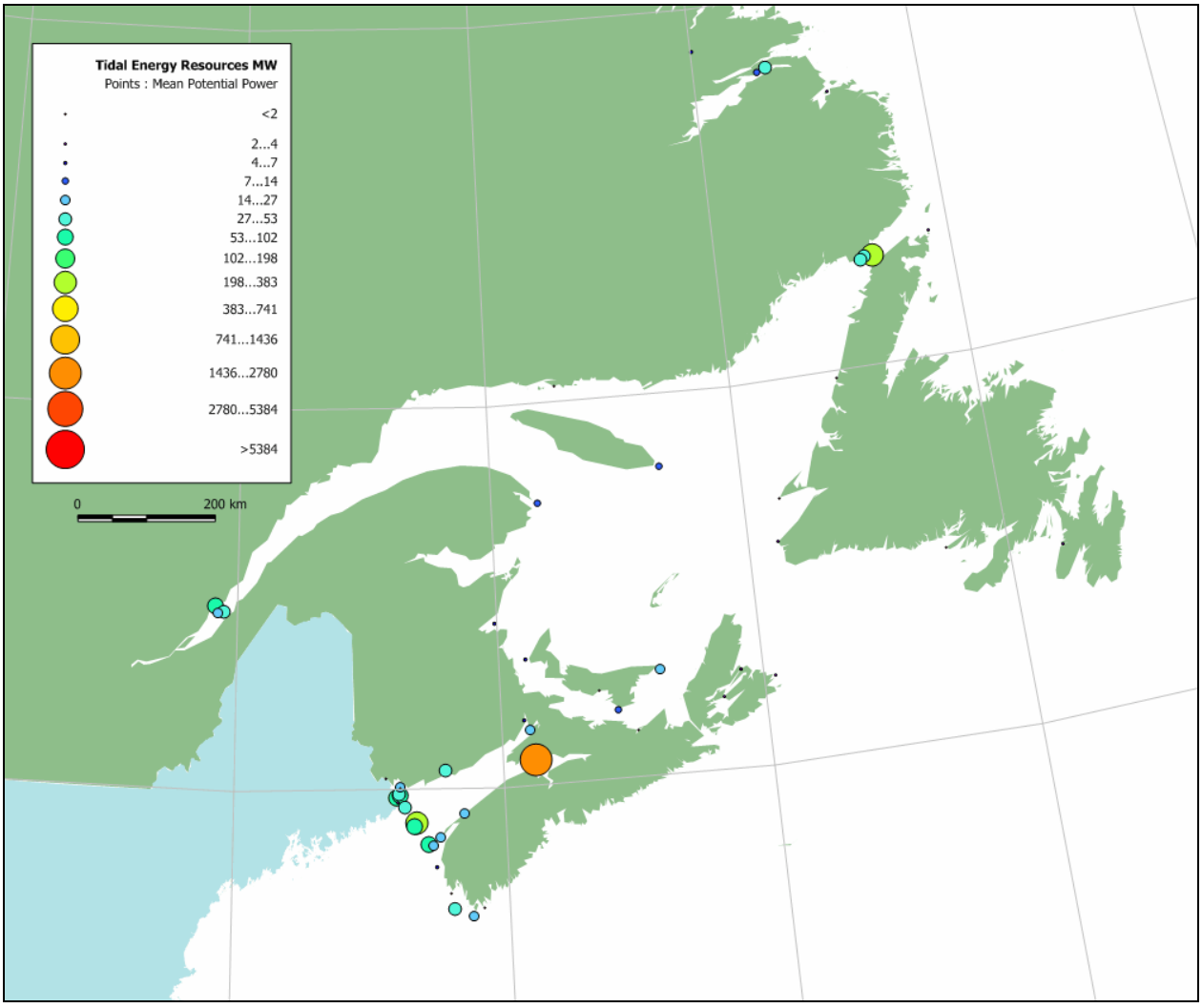


Figure 79. Leading tidal current power sites, Atlantic coast.

# 5. Recommendations for Future Work

Several recommendations for further studies are outlined in what follows. A proposal to conduct these studies has been submitted to Natural Resources Canada for consideration.

## *5.1. Assessment of the Wave Energy Resource*

The wave power along a coast can vary considerably due to sheltering from islands and the interaction between the waves and the local bathymetry. Natural physical processes such as shoaling, refraction and diffraction will create pronounced local variations in wave conditions and energy potential close to shore, particularly in regions where the bathymetry is irregular. These processes can create "hot spots" where the wave energy is significantly greater than (easily more than double) the local average. These hot spots represent prime sites for wave power projects.

The wave energy resources in deep water off Canada's Atlantic and Pacific coasts have been quantified and mapped, however the distribution of wave energy along the coast above the 200 m depth contour remains poorly defined. It is recommended that new wave modelling studies be conducted to quantify and map the wave energy climate above the 200 m contour along the portion of Canada's shoreline where the potential for wave energy extraction is greatest. Third generation shallow water wave transformation models, such as SWAN (Simulating Waves Nearshore), should be applied in these studies. Initially, these studies should be focused on the following coastal areas:

- western shore of the Queen Charlotte Islands;
- western shore of Vancouver Island;
- south-eastern Newfoundland including the Avalon peninsula; and
- south-eastern shore of Cape Breton.

## *5.2. Assessment of the Tidal Current Energy Resource*

Results from numerous existing tide models have been analysed to create maps of tidal currents and the kinetic energy contained therein. In many regions, the resolution of the available model grids is insufficient to obtain reliable predictions of tidal flows near the coast and particularly at high-energy sites. New modelling efforts with refined model grids are required in order to improve the accuracy and detail of the tidal current maps, and the resource estimates derived from them. It is recommended that near-term modelling studies should concentrate on three specific areas:

- Bay of Fundy, Nova Scotia;
- Georgia and Johnstone Straits, British Columbia; and
- Hudson's Strait and Ungava Bay, Québec and Nunavut.

The objective of these modelling studies should be to improve the definition of the tidal current resources available, and to investigate the impact of energy extraction on the tidal flows throughout the region (both levels and currents).

### *5.3. Digital Atlas of Marine Renewable Energy Resources*

The concept of a digital atlas of ocean renewable energy resources is outlined in Chapter 2 of this report. The proposed atlas will feature a geo-referenced database containing tidal current, wave climate and wind data and meta-data for all Canadian waters, integrated with an interactive viewer/mapper and wrapped in a user-friendly interface. The proposed atlas will also include selected climatic, socio-economic and environmental variables relevant to the selection and evaluation of sites for ocean energy projects. The digital atlas will be equipped with a toolbox of statistical, temporal and spatial analysis tools for analysing and interpreting the data. The atlas will be web-enabled, like the Canadian Wind Energy Atlas, so that it can be accessed by all.

The initial content for the atlas will include the results presented in Chapters  and 4 of this report, supplemented by results from new modelling studies conducted to improve the detail and spatial coverage of the initial resource assessments (described above), and by data provided by future collaborators.

## Acknowledgements

The author wishes to thank Michael Tarbotton and Max Larson of Triton Consultants for their many contributions to this work. The hard work and dedication of my colleague Ji Zhang is also acknowledged with sincere gratitude. The author also thanks the following people for supporting and contributing to this study:

- Gouri Bhuyan, Powertech Labs
- Rob Brandon, CTEC, Natural Resources Canada
- Chris Campbell, Ocean Renewable Energy Group (OREG)
- Guoqi Han, NAFC, Fisheries and Oceans Canada
- John Loder, BIO, Fisheries and Oceans Canada
- Marielle Nobert, OERD, Natural Resources Canada
- Val Swail, MSC, Environment Canada
- members of the Federal Ocean Energy Working Group (FOEWG)

The financial support of the Technology and Innovation Research and Development Program, Natural Resources Canada, is gratefully acknowledged.

## 6. References and Bibliography

ABP Marine Environmental Research Ltd. (ABP, 2004) *Atlas of UK Marine Renewable Energy Resources: Technical Report*, Report No. R.1106 prepared for the UK Department of Trade and Industry.

Allievi, A. and Bhuyan, G. (1994) *Assessment of Wave Energy Resources for the West Coast of Canada.* Department of Mechanical Engineering, University of British Columbia, Vancouver.

Baird, W.F. and Mogridge, G.R. (1976) *Estimates of the Power of Wind-Generated Water Waves at Some Canadian Coastal Locations.* NRC Hydraulics Laboratory Report LTR-HY-53.

Briand, M.-H. and Claisse, M. (2004) *Potential for Renewable Energy Development in Nunavik, Canada*. Proc. 2004 Water Power Conference, Austin, Texas, U.S.A.

Cornett, A.M. (2005) *Towards a Canadian Atlas of Renewable Ocean Energy.* Proc. Canadian Coastal Conference 2005. Dartmouth, N.S., November, 2005.

Dupont, Frédéric, Charles G. Hannah and David Greenberg. 2005. *Modelling the Sea Level in the Upper Bay of Fundy*. Atmos.-Ocean. 43(1), 33-47

Dupont, F., C.G. Hannah, D.A. Greenberg, J.Y. Cherniawsky and C.E. Naimie. 2002. *Modelling System for Tides for the Northwest Atlantic Coastal Ocean*. Can. Tech. Rep. Hydrogr. Ocean Sci. 221: vii + 72pp.

Dupont, F., B. Petrie, J. Chaffey. 2003. *Modelling the Tides of the Bras d'Or Lakes*. Can. Tech. Rep. Hydrogr. Ocean Sci. 230: viii + 53pp.

Dunphy, M., F. Dupont, C. Hannah, D. Greenberg. 2005. *Validation of a Modeling System for Tides in the Canadian Arctic Archipelago*. Can. Tech. Rep. Hydrogr. Ocean Sci. XXX: vi + 70pp.

Electrical Power Research Institute (EPRI, 2004) *Offshore Wave Energy Conversion Devices*. E2I-EPRI Report No. WP-004-US, available at www.epri.com.

Electrical Power Research Institute (EPRI, 2005). *Offshore Wave Power Feasibility Project – Project Definition Study, Final Summary Report* E2I-EPRI Report WP-009-US, available at www.epri.com.

Electrical Power Research Institute (EPRI, 2005). *Tidal In Stream Energy Conversion (TISEC) Devices – Survey and Characterization.* E2I-EPRI Report TP-004-NA, available at www.epri.com.

Foreman, M.G.G., W.R. Crawford, J.Y. Cherniawsky, R.F. Henry and M.R. Tarbotton. 2000. *A high-resolution assimilating tidal model for the northeast Pacific Ocean*. Journal of Geophysical Research. 105: 28,629-28,652.

Forrester, W.D. 1983. *Canadian Tidal Manual*. Canadian Hydrographic Service Publication P-252.

Garrett, C., P. Cummins. 2004. *Generating Power from Tidal Currents. J. Waterways, Port, Coastal & Ocean Engineering*. 130(3) ASCE.

Hagerman, G. (2001) *Southern New England Wave Energy Resource Potential* Proc. Building Energy 2001, Tufts University, Boston, MA, March 2001.

Han, G., J.W. Loder. 2003. *Three-dimensional seasonal-mean circulation and hydrography on the eastern Scotian Shelf*. J. Geophysical Research, 108(C5), 3136.

Kliem, Nicolai and David A. Greenberg. 2003. *Diagnostic Simulations of the Summer Circulation in the Canadian Arctic Archipelago*. Atmos.-Ocean. 41.

Mansard, E.P.D. (1978) *Different Methods of Evaluating Wave Power in a Random Seastate: A Comparative Study*. NRC Hydraulics Laboratory Report HY-97, Ottawa.

Mogridge, G.R. (1980) *A Review of Wave Power Technology* NRC Hydraulics Laboratory Report LTR-HY-74

Mollison, D. (1986) *Wave Climate and the Wave Power Resource* in Hydrodynamics of Ocean-Wave Energy Utilization, eds. D.V. Evans and A.F. de O. Falcao, Springer-Verlag, New York.

Pontes, M.T. (1998) *Assessing the European Wave Energy Resource*. J. Offshore Mechanics and Arctic Engineering. Vol. 120, No. 4, pp. 226-231.

Pontes, M.T. and A. Falcao (2001) *Ocean Energies: Resources and Utilisation*. Proc. 18th World Energy Conference, Buenos Aires, Argentina, October 2001.

Pontes, M.T., R. Aguiar and H.O. Pires (2003) *A Nearshore Wave Energy Atlas for Portugal*. Proc. 22nd Int. Conf. on Offshore Mechanics and Arctic Engineering, Cancun, Mexico, June 2003.

Saucier, F.J., F. Roy, D. Gilbert, P. Pellerin and H. Ritchie. 2003. *The Formation and Circulation Processes of Water Masses in the Gulf of St. Lawrence, Canada*. J. Geophysical Research, 108(C8), 3269

Swail, V.R., E.A. Ceccacci, and A.T. Cox (2000) *The AES40 North Atlantic Wave Reanalysis: Validation and Climate Assessment*. Sixth International Workshop on Wave Hindcasting and Forecasting, Monterey, California.

Swail, V.R., V.J. Cardone and A.T. Cox (1998) *A Long Term North Atlantic Wave Hindcast*. Proc. 5th International Workshop on Wave Hindcasting and Forecasting, Melbourne, FL, January 1998.

Tolman, H.L. (2002) *User Manual and System Documentation for WAVEWATCH-III version 2.22*. NOAA-NCEP-MMAB Technical Note 222. U.S. Department of Commerce, Washington, D.C.

Triton Consultants (2002) *Green Energy Study for British Columbia – Tidal Current Energy.* Report prepared for B.C. Hydro.

Triton Consultants (2006) *Potential Tidal Current Energy Resources – Analysis Backgroud*. Report prepared for NRC-Canadian Hydraulics Centre.

WaveNet (2003) *Results from the Work of the European Thematic Network on Wave Energy.* Report prepared for the Energy, Environment and Sustainable Development Programme of the European Union.

# Annex A - Report of Triton Consultants

# Canada Ocean Energy Atlas (Phase 1)

# Potential Tidal Current Energy Resources

# Analysis Background

May 2006

Prepared For:
**Canadian Hydraulics Centre, Ottawa, Ontario as part of a contract for Natural Resources Canada**

Prepared By:
Michael Tarbotton and Max Larson
**Triton Consultants Ltd.**
Vancouver, BC

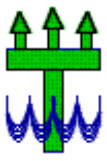

**TRITON CONSULTANTS LTD.**

# TABLE OF CONTENTS

# LIST OF FIGURES

# LIST OF TABLES

# 1. INTRODUCTION

This report provides an analysis background to a preliminary tidal current resource inventory for Canadian waters completed for Phase 1 of the Canada Ocean Energy Atlas Project.

The estimated tidal current energy for Canada is the total potential resource available in tidal flows. The estimates are “potential” resources NOT “economically realisable” resources. At this early stage of the Ocean Atlas development, energy calculations are based on preliminary estimates of existing tidal flows and no consideration has been given to the following factors:

- Environmental Impacts
- Technological developments and limitations in tidal power extraction
- Climate related factors (e.g., ice, global climate change)
- Site location versus power grid accessibility and power demand
- Hydrogen economy developments
- The effect of potential energy extraction schemes on existing flow conditions
- Economic factors.

***Mean vs Rated Site and Turbine Capacity***

There may be some potential for confusion when comparing the power values referenced in this study with those of conventional thermal or hydroelectric generating facilities with which the public is most familiar. With conventional power generation, reference is usually made to the rated power of the facility which is the value stamped on the manufacturer’s nameplate. It is generally the goal of conventional facility owners to operate the facility near this rated capacity. Moreover, the day-to-day variability of conventional energy resources is relatively minor which allows these facilities to operate near their rated capacity for relatively continuous periods of time. This means that rated capacity is generally a good first approximation to the actual power production of a conventional power plant.

For wind power it is often the case that wind farm capacities are quoted in turbine rated capacity rather than the more realistic mean annual power potential. Wind power is much more temporally variable and uncertain than tidal power, but both these sources of renewable energy peak for quite short periods.

In the case of tidal current energy extraction, the resource potential goes to zero two to four times per day and reaches its peak annual value for only a few hours per year. For this reason, it is much more instructive to speak of *mean power* in the context of tidal power as such a definition integrates the effect of the highly variable daily and annual variation of the resource. The Mean Potential Power detailed in this report can be converted to megaWatt.hours per year by multiplying the mean power (MW) by 8,760 (the number of hours in a year).

# 2. DATA SOURCES

Triton has undertaken a preliminary tidal resource inventory for Canadian marine waters including the East and West Coasts and Arctic Canada. This inventory was based on a variety of data sources including:

- Canadian Sailing Directions;
- Nautical Charts and Tide Books;
- Tide and tidal current constituent data;
- Numerical Tidal modelling data

Data from these data sources has been assembled into a database and documented in spreadsheet tables and in the GIS program Manifold (www.manifold.net) for data viewing and interpretation by the study team.

## 2.1 NAUTICAL AND BATHYMETRIC INFORMATION

Nautical data including Canadian Sailing Directions and tide books were purchased for the whole of Canada and reviewed in detail. In addition, all the available electronic nautical charts, a total of 489 charts, were purchased from Nautical Data International (NDI), St. John's, Newfoundland in raster format and areas of potential tidal current resource were identified.

The Canadian Hydrographic Service has a total of 950 nautical charts for all regions of Canada. Deducting approximately 250 charts for the Great Lakes, St. Lawrence River and Mackenzie River systems and interior British Columbia, there are about 700 charts relevant to this study. Therefore, 70% of Canadian (saltwater) Marine Charts are presently available in electronic raster format. A majority of the non-electronic charts are for areas such as Hudson Bay and Strait, Ungava Bay and the Arctic Regions.

Paper copies of the non-electronic charts were reviewed from Triton's own chart database and at the map library at the University of British Columbia.

Table 1 and Table 2 below show the Canadian Sailing Directions and Tide and Current books used for this study.

**Table 1: Canadian Sailing Directions**

| Number | Description |
|---|---|
| P100 | Arctic Canada, Vol. 1, 1994 |
| P102 | Arctic Canada, Vol. 2, 1985 |
| P104 | Arctic Canada, Vol. 3, 1994 |
| P112 | Labrador & Hudson Bay, 1988 |
| P118 | BC (S. Portion), Vol. 1, 2004 |
| P120 | Great Slave Lake & Mackenzie River, 1989 |
| P122 | Gulf of St. Lawrence, 1992 |
| ATL100E | Atlantic Coast, General Information 1992 |
| ATL101E | Newfoundland, Northeast & East Coasts |
| ATL102E | Newfoundland, East and South Coasts |
| ATL103E | Newfoundland, Southwest Coast |
| ATL104E | Cape North to Cape Canso |
| ATL105E | Cape Canso to Cape Sable |
| ATL106E | Gulf of Maine and Bay of Fundy, 2001 |
| ATL107E | St. John River, 1994 |
| ATL110E | St. Lawrence River, Cap Whittle/ |
| ATL111E | St. Lawrence River/Île Verte to Québec, 1999 |
| ATL112E | St. Lawrence River/Cap-Rouge to Montréal |
| ATL120E | Labrador, Camp Islands to Hamilton Inlet |
| ATL121E | Labrador, Hamilton Inlet to Cape Chidley |
| Volume 1 Pacific | British Columbia South 1987 |
| Volume 11 Pacific | British Columbia North 1987 |

**Table 2: Canadian Tide and Current Tables**

| Volume | Description |
|---|---|
| Vol 1 | Atlantic Coast and Bay of Fundy / Côte de l'Atlantique et baie de Fundy, 2006 |
| Vol 2 | Gulf of St. Lawrence / Golfe du Saint-Laurent, 2006 |
| Vol 3 | St. Lawrence and Saguenay Rivers / Fleuve Saint-Laurent et rivière Saguenay, 2006 |
| Vol 4 | Arctic and Hudson Bay / L'Arctique et la baie d'Hudson, 2006 |
| Vol 5 | Juan de Fuca Strait & Strait of Georgia / Détroits de Juan de Fuca et de Georgia, 2006 |
| Vol 6 | Discovery Passage & West Coast of Vancouver Island / Discovery Passage et côte Ouest de l'île de Vancouver, 2006 |
| Vol 7 | Queen Charlotte Sound to Dixon Entrance / Queen Charlotte Sound à Dixon Entrance, 2006 |

## 2.2 TIDAL CONSTITUENT DATABASE

The Canadian Hydrographic Service maintains a database of more than 1030 tidal station constituent files. These tidal (height) constituent files are based on recorded water levels and are used to calculate the tidal heights each year for the CHS Tide and Currents Tables. Because of the practical difficulties of measuring tidal currents, the number of verified tidal current stations available for Canada is quite small (probably less than 50). The Pacific Coast is by far the best serviced area in the country, with a total of 24 stations with current constituents. On the Atlantic Coast there are only two current sites in the Tide and Current tables and these sites are in low current areas of the Bay of Fundy.

It is understood from scientists at the Bedford Institute of Oceanography that many current measurements have been recorded in the Atlantic Region but these have never been assembled into a verified database. CHS headquarters in Ottawa is presently in discussions with their regional offices to agree to a framework for assembling all the current measurement data for Canada.

Figure 1 shows the location of tidal height stations in Canada. The colour of the "dots" indicates the amplitude of the semi-diurnal (twice a day) M2 tidal constituent which gives a good indication of relative tidal range except in places like Juan de Fuca Strait and the Strait of Georgia (Pacific Coast) where the diurnal (once a day) component is also important.

A general overview of the physics of tides and tidal constituents is given in Section 3.1 for reference.

**Figure 1: Tidal Stations in Canada**

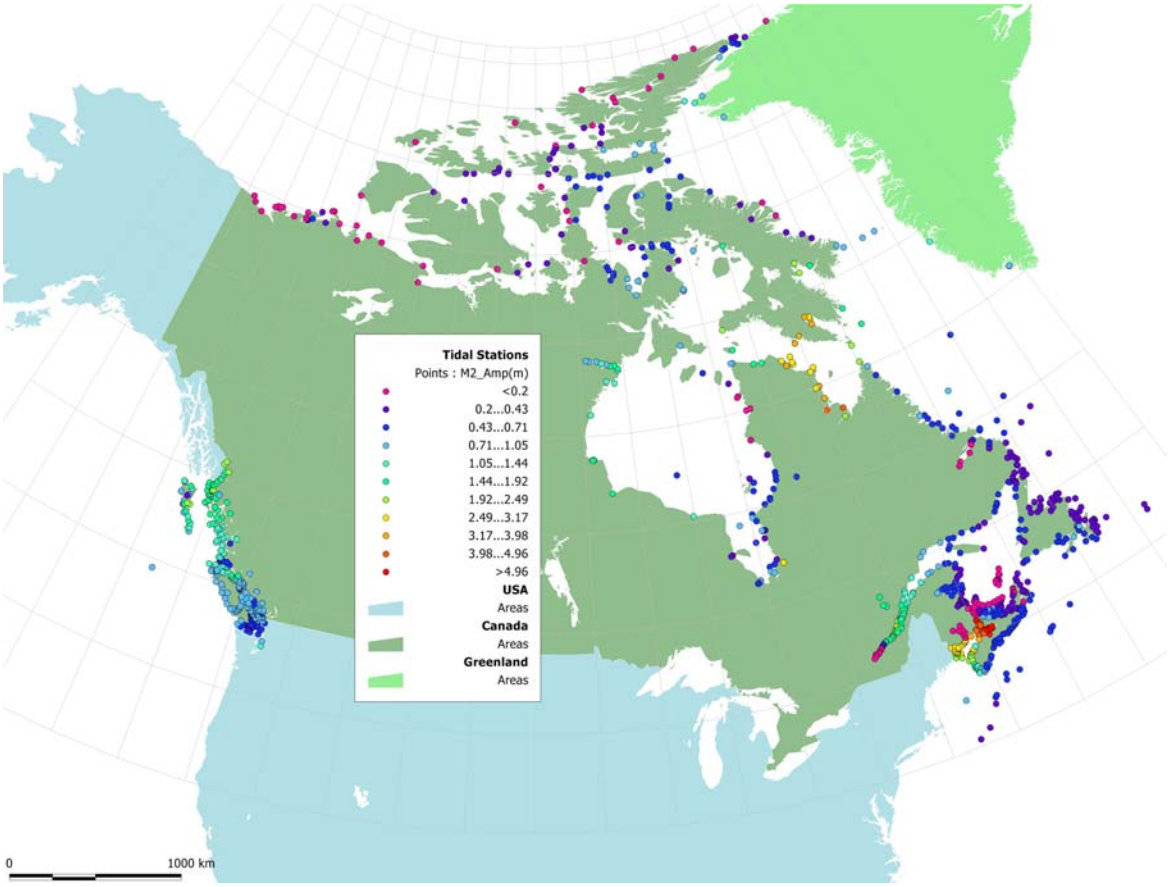


## 2.3 TIDAL MODELLING

Data from numerical tidal models of Canadian Waters was used to provide additional information for the tidal current power assessment. The finite element models used by Triton for this study are shown in Table 3.

**Table 3: Tidal Models**

| Model Region | Model Grid Source | Number of Model Calculation Nodes | Notes |
|---|---|---|---|
| British Columbia South | Triton & IOS* | 132,000 | Model run for this study |
| Queen Charlotte Islands | Triton & IOS* | 7,600 | Model run for this study |
| Hudson's Bay Region | Triton & BIO* | 45,000 | Model run for this study |
| Gulf of St. Lawrence | Triton & PWGSC* | 7,800 | Model run for this study |
| | | | |
| North West Atlantic | BIO/WebTide | 17,100 | Model results provided by BIO |
| Arctic | BIO/WebTide | 17,400 | Model results provided by BIO |
| Bay of Fundy North | BIO/WebTide | 75,000 | Model results provided by BIO |

*original source of model grid; grid further developed and expanded by Triton.

IOS – Institute of Ocean Sciences, Sidney, BC

BIO – Bedford Institute of Oceanography, Bedford, N.S.

Triton's finite element harmonic tidal model Tide2D (see appendix for Tide2D data sheet) was used to provide tidal height and current velocities data at each node in the model domains for a varying number of tidal constituents on the model driving boundary.

Purpose-designed code was written to convert Fundy format (BIO) results to Trigrid (IOS) and to compute for both formats the mean tidal power from the calculated current constituents at each node in the model domains. This latter analysis is equivalent to doing a current prediction for each model node for a full year. Mean current power was then estimated from the indicative formula average $\sum$ (½ x ρ x $U^3$). These conversion codes were implemented in Triton's in-house Coastal Engineering Analysis Package (CEAPack) which is described in the appendix.

The model results (including tide height, current and mean power) were input via CEAPack, into Tecplot (www.tecplot.com) for visualization and analysis. Tecplot allows the user to extract data along cross-section lines. This method was used to estimate potential tidal power at locations where no accurate current measurements are presently available (e.g., Hudson's Strait, Minas Basin and Discovery Pass).

Figure 2 through Figure 6 show the model domains for a selection of tidal models used for this study with contoured depths in metres.

**Figure 2: Hudson Bay Tidal Model Region (depths in metres)**

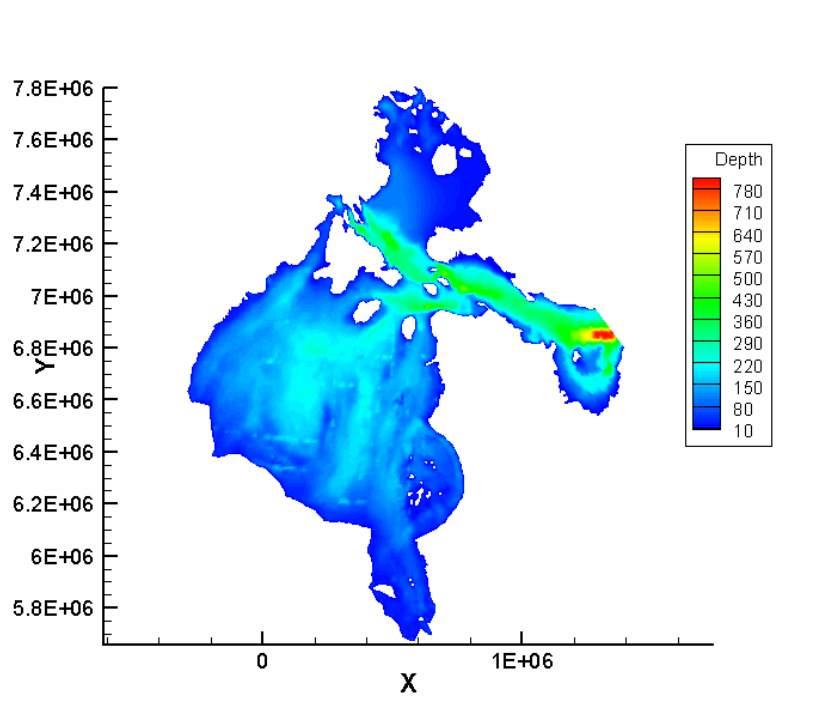


**Figure 3: Gulf of St. Lawrence Tidal Model Region (depths in metres)**

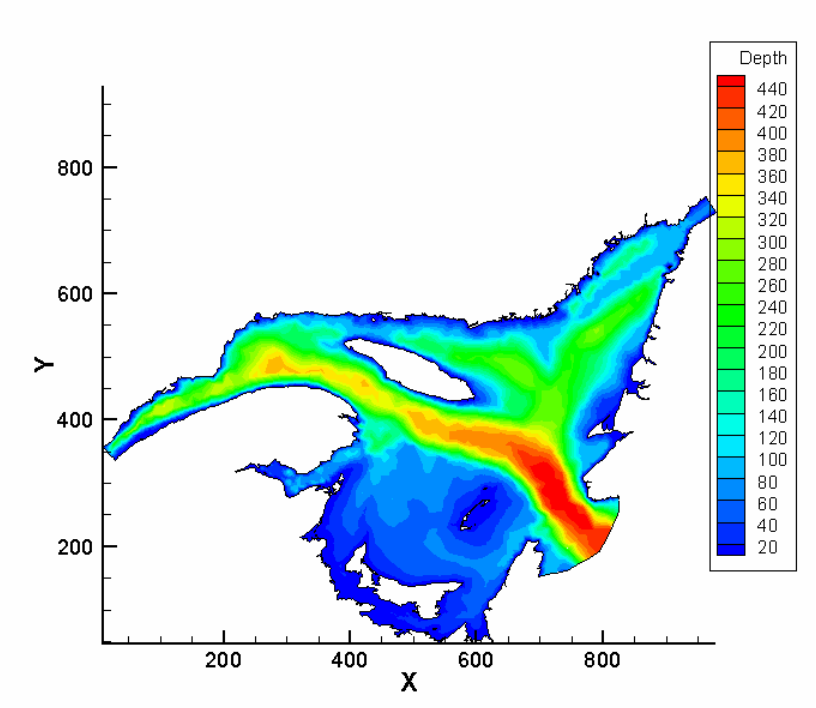

**Figure 4: Bay of Fundy North Tidal Model Region (depths in metres)**

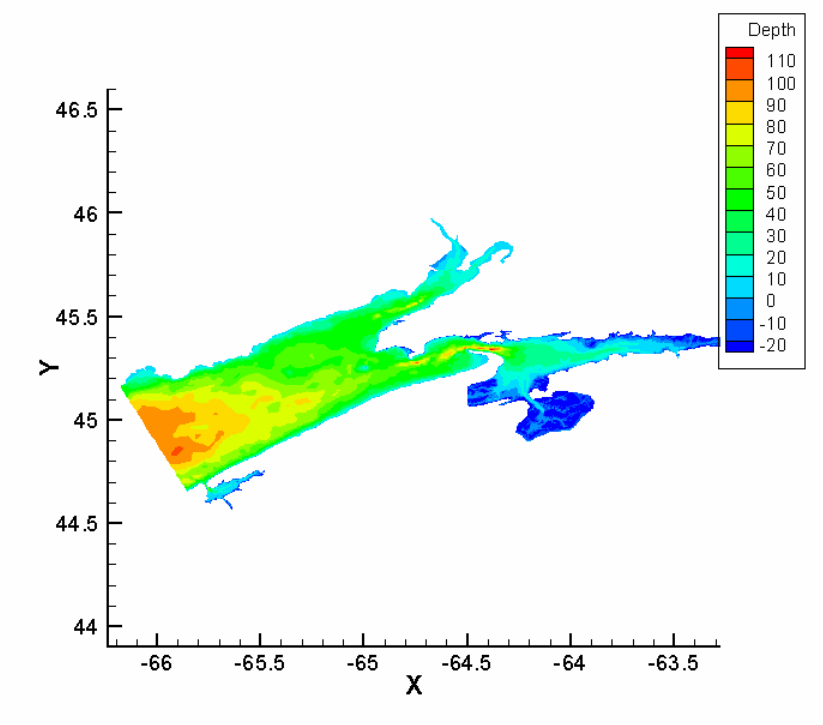


**Figure 5: British Columbia Coast South Tidal Model Region (depths in metres)**

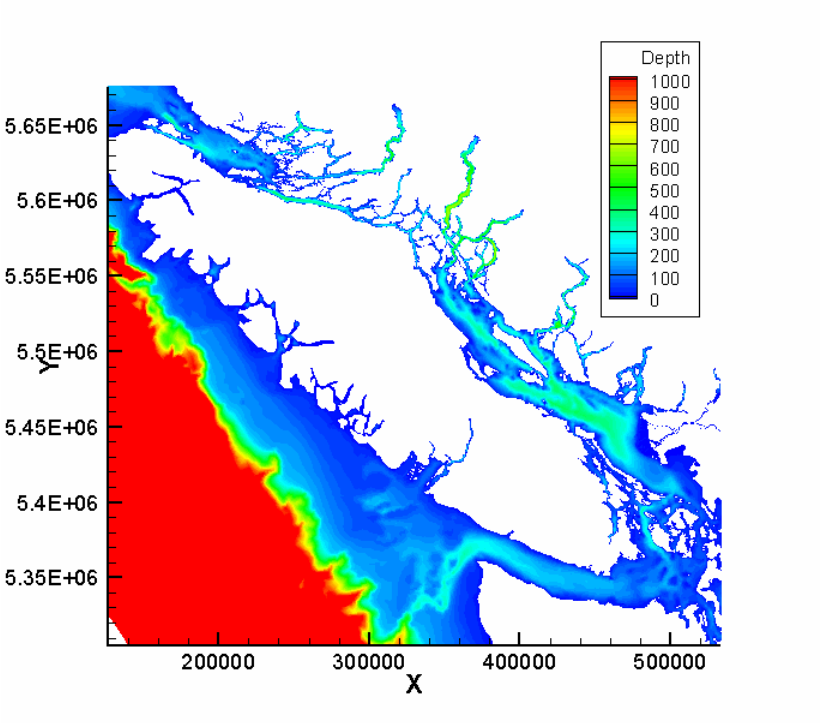

**Figure 6: Queen Charlotte Islands Tidal Model Region (depths in metres)**

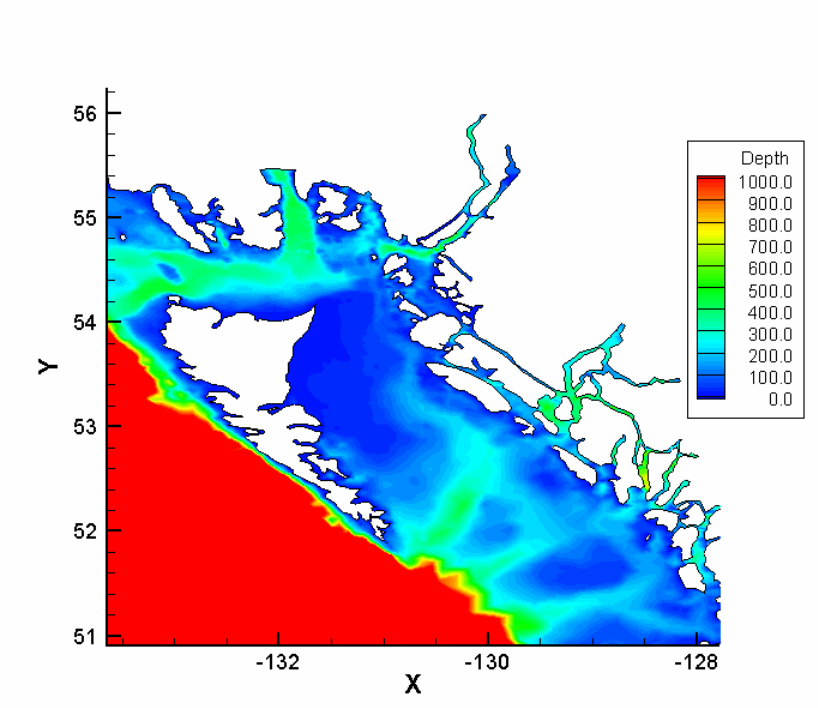

# 3. ANALYSIS METHODOLOGY

## 3.1 TIDES AND TIDAL CURRENTS IN CANADA

Tidal current energy is derived from the flow of coastal ocean waters in response to the tides. A background understanding of tides is helpful in understanding this report, therefore a brief description is included below.

Tides and tidal currents are generated by gravitational forces of the sun and moon on the ocean waters of the rotating earth. Because of its proximity to the earth, the moon exerts roughly twice the tide-raising force of the sun. Tides repeat themselves once every 24 hrs and 50 minutes or the lunar day, which is the time it takes a point on the earth to rotate back to the same position relative to the moon during each daily revolution.

The sun's and moon's gravitational forces creates two "bulges" in the earths ocean waters one directly under or closest to the moon and other on the opposite side of the earth. These "bulges" are the two tides a day observed in many places in the world. Unfortunately, this simple concept is complicated by the fact that the earth's axis is tilted at 22.5 degrees to the moons orbit – the two bulges in the ocean are not equal unless the moon is over the equator. This difference in tide height between the two daily tides is called the diurnal inequality or declinational tides and they repeat on a 14 day cycle as the moon rotates around the earth.

Spring and neap tides have been known for many centuries. Spring tides occur at the time of new or full moon when the sun and moon's gravitational pull is aligned. These tides occur at a 15 day cycle and the combination of this cycle and that of the 14 day declinational tidal cycle explains some of the variability of the tides through the months of the year. There are more than a hundred harmonic constituents or cyclic components of the tide each with a different cycle time. These constituents combine so that tides completely repeat themselves every 18.6 years.

Tides move as shallow water waves in ocean and coastal waters. Despite its name a shallow water waves can exist in any depth of water. Their main characteristic is that the whole depth of water moves as the wave passes. This is unlike wind waves which, except in very shallow water near shore, only move the top few tens of metres of the water column. Shallow water waves move at a celerity related to the square root of the water depth which in the open sea can be several hundred kilometres per hour. In the open ocean tides are small, rarely exceeding 0.5 m. However, as the tidal wave enters coastal waters it slows down, shoals (increases in height) and is reflected in coastal basins. This explains how a small deep ocean tide can result in 15 m tides in Minas Basin (Bay of Fundy), 8 m tides at Prince Rupert (Pacific Coast) and 11 m tides in Ungava Bay (Leaf Bay/Lac aux Feuilles) and Iqualuit.

As discussed above, the total tidal wave is made up of components (constituents) with different harmonic periods and amplitudes. The principal semi-diurnal or twice-daily components are M2 (moon, twice daily) and S2 (sun, twice daily) and the principal diurnal or once-daily components are K1 and O1. Like all diurnal components, the K1 and O1 result from the declination of the moon relative to the earth during the monthly tidal cycle. In coastal waters, these different components may resonate in the bays and straits along the coast depending on their wavelength determined by water depth and the size and shape of the basin. This process is much like the slopping of water in a bathtub. For example, the Bay of Fundy is perfectly "tuned" in terms of water depth and shape to the semi-diurnal tide entering at its mouth. In BC, the small diurnal tides at Victoria and the increasing tide range

as one moves north in Strait of Georgia result from the “tuning out” of the M2 tide in Juan de Fuca Strait and the resonance or tuning of the M2 tide in Strait of Georgia respectively.

Tidal currents result from the passage of the tidal wave. Contrary to popular belief, large tidal currents do not necessarily require a large tidal range. Some of the largest tidal flows in the world occur between the islands on the east side of the Philippines where the tidal range is small but the tide is high in the Pacific at the same time that the tide is low within the Philippine Islands. In technical terms, this is described as the two tides being 180 degrees (or half a cycle) out of phase; the result is very large tidal currents.

Another factor that impacts the magnitude of tidal currents is the presence of narrow passages; these passages result in a narrowing and concentration of tidal flow. However, the flow through a passage is constrained by the loss of energy due to friction. If this loss exceeds a certain value the flow will start to reduce and, in the case of a tidal inlet, (e.g., Minas Channel, NS and Nakwakto Rapids, BC), the tidal range and resulting flows are reduced. There is clearly a limit to the energy that can be extracted, either by nature (in friction) or harnessed (with a tidal power plant).

In British Columbia, some of the highest velocity tidal current flows in Canada occur through the passages between Strait of Georgia and Johnstone Strait. The tidal range is moderate (5 m), but the tides from the Pacific through Johnstone Strait are roughly 180 degrees out of phase with the tides in Strait of Georgia entering south of Vancouver Island.

From a tidal current perspective, it is also important to understand that semi-diurnal tides produce twice the current of the diurnal tide of the same height. This is because the semi-diurnal tide rises in half the time of the equivalent diurnal tide. This is particularly important in British Columbia where many of the potential tidal current power sites are located in areas where the diurnal tide component is strong. On the other coasts of Canada (Arctic and Atlantic), the semi-diurnal tidal component typically dominates the tidal regime (see Section 3.3)

## 3.2 THEORETICAL BASIS

In concept, tidal current energy may be viewed as being extracted directly from the kinetic energy of a tidal stream, or as being extracted from the potential[1] energy of impounded tidal water. In reality, the two are closely related since the extraction of kinetic energy from a tidal stream increases the slope of the hydraulic grade line yielding “partially impounded” water on alternating ends of the tidal channel. Figure 7 shows a hypothetical tidal site that will be used to describe the approach followed in the assessment of tidal stream energy.

[1] Potential (energy) is used here in its technical meaning of energy resulting from vertical position such as tidal height. Elsewhere in this report the common meaning of “latent” is used.

**Figure 7: Definition Sketch**

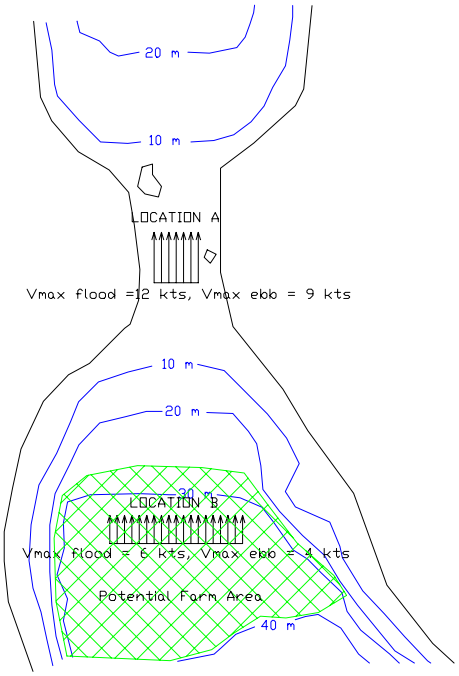


Location A is representative of those locations typically described by the Canadian Hydrographic Service as “narrows” or “tidal rapids” which are critical to marine navigation. For this reason, information pertaining to these areas was used as a primary basis of the overall assessment of Canadian tidal resources.

For the example shown, the flood/ebb maximum currents in the narrows peak at 12 knots/9 knots a few times per year. It is at this location that the theoretical power (energy flux) across the channel cross section is computed and tabulated for potential sites throughout Canada. The theoretical instantaneous power $P_{\text{cross section}}$ (W) in a flow cross-section is given by:

$$P_{cross\,section} = \frac{1}{2}\rho A_{cross\,section} U^3$$

where $\rho$ is the density of water (kg/m$^3$), $A_{\text{cross section}}$ is the cross sectional area (m$^2$), and U is the instantaneous current velocity (m/s). The average value of this parameter throughout the year yields the mean theoretical power at each site considered.

Figure 8 shows the sensitivity of the power calculation to the current speed selected.

**Figure 8: Sensitivity of Power to Current Speed**

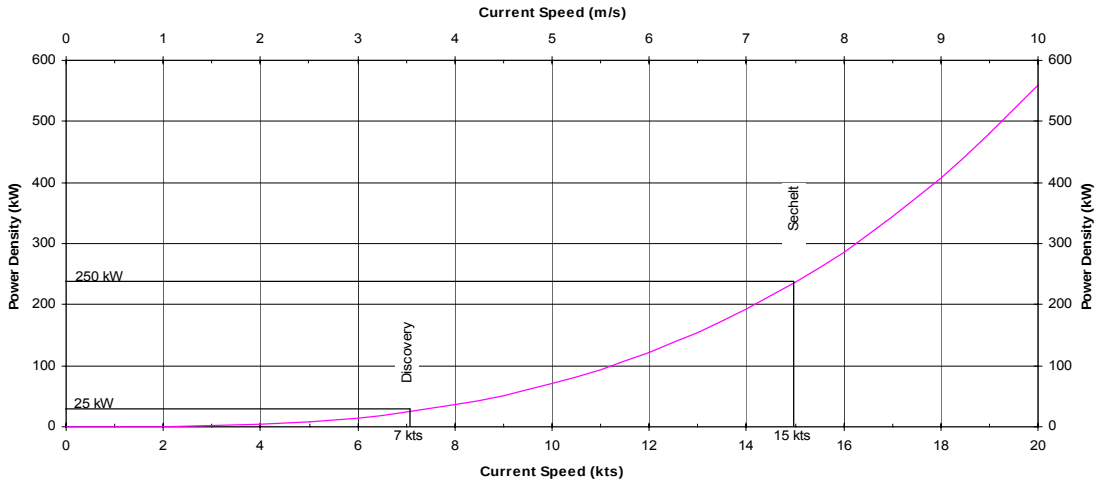


Recent theoretical work by Garrett, Cummins and others at the University of Victoria and the Institute of Ocean Sciences, Sidney, BC, has shown that the kinetic energy approach ($U^3$) described above may have some limitations in a number of tidal current flows such as tidal inlets and tidal passages. This work is described in two papers by Dr. Chris Garrett and Dr. Patrick Cummins (Garrett, 2004; Garrett, 2005). The authors (with help from Dr. Mike Foreman and Dr. Graig Sutherland at IOS) continue to validate their theoretical approach by using a tidal model of Discovery Passage/Johnstone Strait, BC The results of this modelling work will be published in the near future. (pers. comm. Mike Foreman).

A similar modelling approach was used by Triton for the BC Hydro Green Energy Study (Triton, 2002) to investigate the probable magnitude of the extractable tidal energy in the Discovery Passage/Johnstone Strait system. This report is available at www.triton.ca. The results showed that 600 MW of tidal energy could be extracted from this system without significant impacts in the tidal regime in the adjacent tidal water bodies although tidal currents in Discovery Passage were reduced by about 10%. No attempts were made in this study to find the maximum extractable power available from this system. Hopefully, the continuing work of Garrett and Cummins will allow a determination of the extractable power as limited by site specific tidal dynamics.

These new theoretical and modelling studies will provide an improved understanding of the tidal dynamics of tidal current power extraction. Unfortunately, the technical data required for each site, such as detailed tidal models and tidal measurements is considerable, and its application is not appropriate for this early stage of the Canada Ocean Energy Atlas development.

It is therefore believed that theoretical mean power (based on tide stream kinetic energy) remains a reasonable preliminary benchmark to gauge the relative tidal current potential of various sites. The reader must however be aware that kinetic energy is only loosely related to the extractable power since extractable power is highly dependant on the physical characteristics of the site, local tidal dynamics and the technology applied.

## 3.3 PRACTICAL METHODOLOGY

The data sources used for this study are described in Section 2. The practical analysis methodology employed was as follows:

A. Identify and locate all potential current power sites documented in the Sailing Directions and Tide and Current Tables for Canada (see Table 1 and Table 2). Estimate maximum flood and ebb current speeds.

B. Locate these potential sites on the 489 salt water digital charts available for Canada and estimate width and depth of flow.

C. Identify significant potential current sites not covered by digital charts, specifically Hudson's Strait, Ungava Bay and Arctic Region. Review paper chart copies (from UBC map library) and estimate width and depth of flow.

D. Supplement chart data, particularly in remote regions, with satellite mapping data in Google Earth.

E. For large sites with limited (or non-existent) current measurement, estimate potential stream cross-sectional tidal current power from tidal model results (see Section 2.3)

Table 4 shows, in green text, the data collected for each of the identified Canadian tidal current sites. Text in red are calculated parameters. "Column" 1 through 15 correspond to the columns in Table 7 and Table 8 (Section 4 Selected Study Results).

A total of 260 sites were identified: 190 of these sites had an estimated tidal current power potential greater than 1 MW (see Section 4).

**Table 4: Data Assembly**

| Column | Description |
|---|---|
| 1 | Region |
| 2 | Province |
| 3 | Site Name |
| 4 | CHS Chart |
| 5 | Latitude of Site |
| 6 | Longitude of Site |
| 7 | CHS Current Station Number |
| 8 | Maximum Current Speed Flood (Knots) Vf |
| 9 | Maximum Current Speed Ebb (Knots) Ve |
| 10 | Mean Maximum Depth Averaged Current Speed (m/s) Umax = (Vf+Ve)/2 x 0.5148[1] x 0.85[2] |
| 11 | Annual mean power density based on the expression ½ x $^4/_{(3\pi)}$ x $U^3$, where U is the annual mean peak flood and ebb current velocity equal to 0.9 and 0.7[3] times their large tide mean depth and cross-section averaged values respectively. Currents are assumed to vary sinusoidally. |
| 12 | Representative channel width at location of maximum currents (m) |
| 13 | Representative channel depth at location of maximum currents (m) |
| 14 | Representative channel area at mean tide at location of maximum currents ($m^2$) |
| 15 | Mean cross sectional potential power at location of maximum currents computed from the product of the annual mean power density and the mean channel area. (MW) |

Notes:

1. Conversion to m/s
2. Cross-section averaging
3. This factor has been used for all locations except British Columbia, where diurnal tidal currents are strong. In BC, a factor of 0.5 was used in Vancouver Island Mainland and 0.6 used in the Queen Charlotte Islands and Pacific Mainland North regions. This assumption reduces relative BC tidal current power potential compared to the remainder of the country and must be checked with detailed tidal modelling.

# 4. SELECTED STUDY RESULTS

## 4.1 POTENTIAL TIDAL CURRENT ENERGY SUMMARY TABLES

Table 5 shows the estimated mean potential tidal current energy by Provinces in Canada for sites with a mean power greater than 1 MW.

**Table 5: Canada Potential Tidal Current Energy by Province**

| Province | Potential Tidal Current Energy (MW) | Number of Sites (-) | Average Size (MW) |
|---|---|---|---|
| Northwest Territories | 35 | 4 | 9 |
| British Columbia | 4,015 | 89 | 45 |
| Quebec | 4,288 | 16 | 268 |
| Nunavut | 30,567 | 34 | 899 |
| New Brunswick | 636 | 14 | 45 |
| PEI | 33 | 4 | 8 |
| Nova Scotia | 2,122 | 15 | 141 |
| Newfoundland | 544 | 15 | 36 |
| **TOTAL** | **42,240** | **191** | **221** |

Table 6 shows the distribution of mean potential power by Regions with Canada. Note that more than 80% of potential tidal current power is in regions presently impacted by winter ice conditions.

**Table 6: Canada Potential Tidal Current Energy by Region**

| Region | Potential Tidal Current Energy (MW) |
|---|---|
| Vancouver Island Mainland | 3,580 |
| Pacific Mainland North | 353 |
| Queen Charlotte Islands | 81 |
| Arctic | 1,008 |
| Hudson Strait | 29,595 |
| Ungava | 4,112 |
| St. Lawrence River | 153 |
| Gulf of St Lawrence | 537 |
| Atlantic North | 65 |
| Atlantic South | 30 |
| Bay of Fundy | 2,725 |
| **TOTAL** | **42,240** |

Table 7 shows the 50 largest potential tidal current power sites in Canada. Table 8 shows the 50 sites in Canada with the largest Mean Power Density ($MW/m^2$).

## Table 7: Canada Tidal Current Power Sites (50 largest sites)

| Region | Province | Site Name | Chart | Latitude | Longitude | Current Station | Max. Speed Flood (knots) | Max. Speed Ebb (knots) | Mean Max. Depth Ave. Speed (m/s) | Mean Power Density (kW/m2) | Passage Width (m) | Average Depth of Passage (m) | Flow Cross-sectional Area (m2) | Mean Potential Power (MW) |
|---|---|---|---|---|---|---|---|---|---|---|---|---|---|---|
| Hudson Strait | Nunavut | Mill Island-Salisbury Island | 5450 | 63.81 | -77.50 | | 8 | 8 | | 0.887 | 32054 | 204 | 6571070 | 10426 |
| Hudson Strait | Nunavut | Mill Island-Baffin Island | 5450 | 64.15 | -77.57 | | 8 | 8 | | 1.020 | 26125 | 229 | 6008750 | 7584 |
| Hudson Strait | Nunavut | Gray Strait | 5456 | 60.54 | -64.69 | | 6 | 6 | 2.63 | 2.110 | 6000 | 550 | 3307800 | 6979 |
| Hudson Strait | Nunavut | Nottingham Island-Ungava | 5450 | 62.83 | -77.93 | | 8 | 8 | | 0.136 | 64098 | 228 | 14678442 | 1972 |
| Bay of Fundy | Nova Scotia | Minas Basin | 4010 | 45.35 | -64.40 | | 7.5 | 7.5 | 3.28 | 6.036 | 4376 | 56 | 274113 | 1903 |
| Hudson Strait | Nunavut | Salisbury Island-Nottingham Island | 5450 | 63.45 | -77.41 | | 8 | 8 | | 0.360 | 22146 | 147 | 3277608 | 1704 |
| Ungava | Quebec | Smoky Narrows | 5468 | 58.92 | -69.27 | | 12 | 12 | 5.25 | 16.880 | 1500 | 55 | 92400 | 1560 |
| Ungava | Quebec | Algernine Narrows | 5468 | 58.79 | -69.60 | | 10 | 10 | 4.38 | 9.768 | 2000 | 59 | 130400 | 1274 |
| Vancouver Island Mainland | British Columbia | Seymour Narrows | 353902 | 50.13 | -125.35 | 5000 | 16 | 14 | 6.56 | 18.160 | 769 | 41 | 33331 | 786 |
| Hudson Strait | Nunavut | Lacy/Lawson Islands | 5456 | 60.60 | -64.62 | | 7 | 7 | 3.06 | 3.351 | 2750 | 80 | 223575 | 749 |
| Ungava | Quebec | Riviere George Entrance | 5335 | 58.76 | -66.12 | | 8 | 8 | 3.50 | 5.001 | 3000 | 35 | 125100 | 626 |
| Gulf of St Lawrence | Newfoundland | Strait of Belle Isle | 4020 | 51.45 | -56.68 | | | | | 0.201 | 26069 | 49 | 1298236 | 373 |
| Vancouver Island Mainland | British Columbia | N. Boundary Passage | 346201 | 48.79 | -123.01 | | 4 | 4 | 1.75 | 0.498 | 5158 | 140 | 734949 | 366 |
| Vancouver Island Mainland | British Columbia | Discovery Pass. S. | 353901 | 50.00 | -125.21 | | 7 | 7 | 3.06 | 3.676 | 1459 | 42 | 65626 | 327 |
| Arctic | Nunavut | Labrador Narrows | 7487 | 69.71 | -82.59 | | 6 | 6 | 2.63 | 2.110 | 1500 | 100 | 151950 | 321 |
| Vancouver Island Mainland | British Columbia | Boundary passage | 344101 | 48.69 | -123.27 | | 3.5 | 3.5 | 1.53 | 0.334 | 4472 | 175 | 793760 | 265 |
| Ungava | Quebec | Riviere Arnaud (Payne) Entrance | 5352 | 59.98 | -69.84 | | 9 | 9 | 3.94 | 7.121 | 2300 | 9 | 32200 | 229 |
| Bay of Fundy | New Brunswick | Clarks Ground | 4340 | 44.59 | -66.64 | | 6 | 6 | 2.63 | 2.110 | 4092 | 22 | 102300 | 216 |
| Vancouver Island Mainland | British Columbia | Current Passage 2 | 354401 | 50.39 | -125.86 | | 6 | 6 | 2.63 | 1.681 | 1502 | 80 | 123931 | 208 |
| Vancouver Island Mainland | British Columbia | Weyton Passage | 354601 | 50.59 | -126.82 | | 6 | 6 | 2.63 | 1.681 | 1535 | 75 | 118985 | 200 |
| Ungava | Quebec | Koksoak Entrance | 5376 | 58.52 | -68.17 | | 6 | 6 | 2.63 | 2.110 | 2000 | 40 | 92400 | 195 |
| Hudson Strait | Nunavut | Cape Enouolik | 7065 | 64.95 | -78.33 | | 5 | 5 | 2.19 | 1.221 | 5000 | 25 | 142500 | 174 |

| Region | Province | Site Name | Chart | Latitude | Longitude | Current Station | Max. Speed Flood (knots) | Max. Speed Ebb (knots) | Mean Max. Depth Ave. Speed (m/s) | Mean Power Density (kW/m2) | Passage Width (m) | Average Depth of Passage (m) | Flow Cross-sectional Area (m2) | Mean Potential Power (MW) |
|---|---|---|---|---|---|---|---|---|---|---|---|---|---|---|
| Pacific Mainland North | British Columbia | Nakwakto Rapids | 355001 | 51.10 | -127.50 | 6700 | 14 | 16 | 6.56 | 29.062 | 434 | 10 | 5643 | 164 |
| Vancouver Island Mainland | British Columbia | Current Passage 1 | 354401 | 50.41 | -125.87 | | 5 | 5 | 2.19 | 0.973 | 1398 | 100 | 143331 | 139 |
| Vancouver Island Mainland | British Columbia | Dent Rapids | 354301 | 50.41 | -125.21 | 5530 | 11 | 8 | 4.16 | 6.672 | 420 | 45 | 19955 | 133 |
| Vancouver Island Mainland | British Columbia | South Pender Is | 344101 | 48.72 | -123.19 | | 4 | 4 | 1.75 | 0.498 | 1985 | 100 | 203416 | 101 |
| Bay of Fundy | New Brunswick | Devils Half Acre | 4340 | 44.54 | -66.69 | | 6 | 6 | 2.63 | 2.110 | 2133 | 18 | 44793 | 95 |
| Vancouver Island Mainland | British Columbia | Yaculta Rapids | 354301 | 50.38 | -125.15 | | 10 | 10 | 4.38 | 7.782 | 539 | 20 | 12135 | 94 |
| St. Lawrence River | Quebec | Passage de Ile aux Coudre | 1233 | 47.43 | -70.43 | | 5 | 6 | 2.41 | 1.625 | 1700 | 30 | 56100 | 91 |
| Vancouver Island Mainland | British Columbia | Arran Rapids | 354301 | 50.42 | -125.14 | 5600 | 14 | 10 | 5.25 | 13.447 | 271 | 22 | 6629 | 89 |
| Ungava | Quebec | Nakertok Narrows | 5352 | 60.00 | -70.27 | | 9 | 9 | 3.94 | 7.121 | 1100 | 6 | 12100 | 86 |
| Bay of Fundy | New Brunswick | Old Sow | 4114 | 44.92 | -66.99 | | 6 | 6 | 2.63 | 2.110 | 625 | 60 | 39375 | 83 |
| Arctic | Nunavut | Bellot Strait | 7752 | 72.00 | -94.48 | | 8 | 8 | 3.50 | 5.001 | 1000 | 16 | 16400 | 82 |
| Arctic | Nunavut | Cache Pt Channel | 7710 | 68.62 | -113.55 | | 5 | 5 | 2.19 | 1.221 | 6000 | 10 | 62400 | 76 |
| Vancouver Island Mainland | British Columbia | Secheldt Rapids 2 | 351403 | 49.74 | -123.90 | 9999 | 14.5 | 16 | 6.67 | 27.599 | 261 | 8 | 2739 | 76 |
| Arctic | Nunavut | James Ross Strait | 7083 | 66.69 | -95.87 | | 5 | 5 | 2.19 | 1.221 | 5900 | 10 | 61360 | 75 |
| Bay of Fundy | New Brunswick | Head Harbour Passage 1 | 4114 | 44.95 | -66.93 | | 5 | 5 | 2.19 | 1.221 | 890 | 65 | 60520 | 74 |
| Bay of Fundy | Nova Scotia | Northwest Ledge | 4118 | 44.30 | -66.42 | | 4 | 4 | 1.75 | 0.625 | 5334 | 18 | 117348 | 73 |
| Ungava | Quebec | Mikitok Narrows | 5352 | 60.00 | -70.27 | | 9 | 9 | 3.94 | 7.121 | 700 | 8 | 9590 | 68 |
| Arctic | Nunavut | Egg Island | 7735 | 68.55 | -97.40 | | 7 | 7 | 3.06 | 3.351 | 750 | 25 | 19050 | 64 |
| Pacific Mainland North | British Columbia | Otter Passage | 3742 | 53.00 | -129.73 | 8535 | 6 | 6 | 2.63 | 1.860 | 620 | 50 | 32860 | 61 |
| Vancouver Island Mainland | British Columbia | Gillard Passage 1 | 354301 | 50.39 | -125.16 | 5500 | 13 | 10 | 5.03 | 11.835 | 237 | 16 | 4393 | 52 |
| Vancouver Island Mainland | British Columbia | Scott Channel | 362501 | 50.79 | -128.50 | | 3 | 3 | 1.31 | 0.210 | 9970 | 22 | 244256 | 51 |
| Vancouver Island Mainland | British Columbia | Active Pass | 344201 | 48.86 | -123.33 | 3000 | 8 | 8 | 3.50 | 3.984 | 561 | 20 | 12628 | 50 |
| Bay of Fundy | New | Gran Manan Channel | 4340 | 44.78 | -66.86 | | 2.5 | 2 | 0.98 | 0.111 | 5446 | 80 | 452018 | 50 |

| Region | Province | Site Name | Chart | Latitude | Longitude | Current Station | Max. Speed Flood (knots) | Max. Speed Ebb (knots) | Mean Max. Depth Ave. Speed (m/s) | Mean Power Density (kW/m2) | Passage Width (m) | Average Depth of Passage (m) | Flow Cross-sectional Area (m2) | Mean Potential Power (MW) |
|---|---|---|---|---|---|---|---|---|---|---|---|---|---|---|
| | Brunswick | | | | | | | | | | | | | |
| Arctic | Nunavut | Seahorse Point | 7065 | 63.83 | -80.13 | | 5 | 5 | 2.19 | 1.221 | 2000 | 20 | 40800 | 50 |
| Bay of Fundy | Nova Scotia | The Hospital | 4242 | 43.44 | -66.00 | | 4 | 4 | 1.75 | 0.625 | 3600 | 18 | 79200 | 50 |
| Gulf of St Lawrence | Newfoundland | Pointe Armour | 4020 | 51.45 | -56.86 | | 4 | 5 | 1.97 | 0.890 | 1500 | 35 | 53700 | 48 |
| Gulf of St Lawrence | Newfoundland | Forteau | 4020 | 51.41 | -56.95 | | 4 | 5 | 1.97 | 0.890 | 1500 | 35 | 53700 | 48 |
| Pacific Mainland North | British Columbia | Beaver Passage | 3747 | 53.73 | -130.37 | 8545 | 4 | 4 | 1.75 | 0.551 | 810 | 100 | 83430 | 46 |
| Arctic | Nunavut | Nettilling Fiord | 7051 | 66.72 | -72.83 | | 8 | 8 | 3.50 | 5.001 | 1700 | 5 | 9180 | 46 |
| Vancouver Island Mainland | British Columbia | Nahwitti Bar 1 | 354901 | 50.89 | -127.99 | | 5.5 | 5.5 | 2.41 | 1.295 | 2993 | 9 | 34417 | 45 |
| **TOTAL** | | | | | | | | | | | | | | **40697** |

Notes:

1. The tidal current site data shown in yellow in Table 7 and Table 8 were derived from tidal model results (see Section 4.3 and Section 2.3.
2. Some of the tidal current sites shown in Table 7 and Table 8 are located in close proximity to each other in the same tidal channel or tidal inlet (e.g. Seymour Narrows/Discovery Passage in BC and Smoky Narrows and Algernine Narrows in Leaf Bay, Ungava, PQ). The total extractable power available from such adjacent sites will depend on the specific characteristics of the driving tidal dynamics, site geometry and the energy extraction technology used.

## Table 8: Canada Potential Tidal Current Power Sites (50 sites ranked by power density kW/m$^2$)

| Region | Province | Site Name | Chart | Latitude | Longitude | Current Station | Max. Speed Flood (knots) | Max. Speed Ebb (knots) | Mean Max. Depth Ave. Speed (m/s) | Mean Power Density (kW/m2) | Passage Width (m) | Average Depth of Passage (m) | Flow Cross-sectional Area (m2) | Mean Potential Power (MW) |
|---|---|---|---|---|---|---|---|---|---|---|---|---|---|---|
| Pacific Mainland North | British Columbia | Nakwakto Rapids | 355001 | 51.10 | -127.50 | 6700 | 14 | 16 | 6.56 | 29.062 | 434 | 10 | 5643 | 164 |
| Vancouver Island Mainland | British Columbia | Secheldt Rapids 2 | 351403 | 49.74 | -123.90 | 9999 | 14.5 | 16 | 6.67 | 27.599 | 261 | 8 | 2739 | 76 |
| Vancouver Island Mainland | British Columbia | Seymour Narrows | 353902 | 50.13 | -125.35 | 5000 | 16 | 14 | 6.56 | 18.160 | 769 | 41 | 33331 | 786 |
| Ungava | Quebec | Smoky Narrows | 5468 | 58.92 | -69.27 | | 12 | 12 | 5.25 | 16.880 | 1500 | 55 | 92400 | 1560 |
| Bay of Fundy | New Brunswick | Reversing Falls | 4141 | 45.26 | -66.09 | | 12 | 12 | 5.25 | 16.880 | 90 | 15 | 1746 | 29 |
| Pacific Mainland North | British Columbia | Kildidt Narrows | 393701 | 51.89 | -128.11 | | 12 | 12 | 5.25 | 14.880 | 75 | 2 | 375 | 6 |
| Vancouver Island Mainland | British Columbia | Arran Rapids | 354301 | 50.42 | -125.14 | 5600 | 14 | 10 | 5.25 | 13.447 | 271 | 22 | 6629 | 89 |
| Vancouver Island Mainland | British Columbia | Gillard Passage 1 | 354301 | 50.39 | -125.16 | 5500 | 13 | 10 | 5.03 | 11.835 | 237 | 16 | 4393 | 52 |
| Ungava | Quebec | Algernine Narrows | 5468 | 58.79 | -69.60 | | 10 | 10 | 4.38 | 9.768 | 2000 | 59 | 130400 | 1274 |
| Vancouver Island Mainland | British Columbia | Hole-in-the-Wall 1 | 353901 | 50.30 | -125.21 | 5100 | 12 | 9.5 | 4.70 | 9.667 | 189 | 8 | 1985 | 19 |
| Vancouver Island Mainland | British Columbia | Yaculta Rapids | 354301 | 50.38 | -125.15 | | 10 | 10 | 4.38 | 7.782 | 539 | 20 | 12135 | 94 |
| Ungava | Quebec | Riviere Arnaud (Payne) Entrance | 5352 | 59.98 | -69.84 | | 9 | 9 | 3.94 | 7.121 | 2300 | 9 | 32200 | 229 |
| Ungava | Quebec | Nakertok Narrows | 5352 | 60.00 | -70.27 | | 9 | 9 | 3.94 | 7.121 | 1100 | 6 | 12100 | 86 |
| Ungava | Quebec | Mikitok Narrows | 5352 | 60.00 | -70.27 | | 9 | 9 | 3.94 | 7.121 | 700 | 8 | 9590 | 68 |
| Atlantic South | Newfoundland | Placentia Gut | 4841 | 47.25 | -53.96 | | 9 | 9 | 3.94 | 7.121 | 80 | 3 | 336 | 2 |
| Vancouver Island Mainland | British Columbia | Dent Rapids | 354301 | 50.41 | -125.21 | 5530 | 11 | 8 | 4.16 | 6.672 | 420 | 45 | 19955 | 133 |
| Pacific Mainland North | British Columbia | Draney Narrows` | 393102 | 51.47 | -127.56 | | 9 | 9 | 3.94 | 6.277 | 139 | 8 | 1463 | 9 |
| Pacific Mainland North | British Columbia | Hidden Inlet | 399401 | 54.95 | -130.33 | | 9 | 9 | 3.94 | 6.277 | 142 | 3 | 781 | 5 |
| Bay of Fundy | Nova Scotia | Minas Basin | 4010 | 45.35 | -64.40 | | 7.5 | 7.5 | 3.28 | 6.036 | 4376 | 56 | 274113 | 1903 |
| Vancouver Island Mainland | British Columbia | Upper rapids 2 | 353701 | 50.31 | -125.23 | 5030 | 9 | 9 | 3.94 | 5.673 | 242 | 18 | 4955 | 28 |
| Vancouver Island Mainland | British Columbia | Gillard Passage 2 | 354301 | 50.40 | -125.15 | 5500 | 10 | 8 | 3.94 | 5.673 | 393 | 10 | 4916 | 28 |

| Region | Province | Site Name | Chart | Latitude | Longitude | Current Station | Max. Speed Flood (knots) | Max. Speed Ebb (knots) | Mean Max. Depth Ave. Speed (m/s) | Mean Power Density (kW/m2) | Passage Width (m) | Average Depth of Passage (m) | Flow Cross-sectional Area (m2) | Mean Potential Power (MW) |
|---|---|---|---|---|---|---|---|---|---|---|---|---|---|---|
| Vancouver Island Mainland | British Columbia | Gillard Passage 3 | 354301 | 50.39 | -125.16 | 5500 | 10 | 8 | 3.94 | 5.673 | 92 | 5 | 686 | 4 |
| Pacific Mainland North | British Columbia | Outer Narrows | 355001 | 51.09 | -127.63 | | 7 | 10 | 3.72 | 5.288 | 210 | 17 | 4206 | 22 |
| Vancouver Island Mainland | British Columbia | Gabriola Pass. | 347501 | 49.13 | -123.70 | 3300 | 8.5 | 9 | 3.83 | 5.213 | 137 | 8 | 1435 | 7 |
| Ungava | Quebec | Riviere George Entrance | 5335 | 58.76 | -66.12 | | 8 | 8 | 3.50 | 5.001 | 3000 | 35 | 125100 | 626 |
| Arctic | Nunavut | Bellot Strait | 7752 | 72.00 | -94.48 | | 8 | 8 | 3.50 | 5.001 | 1000 | 16 | 16400 | 82 |
| Arctic | Nunavut | Nettilling Fiord | 7051 | 66.72 | -72.83 | | 8 | 8 | 3.50 | 5.001 | 1700 | 5 | 9180 | 46 |
| Vancouver Island Mainland | British Columbia | Porlier Pass | 347303 | 49.01 | -123.59 | 3100 | 9 | 8 | 3.72 | 4.779 | 339 | 15 | 5926 | 28 |
| Vancouver Island Mainland | British Columbia | Quatsino Narrows | 368106 | 50.55 | -127.56 | 9200 | 9 | 8 | 3.72 | 4.779 | 207 | 18 | 4240 | 20 |
| Vancouver Island Mainland | British Columbia | Dodds Narrows | 347501 | 49.14 | -123.82 | 4000 | 9 | 8 | 3.72 | 4.779 | 91 | 9 | 1047 | 5 |
| Pacific Mainland North | British Columbia | Hawkins Narrows | 372201 | 53.41 | -129.42 | | 8 | 8 | 3.50 | 4.409 | 55 | 3 | 301 | 1 |
| St. Lawrence River | Quebec | Travers de Saint-Roch | 1233 | 47.36 | -70.26 | | 7.5 | 7.5 | 3.28 | 4.121 | 500 | 15 | 9000 | 37 |
| Vancouver Island Mainland | British Columbia | Active Pass | 344201 | 48.86 | -123.33 | 3000 | 8 | 8 | 3.50 | 3.984 | 561 | 20 | 12628 | 50 |
| Vancouver Island Mainland | British Columbia | Nitinat Narrows | 364703 | 48.67 | -124.85 | | 8 | 8 | 3.50 | 3.984 | 61 | 20 | 1376 | 5 |
| Vancouver Island Mainland | British Columbia | Discovery Pass. S. | 353901 | 50.00 | -125.21 | | 7 | 7 | 3.06 | 3.676 | 1459 | 42 | 65626 | 327 |
| Hudson Strait | Nunavut | Lacy/Lawson Islands | 5456 | 60.60 | -64.62 | | 7 | 7 | 3.06 | 3.351 | 2750 | 80 | 223575 | 749 |
| Arctic | Nunavut | Egg Island | 7735 | 68.55 | -97.40 | | 7 | 7 | 3.06 | 3.351 | 750 | 25 | 19050 | 64 |
| Bay of Fundy | Nova Scotia | Petit Passage | 4118 | 44.39 | -66.21 | | 7 | 7 | 3.06 | 3.351 | 335 | 18 | 7035 | 24 |
| Ungava | Quebec | McLean Strait | - | 60.35 | -64.63 | | 7 | 7 | 3.06 | 3.351 | 200 | 8 | 2200 | 7 |
| Hudson Strait | Nunavut | McLelan Strait | 4773 | 60.35 | -64.63 | | 7 | 7 | 3.06 | 3.351 | 200 | 8 | 1880 | 6 |
| Bay of Fundy | New Brunswick | Lubec Narrows | 4114 | 44.86 | -66.98 | | 6 | 8 | 3.06 | 3.351 | 180 | 3 | 1080 | 4 |
| Ungava | Quebec | Koksoak Narrows | 5376 | 58.18 | -68.32 | | 5 | 8.5 | 2.95 | 3.004 | 400 | 30 | 14400 | 43 |
| Pacific Mainland North | British Columbia | Porcher Narrows | 3761 | 53.90 | -130.47 | 8551 | 7 | 7 | 3.06 | 2.954 | 120 | 10 | 1560 | 5 |
| Arctic | Nunavut | Wager Bay Narrows | 5440 | 65.31 | -87.74 | | 6 | 7 | 2.84 | 2.683 | 3600 | | 1440 | 4 |
| Vancouver Island | British | Green Pt Rap. 1 | 354301 | 50.44 | -125.51 | | 7 | 7 | 3.06 | 2.669 | 440 | 25 | 12093 | 32 |

| Region | Province | Site Name | Chart | Latitude | Longitude | Current Station | Max. Speed Flood (knots) | Max. Speed Ebb (knots) | Mean Max. Depth Ave. Speed (m/s) | Mean Power Density (kW/m2) | Passage Width (m) | Average Depth of Passage (m) | Flow Cross-sectional Area (m2) | Mean Potential Power (MW) |
|---|---|---|---|---|---|---|---|---|---|---|---|---|---|---|
| Mainland | Columbia | | | | | | | | | | | | | |
| Vancouver Island Mainland | British Columbia | Whirlpool Rapids | 354401 | 50.46 | -125.76 | | 7 | 7 | 3.06 | 2.669 | 321 | 28 | 9804 | 26 |
| Vancouver Island Mainland | British Columbia | Lower Rapids 1 | 353701 | 50.31 | -125.26 | | 7 | 7 | 3.06 | 2.669 | 371 | 8 | 3891 | 10 |
| Vancouver Island Mainland | British Columbia | Race Passage | 344001 | 48.31 | -123.54 | 1200 | 6 | 7 | 2.84 | 2.137 | 884 | 20 | 19885 | 42 |
| Vancouver Island Mainland | British Columbia | Stuart Narrows | 354701 | 50.90 | -126.94 | | 6 | 7 | 2.84 | 2.137 | 261 | 7 | 2478 | 5 |
| Hudson Strait | Nunavut | Gray Strait | 5456 | 60.54 | -64.69 | | 6 | 6 | 2.63 | 2.110 | 6000 | 550 | 3307800 | 6979 |
| Arctic | Nunavut | Labrador Narrows | 7487 | 69.71 | -82.59 | | 6 | 6 | 2.63 | 2.110 | 1500 | 100 | 151950 | 321 |
| Bay of Fundy | New Brunswick | Clarks Ground | 4340 | 44.59 | -66.64 | | 6 | 6 | 2.63 | 2.110 | 4092 | 22 | 102300 | 216 |
| **TOTAL** | | | | | | | | | | | | | | **16441** |

## 4.2 TIDAL RESOURCE MAPS

Figure 9 shows a map (in Manifold GIS) of the Canadian tidal current sites ranked by potential mean power. Figure 10, Figure 11 and Figure 12 show detail areas of this map, namely: Pacific Coast, Hudson's Strait/Ungava Bay and the Atlantic Coast respectively. These latter three maps are at approximately the same scale.

**Figure 9: Canada Potential Tidal Current Resource Sites**

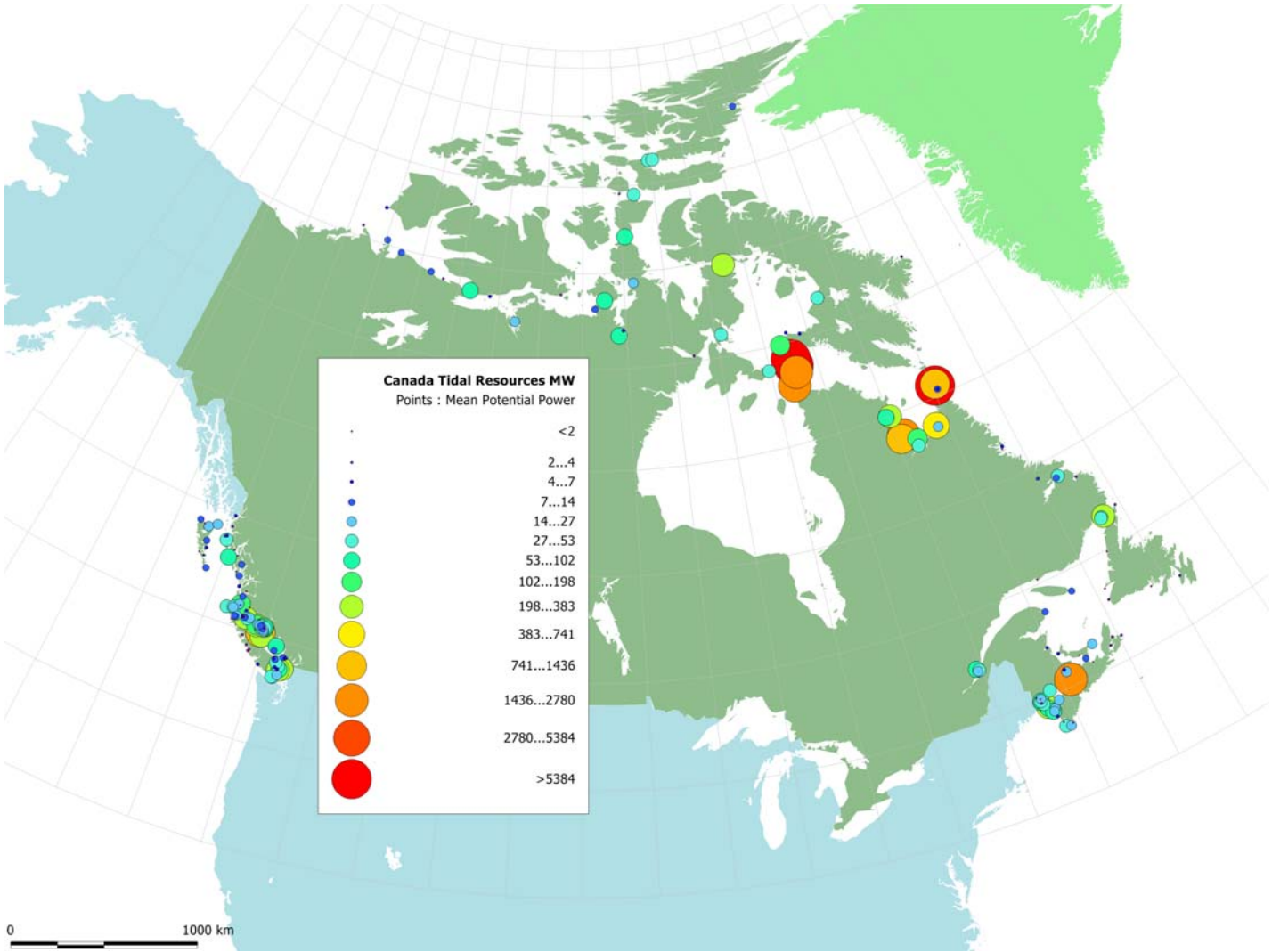

**Figure 10: Potential Tidal Current Resource Sites - Pacific Coast**

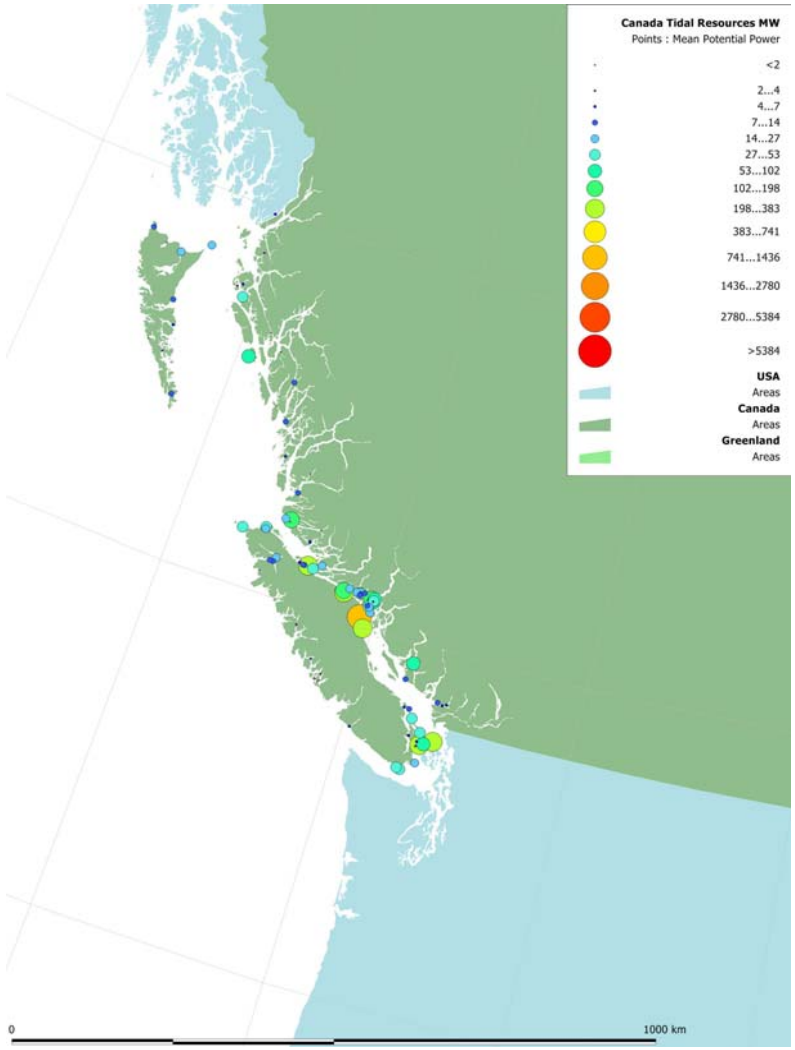

**Figure 11: Potential Tidal Current Resource Sites - Hudson's Strait and Ungava Bay**

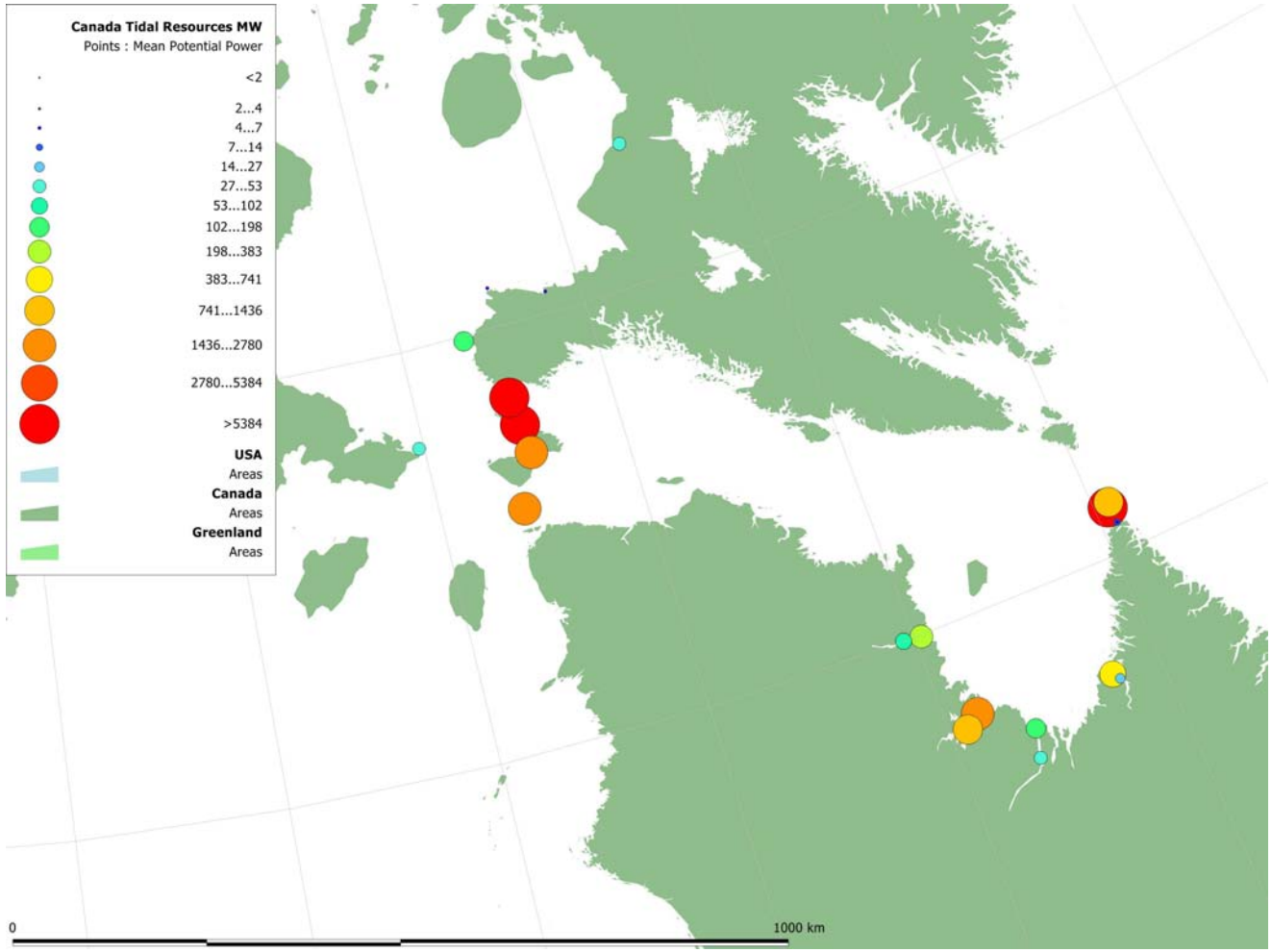

**Figure 12: Potential Tidal Current Resource Sites - Atlantic Coast**

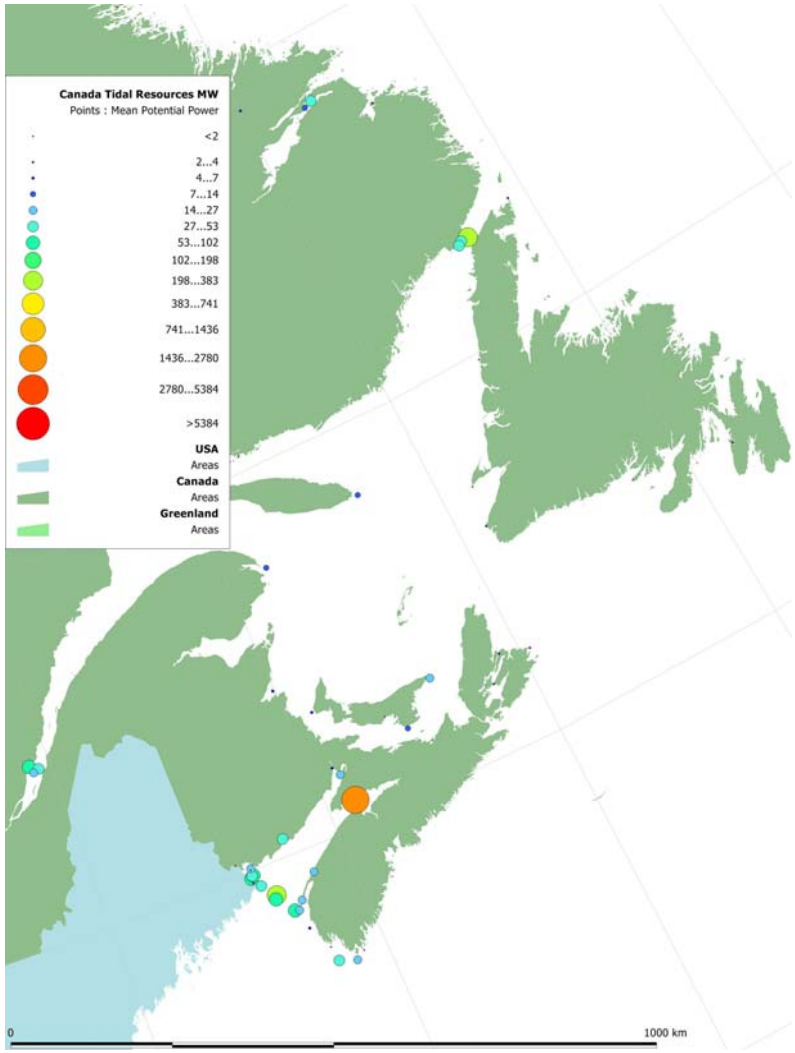

## 4.3 POTENTIAL TIDAL CURRENT ENERGY DENSITY MAPS

Figure 13 through Figure 16 show maps of power density in units W/m for the Pacific Coast, Hudson's Strait, Atlantic Coast and Bay of Fundy North respectively. The power density colour scales for all four maps are similar. These maps were developed from tidal model results.

**Figure 13: Power Density - Pacific Coast**

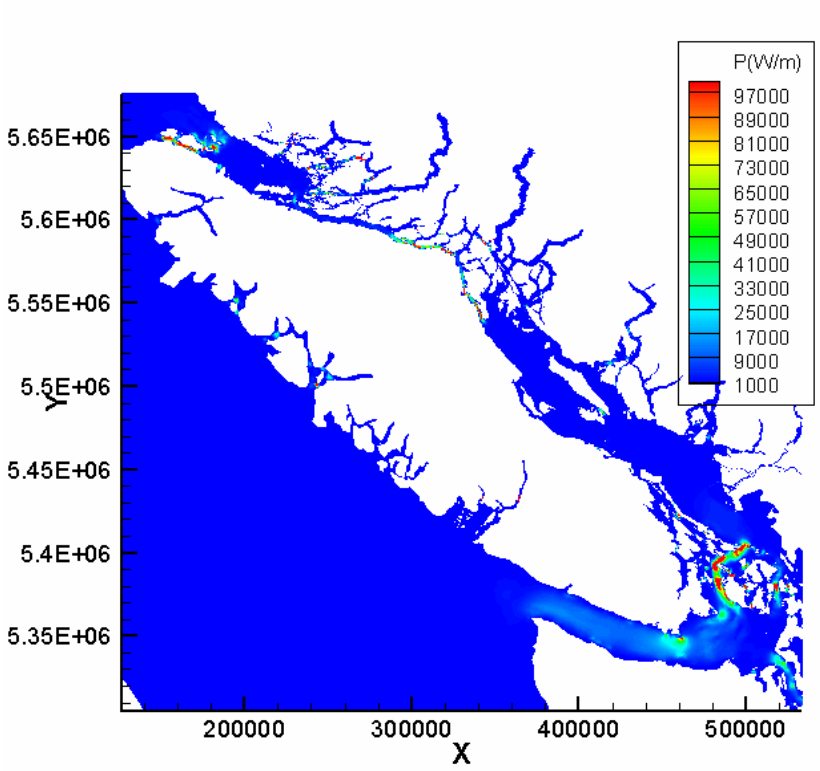

**Figure 14: Power Density - Hudson's Strait**

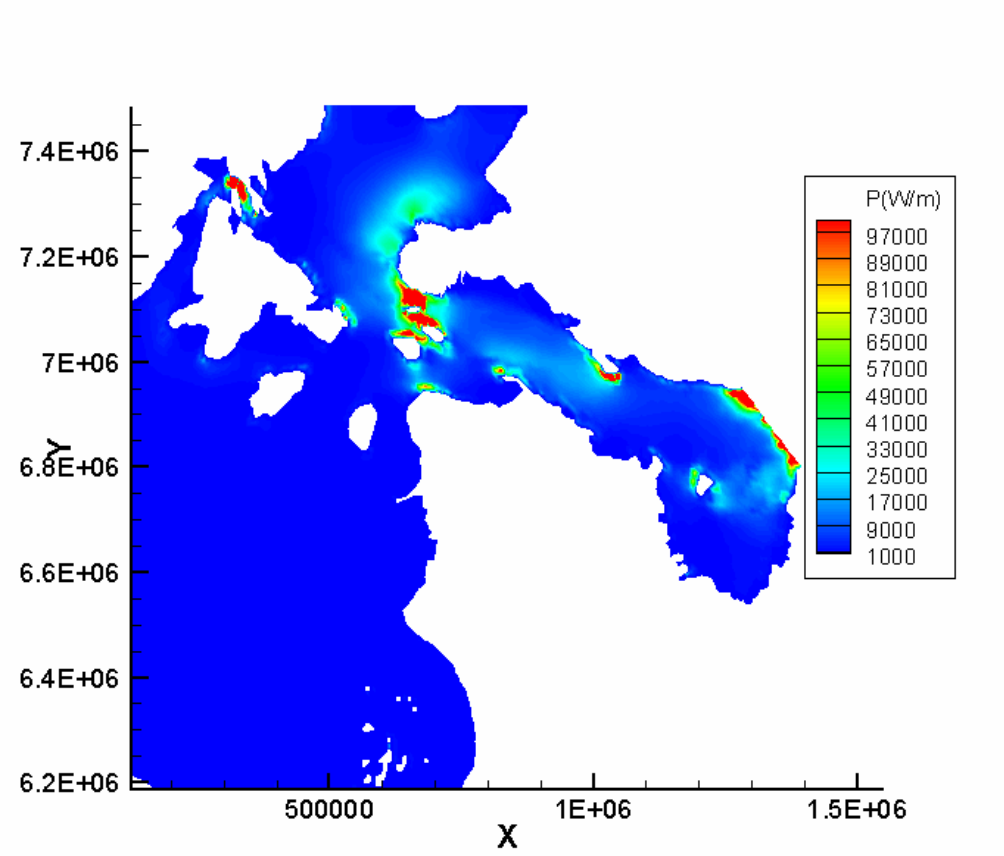

**Figure 15: Power Density - Atlantic Coast**

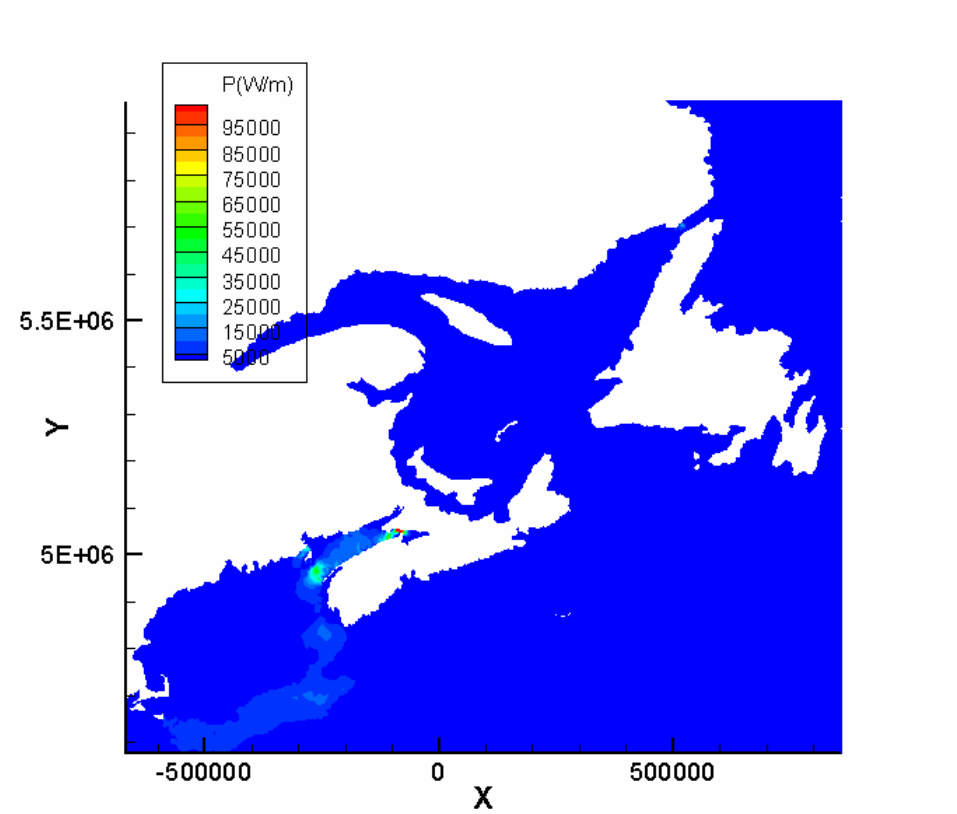

**Figure 16: Power Density - Bay of Fundy North**

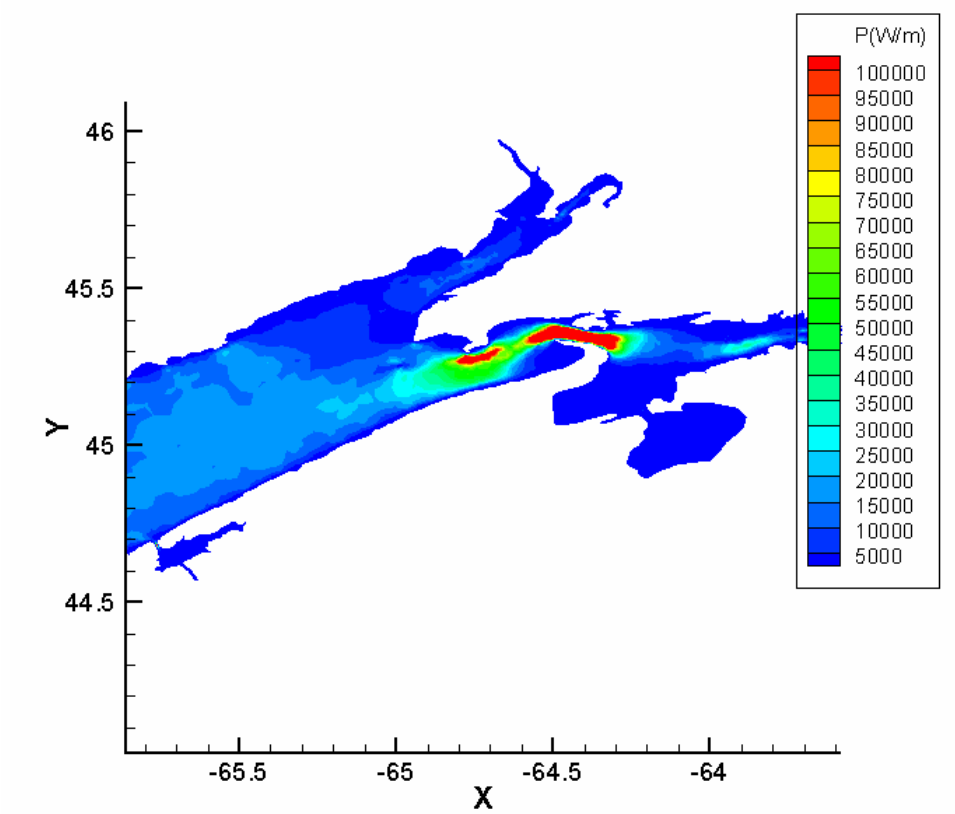

# 5. SUMMARY AND RECOMMENDATIONS FOR FURTHER STUDIES

## 5.1 SUMMARY

As detailed in this summary report, Phase 1 of the Canada Ocean Energy Atlas project has identified a significant tidal current energy resource in Canada. The potential tidal energy in this country is estimated to exceed a mean power of 42,000 MW or about 365 TW.hours/year. To put this figure in perspective, this represents over 70% of Canada's present annual electrical power consumption.

The estimated Canadian tidal current energy resource is an indication of the **potential** energy available, **not** the actual power that can be exploited. Environmental, technological, climate and economic factors will determine what proportion of the potential can be utilised.

## 5.2 RECOMMENDATIONS FOR FUTURE STUDIES

### 5.2.1 Modelling

This preliminary study has identified a number of major tidal current power resources across Canada. It is recommended that near-term modelling studies should concentrate on three specific areas.

- Minas Basin, Nova Scotia
- Georgia and Johnstone Straits, British Columbia.
- Hudson's Strait and Ungava Bay

The objective of these modelling studies should be to improve the definition of the tidal current resources available, to provide estimates of extractable energy and to make an initial evaluation of the environmental impact of tidal energy extraction.

### 5.2.2 Mapping

A principal objective of the Canada Ocean Energy Atlas Project is to make information on Ocean Energy readily available to the Public. As it is clear that Ocean Energy data is primarily geographically-based, the value of a Geographic Information Systems (GIS) for disseminating this information is clear. Over the course of this project, Manifold GIS (www.manifold.net) has been used with success by Triton Consultants. Manifold provides an ideal user-friendly and economic platform for displaying and interrogating geographical-oriented data. GIS packages (such as Manifold) can be easily implemented as web-based applications and this would appear to be the best way to make Canadian Ocean Energy data available to the Public.

It is recommended that a web-based GIS system be implemented during the next phases of the Ocean Energy Atlas Project.

## 6. REFERENCES

Garrett, C. & Cummins, P., 2004. Generating power from tidal currents. J. Waterway Port Coastal Ocean Eng 130 114-118

Garrett, C. & Cummins, P., 2005. The power potential of tidal currents in channels. Proc. R. Soc. A (2005) 461, 2563-2572

Triton Consultants Ltd., 2002. Green energy study for British Columbia. Phase 2: Mainland.

# APPENDICES

# APPENDIX A
# CEAPack Description

# CEAPACK

*Coastal Engineering Analysis Package*

## OVERVIEW

CEAPack is a unified analysis and design toolbox useful to the practicing coastal engineering design consultant. It contains tools for tackling problems as numerically intensive as spectral wave hindcasting and the assessment of the dynamic behaviour of floating bodies, to simple but laborious tasks such as computing pile interference and rubble-mound breakwater volume.

The modules within CEAPack are implemented upon Microsoft Windows .NET framework with a standard user interface and data conventions common to all modules. This standardization frees the user from focusing on data manipulation and allows him to concentrate on the engineering issues.

CEAPack is presently configured with over 30 routines implemented in the following four modules which are called from the CEAPack Launcher interface shown below:

- **CEATools** - Calculates scientific and engineering properties indirectly related to coastal engineering design (e.g., tidal prediction, fluid properties, simple wave generation/propagation, sediment transport)
- **CEADesign** - Design aids directly related to coastal engineering design (e.g., breakwater armour size determination, submarine pipeline stability, floating body stability)
- **CEAData** - 1D, 2D and 3D constant and time-varying dataset conversion, analysis, and visualization (e.g., finite element grid generation, statistical analysis, animation)
- **Models** - A number of individual programs for simulating coastal processes. Many of these are based on existing public-domain or research code that have been modified to fit the CEAPack framework.

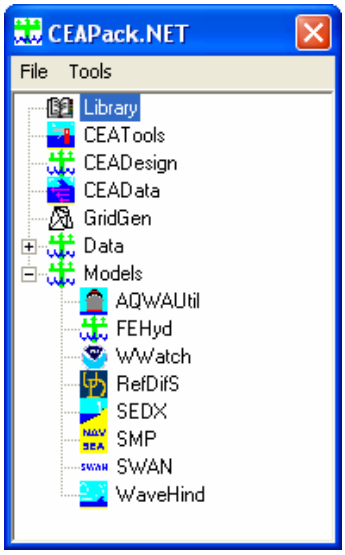


### *CEATools*

CEATools contains routines for completing scientific and engineering calculations such as:

- Tidal harmonic analysis and prediction
- Steady wind wave generation
- Monochromatic and spectral wave transformation
- Wave height distribution
- Propeller wash current generation
- Initiation of sediment transport

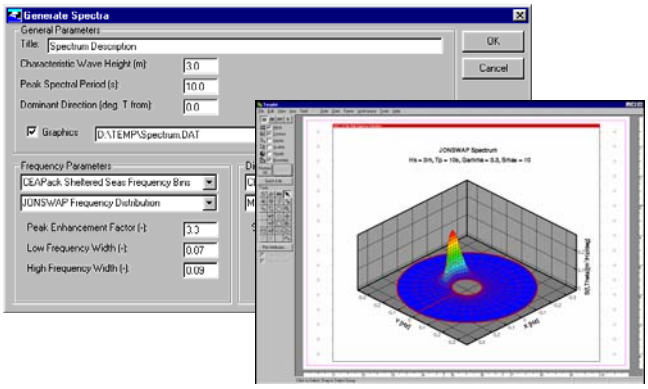


### *CEADesign*

CEADesign contains routines to assist in the design of rubble-mound breakwaters, caisson structures, dredged channels, floating structures, piled structures, pipelines and ports. Design parameters such as minimum structure dimensions, applied forces, and structure response and efficiency are calculated.

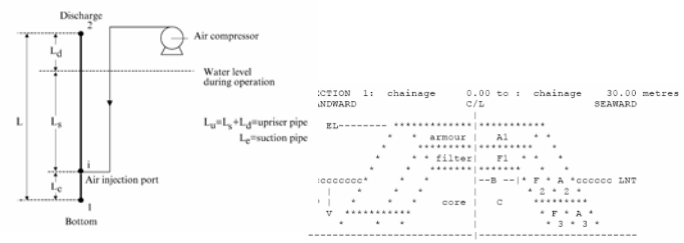


### *CEAData*

CEAData is based on the National Center for Supercomputing Applications Hierarchical Data Format (HDF) with invented conventions for the storage of virtually any type of structured or unstructured mesh and associated scalar and vector time-varying data.

CEAData contains routines for importing data, performing correlation and event analyses, visualizing data and exporting to other formats. In addition, several simple models are included such as 1D wave generation, sediment transport calculation, tide prediction, etc.

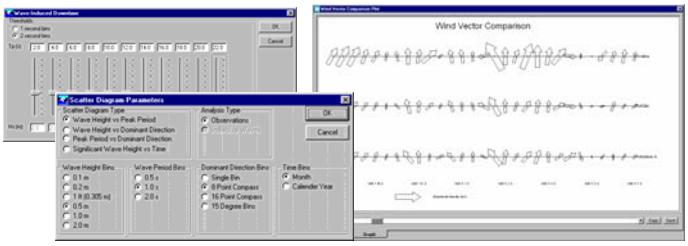

### *Models*

CEAPack contains GUI interfaces and/or pre– and post-processors to several industry-standard numerical models including the following:

- SMP (US Navy)
  - vessel motion analysis for single free-floating vessels of standard shape
- DynMoor (Triton)
  - dynamic mooring analysis model based on SMP results
- AQWA (Century Dynamics)
  - vessel motion and mooring analysis for multiple floating and fixed bodies of arbitrary shape

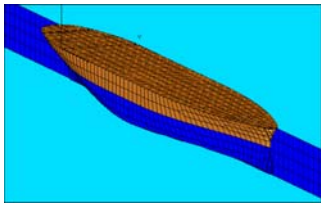
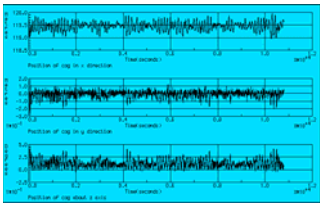

- WaveHind (Triton)
  - 1D wave generation model
- SWAN (Delft University)
  - 2D shallow water wave generation and propagation model
- WaveWatch III (US NOAA)
  - 2D coastal ocean water wave generation and propagation model
- REFDIF (University of Delaware)
  - 2D refraction-diffraction phase-averaging short wave propagation model
- FUNWAVE (University of Delaware)
  - 2D refraction-diffraction phase-resolving short wave propagation model

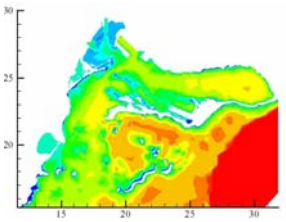

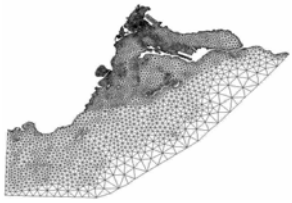

- Tide2D (Roy Walters)
  - 2D harmonic tidal model
- RICOM (Roy Walters)
  - 2D/3D semi-implicit semi-Lagrangian hydrodynamic model
- SEDX (Public Works Canada)
  - alongshore sediment transport calculator
- SBeach and Genesis (US Army)
  - 2D vertical and 2D horizontal shoreline evolution models

### *Supported Data Formats*

CEAPack was designed to leverage the many advanced features that already exist in various industry-standard commercial software packages. In addition to those formats supported implicitly in the models interfaces described previously, a wide variety of import and/or export file format options are supported including:

- Standard
  - ASCII format (DAT, CSV)
  - Binary format (XLS, PDF, MDF, DBF)
  - Images formats (BMP, EMF, GIF, ICO, JPG, PNG, TIF, WMF)
  - Animation formats (AVI)
- Data Visualization
  - Golden Software Surfer Grid format (GRD)
  - TecPlot format (DAT, PLT)
- Grid Generation
  - TriGrid, Institute of Ocean Sci. format (NGH)
- Geographic Information Systems
  - ESRI Shape File format (SHP)
  - Manifold Project format (MAP)
  - MapGen format (DAT)
- Engineering and Scientific
  - AutoDesk AutoCAD formats (DXF, SCR)
  - Danish Hydraulic Institute Litpack formats
  - Canadian Marine Environmental Data Service formats
  - Meteorological Service of Canada formats
  - US NOAA meteorological formats
  - US NOAA raster nautical chart format (BSB)
  - World Meteorological Organization Gridded Binary format (GRB)
  - Unidata NetCDF format (NC, CDF)
  - US National Center for Supercomputing Applications HDF5 format (H5)
  - Canadian Hydrographic Service water level, current and bathymetry formats
  - Geodetic Survey Division, Natural Resources Canada format (GHOST)
  - various meteorological and oceanographic instruments from vendors such as InterOcean, Sontek, Seabird, RD Instruments


**TRITON CONSULTANTS LTD.**

3530 West 43rd Avenue, Vancouver
British Columbia V6N 3J9 CANADA
Telephone: 604 263-3500
Fax: 604 676-2252
Website: www.triton.ca
Email: info@triton.ca

# APPENDIX B
# Hydrodynamic Model Tide 2D Description

# Technical Data Sheet
# HYDRODYNAMIC MODELLING

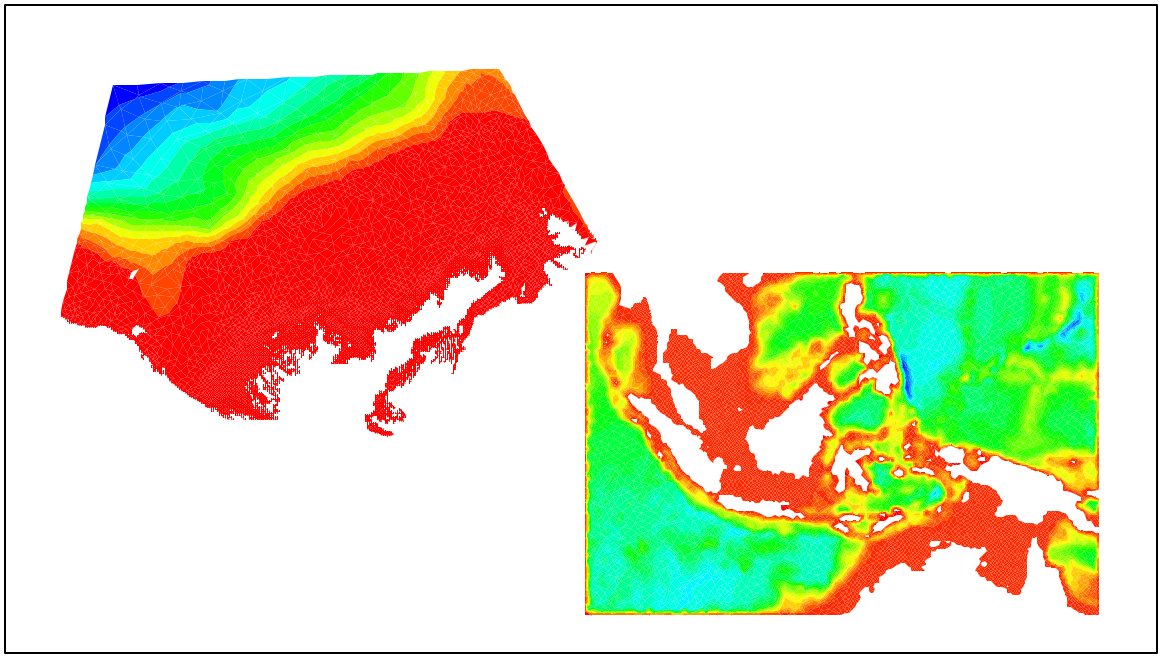

Triton maintains a suite of finite element programs for the assessment of free surface flow in two and three dimensions. All programs were developed by Dr. Roy Walters formerly of the US Geological Survey. The program modules include:

| | | | |
|---|---|---|---|
| Tide2D | Two-dimensional frequency domain solution of the non-linear shallow water equations | WEq | Two dimensional time domain solution of the non-linear shallow water equations |
| Tide3D | Three-dimensional frequency domain solution of the non-linear shallow water equations | XTide | Two dimensional frequency domain solution of the non-linear shallow water and advection-dispersion equations |

Depending on the application, either a frequency domain (harmonic) or time domain (time-stepping) solution may be more appropriate. All modules use a finite element discretisation in space and a harmonic expansion or predictor-corrector approach in time (Walters, 1987). The shallow water equations solve the two or three-dimensional continuity and momentum equations using standard Galerkin techniques. The spatial domain is discretised by defining a set of two-dimensional triangular elements in the horizontal plane, and a sigma coordinate system in the vertical for the third dimension if required.

A typical analysis sequence following the finite element grid generation stage (using the commercially-available TriGrid package) begins with the computationally efficient two-dimesional frequency domain analysis (Tide2D) of steady conditions and harmonic driving components. Short (two to three week) time segments of particular interest are examined using the more-computationally intensive and detailled two-dimensional timestepping solution (WEq). Depending on the importance of three dimensional effects (e.g., salinity, temperature, freshwater influx), Tide3D can be used to with marginal computational penalties over Tide2D. XTide is used to quickly assess dispersion of conservative pollutants.